Magneto-optical Studies of RirA and Cytochrome cd_1

John Derick Holmes

PhD Thesis, July 2012

School of Chemical Sciences

Norwich

Declaration

I declare that the work contained in this thesis, submitted by me for the degree of PhD, is my own original work, except where due reference is made to other authors, and has not been previously submitted by me for a degree at this or any other university.

J. D. Holmes

July 2012

Acknowledgements

Many, many people aided me in the production of this thesis and if it were not for them it would have never been possible. I would firstly like to express my appreciation to my supervisor, Dr. Myles Cheesman, for the unending advice and direction he has given me throughout my studies at the University of East Anglia. As well as this I must also thank Myles for his support through some difficult times and for giving me the strength to carry on when things seemed hopeless. From the first meeting at the Suffield Arms public house sampling their delicious fare to the completion of this thesis he has been there, and for this I will be eternally grateful. On a technical note I must also thank him for using his expert skills to aid me in EPR and simulations. Finally, I would like to thank Myles for being a good friend and rather humorous on many an occasion. I must express thanks to Prof. Andy Johnston and Prof. Nick Le Brun for the enthusiasm, guidance and effort they put into helping me with my studies with RirA, as well as their patience. I would also like to thank Dr. Justin Bradley for his technical assistance on all matters MCD. Again the guidance and support that Justin gave me went a long way to what I achieved. Plus his wit and sunny disposition lightened up any day when the MCD decided to throw a bit of a wobbler. I would also like to express gratitude to Dr. Nicholas Watmough and Dr. Clive Butler for their advice and guidance on improving this thesis. Also thanks to the EPSRC/DTA for the funding for this work, without which nothing at all would have been achievable.

I must give special mention to Dr. Jonathan Todd, Dr. Jason Crack and Dr. Andrew Gates for giving me the skills required working with RirA and the cd_1 proteins, as well as always being approachable when I had queries and doubts. Thank you for the encouragement and guidance (as well as introducing me to Pizza Hut

buffets, the finer points of the British nuclear arsenal and extreme ‘winding me up’ respectively). Along with these fine fellows I must also give praise to the past and present alumni of UEA Biological and Chemical Sciences. They have supported and assisted me from time zero, as well as being friendly and making me feel welcome from the first day as a rookie. These include Dr. Andrew Curson, Dr. Riley Sun, Dr. Rachel Hardingham, Dr. Nefeli Nikolaidou-Katsaridou, Prof. Julea Butt, Dr. Fraser McMillan, Dr. Gaye White, Dr. Benjamin Scott, Dr. Jessica van Wonderen, Dr. Tamara Lawson, Dr Alisa Gaskell, Dr Chloe Singleton, Dr. Allister Crow, Dr Allison Lewin, Dr. Chris Hodson, Dr. Gemma Kemp, Dr Liang Zhou, Dr. Oliver Hecht, Dr. Angelo Figueiredo, Nick Cull, Kate Haynes and Rose-Marie Doyle amongst many others. The latter two I wish every success in the completion of their PhD. I also wish good fortune to Lucy Hume, Rebecca Handley and Raz Abdulqadir in their studies. Apologies for those I have missed, but there are many!

Special thanks must go to Allen Holmes, my father, who supported me financially and every other way through my PhD. His determination through illness is an inspiration to me. The rest of my family, particularly Maureen and Sarah, also deserve my thanks for their help. I must also thank Rev. Canon Roger McPhee for which without his help university life as an undergraduate would not have been possible, let alone this PhD. However Roger, can you stop punching me on the arm now for doing silly things? Many thanks also to Ruth Bird for her unwavering support, and for always thinking of me. A mention must go to the family Appleton for their continued support also. Finally, to all my friends close to and far away from Norfolk. Thank you for shaping me into the person I am today. I am truly blessed to know such an interesting, friendly and diverse bunch of people. I am very lucky. Thanks for the love!

Abstract

Rhizobia are members of the Gram-negative α-proteobacteria. *Rhizobium leguminosarum* controls genes involved in iron uptake through repression under conditions of iron sufficiency. This part of iron regulation is co-ordinated by the dimeric rhizobial iron regulator, RirA. The sequence of RirA contains four cysteines in close proximity, three of which have been shown to be essential to the regulatory functions of RirA and have been proposed as the binding site of an iron-sulfur cluster. RirA has been overexpressed, purified and reconstituted with an iron-sulphur cluster. EPR spectroscopy combined with iron and sulphide assays suggests that the protein binds a [4Fe-4S] or [3Fe-4S] cluster per monomer.

Cytochrome cd_1 is a homodimeric nitrite reductase found in denitrifying bacteria. Each monomer binds a heme *c* that transfers electrons to the structurally unique heme d_1 at the active site. It is shown that the inactive as-prepared form of cd_1 from *Paracoccus pantotrophus* is activated by pre-exposure to the substrate NO_2^-. Although oxidised cd_1 from *Pseudomonas aeruginosa* does not require similar activation, it undergoes the same reaction with NO_2^- to produce a novel form of nitrosyl-heme d_1. The NO derivative of *Pseudomonas aeruginosa* cd_1 was prepared and characterised using variable-temperature variable-field (VTVF) Magnetic Circular Dichroism (MCD) spectroscopy. The novel heme d_1 nitrosyl has thus been identified as an unprecedented Fe^{III}-$NO^{\bullet}$ species. In absorption spectra, this form of nitrosyl-heme d_1 is indistinguishable from the low-spin Fe^{III} state. But simulation of EPR spectra of the oxidised cd_1s has allowed quantitation of the two hemes and shows that there are no populations of the Fe^{III}-$NO^{\bullet}$ product-bound active site heme.

Table of Contents.

Declaration i

Acknowledgements ii

Abstract iv

Table of Contents v

List of Figures xii

List of Tables xx

Abbreviations xxi

Chapter 1. Introduction

1.1 The Nitrogen Cycle 1

1.1.1. Nitrogen Fixation 1

1.1.2. Nitrification 3

1.1.3. ANAMMOX 9

1.1.4. Nitrite Ammonification (Respiratory & Assimilatory) 10

1.1.5. Denitrification 12

1.1.6. Denitrification – Nitrate Reductase 13

1.1.7. Denitrification – Nitrite Reductase 17

1.1.8. Denitrification – Nitric Oxide Reductase 19

1.1.9. Denitrification – Nitrous Oxide Reductase 21

1.1.10. The cd_1 Nitrite Reductases 23

1.1.11. *Pseudomonas aeruginosa* cd_1 Nitrite Reductase 24

1.1.12. *Paracoccus pantotrophus* cd_1 Nitrite Reductase: Differences Between this Enzyme and that of *Pseudomonas aeruginosa.* 34

1.1.13. cd_1 Nitrite Reductases - Nitrite Binding, Mechanism and Catalysis 41

1.1.14. Hemes - Synthesis and Roles 48

1.1.15. Hemes - Physical Properties and Types 53

1.2. Iron Sulphur Clusters and Iron Regulation 57

1.2.1. Iron-Sulphur Clusters – History, Cluster Types and Biosynthesis 58

1.2.2. Iron-Sulphur Cluster Function – Electron Transfer 59

1.2.3. Iron Sulphur Cluster Function – Enzyme Catalysis 62

1.2.4. Iron Sulphur Cluster Function – Structural Functions, Disulphide Cleavage and Sulphur Donation 63

1.2.5. Iron Sulphur Cluster Function – Gene Regulation 63

1.2.6. The Need For Iron Regulation 65

1.2.7. The Classes of Iron Regulators 66

1.2.8. The Rhizobial Iron Regulator (RirA) 75

1.3. Aims of the Work Described in this Thesis 80

1.4. References 81

Chapter 2. Experimental Techniques

2.1. General Materials, Methods and Techniques. 107

2.1.1. Buffer and Growth Media Preparation. 107

2.1.2. Anaerobic Experiments. 108

2.1.3. General Protein Purification Technique. 108

2.1.4. Concentration of Protein Samples. 109

2.1.5. SDS-PAGE. 110

2.2. Materials, Methods and Techniques Used for the RirA Project. 113

2.2.1. Determination of the Extinction Coefficient of RirA Apoprotein. 113

2.2.2. Biorad (Bradford) Protein Assays. 114

2.2.3. Iron Assays. 115

2.2.4. Sulphide Assays 116

2.3. Materials, Methods and Techniques Used for the cd_1 Project. 117

2.3.1. Purification of *Pseudomonas aeruginosa* cd_1. 117

2.3.2. Purification of *Paracoccus pantotrophus* cd_1. 117

2.3.3. Anaerobic Processing. 118

2.3.4. Dialysis. 120

2.3.5. Preparation of NO Solution. 121

2.3.6. Activity Assays for cd_1. 121

2.3.7. Calculation of cd_1 Concentration. 122

2.4. Spectroscopic Applications and Technique. 122

2.4.1. The Theory and Application of Electronic Absorbance Spectroscopy. 122

2.4.2. The Theory and Application of Continuous Wave EPR Spectroscopy. 124

2.4.3. Theory and Application of Magnetic Circular Dichroism (MCD). 127

2.5. References 129

Chapter 3. The Iron-Responsive Regulator RirA in the α-Proteobacteria *Rhizobium leguminosarum*.

3.1. Introduction 130

3.2. Protocols for the Purification and Reconstitution of RirA 131

3.2.1. Construction of the RirA Overexpressing Strain of BL21 *E. coli*. 132

3.2.2. Growth and Preparation of Transformed Cells Containing the RirA Insert. 135

3.2.3. Column Purification of RirA 137

3.2.4. Reconstitution of RirA 138

3.3. Purification, Characterisation and Spectroscopic Analysis of RirA 141

3.3.1. Purification of RirA Apoprotein. 141

3.3.2. Investigation of RirA Overexpression and Breakdown Product 147

3.3.3. Sequencing of the RirA Apoprotein. 152

3.3.4. Characterisation of Protein by Size Exclusion Chromatography 155

3.3.5. Characterisation of Protein by Determination of Extinction Coefficients and Recording of Electronic Absorbance Spectra. 157

3.3.6. Dithionite Reduction and EPR of Reconstituted Protein. 160

3.4. RirA: Summary and Conclusions 169

3.5. References 175

Chapter 4. Novel heme derivatives formed in the reactions of oxidised (as-prepared) *cd*$_1$ with NO_2^- substrate and other nitrogenous ligands.

4.1. Introduction 179

4.2. Oxidised (as Prepared) *Pseudomonas aeruginosa* and *Paracoccus pantotrophus cd*$_1$: Characterisation of Starting Material. 185

4.3. Oxidised (as Prepared) *Pseudomonas aeruginosa cd*$_1$: pH Dependence of Electronic Absorption and EPR. 186

4.4. Oxidised (as Prepared) *Pseudomonas aeruginosa* and *Paracoccus pantotrophus cd*$_1$: Quantitation of EPR Species. 190

4.4.1. Preparation of EPR Samples 193

4.4.2. Simulation of EPR 194

4.5. Activation / Deactivation of *Paracoccus pantotrophus cd*$_1$ – Activation of Oxidised *cd*$_1$ by NO_2^-. 199

4.5.1. Preparation of Experiment 201

4.5.2. Assay Experimental Technique 202

4.5.3. Analysis and Results 202

4.6. Activation / Deactivation of *Pseudomonas aeruginosa cd*$_1$ – Activation of Oxidised *cd*$_1$ by NO_2^-. 204

4.7. Reversion to the Oxidised State by Reaction of Reduced *Paracoccus pantotrophus cd*$_1$ with Hydroxylamine. 207

4.8. MCD and EPR of *Pseudomonas aeruginosa* and *Paracoccus pantotrophus cd*$_1$ Treated with NO and NO_2^-. Reaction of Oxidised *cd*$_1$ with NO. 209

4.8.1. *Pseudomonas aeruginosa* with Bound NO. 210

4.8.2. *Pseudomonas aeruginosa* cd_1 + NO: UV-Visible Electronic Absorbance. 211

4.8.3. *Pseudomonas aeruginosa* cd_1 + NO: EPR. 214

4.8.4. *Pseudomonas aeruginosa* cd_1 + NO: RD-MCD. 215

4.8.5. *Paracoccus pantotrophus* cd_1 + NO: EPR. 216

4.8.6. Reaction of Oxidised cd_1 with NO_2^-. 219

4.8.7. pH on the Nature of NO_2^- Treated *Paracoccus pantotrophus* cd_1. 219

4.9. Reaction of Oxidised cd_1 with N_3^- 222

4.9.1. UV-Visible Absorption Spectra of *Pseudomonas aeruginosa* and *Paracoccus pantotrophus* cd_1 Treated with N_3^-. 223

4.9.2. EPR and MCD of *Pseudomonas aeruginosa* cd_1 Azide Derivative. 224

4.9.3. EPR of the Azide-treated *Paracoccus pantotrophus* cd_1 226

4.10. cd_1: Summary and Conclusions 227

4.11. References 231

Chapter 5. General Discussion

5.1. Introduction 234

5.2. RirA from *Rhizobium leguminosarum* 235

5.3. The cd_1 Nitrite Reductases of *Paracoccus pantotrophus* and *Pseudomonas aeruginosa*. 241

5.4. References 246

Appendix

Experimental and Simulated EPR Spectra of *Paracoccus pantotrophus* and *Pseudomonas aeruginosa* cd_1 251

List of Figures.

Chapter 1.

Figure 1.01 Diagram of the nitrogen cycle.

Figure 1.02 Structure of nitrogenase from *Azotobacter vinelandii*.

Figure 1.03 Structure of specialist co-factors in nitrogenase.

Figure 1.04 Structure of a subunit of hydroxylamine oxidoreductase from *Nitrosomonas europaea*.

Figure 1.05 Structure of heme P460.

Figure 1.06 Structure of siroheme.

Figure 1.07 Structure of a NrfA dimer from *Escherichia coli*.

Figure 1.08 Structure of NapAB from *Rhodobacter sphaeroides*.

Figure 1.09 Structure of NarGHI from *Escherichia coli*.

Figure 1.10 Structure of a CuNIR monomer from *Alcaligenes xylosoxidans*

Figure 1.11 Structure of NorBC from *Pseudomonas aeruginosa*.

Figure 1.12 Structure of the N_2OR homodimer from *Paracoccus denitrificans*.

Figure 1.13 Multiple sequence alignment of cd_1 nitrite reductases from seven different species of bacteria.

Figure 1.14 [A] Structure of the dimeric cd_1 nitrite reductase from *Pseudomonas aeruginosa*.

[B] Structure of the *c* heme of *Pseudomonas aeruginosa* cd_1 and associated amino acid residues.

[C] Structure of the d_1 heme of *Pseudomonas aeruginosa* cd_1 and associated amino acid residues.

Figure 1.15 Structure of the d_1 heme of *Pseudomonas aeruginosa* cd_1 with NO bound and associated amino acid residues.

Figure 1.16 Structures of *c* and d_1 heme.

Figure 1.17 [A] Structure of the dimeric cd_1 nitrite reductase from *Paracoccus pantotrophus*.

[B] Structure of the *c* heme of *Paracoccus pantotrophus* cd_1 and associated amino acid residues.

[C] Structure of the d_1 heme of *Paracoccus pantotrophus* cd_1 and associated amino acid residues.

Figure 1.18 Structure of the d_1 heme of reduced *Paracoccus pantotrophus* cd_1 with NO bound and associated amino acid residues.

Figure 1.19 Structure of the *c* heme of reduced *Paracoccus pantotrophus* cd_1 and associated amino acid residues.

Figure 1.20 Scheme of the general reaction mechanisms of cd_1 nitrite reductases.

Figure 1.21 Scheme of conserved histidines in the d_1 heme pocket in relation to bound nitrite.

Figure 1.22 Scheme of proposed hydrogen-bonding of NO-bound d_1 heme in *Pseudomonas aeruginosa* cd_1.

Figure 1.23 Scheme of heme biosynthesis pathway.

Figure 1.24 Structures of heme *b* and *c*.

Figure 1.25 Energy level diagram showing oxidation / spin states of heme iron.

Figure 1.26 Structures of hemes *a*, *o* and *d*.

Figure 1.27 Structures of common iron sulphur clusters with example proteins, oxidation states and EPR characteristics.

Figure 1.28 [A] Structure of a Fur monomer from *Pseudomonas aeruginosa.*
[B] Structure of a Fur monomer from *Heliobacter pylori*.

Figure 1.29 [A] Structure of DtxR from *Corynebacterium diphtheria* displaying domains and key features.
[B] Structure of DtxR from *Corynebacterium diphtheria* displaying helices with residues key to the reaction mechanism.

Figure 1.30 Multiple sequence alignment of Irr proteins from six bacterial species and compared with *Escherichia coli* Fur.

Figure 1.31 Multiple sequence alignment of RirA proteins from six bacterial species.

Figure 1.32 Multiple sequence alignment of Rrf2 family members RirA, IscR, NsrR and Rrf2.

Chapter 2.

Figure 2.01 Scheme of the workings of the Sparging Fridge.

Figure 2.02 Diagram of path of radiation in a UV-visible spectrophotometer.

Chapter 3.

Figure 3.01 Amino acid sequence of *Rhizobium leguminosarum* RirA.

Figure 3.02 Plasmid map of pET21a with the RirA insert.

Figure 3.03 SDS-PAGE showing RirA overexpression.

Figure 3.04 Elution profile of RirA from the Heparin purification stage.

Figure 3.05 SDS-PAGE showing RirA is not lost in the wash fractions of the Heparin purification stage.

Figure 3.06 SDS-PAGE showing RirA contained in fractions collected during the Heparin purification stage.

Figure 3.07 S200 Gel filtration profile showing RirA and contaminants.

Figure 3.08 SDS-PAGE showing fractions from the gel filtration stage that contain RirA.

Figure 3.09 SDS-PAGE showing RirA degradation over time if IPTG induction is allowed to proceed for too long.

Figure 3.10 SDS-PAGE showing RirA and the formation of breakdown product at room temperature over a period of weeks.

Figure 3.11 SDS-PAGE showing the effects of iron and oxygen on RirA degradation at 4°C.

Figure 3.12 SDS-PAGE showing RirA contained in fractions collected during the Heparin purification stage but with less breakdown product due to addition of EDTA.

Figure 3.13 Sequence of a section of the pET21a plasmid with the RirA insert.

Figure 3.14 Sequence of a section of the pET11a plasmid with the RirA insert.

Figure 3.15 Multiple sequence alignment showing pET21a and pET11a inserts are identical to published RirA sequence.

Figure 3.16 Size exclusion chromatography calibration curve showing RirA is a dimer.

Figure 3.17 Electronic absorption spectrum of RirA apoprotein after removal of cluster.

Figure 3.18 Electronic absorption spectra of 11.8% loaded holoprotein from which the extinction coefficient of 100% loaded RirA holoprotein was calculated.

Figure 3.19 SDS-PAGE of a reconstituted RirA sample.

Figure 3.20 Electronic absorbance spectra of 'as prepared' reconstituted RirA and after treatment with 33.85 μM dithionite.

Figure 3.21 EPR spectra of ferricyanide-oxidised reconstituted RirA recorded at different temperatures.

Figure 3.22 EPR spectra of dithionite-reduced reconstituted RirA measured at different microwave powers.

Figure 3.23 EPR spectra of as reconstituted RirA measured at different microwave powers.

Figure 3.24 EPR spectra of as reconstituted RirA measured at different temperatures.

Chapter 4.

Figure 4.01 Scheme of the two NO conformations formed from NO binding to ferrous and ferric heme.

Figure 4.02 The two Lewis structures for the azide ion.

Figure 4.03 Reaction scheme showing hydroxylamine reoxidation of reduced *Paracoccus pantotrophus* cd_1, followed by gradual reversion to the oxidised form.

Figure 4.04 [A] Electronic absorption spectrum of oxidised, as isolated *Pseudomonas aeruginosa* cd_1.

[B] Electronic absorption spectrum of oxidised, as isolated *Paracoccus pantotrophus* cd_1.

Figure 4.05 Energy level diagram showing the energy differences between low and high spin ferric heme at extremes of pH.

Figure 4.06 Electronic absorption spectra of oxidised, as isolated *Pseudomonas aeruginosa* cd_1 at extremes of pH.

Figure 4.07 EPR spectra of oxidised, as isolated *Pseudomonas aeruginosa* cd_1 at different pHs measured at 10 K and 2 mW, with left panel showing overlaid spectra and feature at ~ 265 mT.

Figure 4.08 Overlaid electronic absorbance spectra of reduced / oxidised horse heart cytochrome c at 500-600 nm with scheme showing the basics of the cd_1 assay reaction.

Figure 4.09 Plots of average initial rates of reaction of *Paracoccus pantotrophus* cd_1 activity at different pHs and buffer conditions (H_2O or D_2O).

Figure 4.10 Plots of average initial rates of reaction of *Pseudomonas aeruginosa* cd_1 activity at different pHs.

Figure 4.11 Plot of initial rates of *Paracoccus pantotrophus* cd_1 activity after hydroxylamine incubation at pH 6.5.

Figure 4.12 Overlaid electronic absorption spectra of *Pseudomonas aeruginosa* cd_1 before and after the addition of NO equivalents.

Figure 4.13 Electronic absorption spectra showing the effect of addition of gaseous NO to oxidised, as isolated *Pseudomonas aeruginosa* cd_1.

Figure 4.14 [A] EPR spectrum of NO bound *Pseudomonas aeruginosa* cd_1 with ~ 55% deuterated glycerol added at 10 K, 2 mW.

[B] EPR spectrum of NO bound *Pseudomonas aeruginosa* cd_1 with ~ 55% deuterated glycerol added at 20 K, 0.64 mW.

Figure 4.15 RD-MCD spectra of NO bound *Pseudomonas aeruginosa* cd_1 at pH 6.5.

Figure 4.16 Overlaid electronic absorption spectra of *Paracoccus pantotrophus* cd_1 treated with gaseous NO at pH 5.5.

Figure 4.17 EPR spectrum of *Paracoccus pantotrophus* cd_1 after overnight exposure to NO at 10 K and 2 mW.

Figure 4.18 EPR spectra of *Paracoccus pantotrophus* cd_1 after overnight exposure to NO, recorded at 10 K / 2 mW and 40 K / 2 mW and focused on the ~ 290-390 mT region.

Figure 4.19 Overlaid electronic absorption spectra of nitrite treated *Paracoccus pantotrophus* cd_1 at three different pHs.

Figure 4.20 RD-MCD spectra of nitrite treated *Paracoccus pantotrophus* cd_1 at three different pHs.

Figure 4.21 Electronic absorption spectra of *Pseudomonas aeruginosa* cd_1 showing the effect of 20 mM azide.

Figure 4.22 Electronic absorption spectra of *Paracoccus pantotrophus* cd_1 showing the effect of 20 mM azide.

Figure 4.23 EPR spectrum of azide treated *Pseudomonas aeruginosa* cd_1 at 10 K and 2 mW.

Figure 4.24 RD-MCD spectra of azide treated *Pseudomonas aeruginosa* cd_1 at pH 6.5.

Figure 4.25 EPR spectrum of azide treated *Paracoccus pantotrophus* cd_1 at 10 K and 2 mW.

Chapter 5.

Figure 5.01 SWISS-MODEL generated structure of RirA using a CymR template.

Appendix

Figure A.01 Experimental and simulated EPR spectra of oxidised *Pseudomonas aeruginosa* cd_1 at 10 K and 2 mW.

Figure A.02 Experimental and simulated EPR spectra of oxidised *Pseudomonas aeruginosa* cd_1 at 20 K and 0.64 mW.

Figure A.03 Experimental and simulated EPR spectra of oxidised *Pseudomonas aeruginosa* cd_1 with ~55% total volume deuterated glycerol at 10 K and 2 mW.

Figure A.04 Experimental and simulated EPR spectra of oxidised *Pseudomonas aeruginosa* cd_1 at 20 K and 0.64 mW.

Figure A.05 Experimental and simulated EPR spectra of oxidised *Paracoccus pantotrophus* cd_1 with ~55% total volume deuterated glycerol at 10 K and 2 mW.

Figure A.06 Experimental and simulated EPR spectra of oxidised *Paracoccus pantotrophus* cd_1 at 20 K and 0.64 mW.

Figure A.07 Experimental and simulated EPR spectra of oxidised *Paracoccus pantotrophus* cd_1 with ~55% total volume deuterated glycerol at 10 K and 2 mW.

Figure A.08 Experimental and simulated EPR spectra of oxidised *Paracoccus pantotrophus* cd_1 with ~55% total volume deuterated glycerol at 20 K and 0.64 mW.

List of Tables

Chapter 2.

Table 2.01 Components of SDS-PAGE stacking and resolving gels.

Table 2.02 Components of SDS-PAGE loading buffer.

Chapter 4.

Table 4.01 EPR g-values of low spin ferric *c* and d_1 hemes in different species and states of cd_1 nitrite reductase.

Table 4.02A Percentage contributions, g-values and linewidths of simulated EPR spectra from oxidised *Pseudomonas aeruginosa* cd_1 at two conditions (10 K / 2mW and 20K / 0.64 mW) and with / without deuterated glycerol.

Table 4.02B Percentage contributions, g-values and linewidths of simulated EPR spectra from oxidised *Paracoccus pantotrophus* cd_1 at two conditions (10 K / 2mW and 20K / 0.64 mW) and with / without deuterated glycerol.

Abbreviations

Å	Angstroms (10^{-10} m)
Abs, A	Absorbance
ΔA	Difference absorption
ADP	Adenosine diphosphate
AEBSF	4-(2-Aminoethyl) benzenesulfonyl fluoride
AMO	Ammonium mono-oxygenase
ANAMMOX	Anaerobic ammonium oxidation
ATP	Adenosine triphosphate
BSA	Bovine serum albumin
CD	Circular dichroism
CM	Carboxymethyl
CuNIR	Copper nitrite reductases
Da (kDa)	Dalton (kilodalton)
DEAE	Diethylaminoethyl cellulose
DMPD	N,N-dimethyl-p-phenylenediamine dihydrochloride
DNA	Deoxyribonucleic acid
DTT	Dithiothreitol
ε	Extinction coefficient ($M^{-1} cm^{-1}$)
Δε	Difference extinction coefficient
e^-	Electron
ECF	Extracytoplasmic function
EDTA	Ethylenediaminetetraacetic acid
EPR	Electron paramagnetic resonance
FNR	Fumarate and nitrate reductase
G	Gauss
HAO	Hydroxylamine oxidoreductase
HCO	Heme-copper oxidase
HEPES	4-(2-hydroxyethyl)-1-piperazineethanesulfonic acid
HiPIP	High potential iron sulphur protein
HPII	Hydroperoxidase II
HRM	Heme regulatory motif
ICE	Iron control element
IPTG	Isopropyl-β-D-galactoside
IRE	Iron responsive elements
IRO	Iron responsive operator
IRP	Iron regulatory protein
ISC	Iron sulphur cluster
K	Kelvin
k_{cat}	Turnover number
K_m	Michaelis constant (association constant)
L (μL, mL)	Litre (microlitre, millilitre)
LB	Luria-Bertani broth
LMCT	Ligand to metal charge transfer
m (nm, μm, mm, cm)	Metre (nanometre, micrometre, millimetre, centimetre)
M (nM, μM, mM)	Mole (nanomole, micromole, millimole)
Mb	Myoglobin
MCD	Magnetic circular dichroism
MES	2-(N-morpholino)ethanesulfonic acid

MGD	Molybdopterin guanine dinucleotide
MLCT	Metal to ligand charge transfer
MNA	Methylnicotinamide
MOPS	3-(N-morpholino)propanesulfonic acid
M_r, mW	Molecular weight
MWCO	Molecular weight cut-off
NIF	Nitrogen fixation
NMR	Nuclear magnetic resonance
NOR	Nitric oxide reductase
N_2OR	Nitrous oxide reductase
OD	Optical density
OM	Outer membrane
PAGE	Polyacrylamide gel electrophoresis
PMSF	Phenylmethanesulfonylfluoride
RD-MCD	Ratio data - magnetic circular dichroism
RNA	Ribonucleic acid
rpm	Revolutions per minute
s	Spin quantum number
S	Spin angular momentum
SDS	Sodium dodecyl sulphate
SUF	Sulphur mobilization
T (mT)	Tesla (millitesla)
TCEP	Tris(2-carboxyethyl)phosphine
TEMED	N,N,N',N'-tetra-methyl-ethylenediamine
Tris	Tris(hydroxymethyl)aminomethane
UV	Ultraviolet
V (mV)	Volt (millivolt)
V_e	Elution volume
v/v	Volume-volume
VTVF	Variable temperature, variable field
V_0	Void volume
W (mW)	Watt (milliwatt)
w/v	Weight-volume

Chapter 1.

Introduction

1.1: The Nitrogen Cycle

Elemental nitrogen is a largely inert diatomic gas that is both tasteless and colourless. It is the fifth most abundant element in the solar system [1] and approximately 79 % of the air in the Earth's atmosphere is nitrogen. It is an essential component of two important groups of biological molecules. The first group comprises amino acids that make up proteins, and the second are bases that are components of DNA and RNA that are fundamental to life on Earth. It is vital that sources of nitrogen can be converted into forms that which living organisms can utilise [2]. Nitrogen can be liberated through the geological recycling of rocks over many millions of years, and this formed the basis for an early nitrogen cycle [3, 4]. However, the nitrogen cycle now involves a more complicated network of microbial mediated redox reactions. The biogeochemistry of nitrogen today is largely reliant on these redox reactions (see Figure 1.01), with the geological recycling of rocks playing a lesser role [3, 5].

1.1.1: Nitrogen Fixation

The nitrogen cycle can be divided into several sections. In a process called nitrogen fixation, atmospheric nitrogen is converted to ammonium by the bacterial enzyme nitrogenase [6]. The nitrogenase acts as a catalyst to lower the activation energy barrier associated with breaking the triple bond of dinitrogen. To do this the nitrogenase hydrolyses 16 ATP molecules to drive what is an endergonic reaction, as well as utilising 8 electrons as shown in Equation 1.

$$N_2 + 8e^- + 8H^+ + 16ATP \rightarrow 2NH_3 + H_2 + 16ADP + 16Pi \quad (1)$$

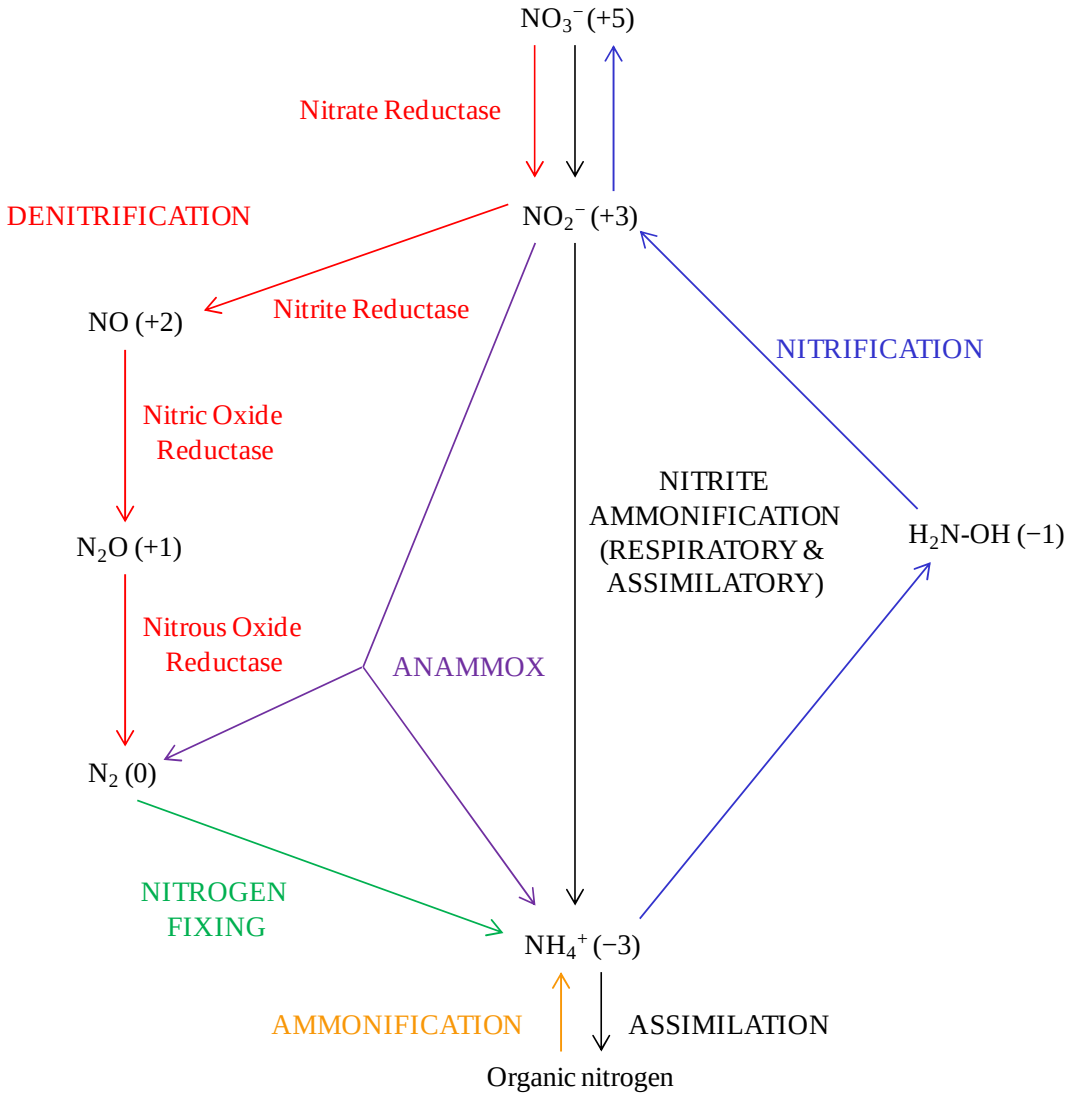

Figure 1.01: The routes of interconversion of compounds in the nitrogen cycle. Nitrogen species are shown with oxidation states of the N atom in brackets. The enzymes involved in the steps of the denitrification pathway are also shown. Subsections of the cycle are labelled in upper case.

The nitrogenase system comprises of a MoFe-protein subunit and a Fe-protein subunit. The MoFe-protein constituent contains a MoFe cofactor at each α subunit and a Fe cofactor (P-cluster) at each β subunit [7]. The Fe-protein constituent contains a [4Fe-4S] cluster (see Figure 1.02 and 1.03). The MoFe-protein of nitrogenase is arranged as a $\alpha_2\beta_2$ tetramer and the Fe-protein section is a α_2 dimer. All

diazotrophs contain the molybdenum nitrogenase enzyme, but there are also vanadium and iron alternatives of this enzyme identified in the obligate, free-living aerobes *Azotobacter vinelandii* and *Azotobacter chroococcum* [8]. From the locations of the cofactors it is suggested that the electron transfer occurs in the order [4Fe-4S] in the Fe-protein to the P-cluster [8Fe8/7S] (some structures have 7 sulphurs and some have 8 sulphurs [9, 10]) in the MoFe-protein, and then to the (7Fe9S[Mo/V/Fe]) cofactor itself. This then donates electrons to the substrate dinitrogen [6]. Two moles of ammonia are produced for each mole of nitrogen gas consumed. Blue-green algae, free-living bacteria such as the aerobe *Azotobacter* and symbiotic bacteria such as *Rhizobium*, that can form root nodules with many leguminous plants such as peas and beans, fix nitrogen [11-13]. Nitrogen fixation allows bacteria to produce nitrogenous compounds that can be used in the synthesis of structural components such as amino and nucleic acids.

1.1.2: Nitrification

As well as assimilation into organic matter, the ammonium can also be used in nitrification [14]. Through nitrification, ammonium is converted via hydroxylamine into nitrites and then nitrates. Nitrification involves the oxidation of ammonium to nitrite by soil bacteria such as *Nitrosomonas.* These are known as nitrosifying bacteria. Bacteria such as *Nitrobacter* then consequentially convert nitrite to nitrates [14]. These are known as nitrifying bacteria. The reaction schemes for these two bacterial types are shown in Equations 2 and 3.

Nitrosifying bacteria: $NH_3 + O_2 \rightarrow NO_2^- + 3H^+ + 2e^-$ (2)

Nitrifying bacteria: $NO_2^- + H_2O \rightarrow NO_3^- + 2H^+ + 2e^-$ (3)

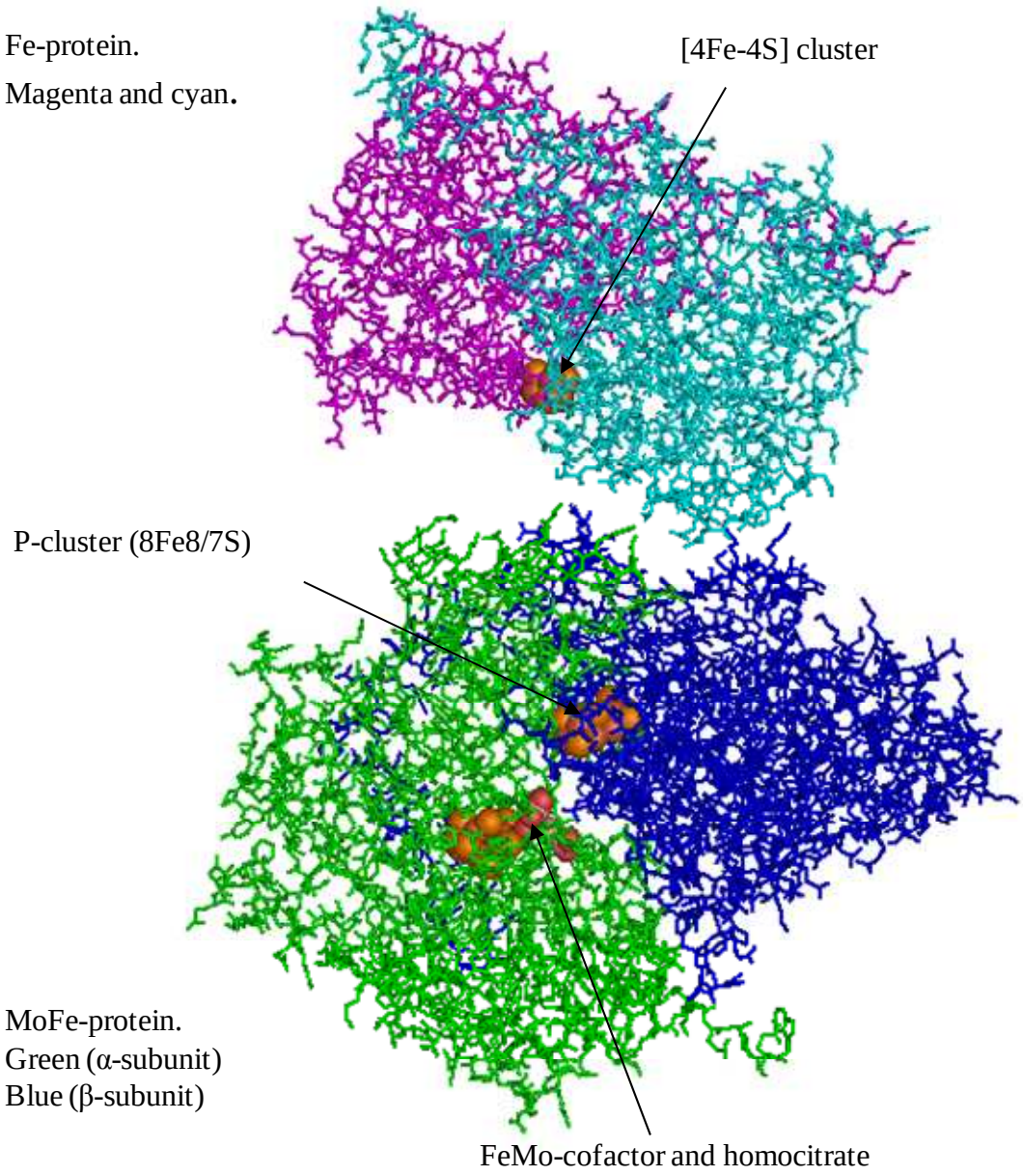

Figure 1.02: The subunit composition and structure of the nitrogenase complex from *A. vinelandii* showing the separate subunits of the Fe-protein constituent (magenta and cyan) and the MoFe-protein constituent (green and blue for α and β subunits respectively). Amino acids are represented by line representations and non-protein groups by spheres. The cofactors are shown in more detail in Figure 1.03. Figure was produced using Pymol. Source: 1M1Y.pdb [9].

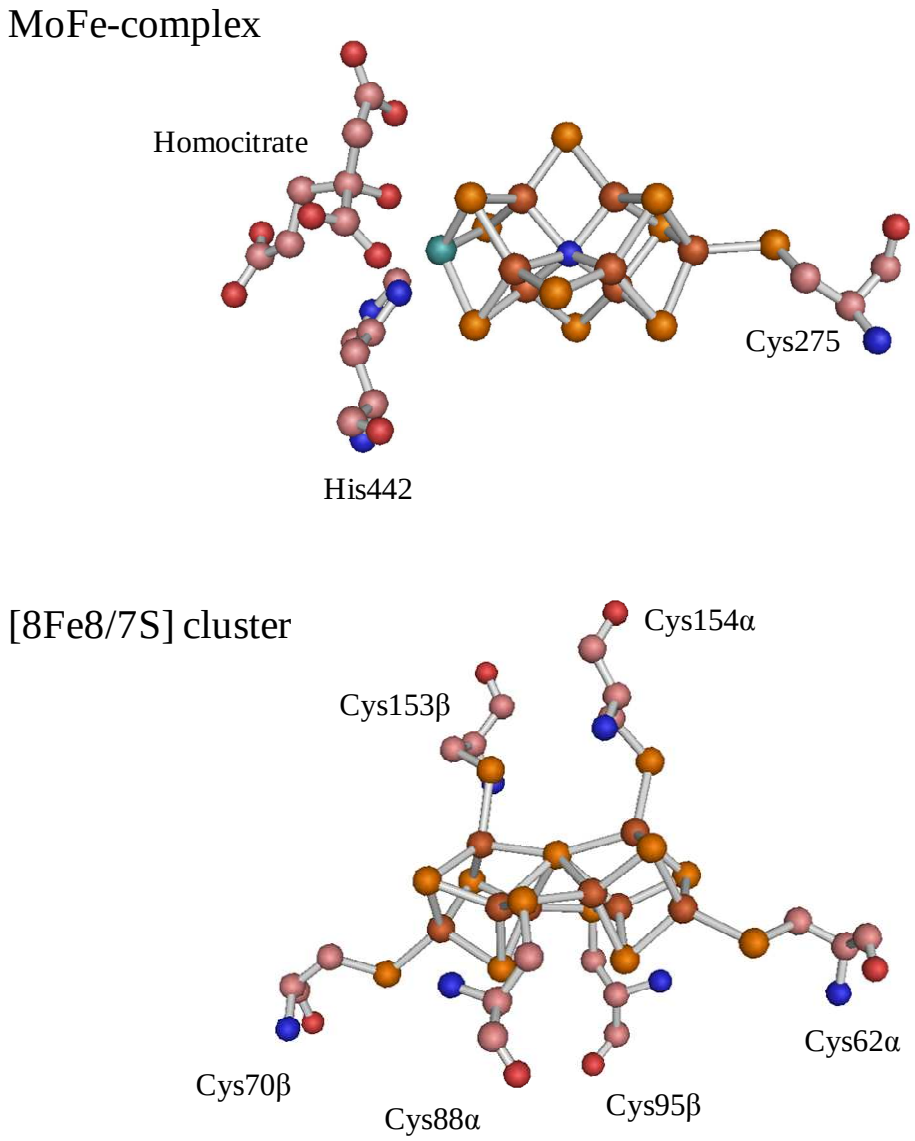

Figure 1.03: Ball and stick models of the MoFe-cofactor and P-cluster with associated ligands. α and β denoted on the cysteines for the P-cluster indicate subunit origins of the cysteines. Colour key is as follows: pink – carbon, red – oxygen, blue – nitrogen (central atom in MoFe complex is predicted), orange – sulphur, brown – iron and cyan – molybdenum. Figure was produced using Pymol. Source: 1M1N.pdb [10].

The two bacterial types are usually found in mixed interdependent communities called consortia. The accumulation of nitrite has an inhibitory effect on *Nitrosomonas*, which therefore relies on species such as *Nitrobacter* to convert any excess nitrate. Conversely, *Nitrobacter* depends on *Nitrosomonas* to generate nitrite that it can utilise. These bacteria derive energy from the oxidation of ammonium and nitrite; they use CO_2 as a carbon source for organic compound synthesis and are therefore chemoautotrophic [14].

Nitrification (see Figure 1.01) firstly involves the oxidation of ammonium to hydroxylamine through the enzyme ammonium mono-oxygenase (AMO). No crystal structure has been resolved as yet for this enzyme. *Nitrosomas europaea* also possesses a membrane bound ammonium monooxygenase. Both are thought to contribute to the conservation of energy [15-17]. The next enzymatic step is the oxidation of hydroxylamine to nitrite by the enzyme hydroxylamine oxidoreductase (HAO) (see Figure 1.04). In *N. europaea* this is a periplasmic, water-soluble trimer [18]. Each monomer has a total of eight covalently attached hemes. Seven of these are bis-histidine coordinated *c* hemes, while the eighth is heme P460 (Figure 1.05). The iron of heme P460 is pentacoordinated and is the substrate binding site. Residues associated with this P460 heme include a unique, covalently bound tyrosine from an adjacent monomer, and an axial histidine ligand. HAO performs the two electron oxidation of hydroxylamine. The *c* hemes allow multiple routes for transfer of electrons which results in the reduction of cytochrome c_{554} [18]. Finally the conversion of nitrite to nitrate is catalysed by nitrite oxidoreductase. There is no definitive crystal structure of this enzyme, but work on *Nitrobacter* organisms has revealed that these membrane-bound proteins contain molybdenum and iron-sulphur centres [19, 20].

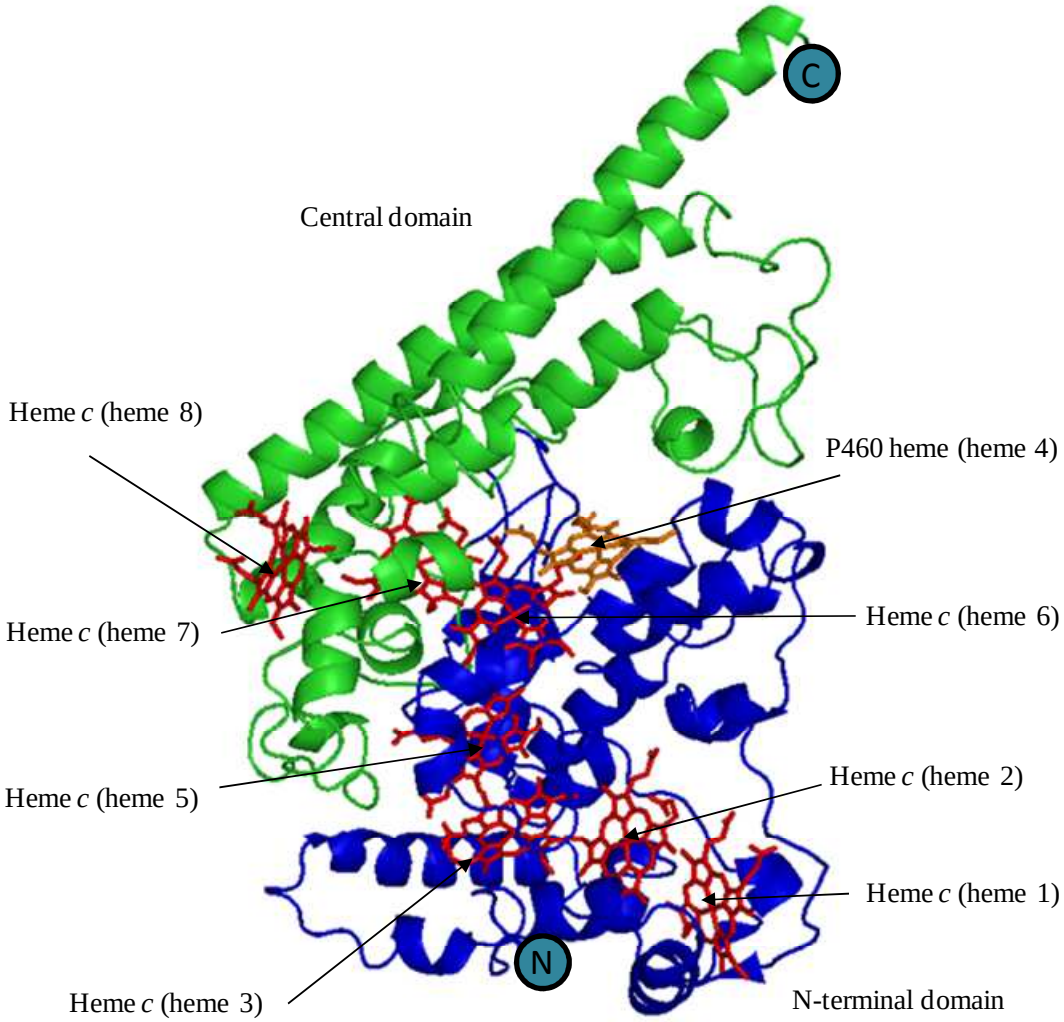

Figure 1.04: A subunit of hydroxylamine oxidoreductase (HAO) from *N. europaea* showing the N-terminal and central domain, in blue and green respectively, as a cartoon representation. Bis-histidine coordinated hemes are shown as red sticks and the P460 heme in orange sticks. Lettered cyan circles denote C and N termini. Figure was produced using Pymol. Source: 1FGJ.pdb [18].

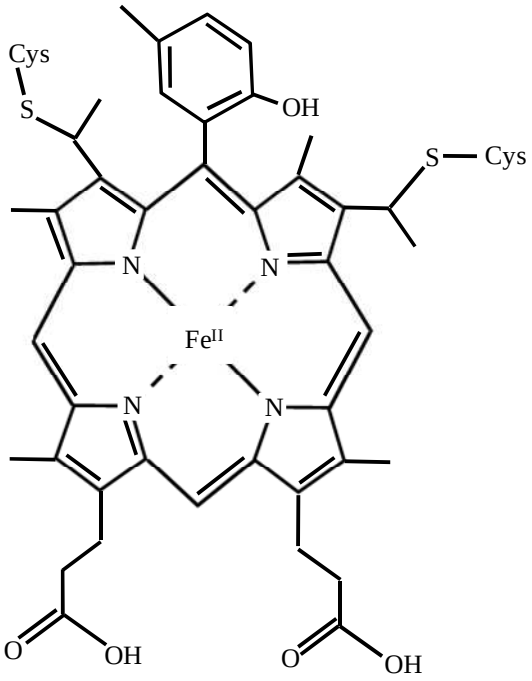

Figure 1.05: Structure of heme P460 showing the covalently bound tyrosine residue.

Nitrification has implications for agriculture and human health. Positively charged ammonium ions are not easily washed out of soils by rainfall. The ammonium readily adsorbs to negatively charged organic matter and clay colloids. Nitrites and nitrates however have a negative charge and bind less effectively to soil components. These are washed from the soil in a process called leaching. The consequences of these nitrites and nitrates leaching are poor soil fertility and accumulation in water sources such as rivers, lakes and groundwater. This can contribute to environmental problems such as eutrophication [21, 22] in which aquatic and marine ecosystems become anoxic or hypoxic, more acidic in nature and overwhelmed by large scale growth of primary producers such as algae. Human health problems can also be associated with eutrophication [22] and inorganic nitrogen compounds. Examples include ‘blue baby syndrome’ and the creation of carcinogenic nitrosamines in the gut which can lead to stomach, bowel and colon cancers [23-26]. ‘Blue baby syndrome’, also known as infant methemoglobinemia, is

a condition caused by nitrites binding to oxyhaemoglobin. This causes the formation of methaemoglobin which does not have the ability to bind oxygen. If methaemoglobin is present in high enough concentrations the infant shows symptoms such as blue colouration of the mucous membranes and lethargy or irritability [23, 24]. It has been shown that high risk groups include infants who ingest well-water or fresh vegetables with high nitrate concentrations [27]. Nitrosamines, which have also been linked to processed foods (such as cured and smoked meats) and tobacco use [28, 29], have been shown in rats to cause specific cancers, dependent on the form of nitrosamine [30]. Certain nitrosamines have the ability to be converted to metabolites that can induce mutagenesis through alkylation of DNA [31]. There is controversy over these two human health issues and the nitrate levels in drinking water, with some scientists calling for nitrate levels to be raised due to health benefits such as cardiovascular wellbeing and defence against infection [32].

1.1.3: ANAMMOX (Anaerobic Ammonium Oxidation)

Many organisms live in, or temporarily endure, anaerobic conditions and therefore cannot gain energy through processes such as nitrification. These organisms can use nitrate as a terminal electron acceptor in the oxidation of organic molecules to obtain energy. Nitrite lies at an important junction in the nitrogen cycle (Figure 1.01) and can be reduced via three different pathways [33]. The first is the ANAMMOX or anaerobic ammonium oxidation pathway [34]. This is the reaction of ammonium and nitrite that creates nitrogen gas as a product as shown in Equation 4.

$$NH_4^+ + NO_2^- \rightarrow N_2 + 2H_2O. \quad (4)$$

An example of a bacterial phylum that performs the ANAMMOX process is the planctomycetes [35]. These ANAMMOX organisms have an important function as a sink for fixed nitrogen in the oceans. They can contribute up to 50 % of the nitrogen gas produced in an ocean. ANAMMOX may offer a route to improvement of nitrogen removal in wastewater treatment, which conventionally would have been removed by nitrification / denitrification methods [36]. Elucidation of the genome of the ANAMMOX bacterium *Kuenenia stuttgartiensis* [37] has initiated work on identifying the proteins in this pathway and the chemical stages that the enzymes undertake to convert ammonium to dinitrogen [38, 39].

1.1.4: Nitrite Ammonification (Respiratory & Assimilatory)

The second pathway by which nitrite can be reduced is nitrite ammonification. This involves the reduction of nitrite to ammonium with no release of intermediate products, as shown in Equation 5 below.

$$NO_2^- + 6e^- + 8H^+ \rightarrow NH_4^+ + 2H_2O \quad (5)$$

Plants, fungi and certain bacteria that utilise nitrite and nitrate as a source of nitrogen possess a cytoplasmic enzyme that can catalyse this conversion. It contains a specialised siroheme co-factor (Figure 1.06) found only in this class of enzyme and a related class of sulphite reductases [40]. This type of enzyme is assimilatory in nature, producing ammonia which is incorporated into cell material. Other bacterial types possess the protein cytochrome *c* nitrite reductase (NrfA) which does the same nitrite-to-ammonium six electron reduction [33]. Unlike the siroheme protein NrfA serves a respiratory role. NrfA contains no specialised co-factors such as siroheme but is instead a homodimeric protein with ten *c* type hemes.

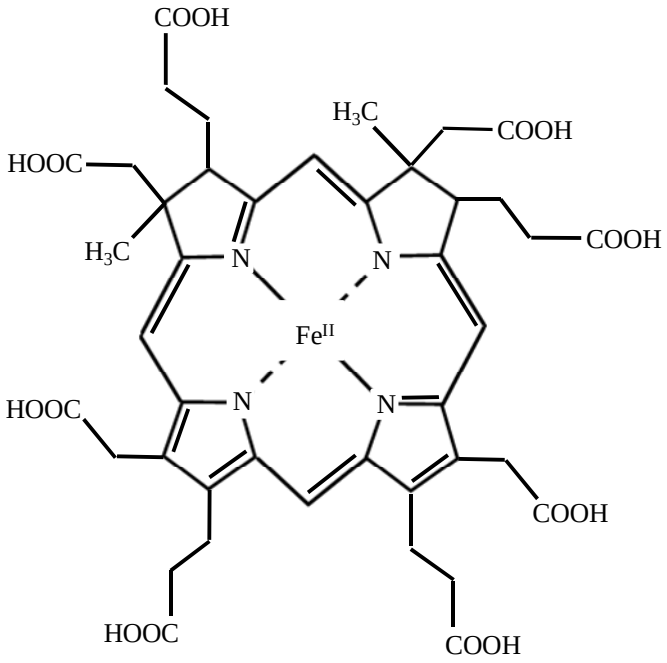

Figure 1.06: The structure of siroheme.

In each monomer, four *c* hemes are spatially arranged in a similar fashion to four of the hemes in hydroxylamine oxidoreductase (HAO) [18]. The fifth heme has the unusual coordination set of a distal lysine ligand and a proximal water/hydroxide ligand. Crystal structures of NrfA exist for several different organisms [41-43]. The homodimeric structure, the five *c* hemes per monomer, the unique active site coordination and an active site calcium that plays a key role in positioning active site residues are conserved in structures of the enzymes from *Sulfurospirillum deleyianum*, *Wolinella succinogenes* and *Escherichia coli* [41-43]. The structure of the NrfA from *E. coli* is shown in Figure 1.07. A structure is also available for the hexameric, octaheme nitrite reductase from *Thioalkalivibrio nitratireducens* (TvNIR) [44]. TvNIR in total contains 48 hemes. It reduces nitrite to ammonium and as with NrfA, there are detectable intermediates. TvNIR and NrfA subunits share the four CXXCH heme-binding motifs, the active site CXXCK motif and the catalytically important active site residues. There is however only ~20% sequence identity

between NrfA and TvNIR [44]. The nitrite ammonium pathway is seen as a short circuit to the stepwise reductions of the denitrification pathway that is discussed next.

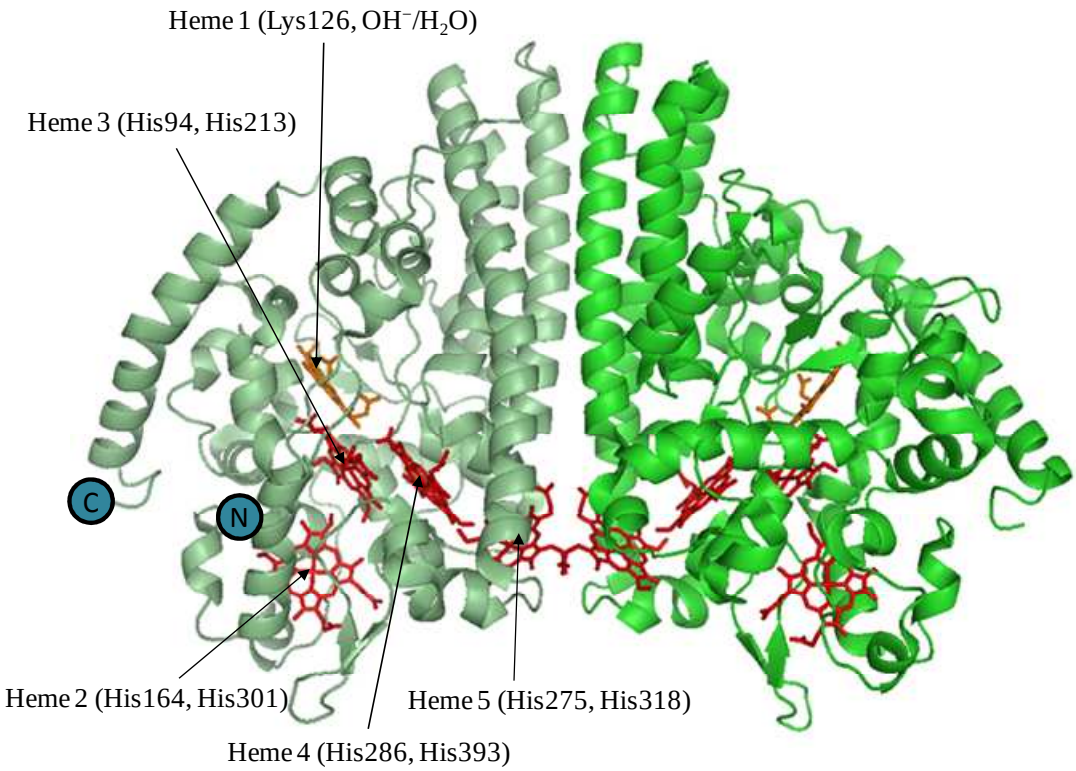

Figure 1.07: Structure of the *E. coli* NrfA dimer showing the separate monomers in different shades of green. Bis-histidine coordinated hemes are shown as red sticks and the lysine ligated heme as orange sticks. Amino acids in brackets are proximal and distal ligands respectively. Lettered cyan circles denote C and N termini for the selected monomer. Figure was produced using Pymol. Source: 1GU6.pdb [45].

1.1.5: Denitrification

The third pathway of nitrite reduction is via denitrification. Denitrification converts nitrates back into atmospheric dinitrogen gas through ordered, reductive enzymatic steps. Nitrate is reduced to nitrogen gas through the intermediates of nitrite, nitric oxide and nitrous oxide [45]. The majority of the denitrifying bacteria are heterotrophic, such as *Paracoccus denitrificans* and *Pseudomonas aeruginosa*.

However there are examples of autotrophic denitrifiers such as *Thiobacillus denitrificans* [46]. The four enzymes responsible for these conversions are nitrate reductase, nitrite reductase, nitric oxide reductase and nitrous oxide reductase. The overall denitrification process is shown in Equation 6.

$$2NO_3^- + 10e^- + 12H^+ \rightarrow N_2 + 6H_2O \quad (6)$$

Denitrification has far reaching environmental consequences as it is linked to the greenhouse effect. The excessive use of nitrogenous compounds in agriculture and the burning of fossil fuels has resulted in additional nitrogen entering the nitrogen cycle, resulting in many human health and environmental problems [47]. The proportions of nitrogen entering the cycle this way is comparable to levels through natural nitrogen fixation. Denitrification can result in the leakage of N_2O through intermediate release or incomplete denitrification. Nitrous oxide is a very efficient greenhouse gas [48, 49]. It is 300 times more potent then carbon dioxide and is the third most important contributor to global warming. Nitrous oxide is thought to be the most important ozone depleting emission [48, 49]. N_2O converts to NO and NO_2 (collectively termed NO_x) which are the gases that react with ozone as shown in Equations 7-9.

$$NO + O_3 \rightarrow NO_2 + O_2 \quad (7)$$

$$O + NO_2 \rightarrow NO + O_2 \quad (8)$$

$$\text{Overall: } O + O_3 \rightarrow 2O_2 \quad (9)$$

1.1.6: Denitrification – Nitrate Reductase

The first enzyme in the denitrification pathway, nitrate reductase, has two distinct types in bacteria. The first type is soluble and periplasmic (NAP) and the second is membrane-bound (NAR). The NAP proteins can be subdivided further in that certain species such as *Desulfovibrio desulfuricans* and *E. coli* produce a

monomeric NapA protein which contains a [4Fe-4S] cluster and a Mo-*bis*MGD cofactor [50, 51]. The [4Fe-4S] cluster is ligated to four cysteine residues and the molybdenum ion is ligated to a cysteine residue, four sulphur ligands from the two MGD molecules and an HO^{-}/H_2O ligand. The other type of NAP, found in bacteria such as *Rhodobacter sphaeroides*, also has an associated NapB as well as a NapA subunit [52]. NapB contains two *c* hemes that are bis-histidine ligated [52-54]. It has been suggested that electrons are donated to *D. desulfuricans* NapA via NapC, NapG or a unique tetraheme cytochrome *c* NapM, but there is no NapB homologue [55]. The NapAB of *R. sphaeroides* is shown in Figure 1.08. Crystal structures are available for the membrane-bound NAR from *E. coli* [56, 57]. It comprises two soluble subunits, NarGH and a hydrophobic cytoplasmic membrane anchor NarI. NarI contains two bis-histidine coordinated *b*-type hemes and receives electrons from the quinol pool via a Q binding site. The NarH subunit contains three [4Fe-4S] clusters and a [3Fe-4S] cluster. These clusters act as a pathway for electrons to reach the catalytic NarG subunit. NarG contains a [4Fe-4S] cluster which is coordinated by three cysteine ligands and one histidine ligand. Mutations of the [4Fe-4S] histidine ligand have significant effects on catalytic rate and on the incorporation of the cofactors during assembly [58]. NarG also contains a Mo-*bis*MGD cofactor, which has different coordination in different published structures [56, 57, 59]. It has been postulated that these coordination changes explain the observed pH dependence of the enzyme activity. In the structure of Jormakka *et al* [57], the aspartate 222 is hydrogen bonded to the conserved residue histidine 546. It has been postulated that the transition from active to inactive forms of the enzyme (low to high pH) is a result of the histidine 546 becoming protonated and dissociating from the aspartate 222. This structural change is then thought to bring about a rotation which results in the formation of a bidentate Mo ligand as seen in Bertero *et al* [56].

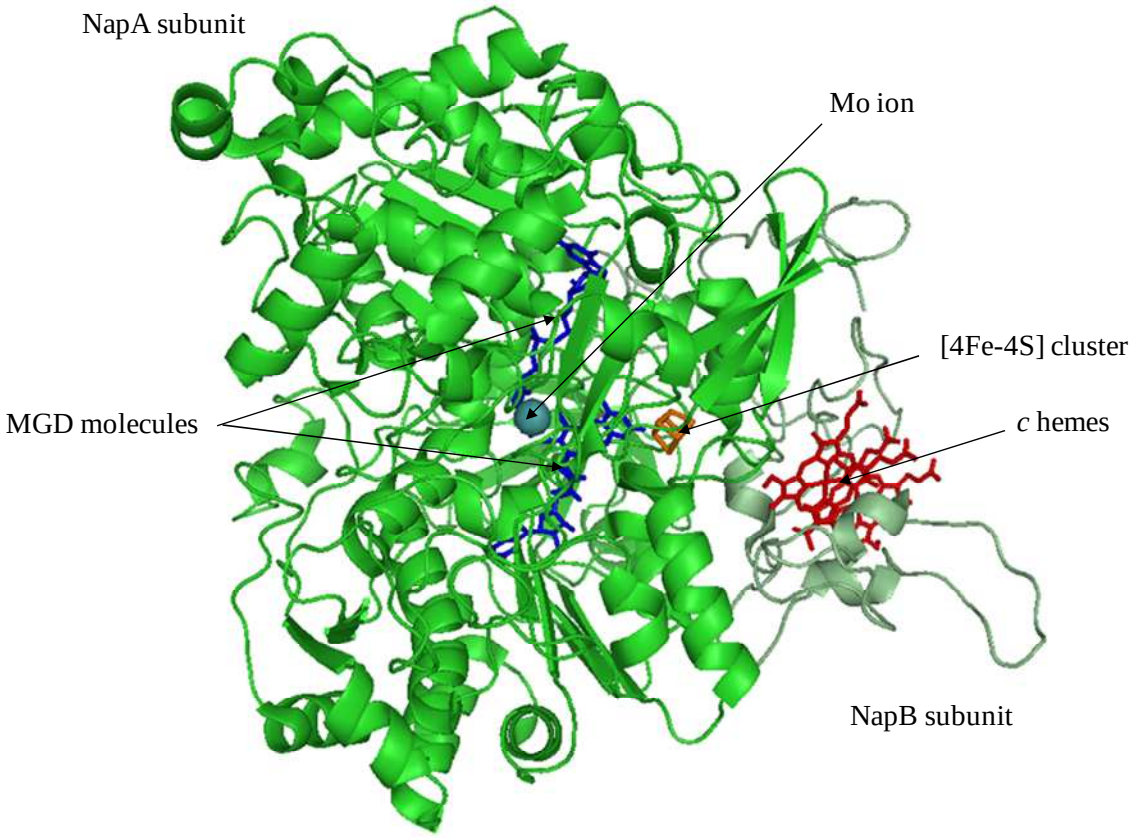

Figure 1.08: Structure of NapAB of *R. sphaeroides* showing the separate monomers in different shades of green as a cartoon representation. The NapA subunit is coloured bright green and the NapB subunit pale green. Bis-histidine coordinated *c* hemes are shown as red sticks, [4Fe-4S] cluster as orange sticks, MGD molecules as blue sticks and Mo ion as a cyan sphere. Model constructed using Pymol. Source: 1OGY.pdb [52].

The bidentate Mo ligand blocks the binding of the substrate nitrate, which renders the enzyme inactive. In the structure from Bertero *et al.* [56], the ligands are side-chain carboxylate group oxygen atoms from aspartate 222 and four sulphur atoms from the *bis*-MGD molecules. Alternatively, the structure of Jormakka *et al.* [57] shows coordination to four sulphur atoms from the *bis*-MGD molecules but only one

carboxylate group oxygen atom from aspartate 222. A sixth ligand is assigned to a water molecule. The NarGHI complex from *E. coli* is shown in Figure 1.09.

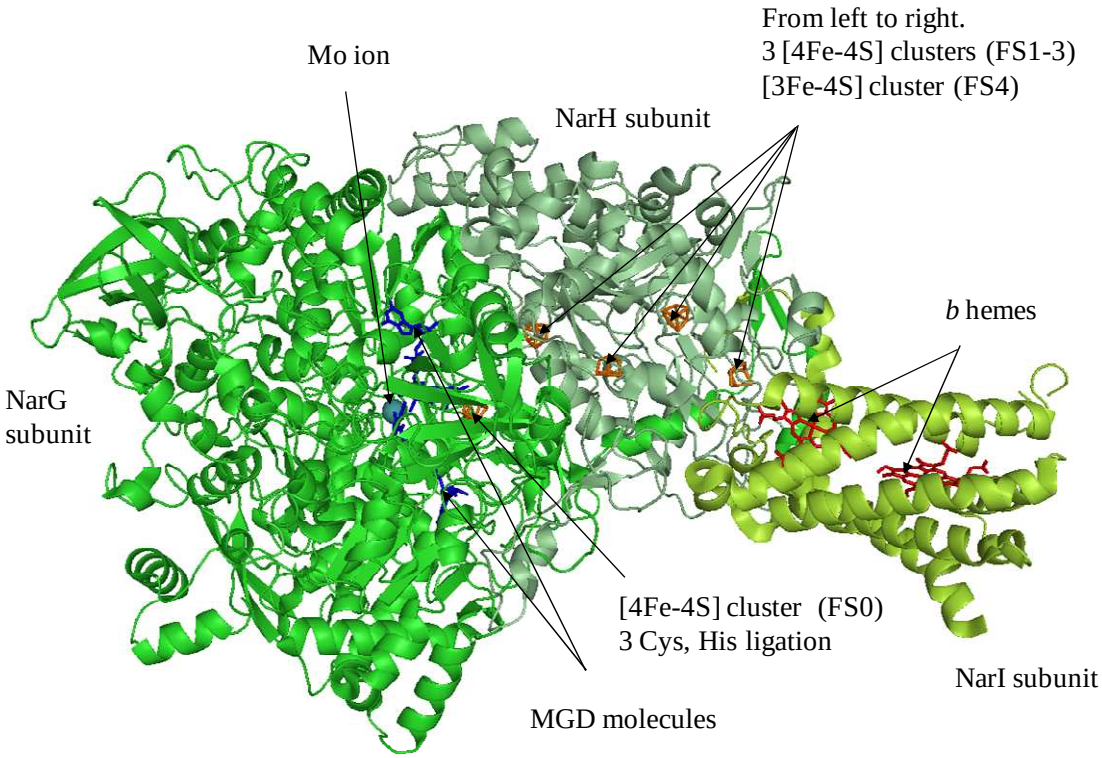

Figure 1.09: Structure of NarGHI of *E. coli* showing the separate monomers in different shades of green as a cartoon representation. The NarG subunit is coloured bright green, the NarH subunit pale green and the NarI subunit lime green. Bis-histidine coordinated *b* hemes are shown as red sticks, [4Fe-4S] and [3Fe-4S] clusters as orange sticks, MGD molecules as blue sticks and Mo ion as a cyan sphere. Model constructed using Pymol. Source: 1Q16.pdb [56].

1.1.7: Denitrification - Nitrite Reductase

Different species of denitrifying bacteria use equivalent metalloproteins in each reduction step, with the exception of the one electron conversion of nitrite to nitric oxide, the second step in the denitrification pathway. This particular step is catalysed by one of two distinct enzymes. One has a copper active site, the other is a heme enzyme containing a *c* heme and a unique d_1 heme [60]. Any particular denitrifying organism will contain one or the other. There is no known denitrifying organism that possesses both. One of the focuses of this work is the nitrite reductase containing *c* and d_1 hemes. This was originally reported to be a cytochrome oxidase on the basis of what is now considered a secondary activity. The cd_1s from *P. pantotrophus* and *P. aeruginosa* will be described in detail in the next section. The alternative nitrite reductases, the copper nitrite reductases or CuNIRs, are homotrimers. Each subunit contains a type I copper centre and a type II copper centre. Both type I and II centres contain a single copper ion. The ligands that coordinate the type I copper ion are two cysteines, a methionine and a histidine. It is thought that that the type I copper site plays a role in transferring electrons from donors such as pseudoazurin, azurin or cupredoxin. The type II copper site in the oxidised state is coordinated by three histidine residues and an HO^-/H_2O. The type II copper site is thought to be the substrate binding site. Structures for CuNIR from *Achromobacter cycloclastes* and *Alcaligenes xylosoxidans* have been published [61, 62]. The structure of a subunit of *A. xylosoxidans* CuNIR is shown in Figure 1.10. CuNIR catalysis results in formation of a copper-nitrosyl intermediate [63-65]. The catalytic residues Asp98 and His255 are directly involved in the mechanism, with Asp98 involved in hydrogen-bonding to substrate and product and His255 thought to be involved in either direct or indirect proton transfer [66, 67].

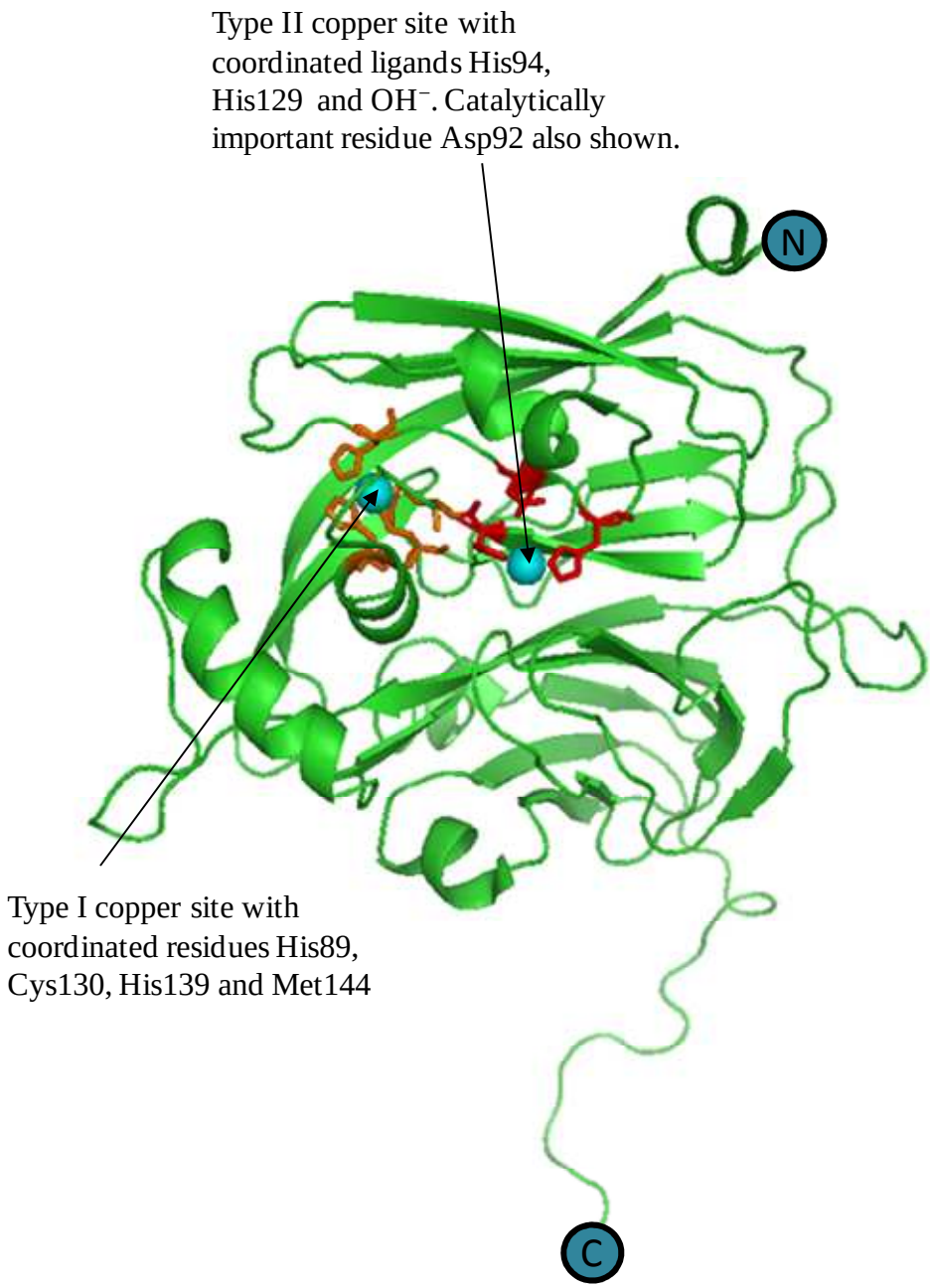

Figure 1.10: Structure of a subunit of *A. xylosoxidans* CuNIR showing the monomer as a cartoon representation. Copper ions are shown as cyan spheres. Coordinated ligands for the type I copper site are displayed as orange sticks. The type II copper ligands are displayed as red sticks. The ligands His249 and His300 coordinated to the type II copper ion are from an adjacent subunit and are therefore missing in this representation. Lettered cyan circles denote C and N termini for the monomer. Model constructed using Pymol. Source: 10E1.pdb [68].

1.1.8: Denitrification – Nitric Oxide Reductase

Following reduction of nitrite, the product nitric oxide is then reduced to nitrous oxide. This reaction is catalysed by nitric oxide reductase (NOR). A structure of NOR from *P. aeruginosa* has recently been published [69]. This is shown in Figure 1.11. These enzymes are members of the superfamily of heme-copper oxidases. Heme-copper oxidases have a heme and a copper in close proximity at their active site. The NOR enzymes however are characterised by the presence of a non-heme iron (Fe_B) in place of the Cu_B of HCOs [70, 71]. Both the NorB and catalytic subunit I of the HCOs have six conserved histidines which correspond to ligands for the dinuclear centre and the low-spin heme. NorB has a conserved glutamate residue as a further ligand to Fe_B. There is also a calcium ion associated with heme *b* and b_3 of NOR. A calcium ion appears to be at the same position in cbb_3 oxidase [72], and is thought to play a role in maintaining structure to allow intramolecular transfer of electrons. The NOR enzyme in bacteria is divided into the subclasses cNOR (cytochrome *c* dependent NOR), qNOR (quinone dependent NOR) and qCu_ANOR [73, 74]. The most complete biochemical, spectroscopic and structural data have been obtained for cNOR [69, 75, 76]. Bacterial cNOR is composed of two distinct subunits [69]. NorB, the larger of the two, contains the heme b_3-Fe_B dinuclear catalytic site. The heme b_3 and Fe_B have a bridging ligand which in a structure of *P. aeruginosa* NorBC is identified as an oxygen species (H_2O, HO^-, O^{2-}) [69]. This subunit also contains a *b* heme which is bis-histidine coordinated. The *b* heme serves to transfer electrons to the active site. The second subunit, NorC, has a single *c* type heme with axial ligation to a histidine and a methionine residue. This *c* heme accepts electrons from an external electron carrier, such as cytochrome c_{551} in *P. aeruginosa*. These are then donated to the *b* heme and subsequently the binuclear centre.

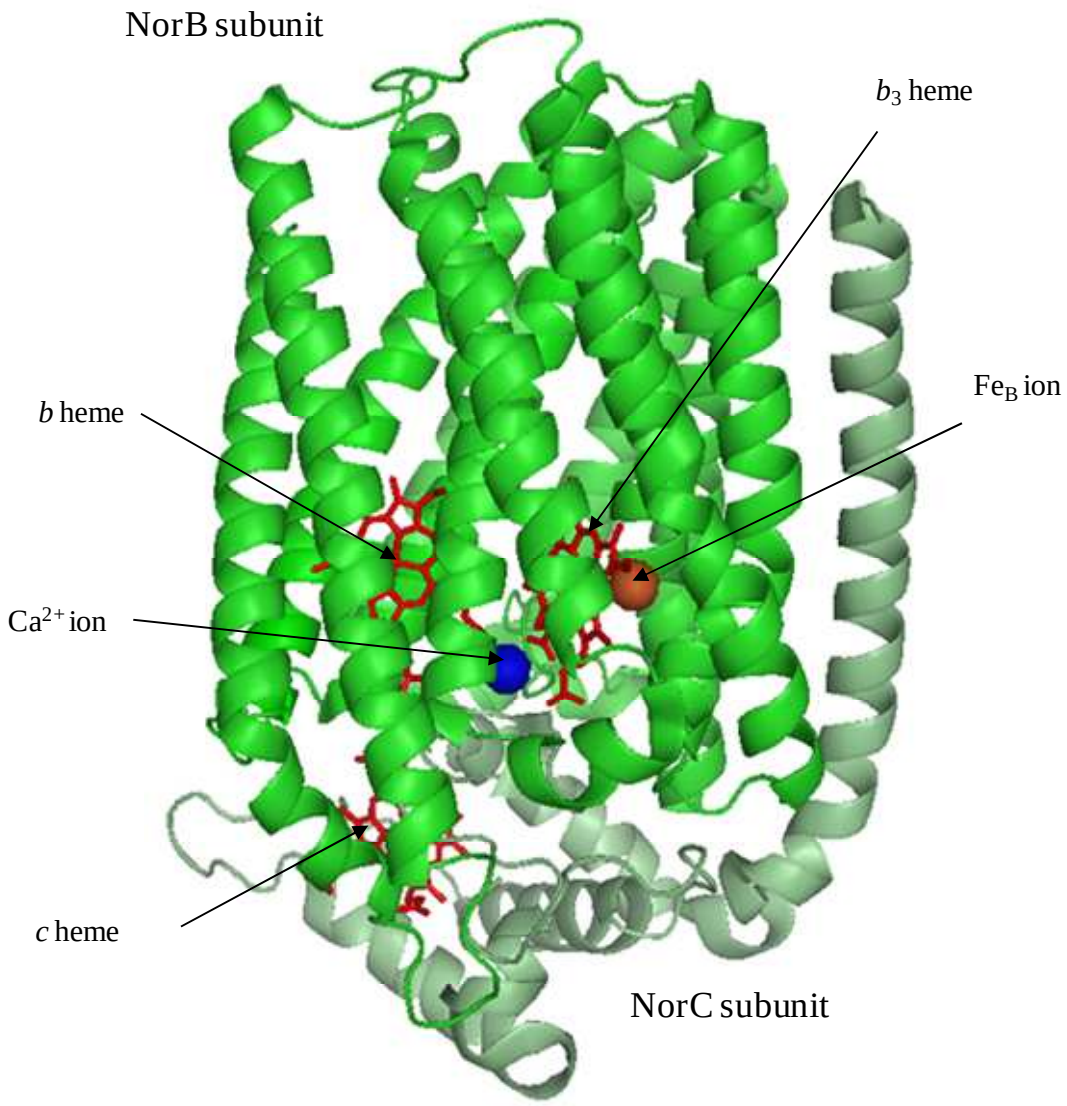

Figure 1.11: Structure of NorBC of *P. aeruginosa* showing the separate monomers in different shades of green as a cartoon representation. The NorB subunit is coloured bright green and the NorC subunit pale green. Hemes are shown as red sticks and labelled with the specific heme type. The Fe_B ion is represented as an orange sphere and the calcium ion as a blue sphere. Model constructed using Pymol. Source: 3O0R.pdb [69].

The electron transfer pathway of NOR from heme *c* to the heme b_3/Fe_B centre shows similarities to the Cu_A to heme *a* pathway in the cytochrome *c* oxidases [69, 77]. There are currently three postulated reaction mechanisms for NORs ability to reduce NO, with all three allowing two NO molecules to bind to the binuclear centre.

These are categorised as the *trans* mechanism where the NO molecules are bound to different metal centres to form an intermediate, the *cis* Fe_B mechanism where the second NO molecule reacts with the first NO molecule bound to the Fe_B centre to form an intermediate, and the *cis* heme b_3 mechanism which is mechanistically identical to the *cis* Fe_B mechanism but the intermediate is formed on heme b_3 [78-81].

1.1.9: Denitrification – Nitrous Oxide Reductase

The final step in denitrification is the conversion of nitrous oxide to dinitrogen by the enzyme nitrous oxide reductase (N_2OR). Structures of N_2OR have been solved for *Pseudomonas nautica*, *Paracoccus denitrificans*, *Achromobacter cycloclastes* and *Pseudomonas stutzeri* [82-85]. The structure of *P. denitrificans* N_2OR is shown in Figure 1.12. This enzyme exists as a homodimer. Each monomer contains two distinct copper sites. The first is the Cu_A site, a metal centre that can also be found in HCOs [86]. This is the site of electron entry, with electrons usually being supplied by single *c* heme cytochromes or cupredoxins. The Cu_A site is binuclear and is contained in a domain that has a cupredoxin fold. The coordinated residues for the two coppers Cu_1 and Cu_2 are two bridging cysteines, a histidine each and methionine for Cu_1 and tryptophan for Cu_2.

The Cu_Z site is the second site and is structurally unique [87]. The Cu_Z site is the centre for catalytic activity. This metal cluster is contained in a bladed propeller structure comprising seven β-sheets. The Cu_Z site is comprised of four copper ions coordinated by seven histidine residues, two OH^- molecules and an inorganic sulphide bridge (two sulphide bridges are present in the structure presented recently by Pomowski *et al* [85]). The subunits lie in such a way that the Cu_A of one monomer receives electrons from the Cu_Z of the other monomer. The distance

between the CuA and CuZ of the different monomers is approximately 10 Å [88]. It has been suggested that the mechanism of nitrous oxide reduction by the Cu_Z site is through the binding of the substrate of one of the four coppers. This allows the other coppers to act as reservoirs for electrons to safeguard against the formation of inhibitory or dead-end products [82, 83, 89]. Through spectroscopic and kinetic analysis of the different forms of CuZ a reaction scheme has been proposed [87 and refs therein], but this has yet to be proven.

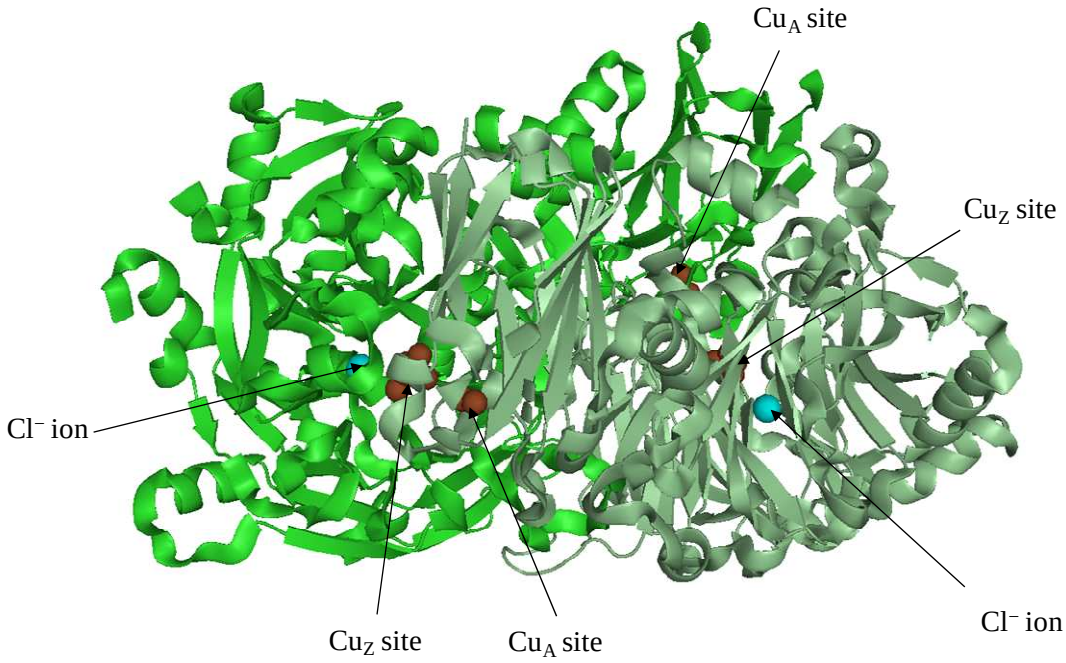

Figure 1.12: Structure of the N_2OR homodimer of *P. denitrificans* showing the separate monomers in different shades of green as a cartoon representation. Copper ions are shown as brown spheres and specific sites indicated by labels. Associated chloride ions are shown as cyan spheres. The small space of 10.75 Å between the Cu_A and Cu_Z sites of different monomers is clear and therefore shows that electron transfer takes place between Cu_A and Cu_Z sites of different monomers. Model constructed using Pymol. Source: 1FWX.pdb [83].

1.1.10: The *cd*$_1$ Nitrite Reductases

The *cd*$_1$ nitrite reductases catalyse the reduction of nitrite to nitric oxide in the denitrification pathway. The first *cd*$_1$ purified was from the organism *P. aeruginosa* [90]. It was shown to be a soluble, periplasmic enzyme. The first activity identified for this *cd*$_1$ was cytochrome oxidase activity, the reduction of dioxygen to water using 4 electrons as shown in Equation 10 [90]. This activity was inhibited by both CO and cyanide [91].

$$O_2 + 4H^+ + 4e^- \rightarrow H_2O \quad (10)$$

The one electron reduction of nitrite to nitric oxide was subsequently recognised as the physiologically relevant activity of *cd*$_1$ (Equation 11). This enzymatic activity is inhibited by cyanide but there is a report that CO has no inhibitory effect [92].

$$NO_2^- + 2H^+ + e^- \rightarrow NO + H_2O \quad (11)$$

A third, non-physiological activity has also been demonstrated: the two-electron reduction of hydroxylamine to ammonia as shown in Equation 12 [93]. Cyanide and carbon monoxide are both effective inhibitors of this reaction.

$$NH_2OH + 2H^+ + 2e^- \rightarrow NH_3 + H_2O \quad (12)$$

Other activities claimed for *cd*$_1$ are the oxidation of carbon monoxide to carbon dioxide and NO reduction to N_2O [94, 95]. However the accepted view is that the nitrite reductase activity is the only physiologically relevant function. This is based on kinetic and equilibrium data [96]. More evidence is provided through the inability of *nirS* inactivated strains of *P. aeruginosa* to proliferate on *N*-oxides [97].

The product of the nitrite reductase activity, nitric oxide, has been found to have a serious impact on the environment. NO is highly reactive, and along with other nitrogen oxides it participates in ozone-depleting gas. N_2O is currently the dominant ozone-depleting emission [49]. Inefficient or incomplete denitrification can

result in the release of NO_x species. Therefore it is important to understand and characterise enzymes such as the nitrite reductases. As discussed, the bacterial nitrite reductases are divided into two distinct types; the CuNIRs and the cd_1 nitrite reductases. cd_1, specifically from the organisms *P. aeruginosa* and *P. pantotrophus*, is a major focus of this work. A general discussion of cd_1 proteins will be presented, using *P. aeruginosa* as an example. This enzyme is very similar to cd_1s from several other species. The cd_1 from *P. pantotrophus* cd_1 will then be described, highlighting the differences between this enzyme and other cd_1s.

1.1.11: *Pseudomonas aeruginosa* cd_1 Nitrite Reductase

The primary structure of the *P. aeruginosa* mature enzyme was determined in 1989 [98]. Comparison between the mature protein sequence and that deduced from DNA translation of *nir*S shows that the enzyme is synthesised with a leader peptide to allow periplasmic export. The sequences of cd_1 nitrite reductases in general show that the d_1 heme containing C-terminal of the monomer sequence is much more conserved among cd_1 proteins than the *c* heme containing N-terminal. In particular, the N-terminus has a low degree of similarity between differing cd_1 proteins [60]. This is highlighted in Figure 1.13, which shows a sequence comparison between the cd_1 nitrite reductases of seven bacterial species [98-104]. The sequence conservation and sequence identity among cd_1 nitrite reductases in the genera featured in Figure 1.13 is at least 66% and 52% respectively.

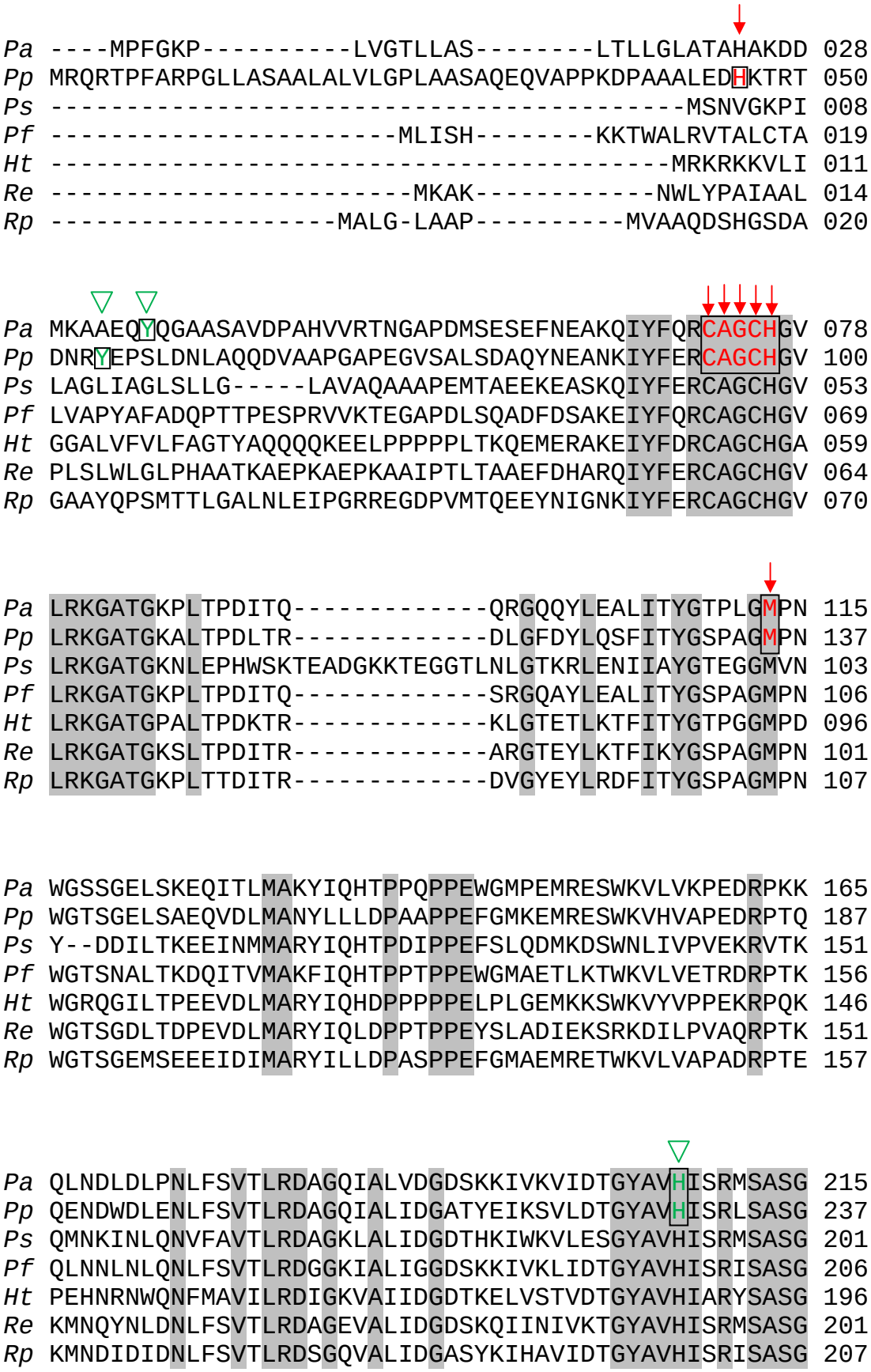
Pa ----MPFGKP----------LVGTLLAS--------LTLLGLATAHAKDD 028
Pp MRQRTPFARPGLLASAALALVLGPLAASAQEQVAPPKDPAAALEDHKTRT 050
Ps --MSNVGKPI 008
Pf ----------------------MLISH--------KKTWALRVTALCTA 019
Ht --MRKRKKVLI 011
Re ----------------------MKAK------------NWLYPAIAAL 014
Rp ------------------MALG-LAAP----------MVAAQDSHGSDA 020
Pa MKAAEQYQGAASAVDPAHVVRTNGAPDMSESEFNEAKQIYFQRCAGCHGV 078
Pp DNRYEPSLDNLAQQDVAAPGAPEGVSALSDAQYNEANKIYFERCAGCHGV 100
Ps LAGLIAGLSLLG-----LAVAQAAAPEMTAEEKEASKQIYFERCAGCHGV 053
Pf LVAPYAFADQPTTPESPRVVKTEGAPDLSQADFDSAKEIYFQRCAGCHGV 069
Ht GGALVFVLFAGTYAQQQQKEELPPPPPLTKQEMERAKEIYFDRCAGCHGA 059
Re PLSLWLGLPHAATKAEPKAEPKAAIPTLTAAEFDHARQIYFERCAGCHGV 064
Rp GAAYQPSMTTLGALNLEIPGRREGDPVMTQEEYNIGNKIYFERCAGCHGV 070
Pa LRKGATGKPLTPDITQ------------QRGQQYLEALITYGTPLGMPN 115
Pp LRKGATGKALTPDLTR------------DLGFDYLQSFITYGSPAGMPN 137
Ps LRKGATGKNLEPHWSKTEADGKKTEGGTLNLGTKRLENIIAYGTEGGMVN 103
Pf LRKGATGKPLTPDITQ------------SRGQAYLEALITYGSPAGMPN 106
Ht LRKGATGPALTPDKTR------------KLGTETLKTFITYGTPGGMPD 096
Re LRKGATGKSLTPDITR------------ARGTEYLKTFIKYGSPAGMPN 101
Rp LRKGATGKPLTTDITR------------DVGYEYLRDFITYGSPAGMPN 107
Pa WGSSGELSKEQITLMAKYIQHTPPQPPEWGMPEMRESWKVLVKPEDRPKK 165
Pp WGTSGELSAEQVDLMANYLLLDPAAPPEFGMKEMRESWKVHVAPEDRPTQ 187
Ps Y--DDILTKEEINMMARYIQHTPDIPPEFSLQDMKDSWNLIVPVEKRVTK 151
Pf WGTSNALTKDQITVMAKFIQHTPPTPPEWGMAETLKTWKVLVETRDRPTK 156
Ht WGRQGILTPEEVDLMARYIQHDPPPPPELPLGEMKKSWKVYVPPEKRPQK 146
Re WGTSGDLTDPEVDLMARYIQLDPPTPPEYSLADIEKSRKDILPVAQRPTK 151
Rp WGTSGEMSEEEIDIMARYILLDPASPPEFGMAEMRETWKVLVAPADRPTE 157
Pa QLNDLDLPNLFSVTLRDAGQIALVDGDSKKIVKVIDTGYAVHISRMSASG 215
Pp QENDWDLENLFSVTLRDAGQIALIDGATYEIKSVLDTGYAVHISRLSASG 237
Ps QMNKINLQNVFAVTLRDAGKLALIDGDTHKIWKVLESGYAVHISRMSASG 201
Pf QLNNLNLQNLFSVTLRDGGKIALIGGDSKKIVKLIDTGYAVHISRISASG 206
Ht PEHNRNWQNFMAVILRDIGKVAIIDGDTKELVSTVDTGYAVHIARYSASG 196
Re KMNQYNLDNLFSVTLRDAGEVALIDGDSKQIINIVKTGYAVHISRMSASG 201
Rp KMNDIDIDNLFSVTLRDSGQVALIDGASYKIHAVIDTGYAVHISRISASG 207

```
Pa RYLLVIGRDARIDMIDLWAKEPTKVAEIKIGIEARSVESSKFKG----YE 261
Pp RYLFVIGRDGKVNMIDLWMKEPTTVAEIKIGSEARSIETSKMEG----WE 283
Ps RYVYTTGRDGLTTIIDLWPEEPMTVATVRFGSDMRSVDVSKFEG----YE 247
Pf RYLLVIGRDAKIDMIDLWPKEPTKVAEIKVGIEARSVETSKFKG----YE 252
Ht RYLYTIGRDGKVVLIDLWMKKPDKVAEVKTCYDGRSLDTSKYKGPKGDFL 246
Re RYLYVIGRDARLDLIDLWLPKPDIVAEVKVGMEARSVETSKYKG----YE 247
Rp RYLFVIGRDALVNMIDLWMETPATVAQIKVGSEARSIETSKFKG----FE 253

Pa DRYTIAGAYWPPQFAIMDGETLEPKQIVSTRGMTVDTQTYHPEPRVAAII 311
Pp DKYAIAGAYWPPQYVIMDGETLEPKKIQSTRGMTYDEQEYHPEPRVAAIL 333
Ps DKYLIGGTYWPPQYSIVDGLTLEPIKVVSTRGQTVDG-EYHPEPRVASIV 296
Pf DKYTVAGSYWPPQFTIMDGETLEPKQIVSTRGMTVDTQQYHPEPRVAAII 302
Ht DKLAIIGCYWPPSFVIVDGQTLEPLKIVATSAYTYDTNEFLREARVASMV 296
Re DKYAVAGSYWPPQYVIMEGDTLKPLKVVSTRGMTVDN-EYHPEPRVAAIV 296
Rp DMYAIAGSYWPPQYVIMDGDTLEPLKIKSTRGMVYDDQSYHPEPRVASIV 303

                                                ▽
Pa ASHEHPEFIVNVKETGKVLLVNYKDIDNLTVTSIGAAPFLHDGGWDSSHR 361
Pp ASHYRPEFIVNVKETGKILLVDYTDLDNLKTTEISAERFLHDGGLDGSHR 383
Ps ASHIKPEWVVNVKETGQIILVDYTDLKNLKTTTIESAKFLHDGGWDYSKR 346
Pf ASHEWPEFIVNVKETGKVMLVNYQDIKNLTITSIDAAPFLHDGGWDSSHR 352
Ht ASHYDPEWVVNVKEAGQIWLVDYSNIHAPKITMIDAERFLHDGGWDASKR 346
Re ASHFHPEFVINAKETGKILMVNYSDLSNLKTTTIDSAKFLHDGGFDATGR 346
Rp ASHFNPEFIVNVKETGKILMIDYSDIKNLKVTEIEAERFLHDGGFDSSKR 353

                                          ▽
Pa YFMTAANNSNKVAVIDSKDRRLSALVDVG-KTPHPGRGANFVHPKYGPVW 410
Pp YFITAANARNKLVVIDTKEGKLVAIEDTGGQTPHPGRGANFVHPTFGPVW 433
Ps YFMVAANASNKVAAVDTKTGKLAALIDTA-KIPHPGRGANFVHPQFGPVW 395
Pf YFMTAANNSNKVAVIDSKERKLTALVDVG-KTPHPGRGANFNHPLYGPVW 401
Ht YFLVAANFRDTISVVDTKEKKLVKNIKVG-TRPHPGRGANIDHPKYGPLW 395
Re YFLVAANASDKIAVVDTKEDKLAALIDVG-KTPHPGRGANFMHPKLGPVW 395
Rp YFLVAANARGKVAVVDTKDSTLTALVETGGQTPHPGRGANLMHPTYGPVW 403

Pa STSHLGDGSISLIGTDPK-----NHPQYAWKKVAELQGQG--GGSLFIKT 453
Pp ATSHMGDDSVALIGTDPE-----GHPDNAWKILDSFPALG--GGSLFIKT 476
Ps STGHLGDDVVSLISTPSEESKYAKYKEHNWKVVQELKMPG--AGNLFVKT 443
Pf ATSHLGDAGVSLIGTDPV-----KHPQYAWKQVASLQGQG--GGSLFIKT 444
Ht CTGHLGDNTIRCIGTDPV-----KHPQYAWKVVVKMEMPGEGGGNLFIKT 440
Re ATSHLGDETISLIGTDPA-----GHPAQAWKVVQTIKGQG--GGSLFIKT 438
Rp ATSHLGDETVALIGTDPE-----GHPDNAWKVVQTLYAQG--GGSLFVKS 446
```

```
Pa HPKSSHLYVDTTFNPDARISQSVAVFDLKNLDAK-----YQVLPIAEWAD 498
Pp HPNSQYLYVDATLNPEAEISGSVAVFDIKAMTGDGSDPEFKTLPIAEWAG 526
Ps HPKSKHFWADAPMNPEREVAESVYVFDMNDLSKAP-----IQLNVAKDSG 488
Pf HPASRHLYVDTTLSPDAKLSQSVAVFNIDKLDAG-----YTVLPIAEYAG 489
Ht HPKSPHLWADRALNNDPKLQRSLFVFDKNTFQIK------KVIEIPP--- 481
Re HPKSSNLWVDTPLNPDAKLNQSVAVFDTRNLEAG-----YKVLPIADWAG 483
Rp HPTSEHLYVDAPLNPDAEISGSVAVFKLGDLAQE--EPEYTVLPIVEWAE 494

Pa LG--EGAKRVVQPEYNKRGDEVWFSVWNGKND--SSALVVVDDKTLKLKA 544
Pp IT--EGQPRVVQGEFNKDGTEVWFSVWNGKDQ--ESALVVVDDKTLELKH 572
Ps LPESKAIRRAVQPEYNKAGDEVWISLWGGKTD--QSAIVIYDDKTLKLKR 536
Pf IK--KGALRVVQPEYNKAGDEVWFSVWSGQED--ESALVVIDDKTLKVKN 535
Ht ----EFQGRAVHLEYNKNGDEVWVAVWSKKNEPEKQAILVYDDKTLTLKK 527
Re LKG-AGARRVVQAEYNKAGDEVWFSVWGTKDG--ESALVVVDDKTRTLKT 530
Rp IG--EGQPRVVQGEFNQEGNEIWFSVWNAKDL--ESAIVVVDDKTLELKA 540

Pa VVKDPRLITPTGKFNVYNTQHDVY 568
Pp VIKDERLVTPTGKFNVYNTMTDTY 596
Ps VITDPAVVTPTGKFNVFNTMNDVY 560
Pf VIKDKRLITPTGKFNVYNTQHDIY 559
Ht AITGNWVATPTGHFNVYNTMKDIY 551
Re VIKDKRLITPTGKFNAYNTQHDVY 554
Rp VIKDPRLITPTGKFNVYNTRADVY 564
```

Figure 1.13: (This and previous pages) Multiple sequence alignment of cd_1 nitrite reductase proteins from seven genera of bacteria (accession numbers from top: P24474.1, P72181.2, P24040.1, AAG34381.1, BAE45629.1, CAJ97059.1, AAV97354.1). A grey highlight denotes the residue is conserved in all seven bacterial species. Residues involved in heme ligand coordination or hydrogen-bonding to heme ligands are boxed for *P. aeruginosa* and *P. pantotrophus*. Red arrows and letters indicate *c* heme residues. Green open triangles and letters indicate d_1 heme residues. Alignment constructed using ClustalW2 and Jalview [105, 106]. **Abbreviations:** *Pa – Pseudomonas aeruginosa, Pp – Paracoccus pantotrophus, Ps – Pseudomonas stutzeri, Pf – Pseudomonas fluorescens, Ht – Hydrogenobacter thermophilus, Re – Ralstonia eutropha, Rp – Ruegeria pomeroyi.*

From Figure 1.13 it can be observed that the C-terminal ends of the seven cd_1 types show a much higher degree of conservation compared to the N-terminal ends. Despite the lack of sequence similarity among the seven cd_1 types at the N-terminal ends the sequence of amino acids that constitute the *c* heme site, as well as the residues in close proximity in the sequence, have a high degree of conservation amongst the cd_1 proteins. This highly conserved sequence of 22 amino acids contains a CXXCH *c* heme binding site. In the cd_1 protein sequence comparison (Figure 1.13) the motif is conserved as CAGCH. These are the only two cysteine residues in the mature sequence of the *P. aeruginosa* subunit, which has over 500 amino acids [98]. These cysteine residues covalently bind to the heme *c* vinyl groups. The histidine residue in the motif is also important as one of the two axial ligands to the *c* heme iron. The other residue involved in heme *c* coordination in *P. aeruginosa* is methionine 88. Although methionine 88 is not in the highly conserved 22 amino acid sequence containing the CAGCH motif, it is also conserved in the sequences featured in Figure 1.13.

Residues that act as ligands for the d_1 heme or involved in hydrogen-bonding to OH^- have also been identified in *P. aeruginosa*. Histidine 182 is the axial ligand in the *P. aeruginosa* sequence associated with the d_1 heme [107]. A sequence of 15 amino acids including histidine 182 has a high degree of conservation amongst the bacterial species in Figure 1.13. Histidines 327 and 369 are also conserved in six of the seven species shown in Figure 1.13. They are hydrogen-bonded directly to the HO^- ligand in oxidised, *P. aeruginosa* cd_1 nitrite reductase [107]. These play an important role in catalysis, with histidine 369 being essential in affinity for nitrite, the physiological substrate [108, 109]. The consensus is these residues are involved in the dehydration and protonation of nitrite. Finally in the amino acid sequence of *P. aeruginosa* cd_1 is tyrosine 10. Tyrosine 10 hydrogen bonds to the OH^- ligand in

the d_1 heme pocket. This is specific to the *P. aeruginosa* enzyme. It is not involved in catalysis and does not influence NO orientation when the enzyme is in a reduced state [110, 111]. Figure 1.14 shows the positions of these key residues.

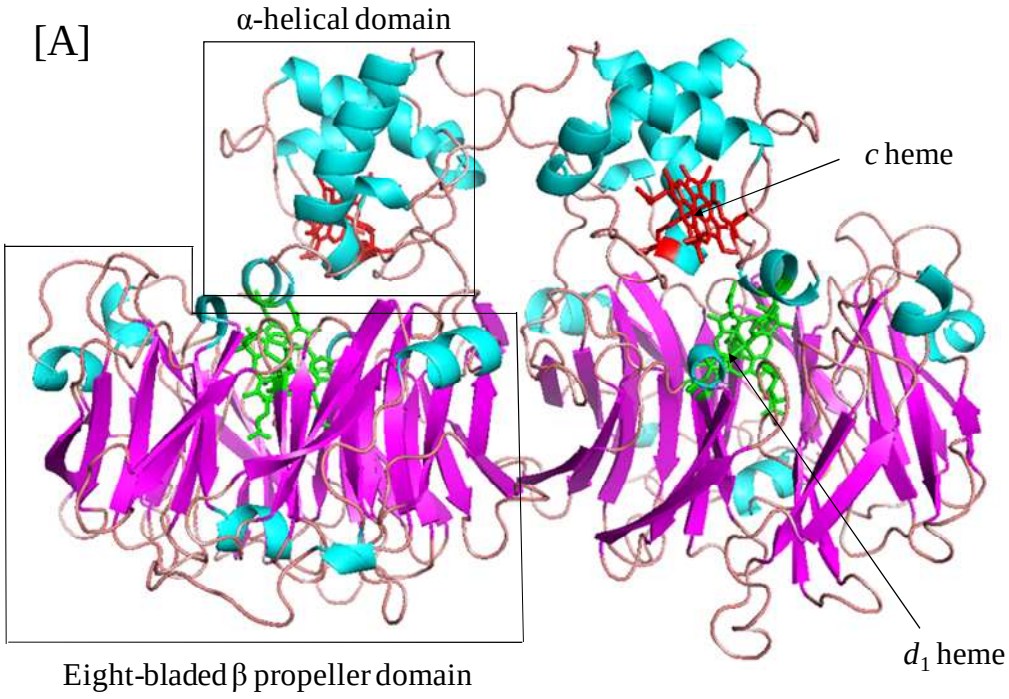

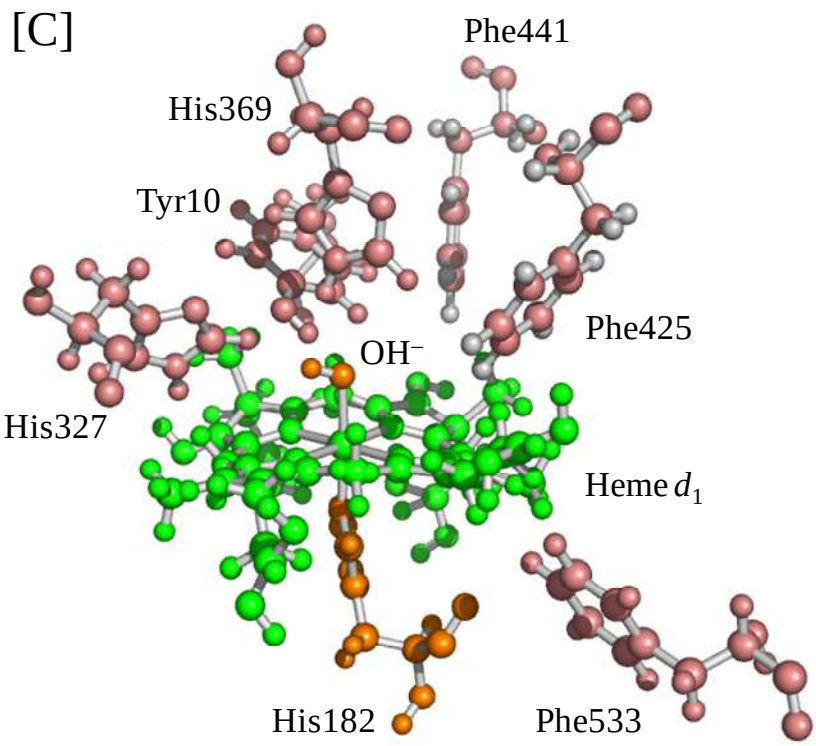

Figure 1.14: (This and previous page) Structures of oxidised *P. aeruginosa* cd_1 nitrite reductase and the *c* and d_1 hemes. [A] *P. aeruginosa* cd_1 homodimer in cartoon representation. α-helices are coloured cyan and β-sheets are coloured magenta. Domains are labelled for one of the subunits for clarity. *c* and d_1 hemes are also shown in stick representation and are coloured red and green respectively. [B] The *c* heme of *P. aeruginosa* cd_1 in ball and stick representation. The heme *c* is shown in red, the covalent cysteine linkages are shown in magenta, the heme iron ligands in orange and close surrounding amino acids in salmon. This conformation applies to oxidised and reduced enzyme. [C] The d_1 heme of oxidised *P. aeruginosa* cd_1 in ball and stick representation. The heme d_1 is shown in green, the heme iron ligands in orange and close surrounding amino acids in salmon (including tyrosine 10, histidine 327 and histidine 369 which hydrogen bond to the OH^- ligand). Figures constructed using Pymol. Source: 1NIR.pdb [107].

Crystal structures for both the oxidised form of *P. aeruginosa* cd_1 and the reduced NO-bound form (Figure 1.15) have been determined [107, 112]. The cd_1 enzyme is homodimeric and has a total M_r of 120000 Da. Each enzyme monomer is structured as two distinctive domains. The N-terminal section is composed of α-helices and the C-terminal section has a β-propeller arrangement as shown in Figure 1.14. In *P. aeruginosa* cd_1 the N-terminal end of each monomer extends into the d_1 site of its neighbour. The quaternary structure shows that non-covalent interactions between monomers that make up the dimer are exceptionally strong. The presence of 6 M urea or 3 M NaCl does not result in dissociation. Only prolonged succinylation or exposure to a pH greater than 11 will yield monomers [113, 114]. Hydrophobic interactions at the interface of the d_1 domain are the majority contributor to the stability of the dimer. This has been confirmed by proteolysis studies and structural analysis [99, 107].

Each subunit contains a *c* heme and a novel d_1 heme as shown in Figures 1.14 and 1.16. The α-helical, N-terminal section of the monomer carries the *c* heme whereas the β-propeller, C-terminal domain binds the d_1 heme at which catalysis takes place [107]. The hemes within a monomer are approximately 11 Å apart, from edge to edge, or 20 Å from iron to iron. All heme-heme distances between subunits are greater than 35 Å. The function of heme *c* is as an electron-accepting site of the protein molecule. *Pseudomonas* uses cytochrome c_{551} and azurin as its electron donors for catalysis [115, 116]. The *c* heme is low-spin and hexacoordinated in both Fe^{II} and Fe^{III} oxidation states [117, 118]. In contrast to heme *c*, the d_1 heme at the active site is a cofactor unique to this reductase in denitrifying bacteria. The d_1 heme is non-covalently bound to the protein and can be removed through an acidic acetone wash [119]. This yields “semi-apoprotein” containing only heme *c*. The d_1 heme can be reconstituted in the protein structure, and this has been achieved using chemically

synthesised d_1 or heme d_1 removed from the protein. The spectroscopic features and activities of the enzyme are then largely restored [120]. Both heme *c* and heme d_1 are low-spin and hexacoordinated in the ferric state. However, on reduction to the ferrous state heme d_1 becomes high-spin and pentacoordinated. The coordination and spin states of both ferrous and ferric *c* and d_1 heme have been elucidated using NMR, EPR and MCD spectroscopies [117, 118, 121].

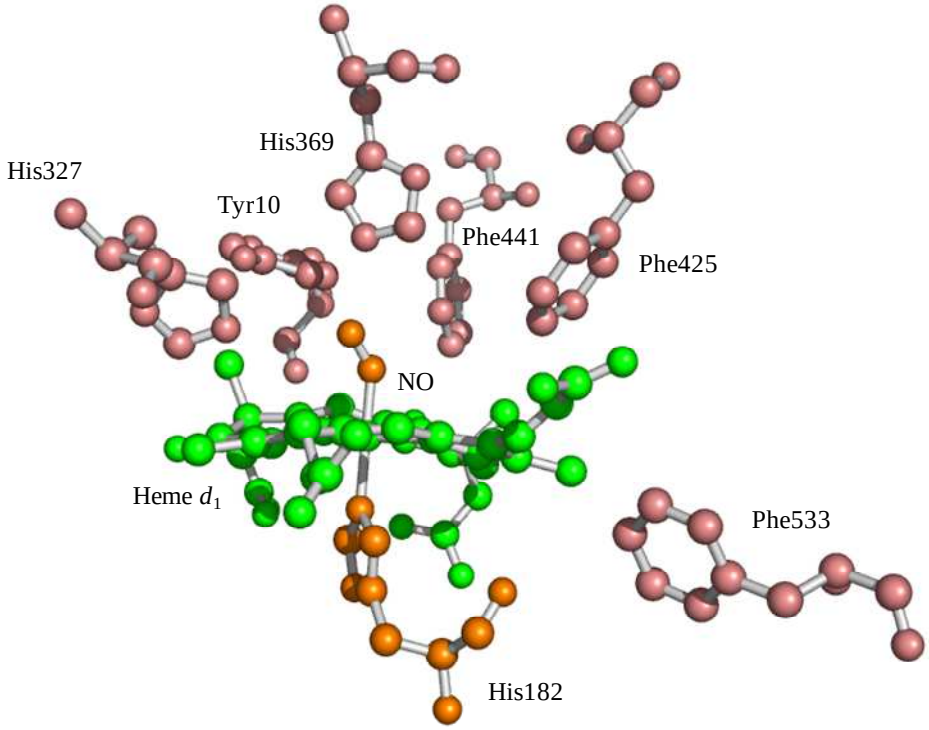

Figure 1.15: Structure of the d_1 site of *P. aeruginosa* cd_1 with NO bound. The representation is shown as a ball and stick model. The d_1 heme is coloured green, the d_1 heme iron ligands (histidine 182 and the product NO) are coloured orange and residues close to the d_1 heme including those involved in hydrogen bonding (tyrosine 10, histidine 327 and histidine 369) are shown in salmon. Figure constructed using Pymol. Source 1NNO.pdb [112].

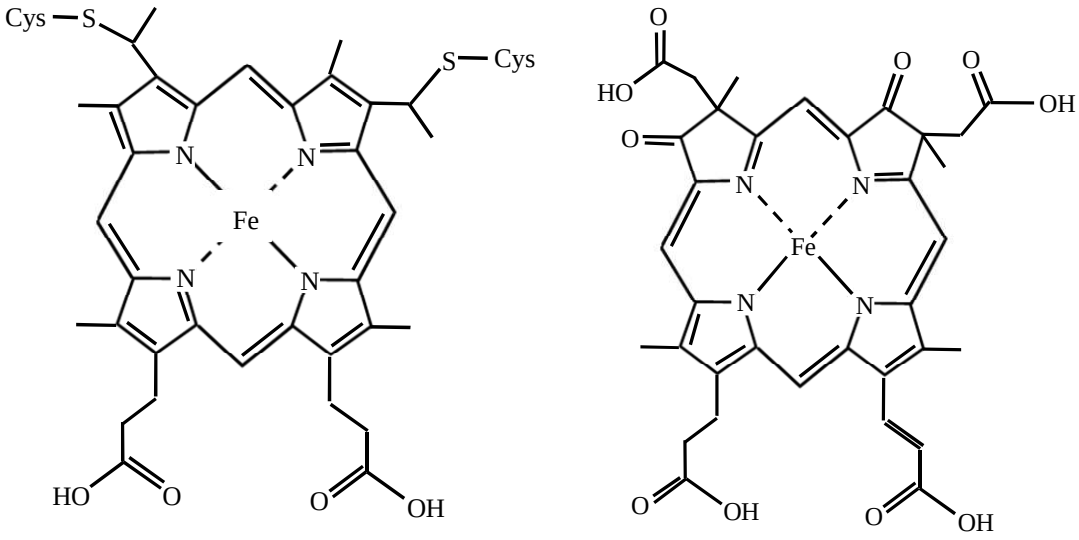

Heme *c* (protoporphyrin IX) Heme d_1 (dioxoisobacteriochlorin)

Figure 1.16: Structures of the two heme types found in cytochrome cd_1.

In the protein, the d_1 heme deviates from planar conformation and instead adopts a distorted saddle shape [99, 107, 112]. In solution, free d_1 heme adopts a domed configuration with an out of plane pentacoordinated iron (III) [122].

In summary *P. aeruginosa* cd_1 nitrite reductase is typical of the majority of cd_1s from organisms such as *P. stutzeri*, *P. fluorescens* and *H. thermophilus*. They are homodimers, with each monomer containing a *c* and d_1 heme. Heme *c* has fixed ligands (histidine and methionine) and the d_1 heme has axial ligation to a histidine and a water or hydroxide molecule in the oxidised state. *P. pantotrophus* cd_1 is also a homodimeric enzyme with one *c* heme and one d_1 heme per monomer. However, *P. pantotrophus* cd_1 differs slightly from the typical cd_1s previously described. The heme *c* has unusual bis-histidine ligation in the oxidised state but revert to histidine / methionine coordination on reduction. The d_1 heme site also has a tyrosine residue as the sixth axial ligand instead of the water / hydroxide molecule in the

oxidised state. The differences of *P. pantotrophus* cd_1 compared to the more typical proteins, such as *P. aeruginosa* cd_1, are described next.

1.1.12: *Paracoccus pantotrophus* cd_1 Nitrite Reductase: Differences Between this Enzyme and that of *Pseudomonas aeruginosa.*

The *P. pantotrophus* enzyme shares many characteristics with the *P. aeruginosa* enzyme and cd_1s from other organisms**.** Like *P. aeruginosa* the enzyme is a soluble 120 kDa homodimer containing an electron accepting *c* heme and a catalytic d_1 heme per monomer as shown in Figure 1.17. However there are some crucial differences between the two enzymes, one being the identity of the sixth ligand of the d_1 heme. In *P. aeruginosa* the sixth ligand is a water / hydroxide ion [107], but in *P. pantotrophus* the sixth ligand is the phenolate of tyrosine 25 [99]. This tyrosine is located in the N-terminal section and therefore is part of the heme *c* domain. Tyrosine-25 has little conservation among cd_1 proteins from other species [60]. Mutagenesis experiments carried out on tyrosine-10 of *P. aeruginosa* and tyrosine-25 of *P. pantotrophus* shows only a minor role in nitrite reduction [110, 123]. Tyrosine 10 of *P. aeruginosa* cd_1 and tyrosine 25 of *P. pantotrophus* cd_1 do not have equivalent roles. Tyrosine 25 in oxidised *P. pantotrophus* cd_1 is a d_1 ligand, whereas the tyrosine 10 of *P. aeruginosa* cd_1 has been shown to hydrogen bond to nitric oxide [111]. Figure 1.13 shows that these tyrosines are not conserved among the cd_1 nitrite reductases. There is a general consensus that the oxidised, tyrosine-coordinated state of the enzyme represents a resting state. This form of the enzyme is inactive catalytically. It has not been observed in any other cd_1.

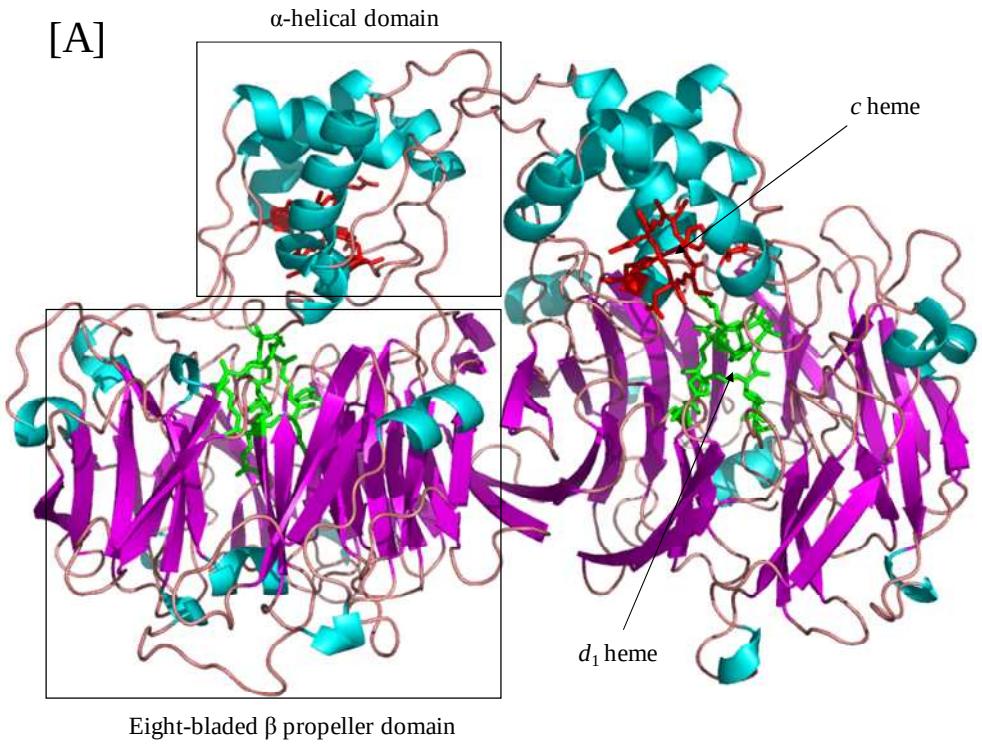
[A]
α-helical domain
c heme
d_1 heme
Eight-bladed β propeller domain

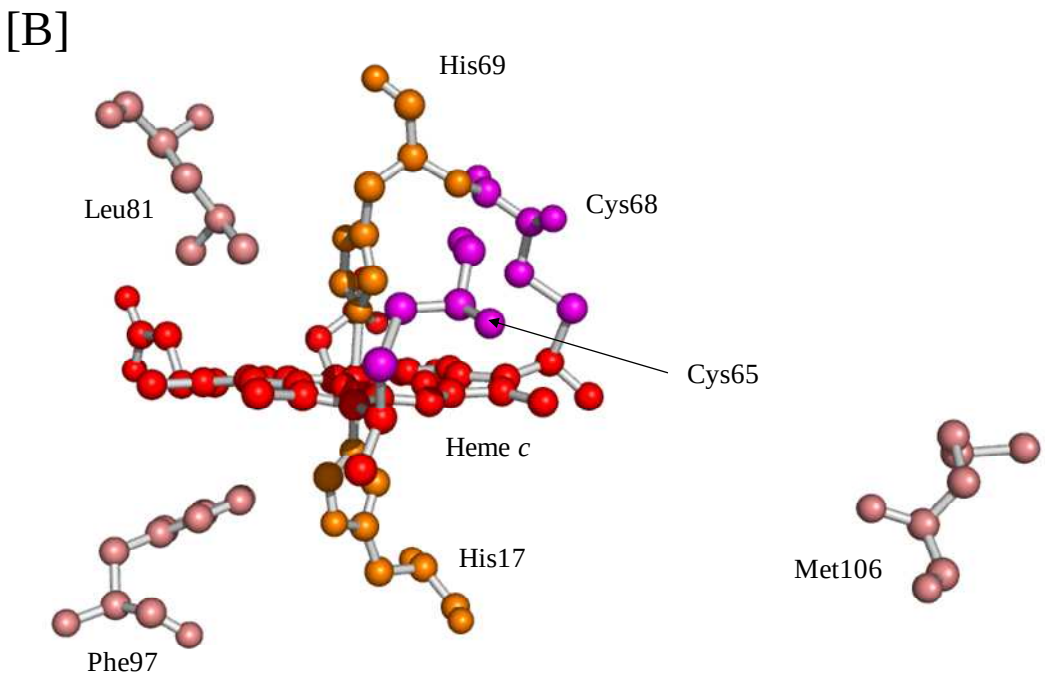
[B]
His69
Leu81
Cys68
Cys65
Heme c
His17
Met106
Phe97

[C]

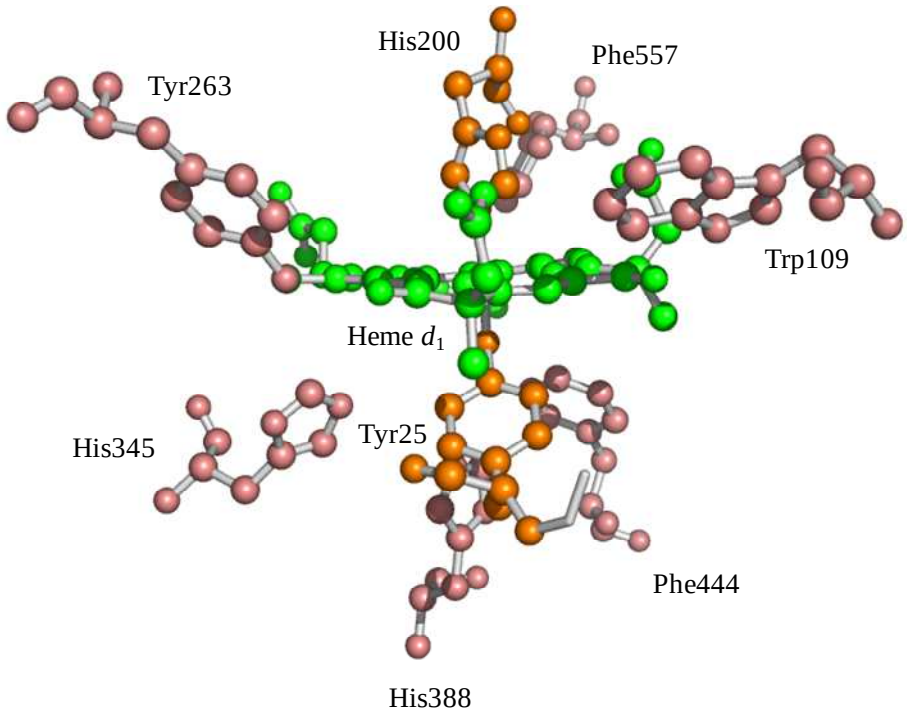

Figure 1.17: (This and previous page) Structures of oxidised *P. pantotrophus* cd_1 nitrite reductase and the *c* and d_1 hemes. [A] *P. pantotrophus* cd_1 homodimer in cartoon representation. α-helices are coloured cyan and β-sheets are coloured magenta. Domains are labelled for one of the subunits for clarity. *c* and d_1 hemes are also shown in stick representation and are coloured red and green respectively. [B] The *c* heme of oxidised *P. pantotrophus* cd_1 in ball and stick representation. The heme *c* is shown in red, the covalent cysteine linkages are shown in magenta, the heme iron ligands in orange and close surrounding amino acids in salmon, including the reduced heme *c* ligand methionine 106. [C] The d_1 heme of oxidised *P. pantotrophus* cd_1 in ball and stick representation. The heme d_1 is shown in green, the heme iron ligands in orange and close surrounding amino acids in salmon (including histidine 345 and histidine 388 which hydrogen bond to a water molecule (not shown) in the oxidised enzyme). Figure constructed using Pymol. Source: 1QKS.pdb [99].

The difference in the sixth ligand of the d_1 heme (water / hydroxide for *Pseudomonas* and tyrosine 25 for *Paracoccus*) results in subtle changes elsewhere in the d_1 heme pocket. The conserved histidines (histidine 327 and histidine 369 in *Pseudomonas*) show differences in hydrogen bonding associations. The oxidised *Pseudomonas* enzyme has the residues in question hydrogen bonded to the hydroxide bound to the d_1 heme [107], but the oxidised *Paracoccus* enzyme is different. The conserved histidines are hydrogen bonded to a water molecule or hydroxide ion [99]. The ligand water / hydroxide in *P. aeruginosa* cd_1 is replaced with the substrate nitrite during catalysis, which is subsequently converted to NO. In *P. pantotrophus* cd_1 it is the tyrosine 25 ligand that is replaced by nitrite before conversion to the product NO. NO bound to the d_1 heme of *P. pantotrophus* cd_1 can be seen in Figure 1.18. The d_1 heme itself also differs in *P. pantotrophus* from other cd_1 proteins in that it assumes a more planar arrangement, as opposed to a twisted saddle arrangement [99, 107, 112, 124]. The *c* heme ligands are also very different between the *Pseudomonas* and *Paracoccus* enzymes. The oxidised *Pseudomonas* ligands are histidine-51 and methionine-88, whereas for the *Paracoccus* enzyme the ligands are histidine-17 and histidine-69. Both oxidised enzymes have been studied through spectroscopic methods [118, 125, 126]. The results confirm that this pattern of *c* heme ligation is also true in solution. When the enzyme is reduced the ligands remain unchanged in *Pseudomonas* [112]. However, in the *Paracoccus* enzyme, axial ligand switching occurs. The histidine-17 and histidine-69 combination changes to histidine-69 and methionine-106 as shown in Figure 1.19, which facilitates large conformational changes that extend to the d_1 domain [124]. The ligand switching to histidine / methionine is thought to be a requirement for enzyme activity, with the bis-histidine coordination proposed as a resting state [127]. A further difference is the rates of electron transfer are different. The rate of electron transfer from the *c* heme to the d_1

heme is much faster in the *Paracoccus* enzyme than for the *Pseudomonas* enzyme [128, 129].

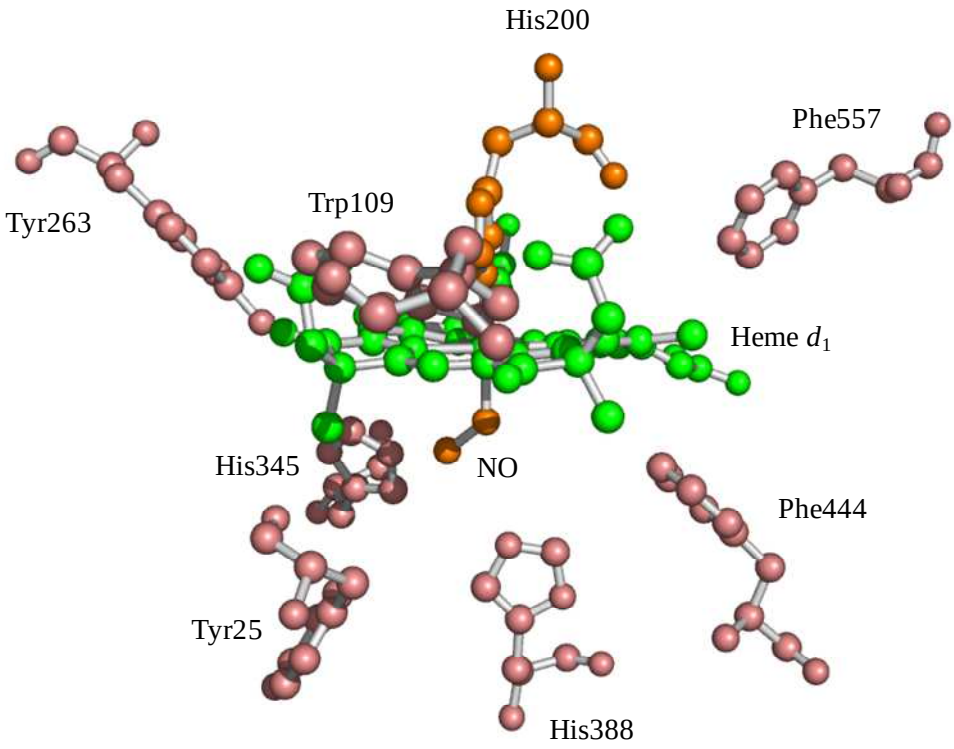

Figure 1.18: The d_1 heme of reduced *P. pantotrophus* cd_1 with NO bound in ball and stick representation. The heme d_1 is shown in green, the heme iron ligands (histidine 200 and the NO molecule) in orange and close surrounding amino acids in salmon (including the oxidised enzyme d_1 ligand tyrosine 25 and the conserved histidine residues involved in catalysis, histidine 345 and histidine 388). Figure constructed using Pymol. Source: 1AOQ.pdb [124].

The *Paracoccus* enzyme has an electron transfer rate of 1400 s^{-1} compared to the *Pseudomonas* enzyme figure of 6 s^{-1}. The rate-limiting step in the *Paracoccus* enzyme is thought to be the rate of NO dissociation. The NO dissociation has been calculated at 65 s^{-1}, which is similar to the overall k_{cat} of 72 s^{-1} per d_1 heme [130, 131]. There also is currently a suggestion that the NO dissociates in a biphasic

manner at different rates between the two monomers [130]. Evidence of inherent asymmetry, supporting anticooperativity between the monomers is reported in kinetic studies with nitrite [132], ligand binding studies [109, 133], potentiometric titrations [134] and studies on intramolecular electron transfer [135, 136].

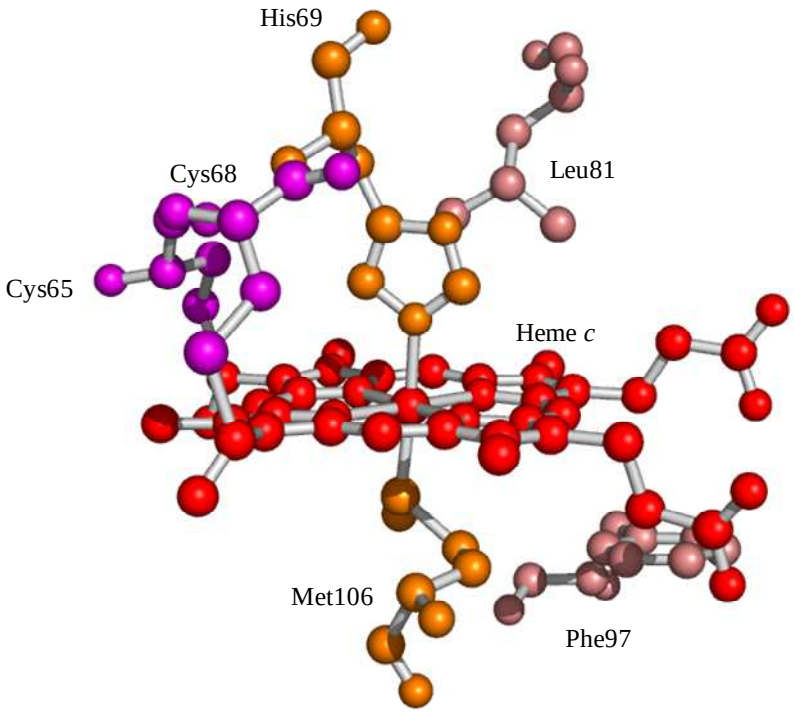

Figure 1.19: The *c* heme of reduced *P. pantotrophus* cd_1 in ball and stick representation. The heme *c* is shown in red, the covalent cysteine linkages are shown in magenta, the heme iron ligands in orange and close surrounding amino acids in salmon. Note that the histidine 17 is replaced by methionine 106 (See Figure 1.17B). The histidine 17 is not shown as the pdb file does not have it represented. Figure constructed using Pymol. Source 1H9X.pdb [137].

Further evidence comes from the crystal structures of *P. pantotrophus* cd_1, both with and without ligands bound. These structures show that the two monomers are different in structural appearance [99, 124, 133]. The high dissociation rate of NO from cd_1 is largely attributed to the d_1 heme cofactor. However, comparison between

cd_1 and d_1-containing myoglobin (Mbd_1) reveals that there is a higher dissociation rate for cd_1, which leads to the possibility that a feature of the protein itself contributes to optimum NO release [130]. A possible candidate thought to be contributing to optimum NO release was a conformational change involving tyrosine 197 and a hinge region, connecting the heme domains comprising residues 132-136 [137]. The identity of the protein moiety responsible has yet to be determined from a molecular level.

Another difference between *P. pantotrophus* cd_1 and *P. aeruginosa* cd_1 is the identity of the preferred electron donor. Both enzymes can accept electrons from a blue copper protein or a simple cytochrome. However, *P. pantotrophus* uses both cytochrome c_{550} and pseudoazurin as its donors. Mutants lacking both these electron donors grow poorly under denitrification conditions [138]. *P. aeruginosa* uses solely cytochrome c_{551} for electron transfer. Azurin has been shown to have no involvement [139]. The two cytochromes share the same basic folding patterns but the *P. aeruginosa* cytochrome c_{551} is significantly smaller at 82 amino acids compared to 134 for the *P. pantotrophus* c_{550} [140, 141]. A large deletion at the bottom of the heme crevice accounts for much of the large difference in the amount of amino acids in the primary structure. Both cytochromes have the CXXCH motif, with the other heme ligand coming from a methionine (methionine 99 in c_{550} and methionine 61 in c_{551}) [140, 142]. The copper proteins pseudoazurin and azurin are both members of the cupredoxins and share the same β-sheet topology. They also share the same rigid backbone dynamics [143, 144]. They differ in the number of helices in their structures and their locations [145]. Pseudoazurin contains two helices located after the VIII β-strand, whereas azurin only has one helix between β-strands IV and V. The copper ligands in the two proteins are also similar, with azurin from *P. aeruginosa* having a claimed extra weak glycine ligand [146]. The pseudoazurin

from *P. pantotrophus* has histidine 40, cysteine 78, histidine 81 and methionine 86 as the copper coordinated ligands [147], whereas the ligands from *P. aeruginosa* azurin are glycine 45, histidine 46, cysteine 112, histidine 117 and methionine 121 [146].

The two cd_1 enzymes also have different oxidised visible absorbance and EPR spectra [96, 125, 148]. Between 620 and 740 nm the UV-visible absorption spectrum of *Paracoccus* cd_1 shows two bands at 644 nm and 702 nm, as opposed to the *Pseudomonas* solitary band in the 640 nm region. The two bands are as a result of two different spin states in thermal equilibrium, as opposed to a single but different species that produces two bands [125]. The EPR spectrum of *Paracoccus* has only one detectable g-value (g_z) at 3.05 for the *c* heme, the other two not easily detected. All three g-values for *c* heme are found in the EPR of *P. aeruginosa*, located approximately at 3.01, 2.29 and 1.40 [125, 148].

1.1.13: cd_1 Nitrite Reductases – Nitrite Binding, Mechanism and Catalysis.

A general reaction mechanism that encompasses all of the cd_1 enzymes including *P. aeruginosa* cd_1 and *P. pantotrophus* cd_1 has been proposed and is shown in Figure 1.20 [130]. This mechanism is generally accepted and is consistent with the majority of published data on cd_1 nitrite reductases. As outlined previously the *Pseudomonas* and *Paracoccus* enzymes differ in terms of the heme ligands. *P. aeruginosa* cd_1 has fixed *c* heme ligands whereas in *P. pantotrophus* cd_1 reduction activates a ligand change. *P. pantotrophus* cd_1 also has a sixth tyrosine ligand at the d_1 heme in the oxidised state, whereas *P. aeruginosa* cd_1 has a bound water / hydroxide molecule at the sixth coordination site.

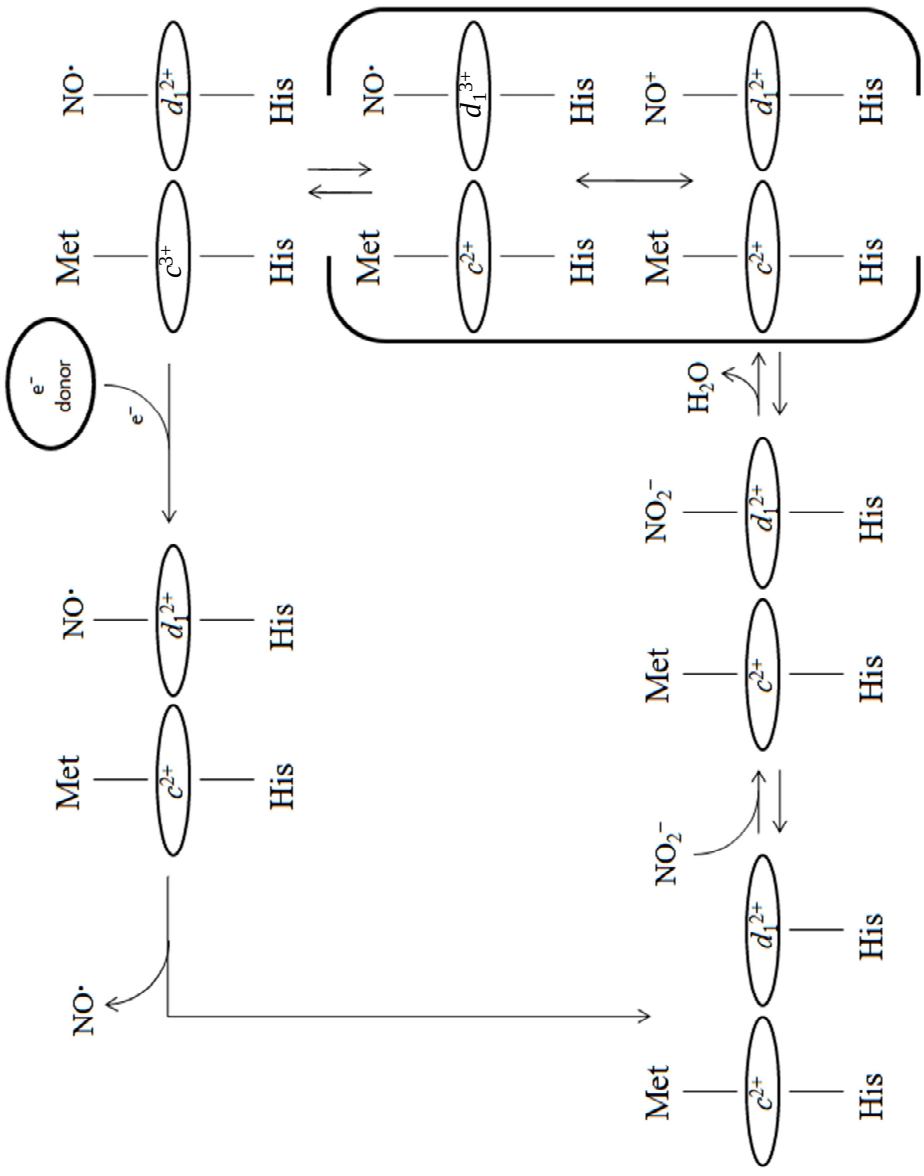

Figure 1.20: Summary of the general reaction mechanisms of cd_1 nitrite reductases. Taken and adapted from Rinaldo *et al.* 2011 [130].

However, the starting point of the mechanism is the reduced state in which the two cd_1 proteins are in terms of ligation the *c* and d_1 hemes. In the reduced form, both have histidine-methionine coordination at heme *c* and an open sixth coordination site for nitrite binding at heme d_1.

It is generally accepted that nitrite binds to the ferrous d_1 iron and through intramolecular electron transfer forms the reduction product NO [149]. The reduced heme d_1 of *P. aeruginosa* cd_1 binds nitrite with an affinity of K_m = 6 μM [108]. This results in the formation of the Michaelis complex [132] with the nitrite molecule binding via the nitrogen atom (a nitro complex). This is based on structural data from *P. pantotrophus* cd_1 nitrite binding [124], nitrite binding from other proteins containing heme [150-153] and synthetic iron porphyrin complexes in both ferrous and ferric states [153-156]. The nitrite N-binding mode is part of the accepted reaction mechanism in which a double protonation event occurs on one of the oxygen atoms of the nitrite [130]. The high affinity of ferrous heme d_1 for nitrite, and other anions such as cyanide [109], is unusual. *b* type hemes commonly bind anions such as nitrite and cyanide more readily when in the ferric state. The high affinity for nitrite exhibited by d_1 heme is thought to be attributed to the presence of histidine 327 and 369 in the active site pocket helping to stabilise the anion. Studies of cyanide-bound reduced *P. pantotrophus* cd_1 show these histidines within hydrogen bonding distance, suggesting that a positive electrostatic potential is required for anion stabilisation [133, 157]. The *E. coli* sulphite reductase, which can bind both sulphite and nitrite with high affinity, has also been shown to have a high charge density [150]. Histidine 327 and 369 have been shown to affect activity of *P. aeruginosa* cd_1 through mutagenesis studies [108, 109]. The mutation of histidine 369 to an alanine residue results in a 100-fold decrease in the rate of turnover [108]. A scheme of the active site with nitrite bound, as proposed by Rinaldo *et al*, is shown

in Figure 1.21 [130]. The structure of nitrite bound *P. pantotrophus* cd_1 also shows both conserved histidines in the d_1 pocket hydrogen-bonded to the nitrite. The histidine nitrogen to nitrite oxygen distances for each histidine are 2.9 - 3.2 Å and therefore are close enough to allow hydrogen bonding [124].

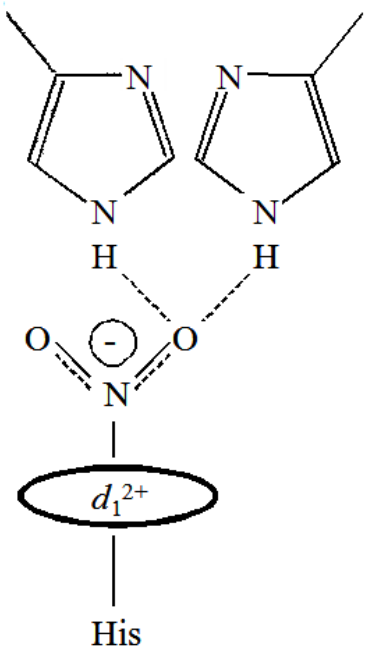

Figure 1.21: Proposed scheme of the d_1 active site from Rinaldo *et al.* 2011 [130] showing the imidazole groups of the two conserved histidine residues in relation to the nitrite. The two protons of the histidine imidazole groups bond to the oxygen to form a molecule of water which is subsequently released. From this a NO bound d_1 heme species is formed.

Once the nitrite is bound to the ferrous d_1 heme reduction to NO occurs. This results in the elimination of a water molecule or a hydroxide ion. Histidine residues provide the protons required. This leaves an iron nitrosyl species that can be described as the resonance species Fe^{III}-NO ↔ Fe^{II}-NO^+. Electron transfer from the *c* heme to the d_1 heme yields a Fe^{II}-NO species. The *c* heme is then rereduced with an electron from a donor protein. The electron transfer from the *c* heme to the d_1

heme has recently been investigated using pulse radiolysis [136]. This technique used 1-MNA (1-methylnicotinamide) and CO_2^- radicals to directly reduce only the heme *c*. The results demonstrated kinetic evidence for negative cooperativity between the d_1 hemes of the two subunits in the dimer. The rates of electron transfer from *c* to d_1 heme have been shown to be significantly affected by increases in the amount of electrons introduced into the enzyme [136]. An increase in electrons introduced to cd_1 results in a decrease in the rate of electron transfer by over an order of magnitude. This has been attributed to the disruption of electronic coupling between the *c* and d_1 heme due to conformational changes in oxidised and reduced species [112]. The differences between oxidised and reduced wild type enzyme is the loss of the sixth ligand hydroxide ion and a shift of tyrosine-10 away from the position it adopts when the enzyme is oxidised. There are also changes in hydrogen-bonding between the interface of the *c* and d_1 domains. The mutation of histidine 369 to an alanine results in an approximate tenfold increase in the rate of intramolecular electron transfer [136]. This is explained by a decrease in the positive charge density of the distal side of the d_1 heme. This results in the destabilization of the OH^- ligand, which in turn lowers the energy barrier that needs to be surmounted for electron transfer to occur, hence the increase in rate. The H369A mutants show great topological changes compared to the wild type. The *c*-heme domain is displaced from the wild type position, part of the d_1 distal section is rearranged and the N-terminal end with tyrosine-10 shifts completely away from the catalytic site. This rearrangement of structure has a pronounced effect on the position of the NO bound to the H369A mutant compared to the wild type.

Transfer of a single electron from the d_1 heme to the nitrite produces NO bound to an oxidised d_1 heme iron, with the release of a molecule of water. In structures of *P. pantotrophus* cd_1 and *P. aeruginosa* cd_1 the NO that is bound to the

reduced, wild type enzyme is bent in its geometry [112, 124]. This nitrosyl conformation results from NO binding to ferrous heme. Ferric heme results in NO binding in a linear nitrosonium conformation. As with the nitrite binding studies, key hydrogen-bonding residues have been identified in NO-bound d_1 [158]. For the wild type enzyme, histidine 369 and tyrosine 10 have been identified as residues that form hydrogen bonds to stabilise the NO-bound complex, with a lesser hydrogen-bonding role for histidine 327. This is shown in Figure 1.22. This contrasts with the crystal structure which shows displacement of tyrosine 10 from the NO [112]. In the tyrosine 10 mutant, histidine 327 is thought to play much more of a role in hydrogen-bonding. Tyrosine 10 is displaced completely in the double histidine mutant [158].

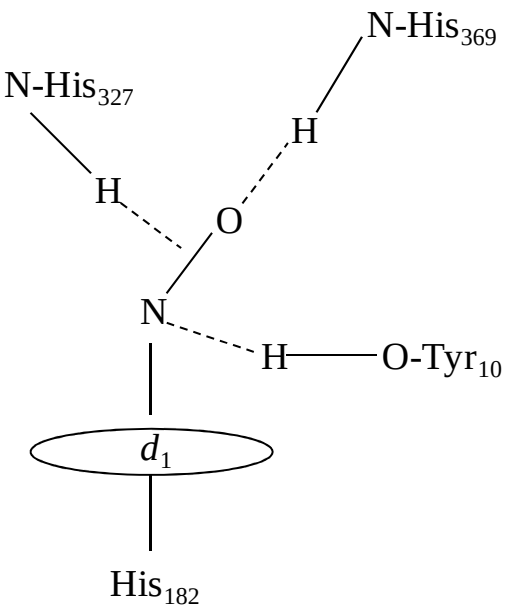

Figure 1.22: Scheme of the proposed hydrogen bonding of NO-bound d_1 heme in wild-type *P. aeruginosa* cd_1. It is not known whether His 327 hydrogen bonds to the N or the O of the nitric oxide and so the hydrogen bond is drawn midway. Adapted from Radoul *et al* [158].

Figure 1.20 shows that d_1Fe^{II}-NO^+ is interconvertable with the isoelectronic d_1Fe^{III}-NO· form. Both d_1Fe^{II}-NO^+ and d_1Fe^{III}-NO· forms are EPR silent. In comparison, nitrosylmyoglobin and nitrosylhaemoglobin bind NO in a Fe^{II}-NO conformation which is EPR active [159]. The d_1Fe^{II}-NO^+ species has been shown to be an intermediate through $^{18}O/^{15}N$ exchange experiments in *P. aeruginosa* cd_1 [160],

through FTIR of NO-bound, oxidised *P. stutzeri* enzyme [161] and in SF-FTIR spectroscopy, as part of a mixture of d_1Fe^{II}-NO^+ and d_1Fe^{III}-NO· species, in *P. pantotrophus* cd_1 [162]. It was initially thought that d_1Fe^{III}-NO· and d_1Fe^{II}-NO^+ were chemically unstable and decayed rapidly to release NO, leaving the heme iron ferric [163, 164]. This was based on comparison with synthetic Fe^{II}-NO^+ complexes [165, 166]. A further reaction mechanism was then proposed, which added NO displacement from $c^{2+}d_1{}^{2+}$-NO by nitrite as well as NO dissociation from d_1Fe^{III}-NO· [167]. For considerable time the formation of $c^{2+}d_1{}^{2+}$-NO was considered to be a stable dead end product [163, 164]. The $c^{2+}d_1{}^{2+}$-NO as a dead-end species was initially observed by Silvestrini *et al* [168] in stopped-flow and EPR studies at pH 8. This was backed up by further examples of NO binding tightly to the ferrous heme of proteins [169]. However, recent work has shown that the physiological substrate nitrite displaces NO from the ferrous enzyme at pH 7, which allows the enzyme to undergo a new catalytic cycle [170]. Further evidence for this is provided by the accumulation of $c^{2+}d_1{}^{2+}$-NO in the histidine 369 mutant. This accumulation is due to the decreased affinity of ferrous d_1 heme for nitrite, which results in the enzyme being trapped in a fully reduced, NO bound state [108, 170]. The latest reaction mechanism, shown in Figure 1.20, shows in addition to the previous mechanisms [167, 171] the need of excess reducing equivalents to stop the enzyme becoming trapped in the d^{3+}-NO bound form [131, 162, 172-174]. Electrons for reduction are provided by an external electron source such as a cytochrome *c* or a copper protein. NO dissociation is then thought to occur from the fully reduced enzyme with NO bound [130, 171]. Once the NO has dissociated from the d_1 heme the enzyme is restored to its fully reduced state and a new catalytic cycle can be initiated.

The respective turnover numbers for *P. aeruginosa* and *P. pantotrophus* cd_1 are 6 s^{-1} and 72 s^{-1} respectively in assays with cytochrome *c* as electron donor [131,

171]. The rate-limiting step in the reaction of *P. aeruginosa* cd_1 and nitrite appears to be the intramolecular electron transfer from the *c* heme to the d_1 heme. It has been reported that the electron transfer rate from the *c* to d_1 heme is in the order of 1-4 s^{-1}, which is comparable to the turnover number of 6 s^{-1} [108, 136]. Earlier studies using pulse radiolysis had calculated the transfer rate to be 3 s^{-1} in *P. aeruginosa* [128] and 23 s^{-1} in the related organism *P. stutzeri* [135]. In *P. pantotrophus* cd_1 the electron transfer rate is many orders of magnitude higher at 1400 s^{-1} [129, 162]. In the case of *P. pantotrophus* cd_1 the slower phase of NO dissociation appears to be the rate-limiting step. The slower and faster rates of NO dissociation are 65 s^{-1} and 200 s^{-1} respectively [130]. The slower rate of 65 s^{-1} closely correlates to the overall turnover number of 72 s^{-1} [131], making it the process most likely to be the rate limiting step. In comparison, *P. aeruginosa* cd_1 has a singular NO dissociation rate of 70 s^{-1} [171].

1.1.14: Hemes - Synthesis and Roles.

As shown in previous sections, many of the enzymes involved in the nitrogen cycle contain heme. Hemes are a class of iron-containing tetrapyrrole co-factors found in a diverse range of proteins spread across the three kingdoms of life [175]. They consist of an iron ion bound in a square planar arrangement by four pyrrole nitrogens from the porphyrin. Along with chlorophylls they are the principal tetrapyrroles in nature. Heme is a very versatile prosthetic group with a diverse array of functions. This range includes oxidation-reduction reactions such as the electron transferring cytochromes [176], the transportation and storage of oxygen such as the well-studied myoglobin and haemoglobin [177], cellular signalling [178], gene regulation [179], and catalysis. Examples of proteins that employ hemes for catalysis include heme copper oxidases [71] and peroxidases [180, 181]. The synthesis of heme occurs through the common intermediate δ-aminolevunic acid as shown in

Figure 1.23. The synthesis then involves condensation reactions of two δ-aminolevunic acid molecules initially to form porphobilinogen, and then four porphobilinogen molecules to produce hydroxymethylbilane. Uroporphyrinogen III synthase then completes the cyclisation of the molecule. Systematic enzymatic steps involving uroporphyrinogen decarboxylase, coproporphyrinogen oxidase and protoporphyrinogen oxidase respectively forms protoporphyrin IX. Ferrochelatase then inserts the iron into the protoporphyrin structure [182, 183]. This product formed is protoheme or heme *b* [184]. Heme *b* is a precursor for the formation of many of the other hemes found in nature. One of the hemes formed as a synthesis product from heme *b* is heme *c*. These two heme types are the most common in nature [185]. Heme *c* is a widely studied and very common heme found in many extensively studied proteins [186]. Both heme *b* and *c* are structurally similar and are shown in Figure 1.24. Heme *b* is bound non-covalently, whereas heme *c* is bound covalently to the protein: the two vinyl groups of the porphyrin form thioether linkages to cysteine residues. The majority of *c* heme proteins have the heme *c* attachment site of CXXCH. This is a pentapeptide section consisting of the cysteines that provide the covalent thioester bonds to the heme, a histidine residue that functions as an axial ligand to the heme iron and two other amino acids (X). In nature the XX section of the attachment motif is so variable in proteins that every amino acid has been found with the exception of cysteine. There are deviations from this signature motif. There are examples that only use a single cysteine to covalently bind to the protein such as the cytochrome *c* of *Euglena gracilis* that has an AXXCH site attachment sequence [188]. Other motifs substitute the axial histidine ligand with another amino acid. An example of this is the pentaheme nitrite reductase NrfA. The motif in question is CXXCK, which binds the high-spin, active site heme. Lysine serves as the axial ligand to iron instead of the histidine [41]. Another type increases

the number of variable amino acids (X) in the motif, from one extra amino acid (CXXXCH) in the diheme cytochrome c_{552} from *P. stutzeri* to $CX_{15}CH$ in MccA from *W. succinogenes* [100, 189].

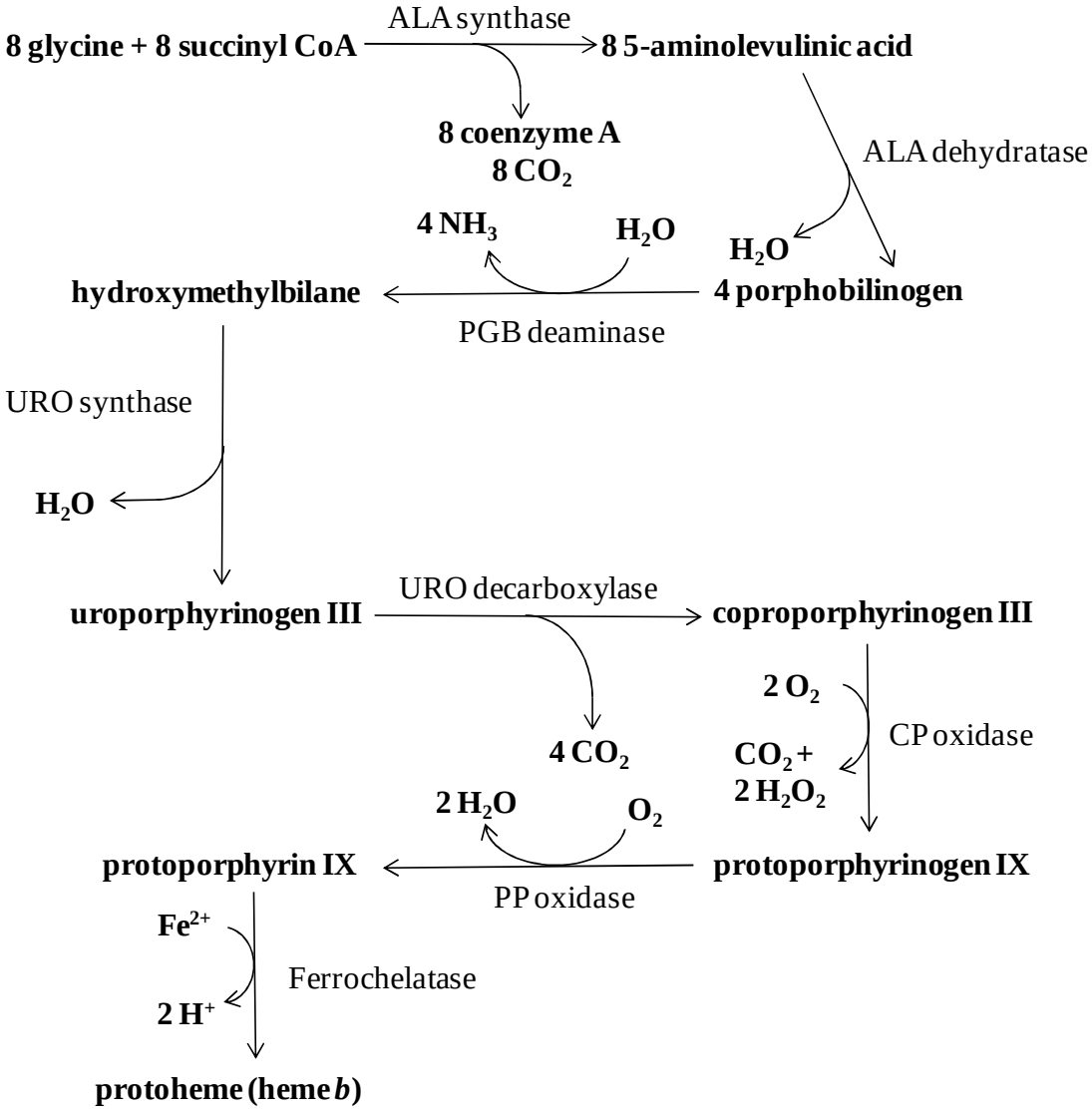

Figure 1.23: Scheme showing the chemical heme biosynthesis pathway. Intermediates, reactants and products are shown in bold type. Enzymes involved in each chemical reaction are shown. Abbreviations: ALA - 5-aminolevulinic acid, PGB - porphobilinogen, URO - uroporphyrinogen III, CP - coproporphyrinogen III, PP - protoporphyrinogen IX. Adapted from Franken *et al*. [187].

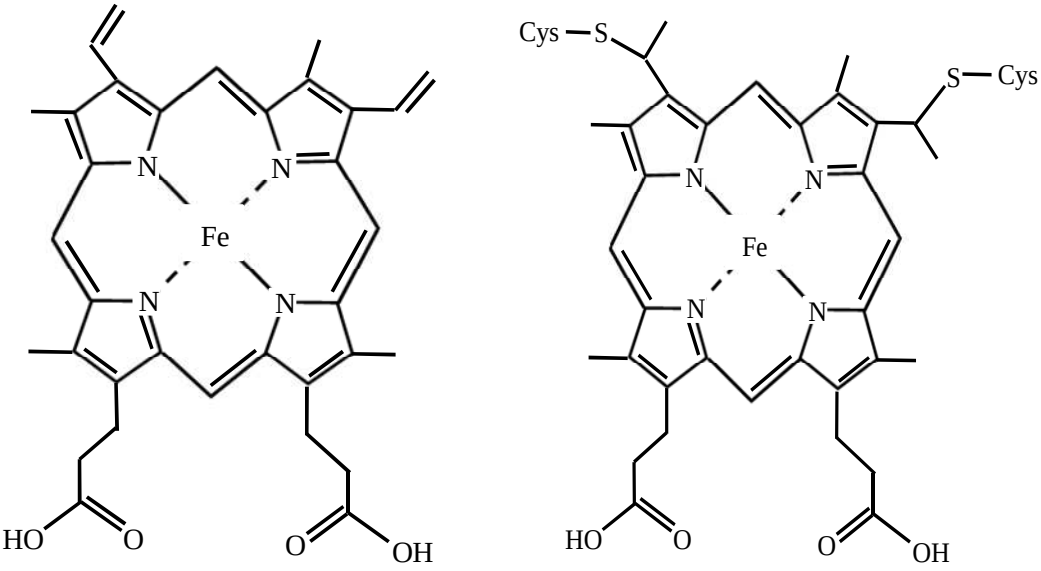

Heme *b* Heme *c*

Figure 1.24: The two most common hemes in nature, heme *b* and *c*. Heme *b* is the precursor to the structural variant heme *c*. Both are very similar structurally apart from the cysteine residues found on heme *c*. This allows heme *c* to covalently bind to the protein structure, whereas heme b is non-covalently bound. Both are found in a diverse assortment of cytochromes and enzymes.

The flexibility of heme and its multiple roles is attributed to the many factors that contribute to the protein environment [190, 191]. One of the most important factors is the type and total number of axial ligands at the iron derived from the protein structure. The heme structure has two free axial coordination sites (proximal and distal) above and below the plane of the porphyrin. Where a heme has a role in carrying or shuttling electrons both axial sites have protein derived ligands. For instance the majority of cytochrome *c* proteins are involved in carrying electrons via oxidation and reduction cycles [192, 193]. The most common residues that act as axial ligands to electron carrier heme proteins are histidine and methionine. The two

most common axial ligand arrangements in hexacoordinated heme for cytochromes are histidine-histidine (*bis*-histidine) or histidine-methionine. Hemes with histidine-histidine coordination include examples such as cytochrome c_{554} [194], cytochrome c_3 [195] and cytochrome b_5 [196]. Histidine-methionine examples include hemes in cytochrome bc_1 and cytochrome b_{562} [197, 198]. These two common ligand sets are found both in hemoproteins working to transfer electrons between other proteins and as intrinsic sites transferring electrons within multicentred structures. For example, in multiheme oxidases such as caa_3 or cbb_3 oxidases [192] the intramolecular hemes allow the shuttling of electrons from an external electron donor, through the protein structure to the catalytic active site. Other more unusual ligand sets include methionine-methionine (*bis*-methionine) in bacterioferritin [199] and N-terminal tyrosine and histidine axial ligation in cytochrome *f* [200].

Hemes do not act exclusively as electron carriers. In many proteins heme functions as an active site for oxygen carriers and enzymes. In the majority of cases the heme has a vacant axial coordination site, or the coordination site has a labile ligand. The labile ligand can take the form of a water or hydroxide molecule, or it can also be an amino acid residue from the protein that can dissociate to allow function. The proximal ligand is often histidine, as in the globins and heme peroxidase. In three related classes of protein, the P450 enzymes, chloroperoxidases and NO synthases, a cysteine is the single protein-derived axial ligand [201]. Less common sole axial ligands include tyrosine in heme catalases [201] and lysine in NrfA [41].

1.1.15: Hemes - Physical Properties and Types.

The electronic configurations of the different oxidation and spin states are shown in Figure 1.25. Hemes exist typically in the ferrous (Fe^{2+}) or ferric (Fe^{3+}) oxidation states. Both these states can have a low and high spin state. A low spin state is one in which as many electrons as possible are placed in the lower-energy d-orbitals before any are placed in the higher orbitals i.e. pairing is maximal. High spin states involve putting in as many unpaired electrons as is possible. Ferric iron in the low and high spin state has a spin of S = 1/2 or S = 5/2 respectively, whereas ferrous iron in the low and high spin state is S = 0 and S = 2 respectively [202]. Typically, axial coordination with two of the amino-acid derived ligands will result in a low-spin heme. If the heme has only one axial ligand then this favours a high spin heme. The oxidation state of iron influences reduction potentials and binding constants of exogenous ligands. For instance the proteins myoglobin and haemoglobin have a single axial histidine ligand coordinated to a ferrous heme. The remaining coordination site allows the physiologically relevant ligand O_2 access to bind the ferrous heme to form a six coordinate complex. Electron rich ferrous heme typically favours a neutral ligand such as O_2 or CO, whereas the positively charged ferric heme iron favours a ligand with a negative charge such as CN^- or F^-. Pentacoordinated, high spin heme often converts to low spin, hexacoordinated heme when an exogenous, sixth axial ligand binds. An example of this is fully reduced heme copper oxidases comprising of cytochrome bo_3 and cytochrome *c* oxidase treated with CO. The CO converts *a*, *o* or *b*-type high-spin pentacoordinated heme into low-spin, CO complexed hexacoordinated heme [203]. The protein environment is also important in tuning the heme for optimum protein function. Reduction potential is thought to be altered by the planarity of the heme [204], which is influenced by interactions of amino acids in the heme pocket.

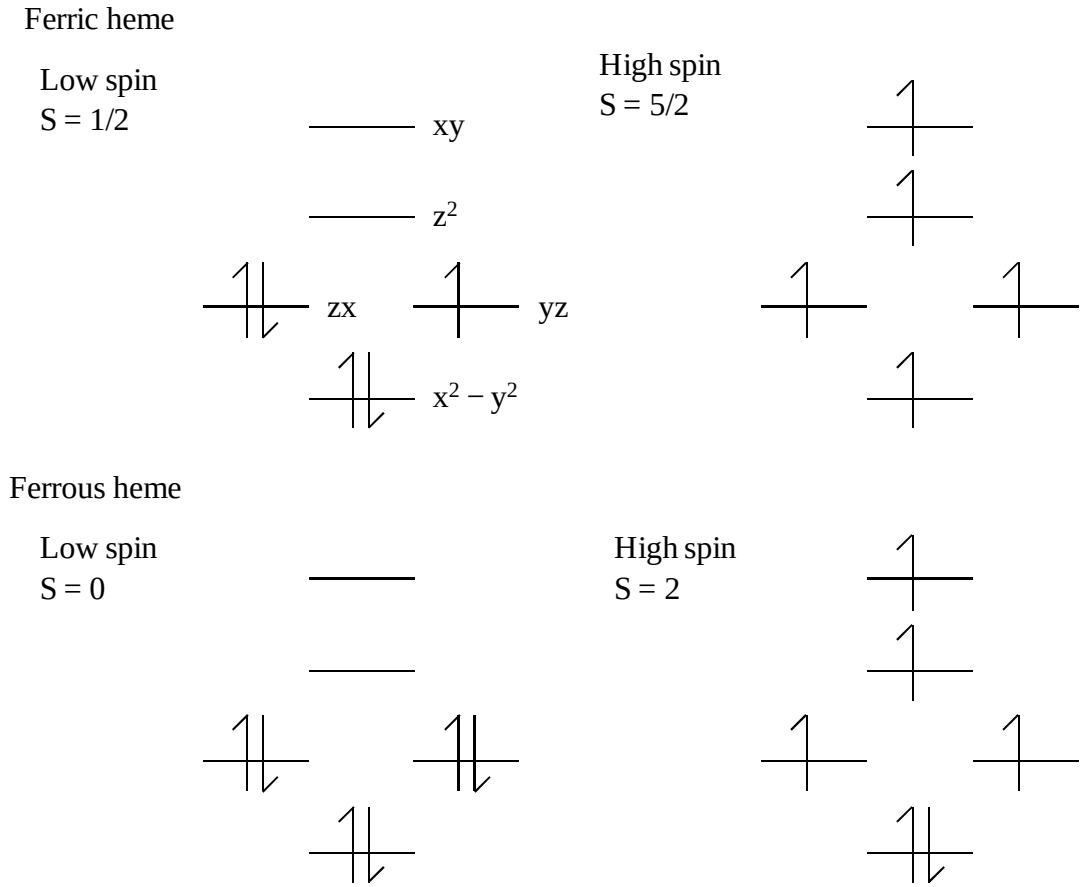

Figure 1.25: Energy level diagrams showing the oxidation and spin states of heme iron. The energy levels (d^5 for ferric and d^6 for ferrous) from highest to lowest for each diagram are xy, z^2, zx and yz, and $x^2 - y^2$.

An example of this is in the heme *b* containing nitrophorins, where high amounts of ruffling are observed [205]. Greater distortion of the heme structure lowers reduction potential. Heme *c* proteins have additional planarity influences through the variations of the CXXCH motif. In tetraheme cytochromes c_3 the composition of heme attachment motif strongly influences planarity, along with effects from the distal ligand and interactions with heme [206]. The heme binding site can also influence reduction potential through altering the histidine-iron bond character and strength. The reduction potential is affected by the strength of the interaction, both in the

oxidised and reduced states, whereas the spin state and reactivity is affected by ligand-field strength. A way in which these factors are tailored to the function of the protein is the level of histidine character the side chain of the histidine axial ligand possesses. It can be of a more neutral imidazole character like histidine, or it can be biased towards an anionic histidinate character. The histidine/histidinate character is adjusted through the heme structure and the axial histidine/heme environment. A lower reduction potential usually results from a more anionic axial histidine residue. Modifications through ligands and protein environments are sometimes not sufficient for function, and the hemes themselves are modified to perform the functions required. Heme *b* is the precursor for the other heme types including heme *c* (Figure 1.24). These however are not the only variations (Figures 1.05, 1.06, 1.16 and 1.26). Heme *o* is synthesised through the addition of a 17-hydroxyethylfarnesyl group at the 2-position. The reaction is catalysed by heme *o* synthase. Heme *o* is a stable intermediate of another variety called heme *a*. Heme *o* is modified to heme *a* by conversion of the 8-position methyl group to a formyl group by heme *a* synthase [207]. Both hemes can be found in the heme-copper respiratory oxidases. It is not clear why these enzymes require these more specialised hemes. Many examples of the heme copper oxidases can function without them, such as the cbb_3 or bb_3 oxidase types [203]. Heme *d* is another variant found in certain catalases [208] and unusual terminal respiratory oxidases [209]. Like the hemes *o* and *a*, there is evidence that heme *d* is not essential in the case of the oxidases, as the structurally related cyanide insensitive oxidases show no spectral characteristics of a heme *d* [210, 211]. The structures of the three heme types are shown in Figure 1.26. One heme variant that is very specific and required for functionality is heme d_1. Heme d_1 has been unambiguously identified as a 3, 8–dioxo–17–acrylate-porphyrindione [212].

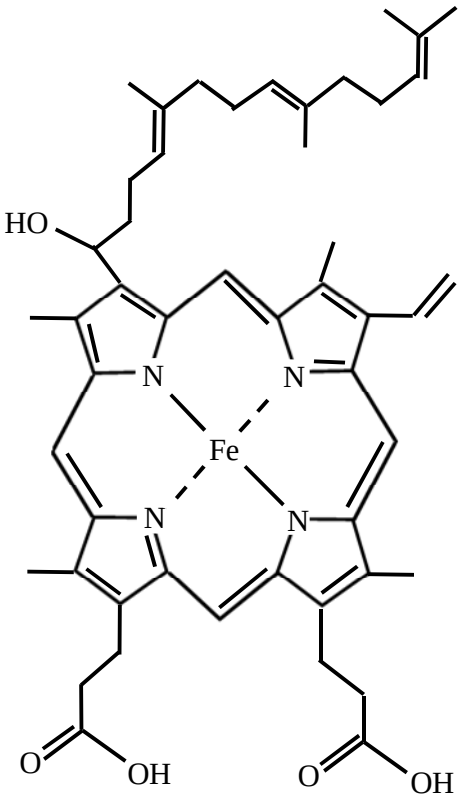

Heme *o*

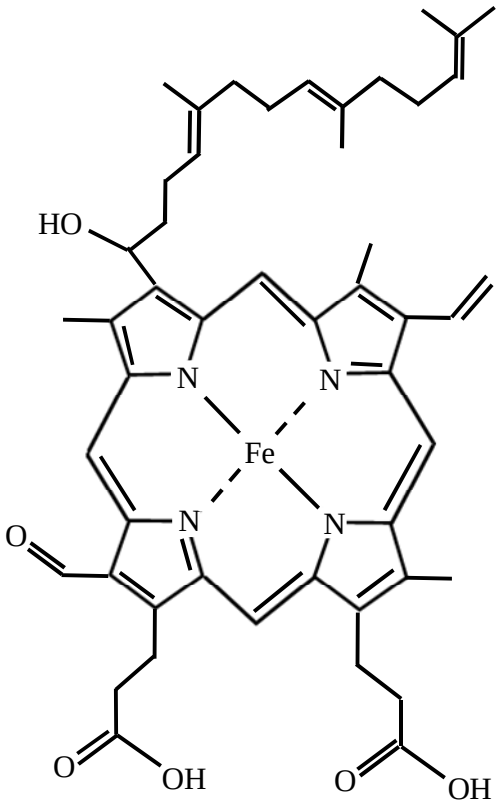

Heme *a*

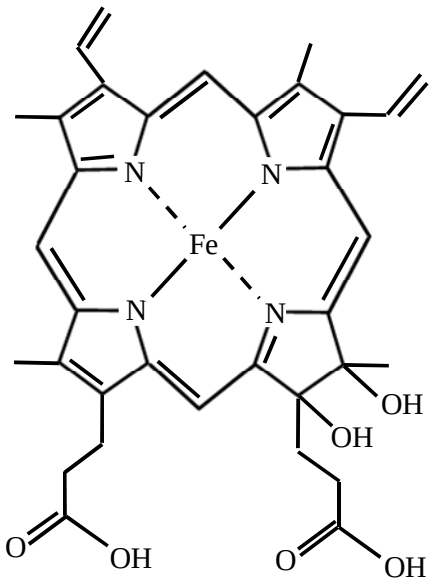

Heme *d*

Figure 1.26: Structure of some of the hemes produced from the heme *b* precursor. Heme *o* and *a* can be found in heme copper respiratory oxidases. Heme *o* is an intermediate of heme *a*. Heme *d* can be found in HPII catalases and terminal respiratory oxidases.

Initially the heme d_1 was thought to have a chlorin core because of its green colour. However, through spectroscopic data [213, 214] and comparisons with compounds used as models for heme d_1 [212, 215] the macrocycle was concluded to be a

porphyrindione. The absolute structure has also been determined through synthesis of an ester of the d_1 heme and comparing circular dichroism spectra with an ester prepared from native d_1 heme [216]. The d_1 heme is exclusive to the denitrifiers that possess the cytochrome cd_1 nitrite reductase. A biosynthesis pathway has been proposed for d_1 heme via δ-aminolevulinic acid and uroporphyrinogen III [60]. The presence of oxo groups, which are electronegative in nature, gives the iron of the heme a more positive redox potential. The result is a Fe(III)/Fe(II) couple redox potential more positive than any porphyrin heme. It also makes the d_1 heme much more difficult to oxidise than any corresponding isobacteriochlorins [217, 218]. Observations on model porphyrins and d_1 heme liberated from cytochrome cd_1 nitrite reductase suggest that there is divergence away from planarity. The structure of heme d_1 is shown in Figure 1.16.

1.2: Iron Sulphur Clusters and Iron Regulation

Along with hemes, iron-sulphur clusters also play multiple roles important to protein function. Similarly to heme, iron-sulphur clusters can also act both as electron carriers and as active sites of enzymes. Further functions that iron-sulphur clusters can perform include structural roles, sulphur donation, disulphide cleavage and gene regulation. Iron-sulphur clusters are used as the sensory element in a diverse range of regulatory proteins, including SoxR, FNR and RirA. The last of these, RirA, is a transcriptional regulator found in many of the α-proteobacteria that repress iron uptake and acquisition genes in iron replete conditions. Regulation of concentration and supply of metal ions is important. Excessive uptake of iron can lead to the formation of toxic products that could have detrimental effects to the bacterial cell, whereas the cells do require the uptake of small amounts of iron to survive. The following section describes iron-sulphur clusters, the importance of iron

regulation and the transcriptional regulators, Fur, DtxR and RirA, the last of which is a focus of this work.

1.2.1: Iron-Sulphur Clusters – History, Cluster Types and Biosynthesis

Iron-sulphurs clusters are omnipresent prosthetic groups that have a diverse array of structures and functions. These prosthetic groups are some of the most ancient in nature. The atmosphere on earth during the first billion years was anaerobic, but with plentiful supplies of iron and sulphur. Ancient organisms utilised these to make iron-sulphur clusters as protein co-factors. Among other functions these co-factors could transfer electrons and bind oxyanions and nitrogenous species. Today iron-sulphur clusters are still spread throughout the three kingdoms of life [219-221].

Iron-sulphur clusters are defined as co-factors containing iron and inorganic sulphur. Sulphur is well suited as a constituent of multi iron clusters. It has the ability to populate 3d orbitals and has a longer, weaker hydrogen bond than oxygen. Chemically, it also has a range of valencies from –II (sulphides) to +VI (sulphates). Combined with abundant iron, which can exist most commonly in ferrous and ferric oxidation states and in different spin states, these important prosthetic groups are created [222]. Iron-sulphur clusters can be found in more than 200 classes of protein. The types of iron-sulphur cluster found in these proteins are also varied [222-224]. The structures of the most common types, [2Fe-2S], [3Fe-4S] and [4Fe-4S] are illustrated in Figure 1.27. Rubredoxin is also included as an example of a species with one iron atom, but is not technically an iron-sulphur cluster due to having no inorganic sulphur in its structure.

Iron-sulphur clusters are produced through three distinct types of assembly machinery. These are the NIF, ISC and SUF systems [221, 225, 226]. The NIF

system is specific for iron-sulphur clusters synthesised for nitrogenase maturation in azototrophic bacterial species such as *A. vinelandii* [227, 228]. The ISC system is the principal machinery of cluster biosynthesis in many bacterial species such as *A. vinelandii* and *E. coli* [229, 230]. There is also an ISC system containing additional components in eukaryotic mitochondria [220]. The SUF machinery operates much like the ISC system in bacterial species by playing a general role in biosynthesising clusters, except that this particular system operates under iron limiting conditions, or when the organism is under oxidative stress [231]. The SUF system also provides the foundation for cluster synthesis in plant chloroplasts [219], archaea and cyanobacteria. There are also bacterial examples of SUF machineries in Gram-positive bacteria, pathogenic bacteria and thermophilic bacteria [231]. All three systems assemble $[4Fe\text{-}4S]^{2+}$ and $[2Fe\text{-}2S]^{2+}$ clusters on scaffolds before transfer and incorporation into proteins. The functions of iron-sulphur clusters are now discussed.

1.2.2: Iron-Sulphur Cluster Function – Electron Transfer

The versatility of iron sulphur clusters allows them to perform a large range of biological functions. One of the primary functions of iron-sulphur clusters is mediating electron transport. The clusters have the ability to delocalise electron density over iron and sulphur atoms, and therefore they are ideally suited for their purpose. Iron has an ability to exist in two stable oxidation states [223]. Therefore in principle a cluster containing iron can exist in 2^n oxidation states but in practice they only operate between two. Depending on the protein environment of the cluster, iron-sulphur clusters can have reduction potentials as negative as −500 mV or as positive as +300 mV [232].

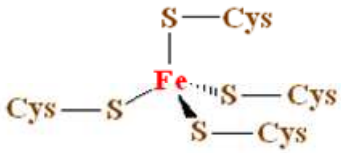

$Fe(Cys)_4$ proteins (technically not a iron-sulphur protein due to no inorganic sulphur atoms).
Example: Rubredoxins
Fe^{3+} (S=5/2) $\xrightarrow{e^-}$ Fe^{2+} (S=2)

Fe_2S_2 proteins.
Examples: Iron hydrogenases, adrenodoxin type and plant type ferredoxins.
$[2Fe\text{-}2S]^{2+}$ (S=0) $\xrightarrow{e^-}$ $[2Fe\text{-}2S]^{+}$ (S=1/2)

Fe_3S_4 proteins.
Examples: Aconitases, some bacterial type ferredoxins, hydrogenase.
$[3Fe\text{-}4S]^{+}$ (S=1/2) $\xrightarrow{e^-}$ $[3Fe\text{-}4S]^{0}$ (S=2)

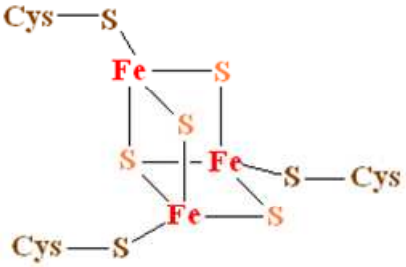

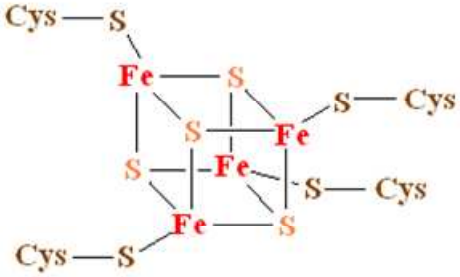

Fe_4S_4 proteins.
Examples: HiPIPs, some bacterialtype ferridoxins, some hydrogenases.
$[4Fe\text{-}4S]^{3+}$ (S=1/2) $\xrightarrow{e^-}$ $[4Fe\text{-}4S]^{2+}$ (S=0) (for HiPIPs)
[4Fe-4S]2+ (S=0) $\xrightarrow{e^-}$ [4Fe-4S]+ (S=1/2) (for ferredoxins, hydrogenases)

Figure 1.27: Crystallographically defined iron-sulphur cluster structures, examples of proteins that contain these clusters, oxidation states and the spin states of these oxidation states. There are other iron-sulphur clusters not shown including [8Fe-7S] iron sulphur clusters found in nitrogenases for example. Taken and adapted from Johnson *et al* [224]. Red denotes iron, brown denotes cysteines and associated sulphur and orange denotes inorganic sulphide.

Specifically, redox potentials for two iron clusters can range from +300 mV to − 110 mV for Rieske clusters, and − 150 mV to − 450 mV for cysteinate bound [2Fe-2S] clusters. Three iron clusters can have reduction potentials ranging from + 100 mV to – 450 mV. Four iron clusters are of two types, high potential and low potential. The former category has a range of reduction potentials + 450 mV to + 50 mV, whereas the latter have negative potentials from – 300 mV to – 600 mV. Reduction potentials reported below − 600 mV have not been proven beyond doubt. Iron-sulphur clusters are involved in a wide range of systems. They are vital components of respiratory electron transfer, such as mitochondrial and bacterial respiratory complexes I, II and III. They are also important in electron transfer in photosynthesis as a component of photosystem I. They also constitute many of the prosthetic groups used in electron transfer in soluble and membrane-bound redox enzymes. Iron-sulphur clusters are also the redox-active component of ferredoxins, a large class of mobile electron carrier proteins. Clusters involved in electron transfer include [2Fe-2S], [3Fe-4S] and [4Fe-4S] as shown in Figure 1.26. Cysteinate commonly completes the sulphur coordination for each of the cluster irons. Variations have been observed and are usually present to adjust reduction potential, facilitate the coupling of proton and electron transport or act as a gate to electron transport [233-235]. These variations include the switch of a cysteinate to an aspartate, serine, histidine or ligation to a backbone amide via an exclusive iron site. Special mention must go to the specialised [8Fe-7S] cluster of nitrogenase. Whereas most clusters act as an electron carrier for one electron, nitrogenase has the capacity to facilitate the transport of two electrons. When the cluster is subjected to two-electron oxidation large structural changes take place that allow the coupling of proton and electron transfer [236, 237].

1.2.3: Iron Sulphur Cluster Function – Enzyme Catalysis

Iron sulphur clusters are also co-factors involved or partly involved in binding sites for a wide variety of enzymes. Enzymes such as aconitase have a [4Fe-4S] cluster including one iron that is not ligated by a cysteinate. This iron serves as a Lewis acid to extract water from citrate to convert it to isocitrate [238]. Dehydration and hydration via iron-sulphur clusters occurs in a large range of dehydratases and hydratases [239].

The radical-S-adenosylmethionine is a superfamily of iron-sulphur cluster proteins that adopts a similar method to the hydratases and dehydratases. These enzymes have roles in radical reaction catalysis involved in the formation and degradation of biological products such as cofactors, herbicides, vitamins and antibiotics. Through binding of carboxylato and amino groups of the methionine fragment to produce a reductive cleavage, a 5'-deoxyadenosyl radical is generated [240].

Some iron-sulphur cluster enzymes are only effective if a metal site that can bind substrate is attached through a cysteinyl bridge. Examples include attachment of a dinickel component in the functional acetyl coenzyme A synthase [241], a siroheme attached to the iron-sulphur cluster in nitrite and sulphite reductase [242] and the presence of a two iron centre in the active site of Fe-hydrogenase [243]. Other metals can also be incorporated into the cluster to allow the activation or binding of substrate, such as CO dehydrogenase that has an unusual [Ni-4Fe-5S] cluster [244].

1.2.4: Iron Sulphur Cluster Function – Structural Functions, Disulphide Cleavage and Sulphur Donation

Other roles that iron-sulphur clusters fulfil in nature are as structural constituents in such as endonuclease III and MutY [245, 246]. Both these DNA repair enzymes use the iron-sulphur cluster to control a protein loop critical for repair and recognition of DNA damage. Iron-sulphur clusters are also involved in enzyme activity regulation. An example is the enzyme glutamine phosphoribosylpyrophosphate amidotransferase from *Bacillus subtilis*. This uses a [4Fe-4S] cluster to stabilise the enzyme. Oxygen-dependent degradation of the cluster results in irreversible denaturation of the enzyme in vitro [247]. Iron-sulphur clusters can also perform the roles of sulphur donation and reduction of disulphides. Sulphur donation is a function of the enzyme biotin synthase. A [2Fe-2S] cluster contained within the protein is degraded, providing sulphur for the catalytic conversion of dethiobiotin to biotin [248]. In terms of disulphide reduction, hetreodisulphide reductase in *Methanothermobacter marburgensis* and the chloroplast enzyme ferredoxin:thioredoxin reductase both use a [4Fe-4S] cluster to carry out cleavage of disulphides through ordered, single electron steps [249, 250].

1.2.5: Iron Sulphur Cluster Function – Gene Regulation

Iron-sulphur clusters are also used in regulation of gene expression at a transcriptional or translational level [251]. The first transcriptional factor identified to contain an iron-sulphur cluster was SoxR, a sensor of NO and superoxide stress. This regulator is activated through oxidation of the [2Fe-2S] cluster in conditions of oxidative stress. The conversion of the cluster stimulates the transcription factor SoxS that in turn activates enzymes involved in the removal of superoxide and the repair of damage caused by its effects [252]. The FNR (fumarate and nitrate

reductase) transcriptional regulator senses oxygen. Activation occurs through oxygen converting the dimeric, DNA-binding $[4Fe\text{-}4S]^{2+}$ form of the protein to the monomeric $[2Fe\text{-}2S]^{2+}$ type. This conversion results in regulated gene expression of aerobic and anaerobic respiratory proteins [253]. A mammalian example is the iron-regulatory protein 1 (IRP1). When iron is plentiful the IRP1 binds a [4Fe-4S] cluster. This allows it to behave as an aconitase. In conditions of iron depletion the IRP1 loses the cluster that gives it the ability to bind iron responsive elements (IRE) found on mRNAs. The IRE binding can inhibit translation if located at the 5' ends through blocking scanning to the AUG start codon by ribosomes. Binding to the IREs through location at the 3' ends can also confer increased translation. This shields the mRNA from nucleolytic degrading [254-256]. Finally, the assembly system for iron-sulphur clusters themselves has regulators that require iron-sulphur clusters. The iron-sulphur cluster assembly proteins in the *isc* operon have a regulatory protein in IscR. It is thought that gene expression of this operon operates on a feedback loop and that the [2Fe-2S] containing IscR is the primary repressor [257].

The iron-regulator RirA, a focus of this work, is also believed to be capable of binding an iron-sulphur cluster, the presence of which allows the protein to repress iron uptake genes when iron is sufficient. Iron regulation is important to microorganisms to prevent formation of toxic byproducts. Iron regulation and the classes of regulator, including RirA, are discussed next.

1.2.6: The Need for Iron Regulation

Apart from a few exceptional examples, the vast majority of microorganisms have a need for iron [258, 259]. Iron has always been an abundant metal on Earth. The atmosphere during the first billion years of Earth's existence was anaerobic, iron was present in the soluble ferrous form and therefore available for early organisms to utilise. Today the atmosphere is aerobic, with most of the iron in the insoluble ferric form. This insolubility presents major difficulties and microbes use various strategies to acquire ferric iron, such as the use of siderophores. Siderophores are organic compounds with a low molecular weight that bind strongly to iron in the ferric (Fe^{3+}) state [260]. These are secreted by the bacteria in order to chelate ferric iron and imported into the cell via dedicated transporters [261]. As well as inorganic iron in ferric form, other types of iron sources are available to bacteria including inorganic iron in ferrous form, heme as a protein constituent or as a free molecule and proteins such as ferritin or transferrin.

As well as the insolubility problem, iron presents another potential problem. It can also be toxic intracellularly. The reactions shown below constitute the Haber-Weiss cycle. Overall these would result in hydrogen peroxide decomposition via radical intermediates. In reality, the second reaction, the 'Haber-Weiss reaction' [262], has a rate constant in water that is essentially zero. The Haber Weiss reaction is shown in Equations 13 and 14.

$$H_2O_2 + OH^{\cdot} \rightarrow H_2O + O_2^{\cdot -} + H^+ \quad (13)$$

$$H_2O_2 + O_2^{\cdot -} \rightarrow O_2 + HO^{\cdot} + HO^- \quad (14)$$

This reaction can however be catalysed by metal ions, particularly *in vivo* by ferrous ions. Hydrogen peroxide can oxidise the Fe^{2+} ions in the Fenton reaction [263] shown in Equations 15 and 16. The Fe^{3+} can then be rereduced by the superoxide ion.

$$Fe^{2+} + H_2O_2 \rightarrow Fe^{3+} + HO^{\cdot} + HO^{-} \quad (15)$$

$$Fe^{3+} + O_2^{\cdot -} \rightarrow Fe^{2+} + O_2 \quad (16)$$

The net result is the Haber-Weiss reaction. Superoxide and hydrogen peroxide are both present in cells. Therefore any free iron species could lead to the production of hydroxyl radicals, which are both highly reactive and potentially damaging. This is one of the important reasons why utilisation and uptake of iron is tightly controlled by the organism. A balance is needed for intracellular iron levels. As a result many genes involved in iron utilization, storage, metabolism and uptake have tight regulation [264]. Expression of these genes increases when iron levels are low.

In terms of the classes of iron responsive regulation, the majority of work has focused on the ferric uptake regulator, or Fur [264-267]. Particular attention has been paid to Fur in the γ-proteobacteria such as *E. coli* and *Pseudomonas* [268-270]. A second type of iron regulator, found in Gram-positive bacteria, performs some of the roles of Fur. An example is the *Corynebacterium diphtheriae* toxin production repressor DtxR [266, 271, 272]. A third class of regulator is rhizobial iron regulator, or RirA, found in the *Rhizobia*, a repressor of genes involved in iron utilisation in conditions of iron sufficiency [273, 274].

1.2.7: The Classes of Iron Regulators

The most widely studied of the iron regulators is Fur. Fur is known to regulate iron acquisition systems in a range of organisms [275-280], and was first described in *E. coli* [281]. In *E. coli* the Fur protein is 17 kDa in size [282] and is thought to be dimeric in both apo and Fe^{2+} binding forms [283]. A two domain structure has been proposed for the Fur protein. The C-terminus is involved in dimerisation and the N-terminus is involved in DNA recognition and binding [284].

In early experiments Fur was thought to operate by binding to *fur* boxes in its Fe^{2+}-Fur form [285]. This is not entirely clear however, as there is evidence that Fur binds DNA with bound metal ions other than iron, and also with no metal ions bound at all [270, 280, 286, 287]. These *fur* boxes are conserved sequences located near promoters of genes whose transcription it regulates [288]. The *fur* box and the interaction of Fur with DNA have also been the subject of much debate. Proposed *fur* box models include a triple 6 base pair repeat sequence, followed by only two of the proposed 6 base pair sequences embedded in a 7-1-7 sequence [265, 289, 290]. The binding of Fe^{2+}-Fur to the *fur* boxes inhibits expression when iron is in abundance. Conversely, when iron is scarce, Fe^{2+} is released from Fur, the protein loses the ability to bind DNA and allows RNA polymerases to bind associated promoters, resulting in gene expression [265, 270]. Many of these genes encode proteins involved in the uptake of iron, examples being those involved in the synthesis of siderophores and their uptake. However, as well as being involved in the repression of many genes, Fur is also responsible for iron-dependent induction of many other operons, for example, through repression of RyhB in the presence of iron. RyhB is a sRNA that regulates the expression of genes involved in metabolism of iron. A sRNA, or small RNA, is a non-coding RNA that is 300 nucleotides or less in size. RyhB inhibits a variety of genes that seem to be Fur induced [291]. The crystal structures of Fur from *P. aeruginosa*, *Vibrio cholerae* and *Heliobacter pylori* have been resolved [292-294], as well as that of the DNA binding domain of *E. coli* Fur [295]. The structure of *P. aeruginosa* and *H. pylori* Fur is shown in Figure 1.28. The *P. aeruginosa* and *V. cholerae* Fur have two metal binding domains [292, 294]. One of the sites is in the dimerisation domain, and the other site bridges both the dimerisation domain and the DNA binding domain.

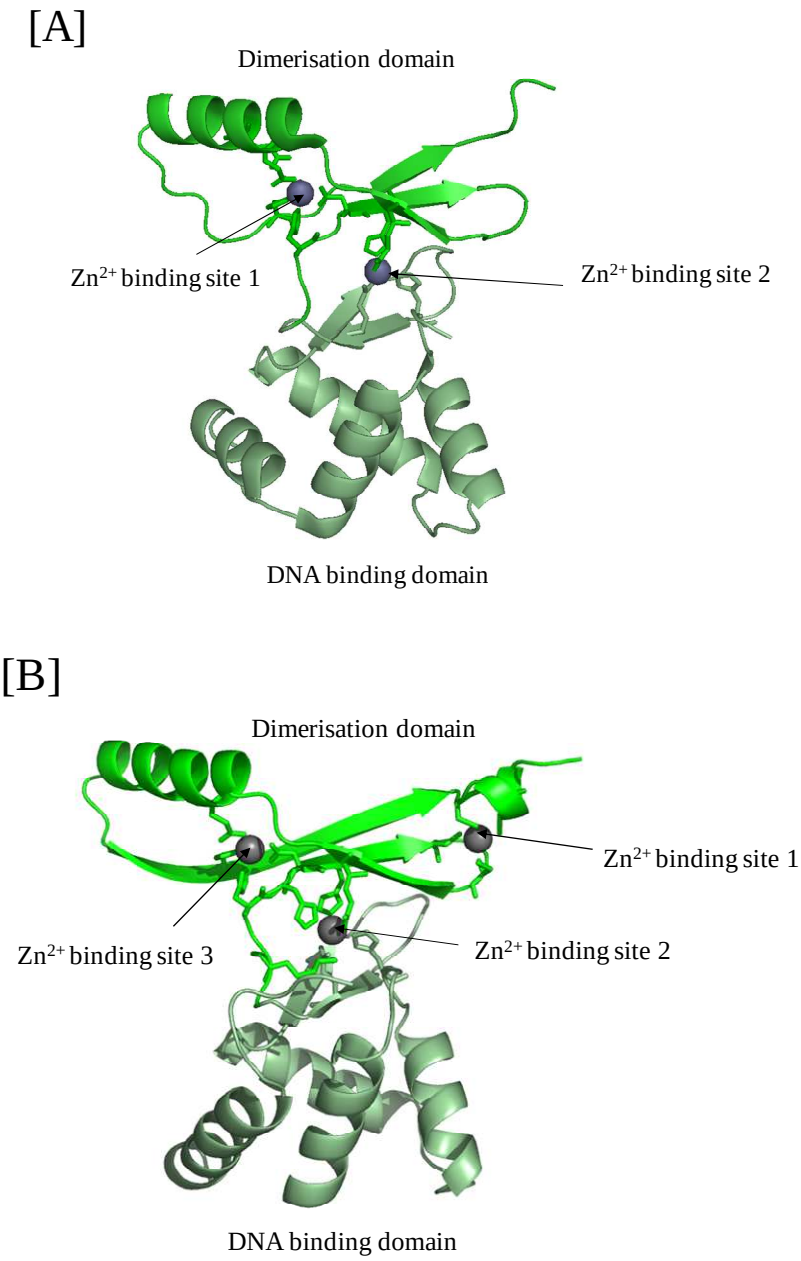

Figure 1.28: Structures of Fur monomers from *P. aeruginosa* [A] and *H. pylori* [B] showing the distinct domains in different shades of green as a cartoon representation. The dimerisation domain is coloured bright green and the DNA binding domain pale green. Zn^{2+} binding site ions are shown as grey spheres with associated amino acid ligands in stick representation, coloured according to the domain type from which the residue belongs. Figure constructed using Pymol. Sources: 1MZB.pdb and 2XIG.pdb [292, 293].

As with the *fur* box and the role of iron in activating Fur to bind DNA, the details of the metal sites are the subject of controversy [270, 292, 294]. It is unclear which site is the iron-sensing binding site, and whether or not the other has a role beyond stabilising protein structure. The *H. pylori* structure has three metal binding sites [293]. One has been identified as a structural metal ion site [296], whereas the other two are homologous to the two binding sites of the *P. aeruginosa* Fur [292]. Iron regulation in some of the *Rhizobia* Gram-negative α-protobacteria can show significant variation from the archetypal Fur regulation. They have the ability to form nitrogen-fixing symbioses with specific members of the legume family. *Rhizobium leguminosarum* can form nodules on beans, peas, lentils, clover and vetches. Differentiated forms of *Rhizobia*, known as the bacteroids, fix atmospheric nitrogen. There is a significant requirement for iron in nitrogen fixation due to it being a component of nitrogenase and other electron transfer proteins such as cytochromes and ferredoxins. As well as these, the plant also produces a large amount of leghaemoglobin. In a free-living state the *Rhizobia* can produce and import siderophores to acquire iron [297]. They can also use ferric citrate and haem. The use of haem is particularly remarkable as iron acquisition from haem (or haemoglobin) is normally a trait of pathogenic bacteria. An example of the differences in iron regulation can be seen in *Bradyrhizobium japonicum*. The Fur of *Bradyrhizobium* recognises sequences that are very different from the usual fur box sequences, such as those of *E. coli*. Also Fur^- mutants have some iron acquisition systems that remain unaffected. *Mesorhizobium loti* has no Fur protein in its proteome, and *R. leguminosarum* and *Sinorhizobium meliloti* have the manganese uptake regulator (or Mur). Mur is a very close homologue of Fur but it responds to Mn^{2+} and not Fe^{2+} [298]. It was found that Mur had no structural Zn^{2+} ion but instead bound two Mn^{2+} ions per dimer [299]. It represses the *sitABCD* ABC transporter

operon under replete conditions of Mn^{2+} [300]. Mur binds to Mur recognition sequences (MRS) under such conditions [301] but has no role in the regulation of iron uptake genes. There are also zinc and nickel uptake regulators in the Fur family [302-304].

As well as Gram-negative bacteria, Fur family proteins have also been discovered in cyanobacteria and Gram-positive bacteria [305-307]. In Gram-positive bacteria, however, there is another important class of iron-responsive regulation proteins. These are the DtxR family members (Figure 1.28) [264, 308]. DtxR was first discovered and identified as a repressor of the production of toxin in the organism *Corynebacterium diphtheriae* [309]. To date, more than 30 DtxR homologues have been identified, including the iron-dependent repressor IdeR from *Mycobacterium tuberculosis* [310]. DtxR and Fur appear to share some structural similarity between bacterial classes. Both have a helix-turn helix motif at the DNA binding site located at the N-terminal domain. Both also have at least two metal binding sites located at the C-terminal domain and N-terminal / C-terminal interface. Both of these metal binding sites are essential for the function of DtxR [311, 312]. The N-terminal domain also contains the dimerisation and metal-binding sites. The C-terminal domain is homologous in structure to eukaryotic SH3 domains [313, 314]. It is unclear what function the C-terminal domain performs. The DtxR proteins, like Fur, also have dual functionality as a repressor and an activator of iron uptake and storage genes [316, 317]. DtxR and Fur however do not share any similarities in sequences [264, 266]. The DtxR protein does not bind Fur boxes, but binds to operators with the common 19 bp core consensus sequence TTAGGTTAGCCTAACCTAA [318, 319]. DtxR has been activated in vitro by many divalent cations other than Fe^{2+}. These include Ni^{2+}, Co^{2+}, Mn^{2+}, Zn^{2+} and Cd^{2+} [320-323].

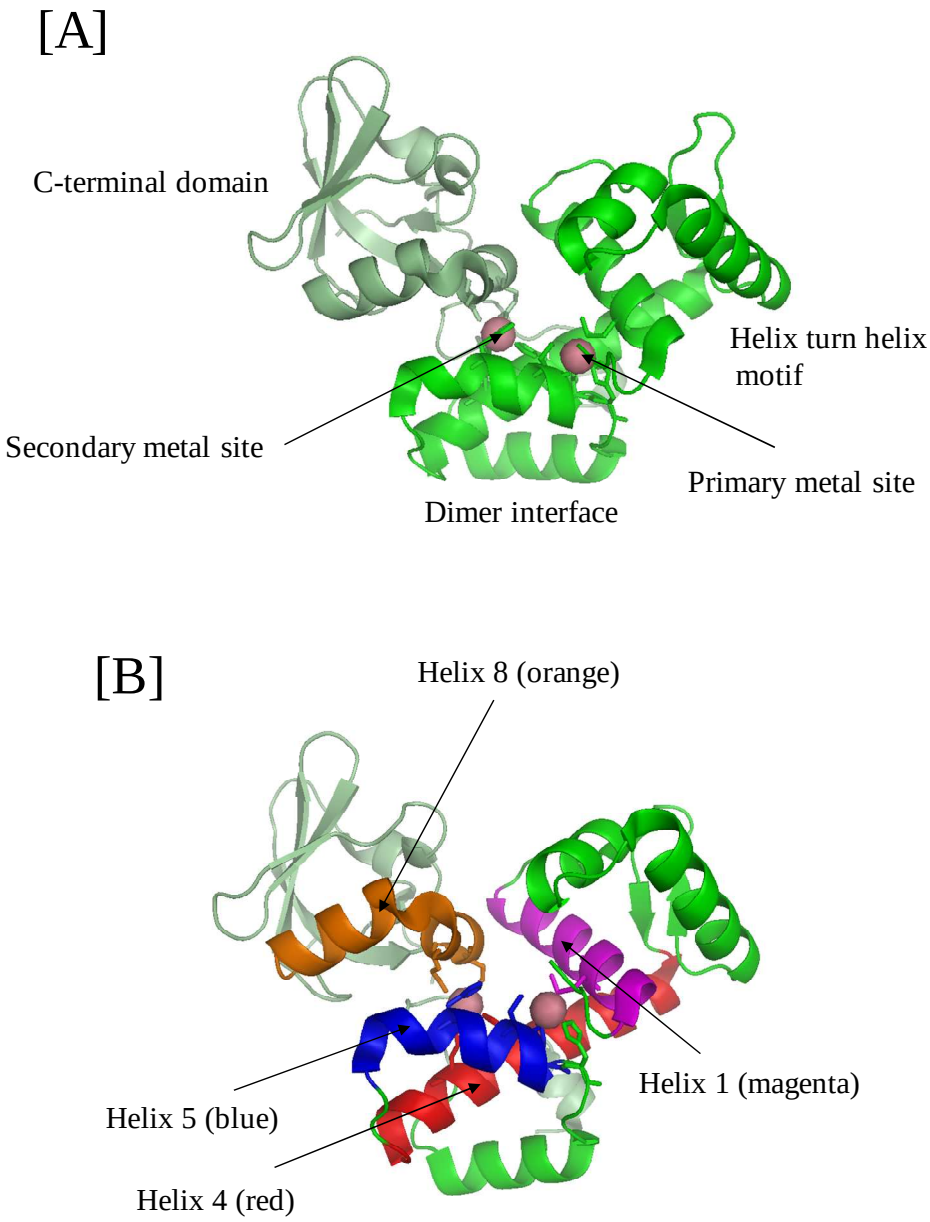

Figure 1.29: Structures of DtxR from *C. diphtheria* shown in cartoon representation. Metal atoms are shown as pink spheres and associated ligands in stick representation coloured according to the domain or helix they belong to. [A] DtxR showing the N-terminal domain in bright green and the C-terminal domain in pale green with key features labelled. [B] DtxR showing the helices that contain key residues associated with the proposed mechanism [315]. Figure constructed using Pymol. Source: 1C0W.pdb [313].

The crystal structures of DtxR have also utilised all of these divalent transition metals [311, 313, 324-327]. The structure of DtxR with bound to the two metal binding sites is shown in Figure 1.29A. A mechanism for the stepwise binding of divalent metal ions and structural changes through calorimetric and spectroscopic studies of wild type and mutant DtxR has been proposed [315]. Binding of the primary metal ion results in the organisation of residues at helix 5 and the subsequent N-terminal loop. The DNA binding domain then associates with the rest of the protein through methionine 10 at helix 1. The metal binding at the secondary site then fixes the positions of helices 4, 5 and 8, completing the folding of the N-domain and the formation of the dimer interface. The positions of the key helices can be found in Figure 1.29B.

Another member of the Fur superfamily is the iron responsive regulator Irr [328]. *R. leguminosarum* Irr is 30% identical to Fur in *E. coli* and 62% identical to Irr in *B. japonicum*. The sequence alignment demonstrating this is shown in Figure 1.30. Irr is a wide-ranging iron-responsive regulator that negatively regulates haem biosynthesis and positively regulates ferric iron transport [329-331]. It is thought to be a haem protein that functions in conditions where there is little iron available. No crystal structure for Irr has so far been published. In *R. leguminosarum* it has been shown that heme binding dramatically reduces the affinity of the Irr protein for its associated DNA operator sequence [332]. As well as this, heme binding at the second, lower-affinity site promotes oligomerization [333]. In *B. japonicum* Irr rapidly degrades via an unknown mechanism when haem or iron is present. *B. japonicum* Irr binds haem at two sites at least. The first site is the haem regulatory motif, or HRM (Gly-Cys-Pro-Trp-His-Asp) and the second is the HxH (Histidine-x-Histidine) [334, 335].

```
Rl MMT------------GAFPIA-------------IEVRLRGAGLRPTRQR 25
At -MA------------FDATLD-------------IGTRLRRSGLRPTRQR 24
Sm -MT------------KATHMS-------------SQERLRSSGLRPTRQR 24
Ba -MHS---------SHTHSTVS-------------MEERLREAGLRPTRQR 27
Bb -MN------------YHSLSE-------------LEEHLRKNGLRLTRQR 24
Bj –MSENTAPHHDDDVHAAALLSGRQPALTGCPWHDVNEMLQSAGLRPTRQR 49

Ec -----------------MTDN-------------NTALKKAGLKVTLPR 19


Rl VALGDLLFAKGDRHLTVEELHEEAVAAGVPVSLATVYNTLHQFTEAGLIR 75
At VALGDLLFAKGDRHLTVEELHDEAVTAGVPVSLATVYNTLHQFTEAGLIR 74
Sm VALADLIFAKGDRHLTVEELHEEAVTAGVPVSLATVYNTLHQFTEAGMIR 74
Ba VALASLIFAQGDRHLSAEDLHEEAVMADVPVSLATVYNTLHQFTEAGMLR 77
Bb LELAHMIFFQGNRHIAAEELYEEAIRSGVPVSLATVYNTLHQFTEAGLLR 74
Bj MALGWLLFGKGARHLTAEMLYEEATLAKVPVSLATVYNTLNQLTDAGLLR 99

Ec LKILEVLQEPDNHHVSAEDLYKRLIDMGEEIGLATVYRVLNQFDDAGIVT 69


Rl VLAVESAKTYFDTNVSDHHHFFVEGDN-EVLDIPVSN---LTIANLPEPP 121
At VLAVEGARTYFDTNVSDHHHFFVEGEN-EVLDIPINN---LQIDNLPEAP 120
Sm VLAVESARTYFDTNVSDHHHFFIEGEN-EVLDIPVSN---IQIDNLPEPP 120
Ba IIAVEGSKTYFDTNISDHQHFFLEGEN-VVFDIPHGEHGQPTVSNMPEAP 126
Bb IIAVEGSKTWFDTNTSDHYHFYIEGEN-RILDIPYNVEGSPIIENLPQPP 123
Bj QVSVDGTKTYFDTNVTTHHHYYLENSH-ELVDIEDPH---LALSKMPEVP 145

Ec RHNFEGGKSVFELTQQHHHDHLICLDCGKVIEFSDDS--IEARQREIAAK 117


Rl EGMEIAHVDVVIRLRAKQG------------ 140
At EGMEIAHVDVVIRLRRKRG------------ 139
Sm EGMEISHVDVVIRLRHKTER----------- 140
Ba EGMEIVNVDIIVRLRRQAR------------ 145
Bb EDMEIVHVDLIIRLKPKIQSDDQE------- 147
Bj EGYEIARIDMVVRLRKKR------------- 163

Ec HGIRLTNHSLYLYGHCAEGDCREDEHAHEGK 148
```

Figure 1.30: (Previous page) Multiple sequence alignment of Irr proteins from six genera of bacteria plus family member *E. coli* Fur for comparison (accession numbers from top: YP_765719.1, AAK85974.2, NP_384335.1, AAO89498.1, YP_989516.1, AAC32183.1, YP_001457481.1). Light grey highlights denote the residue is conserved in all six Irr proteins. Dark grey highlights denote that the residue is conserved in the six Irr proteins and the Fur sequence. Residues involved in the HRF motif for *B. japonicum* and the HxH motif are boxed. Alignment constructed using ClustalW2 and Jalview [105, 106]. **Abbreviations:** *Rl – Rhizobium leguminosarum* Irr, *At – Agrobacterium tumefaciens* Irr-like protein, *Sm – Sinorhizobium meliloti* Irr, *Ba – Brucella abortus* Irr, *Bb – Bartonella bacilliformis* Irr, *Bj – Bradyrhizobium japonicum* Irr, *Ec – Escherichia coli* Fur.

R. leguminosarum Irr has high identity but lacks the HRM site (it does contain the HxH site). Proteins such as ferrochelatase deliver haem to Irr in vivo. Irr^- mutants in *R. leguminosarum* overproduce protoporphyrin [298]. Like RirA mutants, Irr^- mutants are Fix^+ and Nod^+. Irr controls iron-induced expression of genes such as *hemA1* and *rirA* through ICE (Iron Control Element) motifs [328, 336]. These exist near the promoters of many genes controlled by Irr. Irr is thought to bind to the ICE sites. Other genes in *R. leguminosarum* where ICE sequences are located are *mbfA*, which encodes a protein which is thought to be involved in conferring resistance to high iron levels, *fssA*, which has 50% identity to a (FeS) cell cycle regulator interactor protein in humans, and *irpA*, which in *Synechococcus* is a iron-repressed OM protein controlled by Fur. All three of these genes are iron induced by Irr. Irr can work with other iron regulators, for example RirA, to control genes such as *suf*. The *suf* gene is iron-repressed by RirA and repressed under iron deficiency by Irr. The genes *rirA* and *rrp1* (an Irp6A like protein that binds to siderophores) are also under dual control of RirA and Irr [328]. It has also been recently demonstrated that the *irr*

gene in *B. japonicum* is repressed by Fur and antirepressed by Irr [337]. Irr mediates the repression of iron-induced genes when there is a lack of iron in the environment. The opposing regulation in *R. leguminosarum* is co-ordinated by rhizobial iron regulator (RirA). RirA controls the genes involved in the uptake of iron through repression under conditions of iron sufficiency. RirA is a focus of this work and is discussed next.

1.2.8: The Rhizobial Iron Regulator (RirA)

In *R. leguminosarum* and *S. meliloti* the Fur protein is replaced with RirA as the global iron-responsive regulator [273, 274, 338, 339]. Recent work published on *Agrobacterium tumefaciens* has also shown that RirA is the main regulator in iron uptake genes and not Fur [340, 341]. The RirA regulon is fairly extensive in that ~ 100 proteins have been found to be RirA repressed by *R. leguminosarum* and 45 in *S. meliloti* [339, 342, 343]. *R. leguminosarum* RirA is involved in the regulation of vicibactin synthesis (*vbs*) and uptake (*fhu*) genes, genes that are involved in the uptake of haem such as *tonB* and *hmu*, and genes that are thought to be involved in Fe^{3+} transport (*sfu*). As well as these it regulates an ECF RNA polymerase σ factor called *rpoI*. These genes are repressed in wild-type cells with iron in abundance, but not in the $RirA^{-}$ mutants [328, 338, 342]. It has been shown that *rirA* mutants overproduce vicibactin fourfold. Another characteristic is slightly impaired growth. RirA mutants are also Fix^{+} and Nod^{+}. As well as repression, RirA is also thought to positively regulate certain genes. Examples are the RL1019 protein, thought to confer resistance to microcin B17, a tRNA modifying GatB-type enzyme and the ABC transporter binding proteins Rip2, Rip4 and Rip5 [342]. As mentioned previously, RirA also represses genes, such as *suf* and *rrp1*, in tandem with Irr. RirA

is also itself dual-regulated. In iron-replete conditions it is negatively autoregulated, whereas in conditions of low iron it is repressed by Irr [328, 338].

Examples of proteins that *S. meliloti* RirA represses are iron and heme transportation genes *hmuPSTU* and *shmR*, the genes *exoY* and *exoN* involved in exopolysaccharide production and predicted metabolic genes *fixN3, fixP3* and *qxtAB* [339]. Like *R. leguminosarum* RirA it also regulates *suf* genes involved in iron-sulphur cluster formation. Only four unspecified genes were shown to be positively regulated by *S. meliloti* RirA [339]. In addition *S. meliloti* also has a positive regulator called RhrA which is repressed by RirA. RhrA is involved in transcription of *rhb* genes that are thought to be involved in the production of rhizobactin 1021, a siderophore [339, 343].

A single monomer of RirA in *R. leguminosarum* is 17441 Da in size. The RirA amino acid sequence contains four cysteines that are in close proximity to each other. It has therefore been suggested that RirA contains a FeS cluster that is bound by the four cysteines in its sequence. The iron-sulphur cluster availability is thought to be utilised by RirA as a measure of binding to repress target genes. High iron levels result in a high probability of cluster binding and binding to DNA to repress target genes, whereas low iron results in scarcity of clusters and therefore little likelihood of DNA binding to initiate repression [328]. RirA binds to IRO motifs found at promoter regions of RirA repressed genes. These are cis-acting regulatory sequences with the consensus sequence TGA-N_9-TCA [344, 345]. They are located near some of the promoters of the genes RirA represses when responding to the availability of iron.

RirA has very similar homologues in close relatives of *Rhizobium*. They have approximately 70% identity to homologues found in *Sinorhizobium*, *Mesorhizobium*, *Agrobacterium*, *Bartonella* and *Brucella*. The multiple sequence alignment of these

RirA homologues is shown in Figure 1.31. Interestingly, *B. japonicum* has no obvious homologue of RirA in its genome. RirA shows no sequence similarity to DtxR or Fur. Instead RirA also has around 30% sequence similarity to a large family of proteins known as the Rrf2 family. The multiple sequence alignment for the well studied Rrf2 family members is shown in Figure 1.32. Three of the cysteines in the sequence of *R. leguminosarum* RirA are highly conserved (~70%) among the Rrf2 family. These three cysteines have been shown to be essential to all the regulatory functions of *R. leguminosarum* RirA by site-directed mutagenesis. Very few of the Rrf2 family have been studied in detail. No crystal structures have been published for RirA or any of the Rrf2 family. Examples that have been well studied other than RirA include Rrf2, which is found in *Desulfovibrio vulgaris* and is involved in regulation of cytochrome synthesis [346], IscR, a repressor of *iscRSUA* in *E. coli* (This operon is involved in [FeS] production) [257, 347] and NsrR, a transcription regulator in *Nitrosomonas europaea* and *E. coli* that is sensitive to nitrite [348, 349].

```
Rl MRLTKQTNYAVRMLMYCAANDGHLSRIPEIAKAYGVSELFLFKILQPLNK 50
Ar MRLTKQTNYAVRMLMYCAANEGYLSRIPEIAKAYGVSELFLFKILQPLTK 50
Sm MRLTKQTNYAVRMLMYCAANGEKLSRIPEIARAYGVSELFLFKILQPLTR 50
Ba MRLTRQTNYAIRMLMYCAANDGKLSRIPEIARAYNVSELFLFKILQPLVE 50
Ml MRLTRQTNYAMRILMYCAANNDRLSRIPEIATAYSVSELFLFKILQPLVE 50
Bh MRLTKQTNYALRILMYCADNQESLSRIPEIAKAYAVSELFLFKILQPLVE 50

Rl AGLVETVRGRNGGVRLGKPAADISLFDVVRVTEDSFAMAECFEDDGEVEC 100
Ar AGLVETVRGRNGGVRLGKPPTDISLFDVVRVTEDSFAMAECFED-GAVEC 99
Sm AGLVETVRGRNGGVRLPRPASEITLFDVVKVTEDSFAMAECFEA-GEIDC 99
Ba HGLVETVRGRNGGVRLGRASQDISLFDVVRVTEENFSMAECFEN-DASEC 99
Ml NGLVETVRGRNGGVRLGRAAEAISLFDVVRVTEESFAMAECFEN-DAAEC 99
Bh AGFVKTVRGRNGGVKLAKPAAEISVADVVKVTEDNFSMAECFDN-AKSNC 99

Rl PLVDSCGLNSALRKALNAFFAVLSEYSIDDLVKARPQINFLLGITG-EPA 149
Ar PLVDSCGLNSALRKALNAFFDVLTEYSIDDLVKARPQINFLLGLD--ELD 147
Sm PLVDSCGLNAALRKALNAFFEVLQGYTIDDLVKARPQINFLLGLE--EPV 147
Ba PLVDSCGLNAALREALNAFFAVLMKYSIADLVKARPNVRLLLGLD--EME 147
Ml PLVDSCALNSALREALNAFFAVLARYTIADMVAARPNVRNLLGID--MLE 147
Bh PLIDFCSLNTALQKALNAFFDVLSVISLADLQ--RPSFRNQLKIDNREII 147

Rl YR----KPAIVAPAA 160
Ar HRGIAKKMPITAPAA 162
Sm RP--------QTSAA 154
Ba AP---------RIAR 153
Ml RR---------APAA 153
Bh NSN-------HVKGN 155
```

Figure 1.31: Multiple sequence alignment of RirA proteins from six genera of bacteria (accession numbers from top: CAC35510.1, ACM25542.1, CAC45302.1, EFH32853.1, NP_102801.1, YP_033417.1). Grey highlights denote the residue is conserved in all six RirA homologues. The four conserved cysteine residues thought to be ligands for an iron-sulphur cluster are boxed. Alignment constructed using ClustalW2 and Jalview [105, 106]. **Abbreviations:** *Rl – Rhizobium leguminosarum***,** *Ar – Agrobacterium radiobacter, Sm – Sinorhizobium meliloti, Ba – Brucella abortus***,** *Ml – Mesorhizobium loti***,** *Bh – Bartonella henselae*.

```
RirA MRLTKQTNYAVRMLMYCAAN-DGHLSRIPEIAKAYGVSELFLFKI 44
NsrR MRLTNYSDYALRILTYLGLK-REELSTITEIADCYGISRNHVVKI 44
IscR MRLTSKGRYAVTAMLDVALNSEAGPVPLADISERQGISLSYLEQL 45
Rrf2 MKLTTRSRYGTRMLLDIAMHGSEQPVSIKDIAQRQGISVKYLEKL 45

RirA LQPLNKAGLVETVRGRNGGVRLGKPAADISLFDVVRVTEDSFAMA 89
NsrR VHHLGQLGYVDTLRGKNGGIRLAHAPEKINIGEVIRHTETSMDIV 89
IscR FSRLRKNGLVSSVRGPGGGYLLGKDASSIAVGEVISAVDESVDAT 90
Rrf2 IRVLRKAGYITSTLGAHGGYQLAHKAEDIPVGDVVYALEEMEAPV 90

RirA ECFEDDGEVECPLVDSCGLNSALRKALNAFFAVLSEYSIDDLVKA 134
NsrR ECFSNQN--SCIIGCSCVLRTAISEALSAFMAVLDDYTLADLIAP 132
IscR RCQGKG---GCQGGDKCLTHALWRDLSDRLTGFLNNITLGELVNN 132
Rrf2 ECDEENP--CCPRMAVCLTRTIWGEAAKAMYRKLNTFTLADLMRD 133

RirA RPQINFLLGITGEPAYRKPAIVAPAA---- 160
NsrR RRQLSRKLHVMQISDSLSD---------- 151
IscR QEVLDVSGRQHTHDAPRTRIQDAIDVKLRA 162
Rrf2 ASLCPKNACNISPHATH------------ 150
```

Figure 1.32: Multiple sequence alignment of Rrf2 family proteins from four genera of bacteria (accession numbers from top: CAC35510.1, NP841002.1, YP_001459324.1, P33395.1). Grey highlights denote the residue is conserved. The three conserved cysteine residues found in 70% of the Rrf2 members are boxed. Alignment constructed using ClustalW2 and Jalview [105, 106]. **Abbreviations:** RirA– *Rhizobium leguminosarum* rhizobial iron regulator**,** NsrR – *Nitrosomonas europaea* nitrite sensitive repressor, IscR – *Escherichia coli* iron -sulphur cluster regulator, Rrf2 – *Desulfovibrio vulgaris cytochrome* synthesis regulator.

1.3: Aims of the Work Described in the Thesis

The work described in this thesis is divided into two projects. The first subject is RirA, an iron responsive regulator from *R. leguminosarum*. The general objective was a molecular characterisation of RirA, so building on genetic work carried out by the Johnston laboratory at UEA [338, 342]. Specific objectives were as follows:

1. To establish protocols for the growth of *E. coli* strains overexpressing the RirA protein.
2. To establish purification methods in order to obtain quantities of RirA sufficient for detailed characterisation.
3. To determine the fundamental properties of RirA such as oligomeric state and electronic absorption extinction coefficients.
4. By attempting to reconstitute an iron-sulphur cluster in the purified apo-protein, to test the proposal that, in order to function as a repressor, RirA binds such a cluster.
5. To investigate and characterise any iron-sulphur clusters reconstituted in RirA protein using spectroscopic methods such as UV-Visible electronic absorbance, EPR and MCD, and by performing iron and sulphur assays.

The second project involved the cd_1 nitrite reductases from *P. aeruginosa* and *P. pantotrophus* [125, 127]. The objectives for this project were:

1. To adapt previous purification methods to obtain good yields of highly pure protein that did not contain trace contaminants such as pseudoazurin and cytochrome *c*.

2. To investigate the effect of pH on d_1 heme spin state in *P. aeruginosa* cd_1. In the *P. pantotrophus* enzyme, low pH results in a higher proportion of high spin d_1 heme and acceleration of activation by nitrite.

3. To investigate the product of reacting *P. aeruginosa* and *P. pantotrophus* cd_1 with the small ligands NO, NO_2^- and N_3^- and so to investigate the possible existence of a novel Fe^{III}-NO· form of heme nitrosyl at heme d_1.

4. To investigate, by simulation and integration of EPR spectra, whether or not the as prepared samples of *P. aeruginosa* and *P. pantotrophus* cd_1 contain previously unidentified sub-populations of an EPR silent Fe^{III}-NO· form.

5. To investigate the activation of oxidised *P. aeruginosa* and *P. pantotrophus* cd_1 by nitrite through activity assays, and to analyse the effect of pH and H_2O/D_2O on this activation.

6. To investigate the reoxidation of reduced *P. pantotrophus* cd_1 with hydroxylamine. This gives an indication of whether the heme *c* ligand switch, the novel form of d_1 heme or both are required for cd_1 activation.

1.4: References.

1. Anders, E., Grevesse, N. (1989) *Geochim. Cosmochim. Acta* ***53***, 197-214.

2. Sterner, R. W., Elser, J. J. (2002) *Ecological Stoichiometry: The Biology of the Elements from Molecules to the Biosphere.*, Princeton University Press, Princeton.

3. Berner, R. (2006) *Geology* ***34***, 413-415.

4. Boyd, S. R. (2001) *Chem. Geol.* ***176***, 1-30.

5. Canfield, D. E., Glazer, A. N., Falkowski, P. G. (2010) *Science* ***330***, 192-196.

6. Cheng, Q. (2008) *J. Integr. Plant Biol.* ***50***, 786-798.

7. Howard, J. B., Rees, D. C. (2006) *Proc. Natl. Acad. Sci. U. S. A.* ***103***, 17088-17093.

8. Hales, B. J. (1990) *Adv. Inorg. Biochem.* ***8***, 165-198.

9. Rees, D. C., Kim, J., Georgiadis, M. M., Komiya, H., Chirino, A. J., Woo, D., Schlessman, J., Chan, M. K., Joshua-Tor, L., Santillan, G., Chakrabarti, P., Hsu, B. T. (1993) *ACS Symposium series* ***535***, 170-185.

10. Bolin, T. J., Campobasso, N., Muchmore, S. W., Morgan, T. V., Mortenson, L. E. (1993) *Molybdenum Enzymes, Cofactors, and Model Systems*, American Chemical Society, Washington DC.

11. Burns, R. C., Hardy, R. W. F. (1975) *Nitrogen Fixation in Bacteria and Higher Plants*, Springer-Verlag, Berlin.

12. Gage, D. J. (2004) *Microbiol. Mol. Biol. Rev.* ***68***, 280-300.

13. Zehr, J. P. (2011) *Trends Microbiol.* ***19***, 162-173.

14. Prosser, J. I. (1989) *Adv. Microb. Physiol.* ***30***, 125-181.

15. Gilch, S., Meyer, O., Schmidt, I. (2009) *J. Biol. Chem.* ***390***, 863-873.

16. Chain, P., Lamerdin, J., Larimer, F., Regala, W., Lao, V., Land, M., Hauser, L., Hooper, A., Klotz, M., Norton, J., Sayavedra-Soto, L., Arciero, D., Hommes, N., Whittaker, M., Arp, D. (2003) *J. Bacteriol.* ***185***, 2759-2773.

17. Gilch, S., Meyer, O., Schmidt, I. (2010) *Biometals* ***23***, 613-622.

18. Igarashi, N., Moriyama, H., Fujiwara, T., Fukumori, Y., Tanaka, N. (1997) *Nat. Struct. Biol.* ***4***, 276-284.

19. Meincke, M., Bock, E., Kastrau, D. Kroneck, P. M. H. (1992) *Arch. Microbiol.* ***158***, 127-131.

20. Fukuoka, M., Fukumori, Y., Yamanaka, T. (1987) *J. Biochem. (Tokyo)* ***102***, 525-530.

21. Smith, V. H. (2003) *Environ Sci Pollut. Res. Int.* ***10***, 126-139.

22. Camargo, J. A., Alonso, A. (2006) *Environ. Int.* ***32***, 831-849.

23. Camp, N. E. (2007) *J. Emerg. Nurs.* ***33***, 172-174.

24. Majumdar, D. (2003) *Resonance* ***8***, 20-30.

25. Bartsch, H., Spiegelhalder, B. (1996) *Eur. J. Cancer Prev.* ***5***, 11-17.

26. Tricker, A. R., Preussman, R. (1991) *Mutat. Res.* ***259***, 277-289.

27. Greer, F. R., Shannon, M. (2005) *Pediatrics* ***116***, 784-786.

28. Jakszyn, P., Gonzalez, C. A. (2006) *World J. Gastroenterol.* ***12***, 4296-4303.

29. Hecht, S. S. (1999) *Mutat. Res.* ***424***, 127-142.

30. Lijinsky, W., Saavedra, J. E., Kovatch, R. M. (1991) *In Vivo* ***5***, 85-89.

31. Montesano, R. (1981) *J. Supramol. Struct. Cell Biochem.* ***17***, 259-273.

32. Powlson, D. S., Addiscott, T. M., Benjamin, N., Cassman, K. G., de Kok, T. M., van Grinsven, H., L'Hirondel, J. L., Avery, A. A., van Kessel, C. (2008) *J. Environ. Qual.* ***37***, 291-295.

33. Simon, J. (2002) *FEMS Microbiol. Rev.* ***26***, 285-309.

34. Jetten, M. S., Strous, M., van de Pas-Schoonen, K. T., Schalk, J., van Dongen, U. G., van de Graaf, A. A., Logemann, S., Muyzer, G., van Loosdrecht, M. C., Kuenen, J. G. (1998) *FEMS Microbiol. Rev.* ***22***, 421-437.

35. Fuerst, J. (2004) *World Federation for Culture Collections Newsletter.* ***38***, 1-11.

36. Zhang, L., Zheng, P., Tang, C. J., Jin, R. C. (2008) *J. Zheijang Univ. Sci. B.* ***9***, 416-426.

37. Strous, M., Pelletier, E., Mangenot, S., Rattei, T., Lehner, A., Taylor, M. W., Horn, M., Daims, H., Bartol-Mavel, D., Wincker, P., Barbe, V., Fonknechten, N., Vallenet, D., Segurens, B., Schnowitz-Truong, C., Médigue, C., Collingro, A., Snel, B., Dutilh, B. E., Op den Camp, H. J., van der Drift, C., Cirpus, I., van de Pas-Schoonen, K. T., Harhangi, H. R., van Niftrik, L.,

Schmid, M., Keltjens, J., van der Vossenburg, J., Kartal, B., Meier, H., Frishman, D., Huynen, M. A., Mewes, H. W., Weissenbach, J., Jetten, M. S., Wagner, M., Le Paslier, D. (2006) *Nature **440***, 790-794.

38. de Almeida, N. M., Maalcke, W. J., Keltjens, J. T., Jetten, M. S., Kartal, B. (2011) *Biochem. Soc. Trans. **39***, 303-308.

39. Jetten, M. S., Niftrik, L., Strous, M., Kartal, B., Keltjens, J. T., Op den Camp, H. J. (2009) *Crit. Rev. Biochem. Mol. Biol. **44***, 65-84.

40. Murphy, M. J., Siegel, L. M., Tove, S. R., Kamin, H. (1974) *Proc. Natl. Acad. Sci. U. S. A. **71***, 612-616.

41. Einsle, O., Messerschmidt, A., Stach, P., Bourenkov, G. P., Bartunik, H. D., Huber, R., Kroneck, P. M. H. (1999) *Nature **400***, 476-480.

42. Einsle, O., Stach, P., Messerschmidt, A., Simon, J., Kroger, A., Huber, R., Kroneck, P. M. (2000) *J. Biol. Chem. **275***, 39608-39616.

43. Bamford, V. A., Angove, H. C., Seward, H. E., Thomson, A. J., Cole, J. A., Butt, J. N., Hemmings, A. M., Richardson, D. J. (2002) *Biochemistry **41***, 2921-2931.

44. Polyakov, K. M., Boyko, K. M., Tikhonova, T. V., Slutsky, A., Antipov, A. N., Zvyagilskaya, R. A., Popov, A. N., Bourenkov, G. P., Lamzin, V. S., Popov, V. O. (2009) *J. Mol. Biol. **389***, 846-862.

45. Berks, B. C., Ferguson, S. J., Moir, J. W. B., Richardson, D. J. (1995) *Biochim. Biophys. Acta **1232***, 97-173.

46. Zhao, Z., Qiu, W., Koenig, A., Fan, X., Gu, J. D. (2004) *Environ. Technol. **25***, 1201-1210.

47. Galloway, J. N., Townsend, A. R., Erisman, J. W., Bekunda, M., Cai, Z., Freney, J. R., Martinelli, L. A., Seitzinger, S. P., Sutton, M. A. (2008) *Science **320***, 889-892.

48. Wuebbles, D. J. (2009) *Science **326***, 56-57.

49. Ravishankara, A. R., Daniel, J. S., Portmann, R. W. (2009) *Science **326***, 123-125.

50. Dias, J. M., Than, M. E., Humm, A., Huber, R., Bourenkov, G. P., Bartunik, H. D., Bursakov, S., Calvete, J., Caldeira, J., Carneiro, C., Moura, J. J., Moura, I., Romao, M. J. (1999) *Structure **7***, 65-79.

51. Jepson, B. J., Mohan, S., Clarke, T. A., Gates, A. J., Cole, J. A., Butler, C. S., Butt, J. N., Hemmings, A. M., Richardson, D. J. (2007) *J. Biol. Chem. **282***, 6425-6437.

52. Arnoux, P., Sabaty, M., Alric, J., Frangioni, B., Guigliarelli, B., Adriano, J. M., Pignol, D. . (2003) *Nat. Struct. Biol. **10***, 928-934.

53. Butler, C. S., Ferguson, S. J., Berks, B. C., Thomson, A. J., Cheesman, M. R., Richardson, D. J. (2001) *FEBS Lett. **50***, 71-74.

54. Brigé, A., Leys, D., Meyer, T. E., Cusanovich, M. A., van Beeuman, J. J. (2002) *Biochemistry **41***, 4827-4836.

55. Marietou, A., Richardson, D. J., Cole, J. A., Mohan, S. (2005) *FEMS Microbiol. Lett. **248***, 217-225.

56. Bertero, M. G., Rothery, R. A., Palak, M., Hou, C., Lim, D., Blasco, F., Weiner, J. H., Strynadka, N. C. (2003) *Nat. Struct. Biol. **10***, 681-687.

57. Jormakka, M., Richardson, D., Byrne, B., Iwata, S. (2004) *Structure **12***, 95-104.

58. Rothery, R. A., Bertero, M. G., Spreter, T., Bouromand, N., Strynadka, N. C. J., Weiner, J. H. (2010) *J. Biol. Chem. **285***, 8801-8807.

59. Butler, C. S., Richardson, D. J. (2005) *Biochem. Soc. Trans. **33***, 113-118.

60. Zumft, W. G. (1997) *Microbiol. Mol. Biol. Rev. **61***, 533-616.

61. Godden, J. W., Turley, S., Teller, D. C., Adman, E. T., Liu, M. Y., Payne, W. J., LeGall, J. (1991) *Science **253***, 438-442.

62. Kukimoto, M., Nishiyama, M., Murphy, M. E., Turley, S., Adman, E. T., Horinouchi, S., Beppu, T. (1994) *Biochemistry **33***, 5246-5252.

63. Wijma, H. J., Jeuken, L. J., Verbeet, M. P., Armstrong, F. A., Canters, G. W. (2006) *J. Biol. Chem. **281***, 16340-16346.

64. Tocheva, E. I., Rosell, F. I., Mauk, A. G., Murphy, M. E. (2004) *Science **304***, 867-870.

65. MacPherson, I. S., Murphy, M. E. P. (2007) *Cell. Mol. Life Sci. **64***, 2887-2899.

66. Boulanger, M. J., Kukimoto, M., Nishiyama, M., Horinouchi, S., Murphy, M. E. (2000) *J. Biol. Chem. **275***, 23957-23964.

67. Kataoka, K., Furusawa, H., Takagi, K., Yamaguchi, K., Suzuki, S. (2000) *J. Biochem. (Tokyo) **127***, 345-350.

68. Ellis, M. J., Dodd, F. E., Sawers, G., Eady, R. R., Hasnain, S. S. (2003) *J. Mol. Biol. **328***, 429-438.

69. Hino, T., Matsumoto, Y., Nagano, S., Sugimoto, H., Fukumori, Y., Murata, T., Iwata, S., Shiro, Y. (2010) *Science **330***, 1666-1670.

70. Saraste, M., Castresana, J. (1994) *FEBS Lett. **341***, 1-4.

71. van der Oost, J., de Boer, A. P. N., de Gier, J-W. L., Zumft, W. G., Stouthamer, A. H., van Spanning, R. J. M. (1994) *FEMS Microbiol. Lett. **121***, 1-9.

72. Buschmann, S., Warkentin, E., Xie, H., Langer, J. D., Ermler, U., Michel, H. (2010) *Science **329***, 327-330.

73. Zumft, W. G. (2005) *J. Inorg. Biochem. **99***, 194-215.

74. Suharti, S., Heering, H. A., de Vries, S. (2004) *Biochemistry* ***43***, 13487-13495.

75. Field, S. J., Thorndycroft, F. H., Matorin, A. D., Richardson, D. J., Watmough, N. J. (2008) *Methods Enzymol.* ***437***, 79-101.

76. Cheesman, M. R., Zumft, W. G., Thomson, A. J. . (1998) *Biochemistry* ***37***, 3994-4000.

77. Regan, J. J., Ramirez, B. E., Winkler, J. R., Gray, H. B., Malmström, B. G. (1998) *J. Bioenerg. Biomembr.* ***30***, 35-39.

78. Kumita, H., Matusura, K., Hino, T., Takahashi, S., Hori, H., Fukumori, Y., Morishima, I., Shiro, Y. (2004) *J. Biol. Chem.* ***279***, 55247-55254.

79. Ye, R. W., Averill, B. A., Tiedje, J. M. (1994) *Appl. Environ. Microbiol.* ***60***, 1053-1058.

80. Moënne-Loccoz, P. (2007) *Nat. Prod. Rep.* ***24***, 610-620.

81. Watmough, N. J., Field, S. J., Hughes, R. J. L., Richardson, D. J. (2009) *Biochem. Soc. Trans.* ***37***, 392-399.

82. Brown, K., Tegoni, M., Prudencio, M., Perreira, A. S., Besson, S., Moura, J. J., Moura, I., Cambillau, C. (2000) *Nat. Struct. Biol.* ***7***, 191-195.

83. Haltia, T., Brown, K., Tegoni, M., Cambillau, C., Saraste, M., Mattila, K., Djinovic-Carugo, K. (2003) *Biochem. J.* ***369***, 77-88.

84. Paraskevopoulos, K., Antonyuk, S. V., Sawers, R. G., Eady, R. R., Hasnain, S. S. (2006) *J. Mol. Biol.* ***362***, 55-65.

85. Pomowski, A. Z., Zumft, W. G., Kroneck, P. M. H., Einsle, O. (2010) *Acta. Crystallogr. Sect. F. Struct. Biol. Cryst. Commun.* ***66***, 1541-1543.

86. Savelieff, M. G., Lu, Y. (2010) *J. Biol. Inorg. Chem.* ***15***, 461-483.

87. Dell'Acqua, S., Pauleta, S. R., Moura, I., Moura, J. J. (2011) *J. Biol. Inorg. Chem.* ***16***, 183-194.

88. Dell'Acqua, S., Pauleta, S. R., Monzani, E., Pereira, A. S., Casella, L., Moura, J., Moura, I. (2008) *Biochemistry **47***, 10852-10862.

89. Brown, K., Djinovic-Carugo, K., Haltia, T., Cabrito, I., Saraste, M., Moura, J. J., Moura, I., Tegoni, M., Cambillau, C. (2000) *J. Biol. Chem. **275***, 41133-41136.

90. Horio, T., Higashi T., Sasagawa, M., Kusai, M., Nakai, M., and Okunuki, K. (1960) *Biochem. J. **77***, 194-201.

91. Yamanaka, T. (1963) *Anna. Rep. Scient. Works Fac. Sci. Osaka Univ. **11***, 77-115.

92. Yamanaka, T., Ota, A., and Okunuki, K. (1961) *Biochim. Biophys. Acta **53***, 294-308.

93. Singh, J. (1973) *Biochim. Biophys. Acta **333***, 97-173.

94. Timkovich, R., Thrasher, J. S. (1988) *Biochemistry **27***, 5383-5388.

95. Wharton, D. C., Weintraub S. T. (1980) *Biochem. Biophys. Res. Commun. **97***, 236-242.

96. Silvestrini, M. C., Falcinelli, I., Ciabatti, F., Cutruzzolà, F., Brunori, M. (1994) *Biochimie **76***, 641-654.

97. Zennaro, E., Ciabatti, I., Cutruzzolà, F., D'Alessandro, R., Silvestrini, M. C. (1993) *FEMS Microbiol. Lett. **109***, 243-250.

98. Silvestrini, M. C., Galeotti, C. L., Gervais, M., Schininà, E., Barra, D., Bossa, F., Brunori, M. (1989) *FEBS Lett. **254***, 33-38.

99. Fülop, V., Moir J. W. B., Ferguson, S. J., Hadju, J. (1995) *Cell **81***, 369-377.

100. Jüngst, A., Wakabayashi, S., Matsubara, H., Zumft, W. G. (1991) *FEBS Lett. **279***, 205-209.

101. Philippot, L., Mirleau, P., Mazurier, S., Siblot, S., Hartmann, A., Lemanceau, P., Germon, J. C. (2001) *Biochim. Biophys. Acta. **1517***, 436-440.

102. Suzuki, M., Hirai, T., Arai, H., Ishii, M., Igarashi, Y. (2006) *J. Biosci. Bioeng.* ***101***, 391-397.

103. Rees, E., Siddiqui, R. A., Köster, F., Schneider, B., Friedrich, B. (1997) *Appl. Environ. Microbiol.* ***63***, 800-802.

104. Moran, M. A., Buchan, A., González, J. M., Heidelberg, J. F., Whitman, W. B., Kiene, R. P., Henriksen, J. R., King, G. M., Belas, R., Fuqua, C., Brinkac, L., Lewis, M., Johri, S., Weaver, B., Pai, G., Eisen, J. A., Rahe, E., Sheldon, W. M., Ye, W., Miller, T. R., Carlton, J., Rasko, D. A., Paulsen, I. T., Ren, Q., Daugherty, S. C., Deboy, R. T., Dodson, R. J., Durkin, A. S., Madupu, R., Nelson, W. C., Sullivan, S. A., Rosovitz, M. J., Haft, D. H., Selengut, J., Ward, N. (2004) *Nature* ***432***, 910-913.

105. Chenna, R., Sugawara, H., Koike, T., Lopez, R., Gibson, T. J., Higgins, D. G., Thompson, J. D. (2003) *Nucleic Acids Res.* ***31***, 3497-3500.

106. Clamp, M., Cuff, J., Searle, S. M., Barton, G. J. (2004) *Bioinformatics* ***20***, 426-427.

107. Nurizzo, D., Silvestrini, M. C., Mathieu, M., Cutruzzolà, F., Bourgeois, D., Fülop, V., Hadju, J., Brunori, M., Tegoni, M., Cambillau, C. (1997) *Structure* ***5***, 1157-1171.

108. Cutruzzolà, F., Brown, K., Wilson, E. K., Bellelli, A., Arese, M., Tegoni, M., Cambillau, C., Brunori, M. (2001) *Proc. Natl. Acad. Sci. U. S. A.* ***98***, 2232-2237.

109. Sun, W., Arese, M., Brunori, M., Nurizzo, D., Brown, K., Cambillau, C., Tegoni, M., Cutruzzolà, F. (2002) *Biochem. Biophys. Res. Commun.* ***291***, 1-7.

110. Cutruzzolà, F., Arese, M., Grasso, S., Bellelli, A., Brunori, M. (1997) *FEBS Lett.* ***412***, 365-369.

111. Radoul, M., Centola, F., Rinaldo, S., Cutruzzolà, F., Pecht, I., Goldfarb, D. (2009) *Inorg. Chem.* ***48***, 3913-3915.

112. Nurizzo, D., Cutruzzolà, F., Arese, M., Bourgeois, D., Brunori, M., Tegoni, M., Cambillau, C. (1998) *Biochemistry* ***37***, 13987-13996.

113. Kuronen, T., Saraste, N., Ellfork, N. (1975) *Biochim. Biophys. Acta* ***393***, 48-54.

114. Silvestrini, M. C., Tordi, M. G., Citro, G., Vecchini, P., Brunori, M. (1995) *J. Inorg. Biochem.* ***57***, 169-181.

115. Parr, S. R., Barber, D., Greenwood, C., Brunori, M. (1977) *Biochem. J.* ***167***, 447-455.

116. Silvestrini, M. C., Tordi, M. G., Colosimo, A., Antonini, E., Brunori, M. (1982) *Biochem. J.* ***203***, 445-451.

117. Walsh, T. A., Johnson, M. K., Greenwood, C., Barber, D., Springall, J. P., Thomson, A. J. (1979) *Biochem. J.* ***177***, 29-39.

118. Timkovich, R., Cork, M. S. (1983) *Biochim. Biophys. Acta* ***742***, 162-168.

119. Hill, K. E., Wharton, D. C. (1978) *J. Biol. Chem.* ***253***, 489-495.

120. Weeg-Aerssens, E., Wu, W., Ye, R. W., Tiedje, J. M., Chang, C. K. (1991) *J. Biol. Chem.* ***266***, 7496-7502.

121. Muhoberac, B. B., Wharton, D. C. (1983) *J. Biol. Chem.* ***258***, 3019-3027.

122. Montforts, F. P., Mai, G., Romanowski, F., Bats, J. W. (1992) *Tetrahedron Lett.* ***33***, 765-768.

123. Gordon, E. H., Sjogren, T., Lofqvist, M., Richter, C. D., Allen, J. W., Higham, C. W., Hadju, J., Fülop, V., Ferguson, S. J. (2003) *J. Biol. Chem.* ***278***, 11773-11781.

124. Williams, P. A., Fülop, V., Garman, E. F., Saunders, N. F. W., Ferguson, S. J., and Hajdu, J. (1997) *Nature* ***389***, 406-412.

125. Cheesman, M. R., Ferguson, S. J., Moir, J. W. B., Richardson, D. J., Zumft, W. G., Thomson, A. J. (1997) *Biochemistry **36***, 16267-16276.

126. Sutherland, J., Greenwood, C., Peterson, J., Thomson, A. J. (1986) *Biochem. J. **233***, 893-898.

127. van Wonderen, J. H., Knight, C., Oganesyan, V. S., George, S. J., Zumft, W. G., Cheesman, M. R. (2007) *J. Biol. Chem. **282***, 28207-28215.

128. Kobayashi, K., Koppenhofer, A., Ferguson, S. J., Watmough, N. J., Tagawa, S. (2001) *Biochemistry **40***, 8452-8547.

129. Kobayashi, K., Koppenhofer, A., Ferguson, S. J., Tagawa, S. (1997) *Biochemistry **36***, 13611-13616.

130. Rinaldo, S., Sam, K. A., Castiglione, N., Stelitano, V., Arcovito, A., Brunori, M., Allen, J. W. A., Ferguson, S. J., Cutruzzolà, F. (2011) *Biochem. J. **435***, 217-225.

131. Richter, C. D., Allen, J. W., Higham, C. W., Koppenhofer, A., Zajicek, R. S., Watmough, N. J., Ferguson, S. J. (2002) *J. Biol. Chem. **277***, 3093-3100.

132. Sam, K. A., Strampraad, M. J., de Vries, S., Ferguson, S. J. (2008) *J. Biol. Chem. **283***, 27403-27409.

133. Jafferji, A., Allen, J. W., Ferguson, S. J., Fulop, V. (2000) *J. Biol. Chem. **275***, 25089-25094.

134. Koppenhöfer, A., Turner, K. L., Allen, J. W., Chapman, S. K., Ferguson, S. J. (2000) *Biochemistry **39***, 4243-4249.

135. Farver, O., Kroneck, P. M. H., Zumft, W. G., Pecht, I. (2002) *Biophys. Chem. **98***, 27-34.

136. Farver, O., Brunori, M., Cutruzzolà, F.,Rinaldo, S., Wherland, S., Pecht, I. (2009) *Biophys. J. **96***, 2849-2856.

137. Sjogren, T., Hadju, J. (2001) *J. Biol. Chem. **276***, 29450-29455.

138. Pearson, I. V., Page, M. D., van Spanning, R. J., Ferguson, S. J. (2003) *J. Bacteriol.* ***185***, 6308-6315.

139. Vijgenboom, E., Busch, J. E., Canters, G. W. (1997) *Microbiol.* ***143***, 2853-2863.

140. Timkovich, R., Dickerson, R. E. (1976) *J. Biol. Chem.* ***251***, 4033-4046.

141. Almassy, R. J., Dickerson, R. E. (1978) *Proc. Natl. Acad. Sci. U. S. A.* ***75***, 2674-2678.

142. Matsuura, Y., Takano, T., Dickerson, R. E. (1982) *J. Mol. Biol.* ***156***, 389-409.

143. Thompson, G. S., Leung, Y. -C., Ferguson, S. J., Radford, S. E., Redfield, C. (2000) *Protein Sci.* ***9***, 846-858.

144. Kalverda, A. P., Ubbink, M., Gilardi, G., Wijmenga, S. S., Crawford, A., Jeuken, L. J. C., Canters, G. W. (1999) *Biochemistry* ***38***, 12690-12697.

145. Adman, E. T. (1991) *Adv. Protein Chem.* ***42***, 145-197.

146. Adman, E. T., Jensen, L. H. (1981) *Isr. J. Chem.* ***21***, 8-12.

147. Najmudin, S., Pauleta, S. R., Moura, I., Romao, M. J. (2010) *Acta. Crystallogr. Sect. F. Struct. Biol. Cryst. Commun.* ***66***, 627-635.

148. Cutruzzolà, F. (1999) *Biochim. Biophys. Acta.* ***1411***, 231-249.

149. Rinaldo, S., Giardina, G., Castiglione, N., Stelitano, V., Cutruzzolà, F. (2011) *Biochem. Soc. Trans.* ***39***, 195-200.

150. Crane, B. R., Siegel, L. M., Getzoff, E. D. (1997) *Biochemistry* ***36***, 12120-12137.

151. Einsle, O., Messerschmidt, A., Huber, R., Kroneck, P. M. J., Neese, F. (2002) *J. Am. Chem. Soc.* ***124***, 11737-11745.

152. Lukat, P., Rudolf, M., Stach, P., Messerschmidt, A., Kroneck, P. M. H., Simon, J., Einsle, O. (2008) *Biochemistry* ***2008***, 2080-2086.

153. Xu, N., Yi, J., Richter-Addo, G. B. (2010) *Inorg. Chem.* ***49***, 6253-6266.

154. Wyllie, G. R., Scheidt, W. R. (2002) *Chem. Rev.* ***102***, 1067-1090.

155. Nasri, H., Ellison, M. K., Shang, M., Schultz, C. E., Scheidt, W. R. (2004) *Inorg. Chem.* ***43***, 2932-2942.

156. Cheng, L., Powell, D. R., Khan, M. A., Richter-Addo, G. B. (2000) *Chem. Commun.*, 2301-2302.

157. Barber, D., Parr, S. R., Greenwood, C. (1978) *Biochem. J.* ***175***, 239-249.

158. Radoul, M., Bykov, D., Rinaldo, S., Cutruzzola, F., Neese, F., Goldfarb, D. (2011) *J. Am. Chem. Soc.* ***133***, 3043-3055.

159. Antonini, E., Brunori, M. (1971) *Hemoglobin and Myoglobin in their Reactions with Ligands*, North-Holland Publishing Co., Amsterdam.

160. Kim, C. H., Hollocher, T. C. (1983) *J. Biol. Chem.* ***258***, 4861-4863.

161. Wang, Y., Averill, B. A. (1996) *J. Am. Chem. Soc.* ***118***, 3972-3973.

162. George, S. J., Allen, J. W., Ferguson, S. J., Thorneley, R. N. (2000) *J. Biol. Chem.* ***275***, 33231-33237.

163. Cutruzzolà, F., Rinaldo, S., Centola, F., Brunori, M. (2003) *IUBMB Life* ***55***, 617-621.

164. Averill, B. A. (1997) *Chem. Rev.* ***96***, 2951-2964.

165. Fujita, E., Fajer, J. (1983) *J. Am. Chem. Soc.* ***105***, 6743-6745.

166. Olson, L. W., Schaeper, D., Lacon, D., Kadish, K. M. (1982) *J. Am. Chem. Soc.* ***104***, 2042-2044.

167. Rinaldo, S., Arcovito, A., Giardina, G., Castiglione, N., Brunori, M., Cutruzzola, F. (2008) *Biochem. Soc. Trans.* ***36***, 1155-1159.

168. Silvestrini, M. C., Tordi M. G., Musci, G., Brunori, M. (1990) *J. Biol. Chem.* ***265***, 11783-11787.

169. Kharitonov, V. G., Sharma, V. S., Magde, D., Koesling, D. (1997) *Biochemistry* ***36***, 6814-6818.

170. Rinaldo, S., Brunori, M., Cutruzzolà, F. (2007) *Biochem. Biophys. Res. Commun.* ***363***, 662-666.

171. Rinaldo, S., Arcovito, A., Brunori, M., Cutruzzolà, F. (2007) *J. Biol. Chem.* ***282***, 14761-14767.

172. Sam, K. A., Tolland, J. D., Fairhurst, S. A., Higham, C. W., Lowe, D. J., Thorneley, R. N., Allen, J. W., Ferguson, S. J. (2008) *Biochem. Biophys. Res. Commun.* ***371***, 719-723.

173. Sam, K. A., Fairhurst, S. A., Thorneley, R. N., Allen, J. W., Ferguson, S. J. (2008) *J. Biol. Chem.* ***283***, 12555-12563.

174. Zajicek, R. S., Cartron, M. L., Ferguson, S. J., . (2006) *Biochemistry* ***45***, 11208-11216.

175. Munro, A. W., Girvan, H. M., McLean, K. J., Cheesman, M. R., Leys, D. (2008) *Tetrapyroles*, pp 411-434, Landes Bioscience and Springer Science + Business Media.

176. Pettigrew, G. W., Moore, G. R. (1987) *Cytochromes c: Biological Aspects*, Springer-Verlag, Berlin.

177. Lukin, J. A., Ho, C. (2004) *Chem. Rev.* ***104***, 1219-1230.

178. Poulos, T. L. (2006) *Curr. Opin. Struct. Biol.* ***16***, 736-743.

179. Roberts, G. P., Kerby, R. L., Youn, H., Conrad, M. (2005) *J. Inorg. Biochem.* ***99***, 280-292.

180. Shimizu, H., Schuller, D. J., Lanzilotta, W. N., Sundaramoorthy, M., Arciero, D. M., Hooper, A. B., Poulos, T. L. (2001) *Biochemistry* ***40***, 13483-13490.

181. Smulevich, G., Jakopitsch, C., Droghetti, E., Obinger, C. (2006) *J. Inorg. Biochem.* ***100***, 568-585.

182. Layer, G., Reichelt, J., Jahn, D., Heinz, D. W. (2010) *Prot. Sci.* ***19***, 1137-1161.

183. Heinemann, I. U., Jahn, M., Jahn, D. (2008) *Arch. Biochem. Biophys.* ***474***, 238-251.

184. Warren, M. J., Scott, A. I. (1990) *Trends Biochem. Sci.* ***15***, 486-491.

185. Reedy, C. J., Elvekrog, M. M., Gibney, B. R. (2008) *Nucleic Acids Res.* ***36 Database***, D307-313.

186. Bowman, S. E., Bren, K. L. (2008) *Nat. Prod. Rep.* ***25***, 1118-1130.

187. Franken, A. C., Lokman, B. C., Ram, A. F., Punt, P. J., van der Hondel, C. A., de Weert, S. (2011) *Appl. Microbiol. Biotechnol.* ***91***, 447-460.

188. Pettigrew, G. W., Leaver, J. L., Meyer, T. E., Ryle, A. P. (1975) *Biochem. J.* ***147***, 291-302.

189. Hartshorne, R. S., Kern, M., Meyer, B., Clarke, T. A., Karas, M., Richardson, D. J., Simon, J. (2007) *Mol. Microbiol.* ***64***, 1049-1060.

190. Paoli, M., Marles-Wright, J., Smith, A. (2002) *DNA Cell Biol.* ***21***, 271-280.

191. Schneider, S., Marles-Wright, J., Sharp, K. H., Paoli, M. (2007) *Nat. Prod. Rep.* ***24***, 621-630.

192. Bertini, I., Cavallaro, G., Rosato, A. (2006) *Chem. Rev.* ***106***, 90-115

193. Ambler, R. P. (1991) *Biochim. Biophys. Acta.* ***1058***, 42-47.

194. Arciero, D. M., Collins, M. J., Haladjian, J., Bianco, P., Hooper, A. B. (1991) *Biochemistry* ***30***, 11459-11465.

195. Bruschi, M., Woudstra, M., Guigliarelli, B., Asso, M., Lojou, E., Petillot, Y., Abergel, C. (1997) *Biochemistry* ***36***, 10601-10608.

196. Schenkman, J. B., Jansson, I. (2003) *Pharmacol. Ther.* ***97***, 139-152.

197. Xia, D., Yu, C. A., Kim, H., Xia, J. Z., Kachurin, A. M., Zhang, L., Yu, L., Deisenhofer, J. (1997) *Science* ***277***, 60-66.

198. Hamada, K., Bethge, P. H., Mathews, F. S. (1995) *J. Mol. Biol.* ***247***, 947-962.

199. Cheesman, M. R., Thomson, A. J., Greenwood, C., Moore, G. R., Kadir, F. (1990) *Nature **346***, 771-773.

200. Martinez, S. E., Huang, D., Szczepaniak, A., Cramer, W. A., Smith, J. L. (1994) *Structure **2***, 95-105.

201. Rydberg, P., Sigfridsson, E., Ryde, U. (2004) *J. Biol. Inorg. Chem. **9***, 203-223.

202. Walker, F. A., Simonis, V. (1994) *Iron Porphyrin Chemistry, Encyclopedia of Inorganic Chemistry*, Vol. **4**, Wiley, West Sussex, England

203. Garcia-Horsman, J. A., Barquera, B., Rumbley, J., Ma, J., Gennis, R. B. (1994) *J. Bacteriol. **176***, 5587-5600.

204. Jentzen, W., Song, X. Z., Shelnutt, J. A. (1997) *J. Phys. Chem. B. **101***, 1684-1699.

205. Shokhireva, T. K., Berry, R. E., Uno, E., Balfour, C. A., Zhang, H. J., Walker, F. A. (2003) *Proc. Natl. Acad. Sci. U.S.A. **100***, 3778-3783.

206. Ma, J. G., Zhang, J., Franco, R., Jia, S. L., Moura, I., Moura, J. J., Kroneck, P. M., Shelnutt, J. A. (1998) *Biochemistry **37***, 12431-12442.

207. Mogi, T., Saiki, K., Anraku, Y. (1994) *Mol Microbiol. **14***, 391-398.

208. Bravo, J., Verdaguer, N., Tormo, J., Betzel, C., Switala, J., Loewen, P. C., Fita, I. (1995) *Structure **3***, 491-502.

209. Vos, M. H., Borisov, V. B., Liebl, U., Martin, J. L., Konstantinov, A. A. (2000) *Proc. Natl. Acad. Sci. U. S. A. **97***, 1554-1559.

210. Jackson, R. J., Elvers, K. T., Lee, L. J., Gidley, M. D., Wainwright, L. M., Lightfoot, J., Park, S. F., Poole, R. K. (2007) *J. Bacteriol. **189***, 1604–1615

211. Quesada, A., Guijo, M. I., Merchán, F., Blázquez, B., Igeño, M. I., Blasco, R. (2007) *Appl. Environ. Microbiol. **73***, 5118-5124.

212. Chang, C. K., Timkovich, R., Wu, W. (1986) *Biochemistry **25***, 8447-8453.

213. Timkovich, R., Cork, M. S., Taylor, P. V. (1984) *J. Biol. Chem.* ***259***, 1577-1585.

214. Timkovich, R., Cork, M. S., Taylor, P. V. (1984) *J. Biol. Chem.* ***259***, 15089-15093.

215. Chang, C. K., Wu, W. (1986) *J. Biol. Chem.* ***261***, 8593-8596.

216. Micklefield, J., Beckman, M., Mackman, R. L., Block, M. H., Leeper, F. J., Battersby, A. R. (1997) *J. Chem. Soc.* ***Perkin Trans 1***, 2123-2138.

217. Barkigia, K. M., Chang, C. K., Fajer, J., Renner, M. W. (1992) *J. Am. Chem. Soc.* ***114***, 1701-1707.

218. Chang, C. K., Barkigia, K. M., Hanson, L. K., Fajer, J. (1986) *J. Am. Chem. Soc.* ***108***, 1352-1354

219. Balk, J., Lobréaux, S. (2005) *Trends Plant Sci.* ***10***, 324-331.

220. Lill, R., Mühlenhoff, U. (2006) *Annu. Rev. Cell Dev. Biol.* ***22***, 457-486.

221. Ayala-Castro, C., Saini, A., Outten, F. W. (2008) *Microbiol. Mol. Biol. Rev.* ***72***, 110-125.

222. Beinert, H. (2000) *J. Biol. Inorg. Chem.* ***5***, 2-15.

223. Beinert, H., Holm, R. H., Munck, E. (1997) *Science* ***277***, 653-659.

224. Johnson, D. C., Dean, D. R., Smith, A. D., Johnson, M. K. (2005) *Annu. Rev. Biochem.* ***74***, 247-281.

225. Lill, R. (2009) *Nature* ***460***, 831-838.

226. Bandyopadhyay, S., Chandramouli, K., Johnson, M. K. (2008) *Biochem. Soc. Trans.* ***36***, 1112-1119.

227. Jacobson, M. R., Brigle, K. E., Bennett, L. T., Setterquist, R. A., Wilson, M. S., Cash, V. L., Beynon, J., Newton, W. E., Dean, D. E. (1989) *J. Bacteriol.* ***171***, 1017-1027.

228. Jacobson, M. R., Cash, V. L., Weiss, M. C., Laird, N. F., Newton, W. E., Dean, D. R. (1989) *Mol. Gen. Genet.* ***219***, 49-57.

229. Zheng, L., Cash, V. L., Flint, D. H., Dean, D. R. (1998) *J. Biol. Chem.* ***273***, 13264-13272.

230. Takahashi, Y., Nakamura, M. (1999) *J. Biochem.* ***126***, 917-926.

231. Fontecave, M., Ollagnier-de-Choudens, S., Py, B., Barras, F. (2005) *J. Biol. Inorg. Chem.* ***10***, 713-721.

232. Meyer, J. (2008) *J. Biol. Inorg. Chem.* ***13***, 157-170.

233. Link, T. A. (1999) *Adv. Inorg. Chem.* ***47***, 83-157.

234. Calzolai, L., Zhou, Z. H., Adams, M. W. W., La Mar, G. N. (1996) *J. Am. Chem. Soc.* ***118***, 2513-2514.

235. Hunsicker-Wang, L., Heine, A., Chen, Y., Luna, E. P., Todaro, T., Zhang, Y.-M., Williams, P. A., McRee, D. E., Hirst, J., Stout, C. D., Fee, J. A. (2003) *Biochemistry* ***42***, 7303-7317.

236. Lanzilotta, W. N., Christiansen, J., Dean, D. R., Seefeldt, L. C. (1998) *Biochemistry* ***37***, 11376-11384.

237. Peters, J. W., Stowell, M. H., Soltis, S. M., Finnegan, M. G., Johnson, M. K., Rees, D. C. (1997) *Biochemistry* ***36***, 1181-1187.

238. Beinert, H., Kennedy, M. C., Stout, C. D. (1996) *Chem. Rev.* ***96***, 2335-2373.

239. Flint, D. H., Allen, R. M. (1996) *Chem. Rev.* ***96***, 2315-2334.

240. Jarrett, J. T. (2003) *Curr. Opin. Chem. Biol.* ***7***, 174-182.

241. Svetlitchnyi, V., Dobbek, H., Meyer-Klaucke, W., Meins, T., Thiele, B., Römer, P., Huber, R., Meyer, O. (2004) *Proc. Natl. Acad. Sci. U. S. A.* ***101***, 446-451.

242. Crane, B. R., Siegel, L. M., Getzoff, E. D. (1995) *Science* ***270***, 59-67.

243. Nicolet, Y., Cavazza, C., Fontecilla-Camps, J. C. (2002) *J. Inorg. Biochem.* ***91***, 1-8.

244. Dobbek, H., Svetlitchnyi, V., Gremer, L., Huber, R., Meyer, O. (2001) *Science* ***293***, 1281-1285.

245. Kuo, C. F., McRee, D. E., Fisher, C. L., O'Handley, S. F., Cunningham, R. P., Tainer, J. A. (1992) *Science* ***258***, 434-440.

246. Porello, S. L., Cannon, M. J., David, S. S. (1998) *Biochemistry* ***37***, 6465-6475.

247. Smith, J. L., Zaluzec, E. J., Wery, J. P., Niu, L., Switzer, R. L., Zalkin, H., Satow, Y. (1994) *Science* ***264***, 1427-1433.

248. Jameson, G. N., Cosper, M. M., Hernandez, H. L., Johnson, M. K., Huynh, B. H. (2004) *Biochemistry* ***43***, 2022-2031.

249. Duin, E. C., Madadi-Kahkesh, S., Hedderich, R., Clay, M. D., Johnson, M. K. (2002) *FEBS Lett.* ***512***, 263-268.

250. Walters, E. M., Johnson, M. K. (2004) *Photosynth. Res.* ***79***, 249-264.

251. Kiley, P. J., Beinert, H. (2003) *Curr. Opin. Microbiol.* ***6***, 181-185.

252. Demple, B., Ding, H., Jorgenson, M. (2002) *Methods Enzymol.* ***348***, 355-364.

253. Kiley, P. J., Beinert, H. (1998) *FEMS Microbiol. Rev.* ***22***, 341-352.

254. Wallander, M. L., Leibold, E. A., Eisenstein, R. S. (2006) *Biochim. Biophys. Acta* ***1763***, 668-689.

255. Volz, K. (2008) *Curr. Opin. Struct. Biol.* ***18***, 106-111.

256. Rouault, T. A. (2006) *Nat. Chem. Biol.* ***2***, 406-414.

257. Schwartz, C. J., Giel, J. L., Patschkowski, T., Luther, C., Ruzicka, F. J., Beinert, H., Kiley, P. J. (2001) *Proc. Natl. Acad. Sci. U. S. A.* ***98***, 14895-14900.

258. Posey, J. E., Gherardini, F. C. (2000) *Science* ***288***, 1651-1653.

259. Pandey, A., Bringel, F., Meyer, J. -M. (1994) *Appl. Microbiol. Biotechnol.* ***40***, 735-739.

260. Neilands, J. B. (1995) *J. Biol. Chem.* ***270***, 26723-26726.

261. Neilands, J. B. (1982) *Annu. Rev. Microbiol.* ***36***, 285-309.

262. Kehrer, J. P. (2000) *Toxicology* ***149***, 43-50.

263. Neyens, E., Baeyens, J. (2003) *J. Hazard. Mater.* ***98***, 33-50.

264. Andrews, S. C., Robinson, A. K., Rodriguez-Quinones, F. (2003) *FEMS Microbiol. Rev.* ***27***, 215-237.

265. Escolar, L., Pérez-Martín, J., de Lorenzo, V. (1999) *J. Bacteriol.* ***181***, 6223-6229.

266. Hantke, K. (2001) *Curr. Opin. Microbiol.* ***4***, 172-177.

267. Braun, V. (2003) *Front Biosci.* ***8***, 1409-1421.

268. McHugh, J. P., Rodriguez-Quinones, F., Abdul-Tehrani, H., Svistunenko, D. A., Poole, R. K., Cooper, C. E., Andrews, S. C. (2003) *J. Biol. Chem.* ***278***, 29478-29486.

269. Ochsner, U. A., Wilderman, P. J., Vasil, A. I., Vasil, M. L. (2002) *Mol. Microbiol.* ***45***, 1277-1287.

270. Lee, J.-W., Helmann, J. D. (2007) *Biometals* ***20***, 485-499.

271. D'Aquino, J. A., Tetenbaum-Novatt, J., White, A., Berkovitch, F., Ringe, D. (2005) *Proc. Natl. Acad. Sci. U. S. A.* ***102***, 18408-18413.

272. Tao, X., Schiering, N., Zeng, H. Y., Ringe, D., Murphy, J. R. (1994) *Mol. Microbiol.* ***14***, 191-197.

273. Johnston, A. W. B., Todd, J. D., Curson, A. R., Lei, S., Nikolaidou-Katsaridou, N., Gelfand, M. S., Rodionov, D. A. (2007) *Biometals* ***20***, 501-511.

274. Rudolph, G., Hennecke, H., Fischer, H. M. (2006) *FEMS Microbiol. Rev.* ***30***, 631-648.

275. Ernst, F. D., Bereswill, S., Waidner, B., Stoof, J., Mader, U., Kusters, J. G., Kuipers, E. J., Kist, M., van Vliet, A. H., Homuth, G. (2005) *Microbiology* ***151***, 533-546.

276. Holmes, K., Mulholland, F., Pearson, B. M., Pin, C., McNicholl-Kennedy, J., Ketley, J. M., Wells, J. M. (2005) *Microbiology* ***151***, 243-257.

277. Mey, A. R., Wyckoff, E. E., Kanukurthy, V., Fisher, C. R., Payne, S. M. (2005) *Infect. Immun.* ***73***, 8167-8178.

278. Cornelis, P., Matthijs, S., Van Oeffelen, L. (2009) *Biometals* ***22***, 15-22.

279. Delany, I., Rappuoli, R., Scarlato, V. (2004) *Mol. Microbiol.* ***52***, 1081-1090.

280. Bsat, N., Helmann, J. D. (1999) *J. Bacteriol.* ***181***, 4299-4307.

281. Hantke, K. (1984) *Mol. Gen. Genet.* ***197***, 337-341.

282. Saito, I., Wormald, M. R., Williams, R. J. P. (1991) *Eur. J. Biochem.* ***197***, 29-38.

283. Coy, M., Neilands, J. B. (1991) *Biochemistry* ***30***, 8201-8210.

284. Stojiljkovic, I., Hantke, K. (1995) *Mol. Gen. Genet.* ***247***, 199-205.

285. Bagg, A., Neilands, J. B. (1987) *Biochemistry* ***26***, 5471-5477.

286. Althaus, E. W., Outten, C. E., Olson, K. E., Cao, H., O'Halloran, T. V. (1999) *Biochemistry* ***38***, 6559-6569.

287. Mills, S. A., Marletta, M. A. (2005) *Biochemistry* ***44***, 13553-13559.

288. Escolar, L., Pérez-Martín, J., de Lorenzo, V. (1998) *J. Mol. Biol.* ***283***, 537-547.

289. Baichoo, N., Helmann, J. D. (2002) *J. Bacteriol.* ***184***, 5826-5832.

290. Lavrrar, J. L., Mcintosh, M. A. (2003) *J. Bacteriol.* ***185***, 2194-2202.

291. Masse, E., Gottesman, S. (2002) *Proc. Natl. Acad. Sci. U. S. A.* ***99***, 4620-4625.

292. Pohl, E., Haller, J. C., Mijovilovich, A., Meyer-Klaucke, W., Garman, E., Vasil, M. L., . (2003) *Mol. Microbiol.* ***47***, 903-915.

293. Dian, C., Vitale, S., Leonard, G. A., Bahlawane, C., Fauquant, F., Leduc, D., Muller, C., De Reuse, H., Michaud-Soret, I., Terradot, L. (2011) *Mol. Microbiol.* ***79***, 1260-1275.

294. Sheikh, M. A., Taylor, G. L. (2009) *Mol. Microbiol.* ***72***, 1208-1220.

295. Pecqueur, L., D'Autreaux, B., Dupuy, J., Nicolet, Y., Jacquamet, L., Brutscher, B., Michaud-Soret, I., Bersch, B. (2006) *J. Biol. Chem.* ***281***, 21286-21295.

296. Vitale, S., Fauquant, C., Lascoux, D., Schauer, K., Saint-Pierre, C., Michaud-Soret, I. (2009) *Biochemistry* ***48***, 5582-5591.

297. Johnston, A. W. B., Yeoman, K. H., Wexler, M. (2001) *Adv. Microb. Physiol.* ***45***, 113-156.

298. Wexler, M., Todd, J. D., Kolade, O., Bellini, D., Hemmings, A. M., Sawers, G., Johnston, A. W. B. (2003) *Microbiology* ***149***, 1357-1365.

299. Bellini, P., Hemmings, A. M. (2006) *Biochemistry* ***45***, 2686-2698.

300. Diaz-Mireles, E., Wexler, M., Sawers, G., Bellini, D., Todd, J. D., Johnston, A. W. B. (2004) *Microbiology* ***150***, 1447-1456.

301. Diaz-Mireles, E., Wexler, M., Todd, J. D., Bellini, D., Johnston, A. W. B., Sawers, G. (2005) *Microbiology* ***151***, 4071-4078.

302. Patzer, S. I., Hantke, K. (1998) *Mol. Microbiol.* ***28***, 1199-1210.

303. Gaballa, A., Helmann, J. D. (1998) *J. Bacteriol.* ***180***, 5815-5821.

304. Ahn, B. E., Cha, J., Lee, E. J., Han, A. R., Thompson, C. J., Roe, J. H. (2006) *Mol. Microbiol.* ***59***, 1848-1858.

305. Ghassemian, M., Straus, N. A. (1996) *Microbiology **142***, 1469-1476.

306. Bsat, N., Herbig, A., Casillas-Martinez, L., Setlow, P., Helmann, J. D. (1998) *Mol. Microbiol. **29***, 189-198.

307. Heidrich, C., Hantke, K., Bierbaum, G., Sahl, H. G. (1996) *FEMS Microbiol. Lett. **140***, 253-259.

308. Holmes, R. K. (2000) *J. Infect. Dis. **181 Supp. 1***, S156-167.

309. Boyd, J., Oza, M. N., Murphy, J. R. (1990) *Proc. Natl. Acad. Sci. U. S. A. **87***, 5968-5972.

310. Schmitt, M. P., Predich, M., Doukhan, L., Smith, I., Holmes, R. K. (1995) *Infect. Immun. **63***, 4284-4289.

311. Ding, X., Zeng, H., Schiering, N., Ringe, D., Murphy, J. R. (1996) *Nat. Struct. Biol. **3***, 382-387.

312. Goranson-Siekierke, J., Pohl, E., Hol, W. G. J., Holmes, R. K. (1999) *Infect. Immun. **67***, 1806-1811.

313. Pohl, E., Holmes, R. K., Hol, W. G. J. (1999) *J. Mol. Biol. **292***, 653-667.

314. Wang, G., Wylie, G. P., Twigg, P. D., Caspar, D. L. D., Murphy, J. R., Logan, T. M. (1999) *Proc. Natl. Acad. Sci. U. S. A. **96***, 6119-6124.

315. Rangachari, V., Marin, V., Bienkiewicz, E. A., Semavina, M., Guerrero, L., Love, J. F., Murphy, J. R., Logan, T. M. (2005) *Biochemistry **44***, 5672-5682.

316. Brune, I., Werner, H., Hüser, A. T., Kalinowski, J., Pühler, A., Tauch, A. (2006) *BMC Genomics **7:21***.

317. Wennerhold, J., Bott, M. (2006) *J. Bacteriol. **188***, 2907-2918.

318. Tao, X., Murphy, J. R. (1994) *Proc. Natl. Acad. Sci. U. S. A. **91***, 9646-9650.

319. Lee, J. H., Wang, T., Ault, K., Liu, J., Schmitt, M. P., Holmes, R. K. (1997) *Infect. Immun. **65***, 4273-4280.

320. Spiering, M. M., Ringe, D., Murphy, J. R., Marletta, M. A. (2003) *Proc. Natl. Acad. Sci. U. S. A.* ***100***, 3808-3813.

321. Tao, X., Murphy, J. R. (1992) *J. Biol. Chem.* ***267***, 21761-21764.

322. Tao, X., Boyd, J., Murphy, J. R. (1992) *Proc. Natl. Acad. Sci. U. S. A.* ***89***, 5897-5901.

323. Schmitt, M. P., Holmes, R. K. (1993) *Mol. Microbiol.* ***9***, 173-181.

324. Qiu, X., Pohl, E., Holmes, R. K., Hol, W. G. J. (1996) *Biochemistry* ***35***, 12292-12302.

325. Qiu, X., Verlinde, C. L. M. J., Zhang, S., Schmitt, M. P., Holmes, R. K., Hol, W. G. J. (1995) *Structure* ***3***, 87-100.

326. Schiering, N., Tao, X., Zeng, H., Murphy, J. R., Petsko, G. A., Ringe, D. (1995) *Proc. Natl. Acad. Sci. U. S. A.* ***92***, 9843-9850.

327. Pohl, E., Qiu, W., Must, L. M., Holmes, R. K., Hol, W. G. J. (1997) *Prot. Sci.* ***6***, 1114-1118.

328. Todd, J. D., Sawers, G., Rodionov D. A., Johnson, A. W. B. (2006) *Mol. Genet. Genomics* ***275***, 564-577.

329. Small, S. K., Puri, S., Sangwan, I., O'Brian, M. R. (2009) *J. Bacteriol.* ***191***, 1361-1368.

330. Hamza, I., Chauhan, S., Hassett, R., O'Brian, M. R. (1998) *J. Biol. Chem.* ***273***, 21669-21674.

331. Small, S. K., Puri, S., O'Brian, M. R. (2009) *Biometals* ***22***, 89-97.

332. Singleton, C., White, G. F., Todd, J. D., Marritt, S. J., Cheesman, M. R., Johnston, A. W. B., Le Brun, N. E. (2010) *J. Biol. Chem.* ***285***, 16023-16031.

333. White, G. F., Singleton, C., Todd, J. D., Cheesman, M. R., Johnston, A. W. B., Le Brun, N. E. (2011) *FEBS J.*, [Epub ahead of print].

334. Yang, J. H., Ishimori, K., O'Brian, M. R. (2005) *J. Biol. Chem.* ***280***, 7671-7676.

335. Ishikawa, H., Nakagaki, M., Bamba, A., Uchida, T., Hori, H., O'Brian, M. R., Iwai, K., Ishimori, K. (2011) *Biochemistry* ***50***, 1016-1022.

336. Sangwan, I., Small, S. K., O'Brian, M. R. (2008) *J. Bacteriol.* ***190***, 5172-5177.

337. Hohle, T. H., O'Brian, M. R. (2010) *J. Biol. Chem.* ***285***, 26074-26080.

338. Todd, J. D., Wexler, M., Sawers, G., Yeoman, K. H., Poole, P. S., Johnston, A. W. B. (2002) *Microbiology* ***148***, 4059-4071.

339. Chao, T. C., Buhrmester, J., Hansmeier, N., Puhler, A., Weidner, S. (2005) *Appl. Environ. Microbiol.* ***71***, 5969-5982.

340. Ngok-Ngam, P., Ruangkiattikul, N., Mahavihakanont, A., Virgem, S. S., Sukchawalit, R., Mongkolsuk, S. (2009) *J. Bacteriol.* ***191***, 2083-2090.

341. Kitphati, W., Ngok-Ngam, P., Suwanmaneerat, S., Sukchawalit, R., Mongkolsuk, S. (2007) *Appl. Environ. Microbiol.* ***73***, 4760-4768.

342. Todd, J. D., Sawers, G., Johnston, A. W. B. (2005) *Mol. Genet. Genomics* ***273***, 197-206.

343. Viguier, C. O., Cuiv, P., Clarke, P., O'Connell, M. (2005) *FEMS Microbiol. Lett.* ***246***, 235-242.

344. Yeoman, K. H., Curson, A. R. J., Todd, J. D., Sawers, G., Johnston, A. W. B. (2004) *Microbiology* ***150***, 4065-4074.

345. Rodionov, D. A., Gelfand, M. S., Todd, J. D., Curson, A. R. J., Johnston, A. W. B. (2006) *PLoS Comput. Biol.* ***2***, e163.

346. Keon, R. G., Fu, R. D., Voordouw, G. (1997) *Arch. Microbiol.* ***167***, 376-383.

347. Giel, J. L., Rodionov, D., Liu, M., Blattner, F. R., Kiley, P. J. (2006) *Mol. Microbiol.* ***60***, 1058-1075.

348. Beaumont, H. J. E., Lens, S. I., Reijnders, W. N. M., Westerhoff, H.V., van Spanning, R. J. M. (2004) *Mol. Microbiol.* ***54***, 148-158.

349. Bodenmiller, D. M., Spiro, S. (2006) *J. Bacteriol.* ***188***, 874-881.

Chapter 2.

Experimental techniques

2.1: General Materials, Methods and Techniques.

This chapter describes the techniques, procedures and methods used in all parts of this work. Methods that are unique to specific projects, such as the purification of RirA, are described in more detail in later chapters.

2.1.1: Buffer and Growth Media Preparation.

All buffer and growth media components were weighed out in weighing boats using either Ohaus Adventurer weighing scales for quantities in grams or Ohaus Explorer weighing scales for quantities in milligrams. All buffer solutions and growth media were prepared using distilled water or D_2O in some experimental cases. Buffers made with D_2O are given a pH* value, where pH* is the apparent pH of the D_2O solutions measured using a standard glass electrode. pH was measured using a Hanna Instruments pH 210 Microprocessor pH meter. Unless stated, concentrated hydrochloric acid was used to lower the pH and 5 M sodium hydroxide used to raise the pH. Whilst adjusting the pH, the buffer is stirred using a stirrer bar powered by a Stuart SB161 stirrer plate. Buffer required for anaerobic use was sparged with nitrogen or argon (depending on buffer volume and headspace) for at least an hour. The gas used for sparging was fed through a line and bubbles through the buffer via a needle. Any possible points of entry for oxygen were sealed with Parafilm except for a pressure outlet. This outlet was a second needle. The buffer was kept moving slowly with a stirrer bar and a Stuart SB161 stirrer plate. Growth

media once made was autoclaved in a LTE Scientific Kestrel autoclave on a media cycle before any bacterial growth cultures were commenced.

2.1.2: Anaerobic Experiments.

Anaerobic work was performed in multiple glove boxes. A Faircrest anaerobic glove box was used in the preparation of reconstituted RirA and NO saturated solutions. A Belle glove box containing a small Belle anaerobic fridge was used to store sensitive reconstituted RirA samples and carry out oxygen experiments on reconstituted RirA. Finally another Belle anaerobic glove box was used in preparing cd_1 for EPR and MCD spectroscopy and to carry out activity assays on cd_1. Anaerobic solutions of certain compounds or proteins such as nitrite and reduced horse heart cytochrome *c* in cd_1 assays were prepared by weighing out the correct amount before transferring into the glove box. The solutions were then prepared in the anaerobic glove box using prepared anaerobic buffer. All buffers were thoroughly sparged (see buffer and growth media preparation section) and left at least overnight before being used as anaerobic buffer solutions.

2.1.3: General Protein Purification Technique.

The S200 gel filtration column, DEAE-Sepharose column, Phenyl-Sepharose column and all HiTrap columns were stored in 20% ethanol (absolute ethanol diluted with water) at room temperature when not in use. In the *Pseudomonas aeruginosa* cd_1 and RirA preparations the CM, DEAE and Heparin columns were from the HiTrap range of columns. The gel filtration column used in all three preparations was a HiPrep 26/60 S200 gel filtration column. The 500 mL volume of DEAE-Sepharose used in the preparation of *Paracoccus pantotrophus* cd_1 was contained in a XK 50

column. The column was packed using a reservoir to obtain uniform packing of the DEAE-Sepharose medium. The Phenyl-Sepharose column in the *P. pantotrophus* cd_1 preparation was also packed by hand. The 15 mL of Phenyl-Sepharose medium was contained in a 16/20 column. This column was regularly cleaned and repacked as contaminants that tightly bind to the medium tend to build up quickly and proteins can precipitate in the medium causing blockages. The cleaning procedure involved pouring the medium out of the column. The medium was then washed in 1 M sodium hydroxide to remove precipitated protein and 70% ethanol to remove any tightly bound protein. The medium was washed in distilled water before being repacked. 10 column volumes of distilled water were then run through the column before storage in 20% ethanol to stop microbiological growth. Columns are used either in conjunction with an ÄKTAprime Plus purification system connected to Primeview, or they were fitted with a syringe adaptor so buffer could be syringed through the medium. Purification steps using the ÄKTAprime Plus system use the fraction collector with 13 mL plastic test tubes to collect protein fractions.

2.1.4: Concentration of Protein Samples.

The concentration of protein samples used different methods depending on sample volumes. When the volume of protein was in the microlitre to low millilitre range, 10000 MWCO Microcons were used with a Sigma bench top microcentrifuge. Millipore 3000 MWCO Centricons were used in conjunction with an ALC PK121R centrifuge with an A-M10 rotor for volumes of tens of millilitres. Larger volumes than this are concentrated using an Amicon 8050 ultrafiltration cell under argon pressure with an YM10 filter disc.

2.1.5: SDS-PAGE.

SDS-PAGE was carried out using Hoefer SE 250 gel apparatus. Firstly the back plate, glass front plate and side pieces were clamped together. The gel caster was then assembled as per instructions but molten agar was pipetted along the rubber seal. This was allowed to set to provide a tighter seal when the unset liquid gel is transferred to the plates. Table 2.01 shows the components required to make two separating gels of different percentages.

Required chemicals / solvents	**12% Running Gel**	**15% Running Gel**	**4% Stacking Gel**
Water	10 mL	7 mL	6.15 mL
Tris (1M) pH 8.8	7.5 mL	7.5 mL	n/a
Tris (1M) pH 6.8	n/a	n/a	2.5 mL
SDS (10% w/v)	300 μL	300 μL	50 μL
30% Acrylamide/Bis Solution (37.5:1)	12 mL	15 mL	1.35 mL
Ammonium persulphate (10% w/v)	150 μL	150 μL	50 μL
TEMED	20 μL	20 μL	10 μL

Table 2.01: The volumes required for the different components of resolving and stacking gels in SDS-PAGE. These were scaled up and down as required. Abbreviations, Tris - tris(hydroxymethyl)aminomethane, SDS - sodium dodecyl sulphate, TEMED - N,N,N’,N’-tetra-methyl-ethylenediamine.

The 15% gel gives a better resolution for the smaller proteins, whereas the 12% is better for higher molecular proteins. Once the percentage is chosen, the components listed in Table 1.01 were combined apart from the ammonium persulphate and N,N,N’,N’-tetra-methyl-ethylenediamine (TEMED). The ammonium persulphate and

TEMED were only added when the separating gels were ready to be cast. A 1.5-2 cm gap is left at the top for the stacking gel. Water was carefully layered onto the top of the separating gel to remove bubbles and level up the top. The separating gel was then left to set. Once the gel was completely set then the water was carefully poured off. The stacking gel was then prepared. Again, the components listed in Table 1.01 were combined except for the ammonium persulphate and the TEMED. They were only added when the stacking gel was ready to pour. The stacking gel was poured such that the gel level reached the top of the plate. A comb was then placed at the top of the plate to create lanes for protein loading. The stacking gel was then left to set. Once this had set, the plates with the contained gel could be removed from the caster and clamp. The plate was then clipped onto the tank and buffer chamber core. The sample wells and tank were then filled with running buffer. A 5x concentrated solution of running buffer contains 15 g/L tris(hydroxymethyl)aminomethane (Tris), 72 g/L glycine and 5 g/L sodium dodecyl sulphate (SDS). This was then diluted 5 times to create a 1x solution to use in SDS-PAGE. A running lane decal was then placed on the plate to show the position of the lanes. The comb was then removed so loading can proceed. The first lane was filled with 5 μL of Biorad Precision plus All Blue Standard. This is the protein marker with a range of 10 – 250 kDa. The protein sample concentration was dependant on the purpose of the gel. As a general rule the sample should contain at least 10 μg of protein, but some gels in this work are heavily overloaded so trace contaminating protein could be detected. A maximum of 20 μL could be transferred into each well. This consisted of 10 μL of a suitably concentrated protein sample and 10 μL of loading buffer. Loading buffer consists of the components listed in Table 2.02

Required chemicals / solvents and final concentrations	**Stock solution**	**Required volume / weight**
100 mM Tris pH 6.8	1 M Tris pH 6.8	1 mL of stock solution
200 mM DTT	1 M DTT	2 mL of stock solution
4% SDS (w/v)	10% SDS	4 mL of stock solution
20% Glycerol	100% Glycerol	2 mL of 100% Glycerol
0.2% Bromophenol Blue (w/v)	n/a	20 mgs
Water	n/a	1 mL

Table 2.02: Components required for making 10 ml of protein loading buffer. Abbreviations, Tris - tris(hydroxymethyl)aminomethane, DTT – dithiothreitol, SDS - sodium dodecyl sulphate.

Each sample to be tested was transferred to a well using a 20 μL Gilson pipette. Once all the samples were loaded the decal was removed, the buffer levels were checked and the lid was clicked into place. The cables from the lid were connected to a Consort E844 power pack. The power pack was switched on and the voltage adjusted to 180 mV. The gel was left to run for 45 mins to 1 hour until the markers are clearly resolved. The gel was then removed from the apparatus and put into a plastic tray. A sufficiently amount of Coomassie stain to cover the gel was poured into the tray. The stain is prepared by dissolving 1 g of Brilliant Blue in 500 mL water, 400 mL methanol and 100 mL acetic acid. The gel was left in the stain for an hour on a Thermo Scientific MaxQ 2000 shaker. The stain was then discarded and replaced with a destain solution. This was prepared by mixing 700 mL water, 200 mL methanol and 100 mL acetic acid. The gel was then left on the shaker and in destain until all markers and protein bands could be clearly seen. Once the bands were clear

to see the gel could be put between two pieces of transparency film and scanned using a HP Scanjet 2400 scanner.

2.2: Materials, Methods and Techniques Used for the RirA Project.

The following techniques and procedures were used only in the RirA project.

2.2.1: Determination of the Extinction Coefficient of RirA Apoprotein.

A 2 ml sample of 40 μM RirA protein in 50 mM HEPES pH 7.5 was prepared. Sample and reference quartz cuvettes were then prepared with 2 mL of 50 mM HEPES pH 7.5 in each. These cuvettes were then measured in a Helios spectrophotometer to establish a baseline. Once the baseline was established, 1 mL of RirA sample was then placed into a 1 cm pathlength quartz cuvette. The volume was then made up to 2 mL by addition of 1 mL of 50 mM HEPES pH 7.5. The solutions were then stirred carefully using a glass rod. The cuvette was then placed in the spectrophotometer. A spectrum is then measured from 260-360 nm. The absorbance at 280 nm was then recorded. This was the 280 nm native absorbance value.

A further 1 mL of RirA was placed into a 1 cm pathlength quartz cuvette. The volume was then again made up to 2 mL through addition of 6.6 M guanidine-HCl in 75 mM HEPES pH 7.5. A glass rod was again used to carefully stir the solutions together. The cuvette is placed in the spectrophotometer and a spectrum was recorded at 260-360 nm. The absorbance at 280 nm was again recorded. This was the 280 nm denatured absorbance value. The estimated extinction coefficient is then calculated using Equation 1.

$$\varepsilon_{\text{Native 280 nm}} = \varepsilon_{\text{Denatured 280 nm}} \times (A_{\text{Native 280 nm}}/A_{\text{Denatured 280 nm}}) \quad (1)$$

The $\varepsilon_{\text{Denatured 280 nm}}$ was calculated from the amount of tryptophans, tyrosines and cysteines in the amino acid sequence. In RirA there are five tyrosines and four cysteines. From model compounds the extinction coefficients are known at 280 nm for tyrosine and cysteine, 1,490 and 125 M^{-1} cm^{-1} respectively [1]. Therefore a RirA monomer has a $\varepsilon_{\text{Denatured 280 nm}}$ of 6925 M^{-1} cm^{-1}. This extinction coefficient then needs to be multiplied by the ratio of $A_{\text{Native 280 nm}}/A_{\text{Denatured 280 nm}}$ to get an estimated $\varepsilon_{\text{Native 280 nm}}$.

2.2.2: Biorad (Bradford) Protein Assays.

A 1 mg/mL solution of bovine serum albumen (BSA) was made using the buffer that the sample protein is contained in. The stock solution of BSA was transferred to 13 mL plastic test tubes in volumes of 0, 20, 40, 60, 80 and 100 μL. These stock solutions were diluted accordingly with buffer to make the final volume 100 μL. This gave a range of concentrations from 0 mg/mL BSA to 1.0 mg/mL BSA in increments of 0.2 mg/mL. As well as these standards, two samples of protein of unknown concentration, volumes 25 and 50 μL were transferred to two 13 mL test tubes. These unknown samples were also diluted to a final volume of 100 μL. A working strength Biorad dye is then made by adding one part Biorad dye-reagent concentrate with four parts buffer. To each of the 13 mL test tubes was added 5 mL of working strength Biorad dye. Each test tube was vortexed briefly to mix. The samples were left for 15 mins to allow colour to develop. In the presence of protein the dye-reagent will change from red-brown to blue. After 15 mins had elapsed the samples were measured in a Helios spectrophotometer using 1 mL, 1 cm pathlength cuvettes. Because absorbance increases over time with this assay, three runs were performed in succession. A standard curve for each run is drawn from which the

concentrations of protein can be calculated. If the values are close for the multiple runs then an average was used. If the subsequent concentration calculations for the two unknown samples are also close then again an average was used. This is used as the final protein concentration.

2.2.3: Iron Assays.

112 μL of BDH Spectrosol standard iron solution was diluted to 10 mL with water to give a final iron standard concentration of 200.133 μM. Incremental volumes of the standard iron solution (0, 10, 20, 30, 40, 50, 60, 70, 80, 90 and 100 μL) were transferred to 2 mL screw top Eppendorf tubes. Screw top Eppendorf tubes were used so the lids did not open when tubes were heated at 90°C after nitric acid addition later in the assay preparation. Each Eppendorf tube containing the iron solution was diluted with water to give a final volume of 100 μL. This gives a range of iron concentrations from 0 to 200.133 μM. Two more Eppendorf tubes containing 10 μL and 20 μL of solution with unknown iron concentration were prepared. These were also diluted with water to give a final volume of 100 μL. To each of the samples was added 100 μL of 21.7% nitric acid. The samples were incubated on a Grant heat block for 30 min at 90°C. The heated samples were then placed in a freezer to cool for 20 min. The samples were then centrifuged at 9000 x g (10000 rpm) for 30 seconds in a Sigma bench top centrifuge to collect the resulting condensate. Then 0.6 mL of 7.5% ammonium acetate, 100 μL of ascorbic acid and 100 μL of 10 mM ferene were added to the samples. Each sample was vortexed briefly to allow mixing. The reactions were allowed to develop for 30 mins before each sample was analysed at an absorbance of 593 nm. Assay mixtures produce a dark blue colour in the presence of iron. A standard curve was drawn and the iron

concentrations of the two unknown samples were calculated. If the calculated iron concentrations were similar then an average could be taken to give a final iron concentration.

2.2.4: Sulphide Assays.

A 500 mL solution of 10 mM NaOH solution was prepared. The solution was then sparged with nitrogen to make the solution anaerobic. Approximately 0.25 g of sodium sulphide was added to the anaerobic solution to make a sulphide standard solution. In Eppendorf tubes were added 0, 5, 10, 15, 20 and 25 μL of the sulphide solution. These were diluted with water to make a final volume of 200 μL. A 10 μL and 20 μL aliquot of solution with an unknown sulphide concentration were transferred to Eppendorf tubes. These aliquots were diluted to a volume of 200 μL with water. Separately to each tube is added 0.6 mL 1% zinc acetate and 50 μL 12% sodium hydroxide. The two unknown sulphide concentration samples were left last. The precipitation was allowed to occur for 15 min. The samples were placed in a Sigma bench top centrifuge and spun at 500 x g (1500 rpm) for 5 minutes to collect the precipitate. Then separately for each tube, 150 μL of 0.1% DMPD (in 5 M HCl) was added slowly in a swirling motion so that the precipitate disappeared. As soon as the precipitate disappeared, 150 μL of 10 mM iron chloride (in 1 M HCl) was added. The samples were vortexed and allowed to develop a turquoise colour for 30 mins. The sample absorbance was then measured at 670 nm. A standard curve was drawn from which the concentrations of sulphide could be calculated. If the two calculations were of similar value then the average was taken as the final sulphide concentration.

2.3: Materials, Methods and Techniques Used for the cd_1 Project.

The following techniques and procedures were applied only to the cd_1 project.

2.3.1: Purification of *Pseudomonas aeruginosa* cd_1.

The purification of *P. aeruginosa* cd_1 was performed as described in the thesis of Parr [2] with the following modifications. The *P. aeruginosa* cells were subjected to an anaerobic processing stage after harvesting (see Anaerobic Processing). This was to ensure that the cells produced a good yield of cd_1 protein. Omitting this stage can occasionally result in the absence of cd_1 in the cell extract. The column stages were also altered from the Parr thesis. The DEAE stage was conducted using a Hi-Trap column and not a DEAE gel slurry. The DEAE stage was performed multiple times to ensure complete removal of contaminants such as flavoproteins. The Sephadex G75 gel filtration column was replaced with a S200 26/60 gel filtration column and the Amberlite CG-50 was replaced with a Hi-Trap CM ion-exchange column. The cd_1 protein was deemed ready for use if there were no contaminating bands on SDS-PAGE corresponding to azurin or cytochrome *c* and the A_{412nm}/A_{280nm} was greater than 1.25.

2.3.2: Purification of *Paracoccus pantotrophus* cd_1.

The purification of *P. pantotrophus* cd_1 is performed as described in Moir *et al*. [3] with the following modifications. As with the *P. aeruginosa* cd_1 preparation, the *P. pantotrophus* cells were subjected to an anaerobic processing stage after harvesting to ensure a good yield. The only chromatography column change was the replacement of the sometimes used second DEAE stage with a S200 26/60 gel

filtration column. This was found to remove smaller protein contaminants such as pseudoazurin much more effectively than DEAE ion-exchange and without the need to dialyse out any salt afterwards. Removing proteins such as pseudoazurin is important as they have been shown to affect kinetic and spectroscopic data [4]. Like with the *P. aeruginosa* preparation, the cd_1 protein was deemed ready for use if there were no contaminating bands on SDS-PAGE corresponding to pseudoazurin or cytochrome *c* and the A_{412nm}/A_{280nm} was greater than 1.25.

2.3.3: Anaerobic Processing.

Once the cells were harvested from the cultures they were resuspended in a minimum volume of the spent medium supernatant. This decrease in volume creates a dense culture which will go anaerobic rapidly during sparging in the sparging fridge. The arrangement of the anaerobic fridge is shown schematically in Figure 2.01. Initially the gas delivery system taps for both INLET and OUTLET lines were switched to the off position. The gas delivery system and lid of the anaerobic bottle were wiped with a tissue saturated in 70% (v/v) ethanol. This includes the delivery tubing for both INLET and OUTLET lines, the glass frit and the inside of the screw top lids. This was done for at least a minute to ensure that contamination was kept to a minimum. The delivery system was then screwed onto a pre-sterilised 1 L screw-top bottle which acted as an anaerobic growth flask. Using sterile technique, the newly resuspended culture was transferred to the anaerobic growth flask, ensuring that the level of culture in the bottle was 700-800 mL as a maximum volume. The culture then had 10 g/L $NaNO_3$ added. This was mixed well via vigorous swirling of the bottle. Then 0.2% (v/v) or 2 mL per litre Antifoam 204 was added to the culture

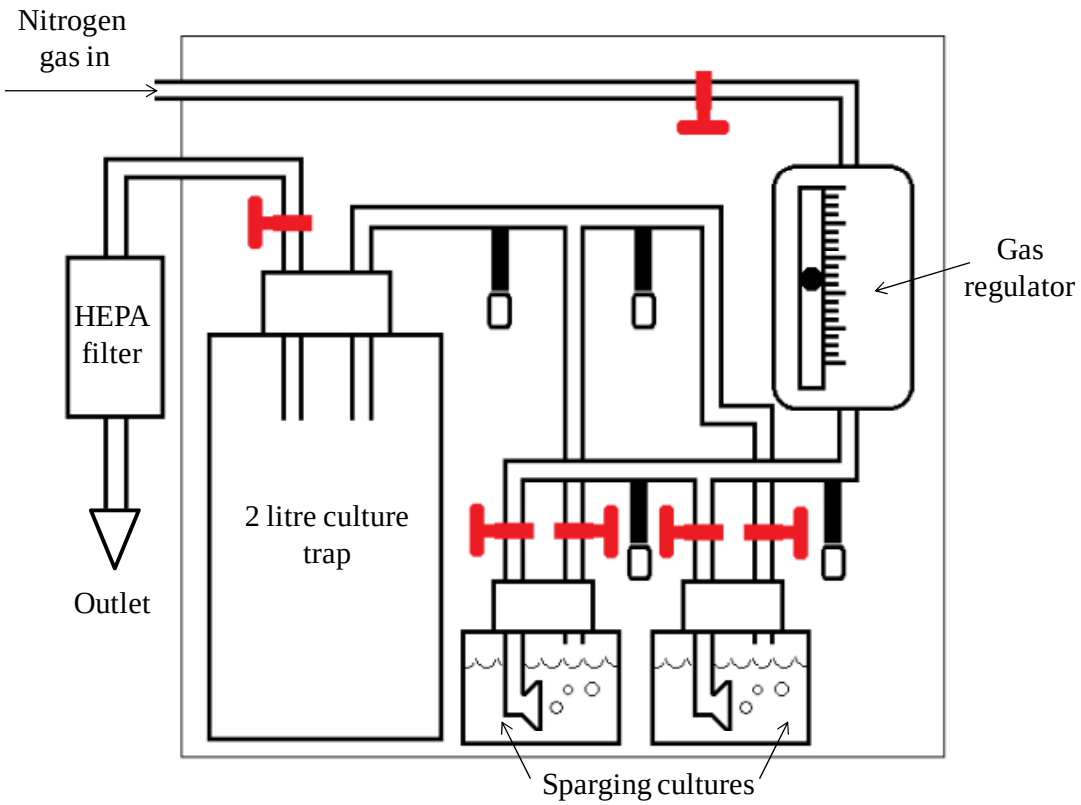

Figure 2.01: The arrangement of the Sparging Fridge. Items in RED are taps. Nitrogen flow is controlled by the gas regulator and delivered to a four-way INLET manifold. Only two sparging cultures are shown. Unused lines are plugged with "Suba-Seals". Nitrogen gas enters the cultures through glass frits, leaves through OUTLET lines leading to a 2 L culture trap and on to an external HEPA-CAP filter before being fed into a fume hood.

to stop foaming when nitrogen was bubbled through. Again the culture was swirled well to mix the culture and Antifoam 204. The neck of the screw top bottle and bottom of the screw cap were then sealed with Para-film. This ensured that no oxygen could get into the bottle nor any culture escape. The culture was then transferred to the "sparging fridge". The IN line of the gas delivery system of the anaerobic growth flask was connected to one of the lines of the four way splitter from the fridge INLET line. There is capacity for four growth flasks, so any unused

lines were plugged with Suba-Seals and sealed with electrical tape. The OUT line of the gas delivery system of the growth flask was then connected to the four way splitter of the fridge OUT line. Again any unused lines were plugged. Checks were made to ensure the correct lines were connected together so culture does not flood the fridge. The gas in line outside of the fridge was then connected to the nitrogen gas tap using a screw clip. This prevented the tube from coming off the gas tap and rendering the culture aerobic. The OUT line outside of the fridge was also secured in the fume cupboard. The nitrogen gas tap was turned to ~50% of the maximum. The taps that close the gas in and gas out lines for both the splitters and growth culture were switched to the open position. The flow monitor was then set to 6 L/min by adjusting the control knob resulting in a stream of nitrogen bubbling through the culture. If the connections are incorrect there is a fluid trap to catch any culture flowing out. There is also a 0.2 μm HEPA cap filter to trap any microorganisms that may reach the OUT line outside of the fridge. If the cultures were still sparging with nitrogen correctly after 10 minutes then they were left to incubate overnight or for ~16 hours. The cells are then harvested ready for resuspension and sonication in the preparation of *P. aeruginosa* cd_1, or resuspended in spheroblast buffer and lyzozyme treated for *P. pantotrophus* cd_1.

2.3.4: Dialysis.

Dialysis was used in the preparation of *P. aeruginosa* cd_1 and to buffer exchange pure cd_1 protein from both *Pseudomonas* and *Paracoccus* for use in spectroscopic measurements. Spectra/Por molecular porous membrane tubing with a capacity of 6.4 mL/cm was used for dialysis. The tubing was thoroughly washed in distilled water first before the solution to be dialysed was transferred to the tubing.

The tubing was tied and fastened with clips at both ends to keep the solution securely in the tubing. The tubing containing the solution was placed in a 5 L plastic beaker of dialysis buffer. There was a stirrer bar in the 5 L of dialysis buffer powered by a Stuart SB161 stirrer plate to keep the buffer moving for more effective dialysis. The dialysis was kept at ~ 4°C in a cold room. Each dialysis step was carried out for at least 10 hours. The 5 L beaker of dialysis buffer was then replaced if the first step had not been effective in removal of the unwanted solute.

2.3.5: Preparation of NO Solution.

NO solution was prepared by adding a small volume of buffer to a pear-shaped pyrex flask in an anaerobic glove box. A magnetic flea was placed in the pear-shaped flask along with the buffer. A NO bulb was then clamped to the arm of the pear-shaped flask. The pear-shaped flask was then clamped in place to a stirrer plate so that the flea spins in the buffer. A Suba-Seal was then used to plug the neck of the pear-shaped flask to prevent the NO escaping. The glass taps on both the bulb and the pear-shaped flask were then switched to the 'open' position to allow the NO gas to flow into the pear-shaped flask. The dissolving of NO gas into the buffer to create a saturated solution took approximately twenty minutes to complete. The concentration of NO in the saturated solution is ~ 1.75 mM in the temperature ranges 5 - 40°C [5]. Saturated binding of NO to protein could also be achieved by substitution of the buffer for a concentrated protein solution.

2.3.6: Activity Assays for cd_1.

Activity assays on cd_1 protein were performed as described by Richter *et al* [6]. Further details are given in Chapter 4.

2.3.7: Calculation of cd_1 Concentration.

The concentrations of cd_1 for both *Pseudomonas* and *Paracoccus* were calculated using the absorbance of the 411 nm Soret band and applying the extinction coefficient of 149,000 $M^{-1}cm^{-1}$. All concentrations therefore are per monomer.

2.4: Spectroscopic Applications and Technique.

Both projects involved the use of multiple spectroscopic techniques to probe the metal cofactors of both RirA and cd_1. The three techniques used are described below.

2.4.1: The Theory and Application of Electronic Absorbance Spectroscopy.

Electronic absorbance spectroscopy is a technique associated with the excitation of molecules from a ground state to an excited state by promotion of electrons within an orbital ladder. The radiation used to excite the electrons fall into two regions, ultraviolet (200 to 400 nm) and visible (400 to 800 nm). Electronic absorbance spectroscopy measured in the UV-visible range is useful in the detection of chromophores such as the metal ions in proteins and the aromatic rings of tryptophan, tyrosine and phenylalanine. From the spectra can be deduced protein concentration and metal ion oxidation state. Absorbance of the aromatic side chains of tryptophan, tyrosine and phenylalanine is due to excitation of electrons in π to π^* transitions. This accounts for the absorbance of proteins at 230-300 nm. If the protein contains a metal then charge-transfer bands can also contribute to absorbance across the UV-visible range. These charge transfer bands can be classed as ligand to metal charge transfer (LMCT) or metal to ligand charge transfer (MLCT). d-d (metal-centred transitions) can also contribute but these transitions are symmetry forbidden

through Laporte's selection rule (t_{2g} to e_g is forbidden) and can also be spin forbidden (for example d^5 ion transition from t_{2g} to e_g). They are therefore of extremely weak intensity ($\varepsilon << 500$ м$^{-1}$ cm^{-1}).

UV-visible spectrometers usually have two radiation sources, a source of light in the visible region and an ultraviolet light source. These two sources combine to give a continuous wavelength range over the UV-visible region (200-800 nm). A prism or diffraction grating separates the radiation into component wavelengths. Each monochromatic beam is then split into two beams often by a half-mirrored component. The first beam passes through the sample path, which contains the compound or protein of interest in solution. The second beam passes through a reference path, which only contains the solvent / buffer used to dissolve the compound or protein. The intensities of these beams are then compared.

Absorbance is defined as $A = \log_{10} I_0 / I$, where I_0 is the intensity of the light travelling to the sample and I is the lower light intensity that leaves the sample after a proportion is absorbed (Figure 2.02). At a particular wavelength, absorbance intensity can be used to calculate concentration of the compound through the Beer-Lambert law. This is shown in Equation 2.

$$A = \log_{10} I_0 / I = \varepsilon_\lambda cl \quad (2)$$

The ε_λ is defined as the molar absorption coefficient or extinction coefficient of a chromophore at a given wavelength λ. It is a measure of the strength of interaction between a chromophore and radiation of a given wavelength. c is defined as the concentration of the chromophore species in the sample and l is the pathlength of the radiation through the sample. Together, c and l is a measure of the quantity of molecules in the path of the radiation.

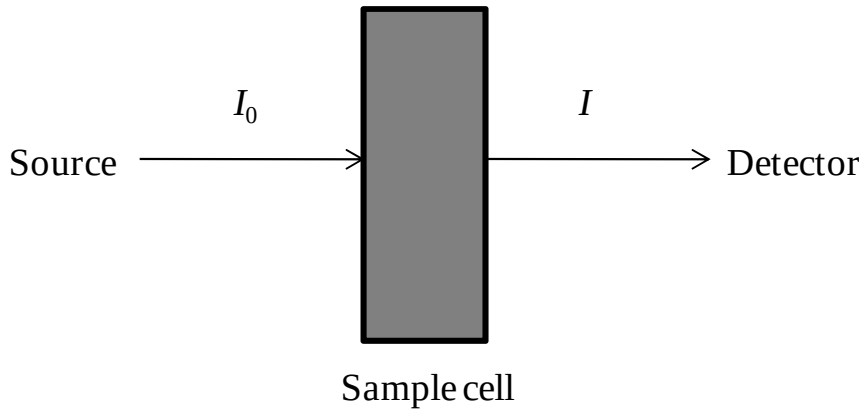

Figure 2.02: Diagram showing the path taken by the radiation in a UV-visible spectrophotometer

Most spectroscopic measurements were carried out on a Hitachi U4100 spectrometer. However for measurements involving the use of anaerobic glove boxes a Jasco V550 spectrometer was used. The majority of spectra were obtained using a 1 mm pathlength quartz cuvette. For anaerobic measurements a gas-tight cap was used to stop oxygen entering the cuvette. A baseline was always obtained through zeroing against the buffer solution.

2.4.2: The Theory and Application of Continuous Wave EPR Spectroscopy.

Electron Paramagnetic Resonance or EPR is a technique that can be used to study species that contain unpaired electrons using microwave frequencies [7, 8]. Free radicals and some transition metal ions possess unpaired electrons and are paramagnetic. There are many examples of proteins that require one or both of these to function. As a consequence of its spin (S = ½) and charge, an unpaired electron gives rise to a magnetic moment. The interaction of this magnetic moment with an applied magnetic field is known as the Zeeman effect. The magnetic moment can take one of two allowed orientations relative to the magnetic field. These are labelled

m_s = +1/2 and m_s = −1/2 according to whether the spin is roughly parallel or anti-parallel to the field [7, 8]. The difference in energy between the orientations is given in Equation 3 [9].

$$\Delta E = g\beta \mathbf{B} \quad (3)$$

In the equation, g is the measure of the Zeeman interaction strength termed a g-value, β is the Bohr magneton constant and **B** is the magnetic field. From this it can be seen energies of the two m_s states diverge linearly in an increasing magnetic field. By keeping the electromagnetic frequency constant and scanning the magnetic field, resonance can be reached and microwave absorption detected. Absorption occurs when the energy difference of the two m_s states matches the photon energy. The spectrum is recorded as the first derivatives of absorption for instrumental reasons. Differences between paramagnetic species arise from the electron environment and the orientation between molecule and magnetic field. The environment changes the strength of the Zeeman effect. This in turn is reflected in the magnitude of the g-value and consequently the rate of divergence between energies of the parallel and antiparallel states. The variation of g-values due to orientations of the molecule with the magnetic field is known as g-value anisotropy [7-9]. For transition metal ion EPR, fast relaxation rates mean that low temperatures are often needed for detection. Freezing the solution containing the molecule to be studied will result in molecules distributed randomly over all possible orientations relative to the magnetic field. This results in a spectrum covering a broad magnetic field with a range of g-values. Through these spectra characteristic axial and rhombic lineshapes can be observed. Axial lineshapes occur when g-values are equivalent for the x and y-axis but not the z-axis. Rhombic spectra arise when the x, y and z-axis are not equivalent to each other. There are also other effects which can influence lineshape, including the

presence of orbital angular momentum from delocalised electrons and hyperfine coupling [7, 8]. The latter results from an electron interacting with an atom that has a non-zero nuclear spin. The consequence is the splitting of EPR resonance signals in doublets, triplets and other multiple types.

The type of EPR used in this work is continuous wave, X-band EPR. X-band EPR uses a frequency of 9-10 GHz. Each sample is frozen in an EPR tube using liquid nitrogen. A typical volume of sample would be 250 μL. As the measurements would be conducted from 5-100 K temperatures liquid helium is used in the EPR spectroscopy. The EPR spectrometer is supplied by Bruker and consists of the following components. It has an EPR cavity in which the flash frozen sample contained in an EPR tube is placed. In simple terms a cavity is a metal container which creates a standing wave, such that the microwave energy is stored in the cavity. When the sample absorbs microwave energy it lowers the quality factor (a measure of the efficient storage of microwave energy by the cavity, denoted Q). This is due to coupling changes and increasing energy losses through changes in cavity impedance by sample absorption. This results in the cavity no longer being critically coupled, therefore permitting the reflection of microwaves to the bridge component. The bridge contains the electromagnetic radiation source and the detector. The EPR apparatus also uses a magnet to tune electronic energy levels. The magnet is regulated through a Hall probe located in the magnet gap. The Hall probe compares voltages between itself and a reference voltage. Any error results in a corrective voltage being sent to the magnet. This alters current flow, and consequently the magnetic field. Once corrected through adjusting the error voltage to zero, the field is stabilised. The EPR apparatus also uses a phase sensitive detector to enhance spectrometric sensitivity. The phase sensitive detector compares the modulated

signal with a reference signal. It then senses only those signals with the same frequency and phase as the field modulation to remove noise and electrical interference. Electronic damping with a chosen time constant is also used to filter random noise. Modulation amplitude, frequency and time constant can be adjusted and are crucial to the clarity of EPR spectra. High modulation amplitude can result in signal broadening and poor resolution, long time constants can result in distortion or the disappearance of signals and high modulation frequency can also result in broad signals with poor resolution.

2.4.3: Theory and Application of Magnetic Circular Dichroism (MCD).

MCD spectroscopy measures intensity difference between the absorbance of left and right circular polarised light when a magnetic field is applied. The magnetic field is parallel to the direction of circular polarised light propagation. The quantity measured in MCD is the ΔA ($A_{LCP} - A_{RCP}$) against wavelength. Molecular properties can be deduced from the magnitude of observed MCD via the Beer-Lambert law ($\Delta A = \Delta\varepsilon.c.l$). As a technique MCD is more useful then absorption spectroscopy through having a greater wavelength range (200-3000+ nm) and offering more detailed spectra by virtue of its double-signed nature. The greater wavelength range allows detection of metal bands in UV and near-infrared wavelengths. Through MCD fingerprinting, co-factor type, oxidation state, spins and even axial ligands can be identified. This is very useful in characterising biomolecules such as metalloproteins [10]. Using a magnetic field lifts the degeneracies of electronic orbital and spin states, as well as causing the mixing of electronic states. This results in slightly different energies for the absorptions of left and right polarised light. The angular momentum selection rule is $\Delta M_L = +1$ for left polarised light and $\Delta M_L = -1$ for right

polarised light. The equation for total MCD intensity (Equation 4) can be written as follows.

$$I \sim [A_1 (-\delta f(E)/\delta(E)) + (B_0 + C_0/kT) f(E)] \quad (4)$$

From the equation three contributions to the MCD spectrum can be discerned. These are known as A, B and C-terms [10, 11]. The A-term is temperature independent and occurs due to ground or excited state degeneracy (sometimes both) through the Zeeman effect. The B-term is also temperature independent and results from zero-field electronic states experiencing field-induced mixing. Finally the C-term is temperature dependant and arises due to a population change over the Zeeman sublevels of a species with ground-state paramagnetism. By lowering temperature the C-term intensifies. Through variation of temperature and field the ground state parameters such as zero-field splitting, spin and g-factor can be determined [12].

The MCD apparatus consists of a Jasco J-810 CD spectropolarimeter and an Oxford Instruments SM4 split-coil superconducting magnet. Radiation from a xenon-arc lamp is prism monochromated and then circularly polarised by a polariser and photoelastic modulator. The circularly polarised light then impinges on the sample. The sample is held in a modified quartz cuvette of pathlength 1 mm and volume 120-360 μL. For low temperatures, the sample has a glassing agent such glycerol or ethanediol added, such that the ratio of glassing agent to sample is 55:45. If measurement at 1400-3000 nm is required then the samples are prepared in D_2O buffers. The cuvette is held in a long probe with a Hall probe and a carbon glass resistor to allow measurement of field and temperature. The probe is placed in the sample space of the cryostat such that the cuvette is visible through the optical windows, located at the bottom of the cryostat, in the position of maximum field. Temperature control can be achieved through the main liquid helium can of the

cryostat. Raising the temperature is achieved through emptying and heating the sample space or lowering temperature can also be carried out through filling and pumping on the sample space. The superconducting magnets used here allowed the generation of fields up to 8 T (room temperature samples) or 5 T (low temperature).

2.5: References

1. Pace, C. N., Vajdos, F. Fee, L., Grimsley, G., Gray, T. (1995) *Protein Sci.* ***4***, 2411-2423.
2. Parr, S. R. (1974) *Thesis*, 39-44.
3. Moir, J. W. B., Baratta, D., Richardson, D. J., Ferguson, S. J. (1993) *Eur. J. Biochem.* ***212***, 377-385.
4. Sam, K. A., Fairhurst, S. A., Thorneley, R. N. F., Allen, J. W. A., Ferguson, S. J. (2008) *J. Biol. Chem.* ***283***, 12555-12563.
5. Mesáros, Š., Grunfeld, S., Mesárošová, A., Bustin, D., Malinski, T. (1997) *Anal. Chim. Acta.* ***339***, 265-270.
6. Richter, C. D., Allen, J. W., Higham, C.W., Koppenhöfer, A., Zajicek, R. S., Watmough, N. J., Ferguson, S. J. . (2002) *J. Biol. Chem.* ***277***, 3093-3100.
7. Wertz, J. E., Bolton, J. R. (1972) *Electron Spin Resonance: Elementary Theory and Practical Applications*, McGraw-Hill, New York.
8. www.Bruker-biospin.com/cw.
9. Hagen, W. R. (2006) *Dalton Trans.*, 4415-4434.
10. Stephens, P. J. (1974) *Ann. Rev. Phys. Chem.* ***25***, 201-232.
11. Sutherland, J. C., Holmquist, B. (1980) *Annu. Rev. Biophys. Bioeng.* ***9***, 293-326.
12. Neese, F., Solomon, E. I. (1999) *Inorg. Chem.* ***38***, 1847-1865.

Chapter 3.

The Iron-Responsive Regulator RirA in the α-Proteobacteria *Rhizobium leguminosarum*.

3.1: Introduction

As described in Chapter 1, *R. leguminosarum* possesses a monomeric 17441 Da protein called RirA (rhizobial iron regulator) that represses iron uptake genes when iron is sufficient. RirA is a 160 amino acid protein that has four essential cysteine residues in its amino acid sequence as shown in Figure 3.01. The three cysteines at positions 92, 101 and 107 are conserved in 70% of the Rrf2 family of proteins that RirA belongs to. These cysteines are thought to be ligands for an iron-sulphur cluster. Members of the Rrf2 family such as NsrR [1, 2] and IscR [3] have been shown to contain iron sulphur clusters. NsrR and IscR are members of the Rrf2 family that have the three conserved cysteine residues that RirA possesses, and therefore it is assumed that RirA also has an iron sulphur cluster that is key to its function.

```
MRLTKQTNYA VRMLMYCAAN DGHLSRIPEI AKAYGVSELF 40
LFKILQPLNK AGLVETVRGR NGGVRLGKPA ADISLFDVVR 80
VTEDSFAMAE CFEDDGEVEC PLVDSCGLNS ALRKALNAFF 120
AVLSEYSIDD LVKARPQINF LLGITGEPAY RKPAIVAPAA 160
```

Figure 3.01: Sequence of RirA from *R. leguminosarum* showing in boxes the four conserved cysteine residues that are thought to be involved as ligands to the iron-sulphur cluster. Accession number: CAC35510.1.

Currently, the published work on *R. leguminosarum* RirA has focused on genetic expression and regulation [4-6]. The majority of work published on RirA from other species is also focused on the genetics [7-10]. Very little has been reported on the characterisation of the protein and of the postulated iron sulphur cluster for any of the organisms that has RirA regulation. Jonathan Todd (School of Biological Sciences, UEA) constructed BL21 *E. coli* with a pET21a plasmid containing the RirA insert from which RirA could be successfully overexpressed. He also performed preliminary purification of the overexpressed RirA. This chapter describes work following on from these preliminary studies. After two years of use, this pET21a plasmid failed to overexpress any RirA protein and was replaced with a pET11a plasmid containing a RirA insert synthesised by GenScript.

The chapter describes the establishment of a protocol to grow transformed *E. coli* BL21 cells containing the RirA insert, to overexpress the RirA protein and to purify the protein so it can be used for spectroscopic study. Following purification, the RirA is then reconstituted with an iron-sulphur cluster, which is subsequently investigated through assays and spectroscopy to determine the nature of the cluster.

3.2: Protocols for the Purification and Reconstitution of RirA.

Analysis and characterisation of proteins requires the generation of soluble, purified protein in high quantity. Native strains seldom meet the requirements for quantity and ease of purification. Recombinant protein expression is often employed to generate high yields of purified protein. The gene that encodes the protein can be introduced into a vector such as a plasmid. The plasmid contains an expression system such as the *lac* operon to regulate transcription and translation of the

recombinant gene. An inducer, such as IPTG in the case of the *lac* operon, is used to activate gene expression.

The plasmid is transformed into a host bacterial strain. *E. coli* is commonly used as such a host strain for recombinant protein expression [11]. It can be cultivated at high cell densities, the genetics are well understood, it is a relatively simple organism to work with and it is inexpensive. In this study, BL21 *E. coli* transformed with either a pET21a or pET11a plasmid is used. These plasmids contain the RirA gene from *R. leguminosarum*.

If the recombinant protein is a metalloprotein, it can sometimes lack the metal cofactor when overexpressed. RirA was expressed and purified in apo-form in this study. It is generally agreed that RirA binds an iron-sulphur cluster, and therefore incorporation of a cluster into the protein was attempted. Iron-sulphur clusters can be inserted into apoprotein by several methods. For example in FNR iron-sulphur clusters can be reconstituted into purified apoprotein [12] or produced *in vivo* by supplementing anaerobic cultures with ferric ammonium citrate and methionine [13]. In this work, RirA is reconstituted with a cluster using ferrous ammonium sulphate, L-cysteine / DTT and NifS.

The following section describes the protocols used to overexpress, purify and reconstitute RirA.

3.2.1: Construction of the RirA Overexpressing Strain of BL21 *E. coli*.

These methods apply to both preparations performed with the pET21a and pET11a plasmid. The pET21a plasmid containing a RirA insert, obtained from the Johnston group at the School of Biological Sciences (UEA), is shown in Figure 3.02. The pET11a with RirA insert was synthesised by and purchased from GenScript.

BL21 cells were freshly transformed with the pET plasmid and checked for overexpression before any growth and purification commenced.

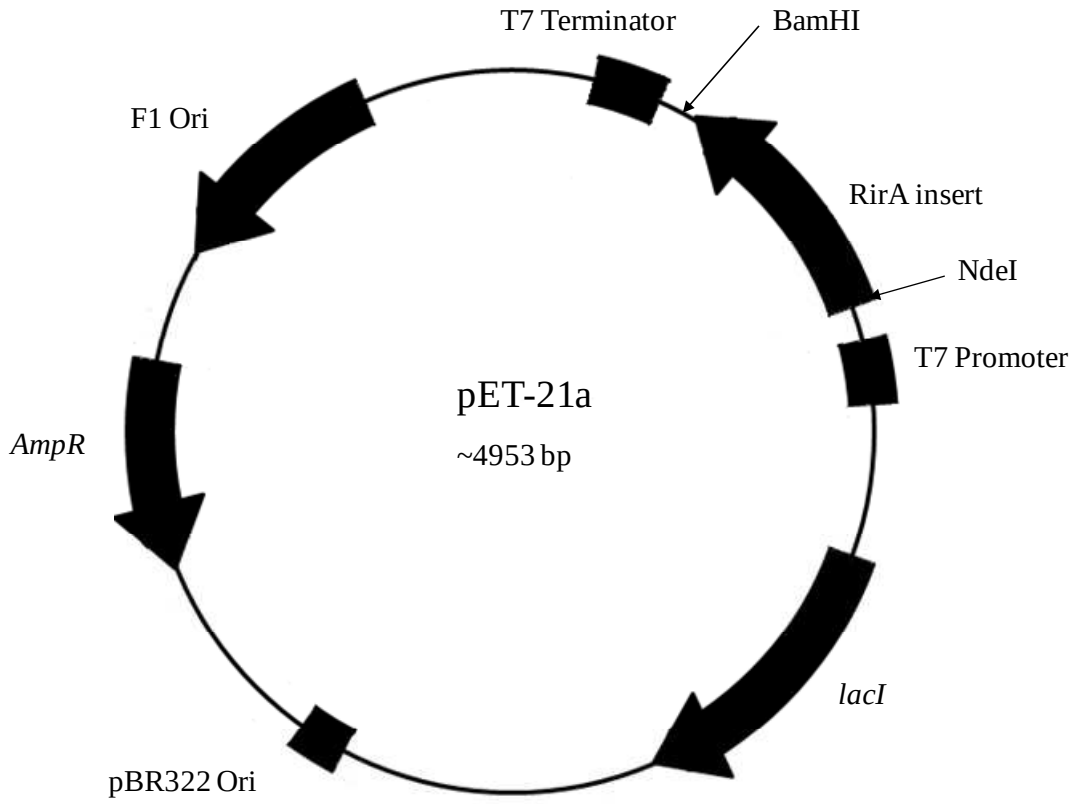

Figure 3.02: Plasmid map of pET21a containing the RirA insert and showing the major sequence landmarks. The RirA insert is in the multiple cloning region that contains the restriction enzyme sites BamHI and NdeI. Abbreviations: F1 Ori: F1 origin of replication, *AmpR*: ampicillin resistance gene, pBR322 Ori: pBR322 origin of replication, *lacI*: gene encoding lac repressor protein.

Following an established protocol, competent *E. coli* cells were prepared for both BL21 and the storage strain DH5α. A 5 mL culture of Luria-Bertani medium (5 g NaCl per litre, 10 g tryptone per litre, 5 g yeast extract per litre) was inoculated with the *E. coli* strain of choice. The culture was incubated overnight at 37°C. 0.4 mL of the 5 mL culture was then used to inoculate 40 mL of LB medium in a

250 mL conical flask. The 40 mL culture was then grown at 37°C and agitated at 200 rpm until the A_{650} reached 0.4-0.5. The culture was then transferred to a sterile 50 mL Falcon tube. The cells were then centrifuged at 8000 rpm for 8 minutes at 4°C, using an ALC PK121R centrifuge with an A-M10 rotor. The pellet was drained and resuspended in TF-1 buffer. TF-1 buffer consists of 7.4 g/L KCl, 30 mL of 1 M CH_3COOK, pH 7.5, 1.5 g/L $CaCl_2.2H_2O$ and 150 g/L glycerol. This was made up to a volume of 950 mL, pH adjusted to 6.4 with 0.2 M acetic acid, divided into 95 mL volumes and autoclaved. Once the autoclaved TF-1 was cooled, 5 ml of filter sterilised 1 M $MnCl_2.4H_2O$ was added to each 95 mL aliquot. The TF-1 resuspended cells were then placed on ice for 15 minutes. The cells were then centrifuged again using an ALC PK121R centrifuge. The cells were spun at 8000 rpm for 8 minutes at 4°C. The cell pellet was then drained thoroughly of TF-1 buffer and resuspended in 4 mL of TF-2 buffer. TF-2 consists of 0.74 g/L KCl, 11 g/L $CaCl_2.2H_2O$ and 150 g/L glycerol. The volume was made up to 980 mL and divided into 98 mL aliquots. The TF-2 buffer was then autoclaved. After cooling, 2 mL of filter sterilised 0.5 M MOPS buffer at pH 6.8 (KOH adjusted) was added to each 98 mL of TF-2 buffer. The resuspended cells were then kept on ice ready for transformation.

For each transformation, 0.2 mL of competent cells were transferred to 2 mL chilled Eppendorf tubes. Up to 4 μL of prepared plasmid DNA (via DH5α storage strain containing the plasmid and QIAprep® Spin Miniprep Kit) was then added to the competent cells. The tubes were gently rolled on ice to mix. The cells were then left on ice to incubate for 40 minutes. The competent cells were then placed in a heat block set at 42°C for 2 minutes. This heat shocks the cells into taking up the plasmid DNA. After the heat shock treatment the cells were returned to the ice for a further 5 minutes incubation. Once the incubation period was over then 0.7 mL LB medium

(pre-warmed in an incubator) was added to each of the 0.2 mL competent cells. These were then incubated in a heat block at 37°C for 1 hour to allow resistance gene expression. Once incubated, the cells were centrifuged in a bench top micro-centrifuge at 10000 rpm for 5 mins. Approximately 0.5 mL to 0.7 mL of the supernatant was then removed and discarded. The cells were then resuspended in the remaining supernatant. A 200 mL aliquot of the newly resuspended cells was then used for plating out. LB agar plates containing the antibiotic ampicillin were used to select for those containing the plasmid. The LB agar plates were then incubated overnight at 37°C. The plates were checked for sufficient colonies before a sterile loop was used to transfer a colony into fresh 5 mL volumes of LB media containing ampicillin. Test cultures were grown using isopropyl-β-D-thiogalactopyranoside (IPTG) to check for overexpression before commencing with a purification run.

3.2.2: Growth and Preparation of Transformed Cells Containing the RirA Insert.

Four 5 mL LB cultures were inoculated with freshly transformed BL21 *E. coli* containing a pET21a or pET11a plasmid with the RirA insert. The chosen media was LB (Luria-Bertani) broth. Each of the 5 mL LB liquid media also contained 5 μL of 100 mg/mL ampicillin. The cultures were incubated with shaking at 37°C until there are a sufficient number of cells to give an OD_{600nm} of at least 1.0. The OD, or optical density, is the absorbance of an optical element for a given wavelength λ per unit distance i.e. 1 cm. Each 5 mL culture was then added to a 2 L conical flask containing 500 mL of LB. Each flask was plugged with a foam bung. A 500 μL volume of 100 mg/mL ampicillin was added to each of the 500 mL of LB. This was incubated at 37°C aerobically with shaking until the OD_{600nm} was in the

region of 0.4 – 0.6 for each flask. A 1 mL sample of the culture was then removed to determine the level of overexpression of RirA using SDS-PAGE electrophoresis. The cultures were then inoculated with 500 μL of 1 M isopropyl-β-D-thiogalactopyranoside (IPTG) each to trigger the overexpression of RirA in the *E. coli* cells. The newly inoculated cultures were then incubated at 37°C with shaking for 3 hours. A sample of IPTG-induced culture was then compared to a sample that contained no IPTG by SDS-PAGE analysis. If RirA overexpression was detected then the next stage could proceed.

The cultures were transferred to 250 mL centrifuge containers and balanced to within 0.1 g. This involves transferring amounts of culture to each other until they weigh approximately the same. The cultures were then centrifuged using a Beckman J20 Avanti centrifuge and the JA14 rotor. They were centrifuged at 10000 rpm (12500 x g) for 15 minutes. The supernatant was removed and discarded, while the pellet was kept and stored in the freezer after flash freezing in liquid nitrogen. A 2 L conical flask with 500 mL culture yields roughly 2.5 g of wet cell paste. If SDS-PAGE electrophoresis reveals a good degree of overexpression then the purification can proceed. The frozen cell pellets were resuspended in 40 mL Buffer A (25 mM HEPES, 2.5 mM $CaCl_2$, 50 mM NaCl and 10 mM diaminoethanetetra-acetic acid disodium salt (EDTA), pH 7.5). The resuspension was then sonicated for 8 minutes and 20 seconds in an aerobic microbiological cabinet. This was carried out twice. The sonicator was set at 50% of its maximum power output and sonicating for 0.2 seconds in every second. The sonicated suspension was then transferred to Falcon tubes. These were balanced and centrifuged at 10000 rpm (12500 x g) for 30 minutes. The result was a yellow supernatant, with a pellet of cell debris. The cell pellet was discarded and the yellow supernatant was retained. The yellow

supernatant containing RirA was then filtered using a Sartorius syringe filter (0.20 μm pore size) ready for the Heparin column purification.

3.2.3: Column Purification of RirA

For the purification, two buffers were prepared. Buffer A, used to resuspend the frozen cell pellets, contains 25 mM HEPES, 2.5 mM $CaCl_2$, and 50 mM NaCl at pH 7.5. Buffer B contains 25 mM HEPES, 2.5 mM $CaCl_2$, 50 mM NaCl and 750 mM KCl at pH 7.5 and is used for elution purposes. Both buffers were filtered using a Sartorius syringe filter (0.45 μm pore size) before being used in the column chromatography.

The column stage uses a 5 mL HiTrap Heparin HP column connected to an ÄKTA Prime system. A Heparin column consists of naturally occurring sulphated glucosaminoglycan ligands covalently coupled to agarose beads. The column has two modes of interaction. It can act either as an affinity ligand or as a high capacity cation exchanger (due to the anionic sulphate groups). The lines were washed out first before equilibrating the column with 10 column volumes (50 mL) of Buffer A at 5 mL/min. 5 mL of the filtered crude extract was then applied to the column through a 5 mL syringe. Then the column was washed with Buffer A. 5 mL fractions were collected. A total of 15 x 5 mL wash fractions were collected altogether at a flow rate of 5 mL/min. The elution stage followed. The gradient of Buffer A to Buffer B was from 0% B to 100% B over a total of 50 mL. Elution fractions were again 5 mL. A total of 15 x 5 mL elution fractions were collected at 5 mL/min. 10 column volumes of Buffer A were then used to regenerate the column before repeating this purification stage. The fractions were checked by measuring the absorbance at 280 nm. This was done using a quartz cuvette and a Helios UV/Vis

spectrophotometer. The RirA fractions eluted at 50% Buffer B. The fractions corresponding to the highest absorbances at 280 nm were analysed on SDS-PAGE. Those fractions containing the RirA at high concentration and purity were pooled.

In some instances further column purification was required to purify the RirA fractions. This was achieved using a HiPrep 26/60 S200 gel filtration column connected to an ÄKTA Prime system. The S200 was equilibrated with a column volume of Buffer A, containing 25 mM HEPES, 2.5 mM $CaCl_2$, and 50 mM NaCl at pH 7.5. Once equilibration was complete 4 mL of the pooled RirA was injected by syringe and pumped onto the column at 1 mL/min. Again the pooled protein was not concentrated as this risked precipitation. The A_{280nm} trace was monitored using Primeview, since all of the contaminating proteins and RirA are colourless. The fractions were collected in volumes of 2 mL and so the RirA was spread over several collection tubes. SDS-PAGE gels were used to determine the best fractions to pool. Concentration using an Amicon ultrafiltration stirred cell model 8050 (using an YM5 membrane disc) or spin columns was required if the protein was too dilute. The concentration of protein was estimated using a Biorad protein assay. This was required as the concentration of ammonium iron (II) sulphate that will be required in the reconstitution is dependent on the protein concentration. The pooled protein fractions were flash frozen and stored in a − 80°C freezer until needed for reconstitution.

3.2.4: Reconstitution of RirA

The reconstitution involves the addition of ammonium iron (II) sulphate, L-cysteine, DTT and NifS protein to the purified RirA protein. The mixture was placed in a conical flask sealed into a beaker. The beaker has an inlet and an outlet for

temperature control via a water bath. A stirrer bar was also present in the conical flask part of the container to thoroughly mix the reactants during reconstitution. After there is sufficient yellow colour in the reaction mixture the reconstituted protein was cleaned of excess reactants using a Heparin column. Finally the reconstituted protein was checked by recording an absorbance spectrum. The experiments were attempted using samples where RirA and breakdown product were in a 50:50 ratio, with a little high molecular weight contaminating protein also present.

To begin the reconstitution of the RirA samples the following were weighed out: - 78.5 mg of ammonium iron (II) sulphate hexahydrate into a 2 mL screw top Eppendorf tube. 12.8 mg of L-cysteine into a 3 mL screw top Eppendorf tube and 41.7 mg of DTT into a 2 mL screwtop Eppendorf tube. The screw top lids were pierced four times with a needle as they are transferred to an anaerobic cabinet. 1 mL of anaerobic Buffer A was used to dissolve the ammonium iron (II) sulphate in the anaerobic cabinet. The 1 mL solution was then transferred to a 10 mL volumetric flask. Another 9 mL of anaerobic Buffer A was added to make the ammonium iron (II) sulphate solution to 10 mL. For the L-cysteine and DTT 1 mL of anaerobic Buffer A was added to each tube in the anaerobic cabinet. The 1 mL solution of DTT was then transferred to the 1 mL solution of L-cysteine to create a 2 mL solution of DTT / L-cysteine in a 3 mL screw top Eppendorf vial. 15 mL of the RirA protein was then pipetted into the special container. The water bath was set to 25°C and turned on to allow the protein to reach temperature. Then the following were added; an appropriate volume of the DTT / L-cysteine solution so that the total concentration is 1 mM, an appropriate volume of ammonium iron (II) sulphate solution so the concentration is 7 times that of the protein and 60 μL of purified NifS protein. NifS is a cysteine desulphurase that catalyses the removal of sulphur from L-cysteine,

which results in the production of elemental sulphur and L-alanine. The DTT donates electrons to the elemental sulphur to produce sulphide (Equation 1).

$$R\text{-}CH_2\text{-}SH \xrightarrow[2e^-]{NifS} R\text{-}CH_3 + S^{2-} \quad (1)$$

The temperature of the circulating water was then increased to 37°C. The reconstitution reaction was carried out for up to four hours. A yellow colour starts to develop as the reaction proceeds. Once the reaction was deemed to be complete, through no further changes in colour, the reconstitution mixture was purified of excess iron and sulphur using a 1 mL HiTrap Heparin HP column fitted with syringe adaptors. 15 mL of Buffer A was applied to the column using a 5 mL syringe from the top. The yellow protein solution was then applied at the bottom of the column. A 1 mL syringe with filter and adaptor was used for this process. Up to 10 mL of the yellow reconstituted protein was loaded. The column was then washed using Buffer A from the top of the column, again using a 5 mL syringe. 15 mL of Buffer was used to wash the column. The bound protein was then eluted with anaerobic Buffer B from top to bottom. The samples were collected in 1.5 mL Eppendorf tubes. Each fraction contained 50 µL to 200 µL volumes. A brown / yellow band was observed. The fractions with the reconstituted protein were transferred to a glass screw top vial, sealed with Parafilm and transferred to an anaerobic fridge for storage at 4°C. A sample of reconstituted protein was analysed by recording a spectrum on a V550 UV-Vis spectrophotometer (see Figure 3.18) to see if the protein has any characteristic features of an iron-sulphur cluster. A protein assay was also performed to obtain the protein concentration after reconstitution.

If removal of the cluster was required, 125 µM of holoprotein was incubated with 1 mM EDTA and 1 mM TCEP aerobically for three hours. The sample was then

carefully buffer exchanged using 10000 MWCO microcons to remove any free sulphide and iron in solution.

3.3: Purification, Characterisation and Spectroscopic Analysis of RirA

The following section describes the results of the purification, characterisation and spectroscopic analysis of RirA.

3.3.1: Purification of RirA Apoprotein.

The materials and methods for the preparation of RirA are described in Section 3.2.3. The first stage of the purification was to check for RirA overexpression. Once the incubation time has elapsed, a 1 mL sample of the newly induced culture was then removed for SDS-PAGE electrophoresis. This sample can then be compared to the other sample (500 μL culture with no IPTG) to check for overexpression (Figure 3.03).

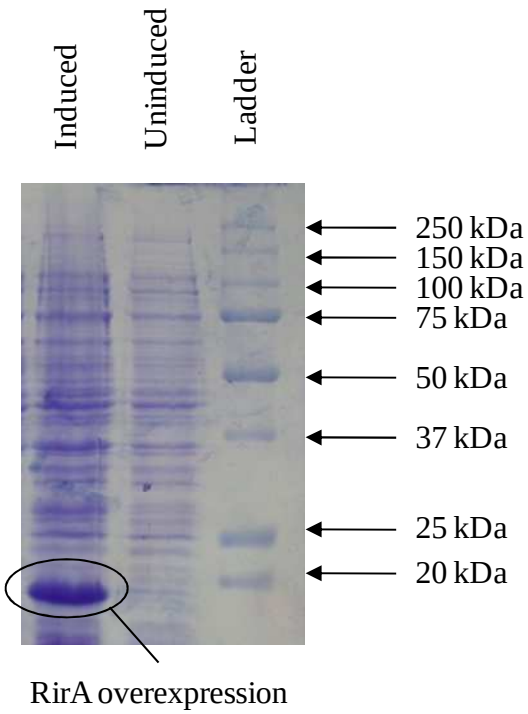

Figure 3.03: 12% SDS-PAGE gel showing the overexpression of RirA. RirA was induced by using IPTG. The first lane shows the induced cell protein with the overexpressed RirA (band indicated), the second shows the protein in the uninduced cells with clearly no overexpression and the third shows the ladder with key markers indicated.

From Figure 3.03 it is clear to see there was a clearly defined band at around 20 kDa where the protein has overexpressed in the 'induced' lane. This band is not present in the 'uninduced' lane, and therefore the band is the result of overexpression through the induction of IPTG. RirA is 17441 Da in size, which correlates with the induced band just below the 20 kDa marker.

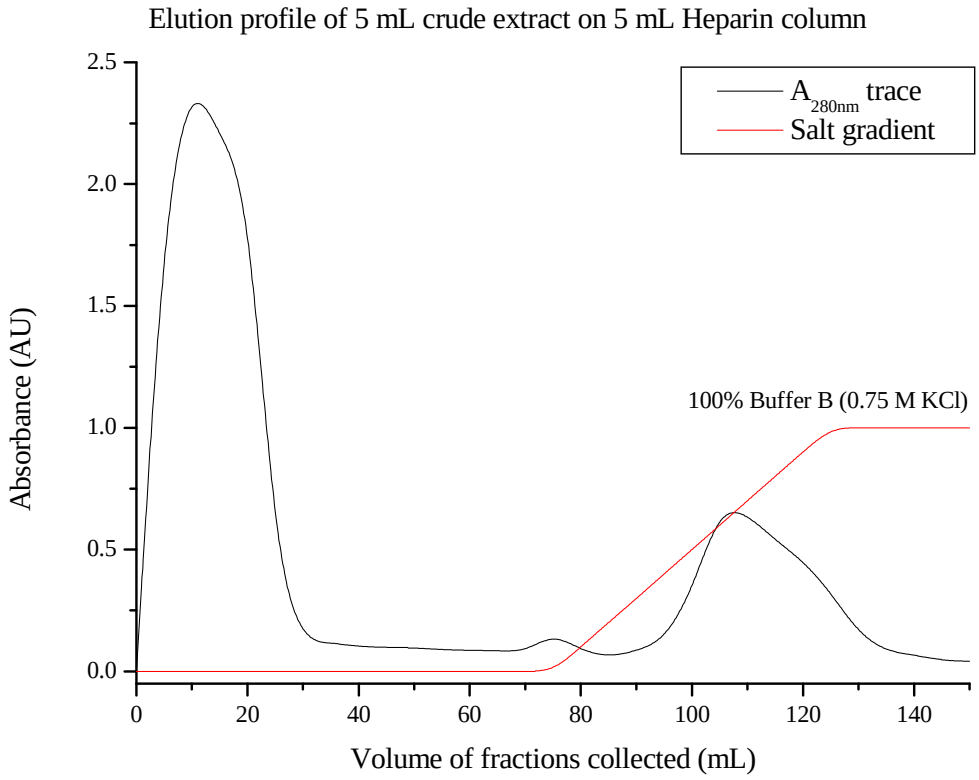

Figure 3.04: Elution profile of the 5 mL HiTrap Heparin column. The black line indicates the A_{280nm} trace used to track proteins eluting from the column. The red line indicates the Buffer B gradient used to elute the Heparin bound protein. For the red line, 1.0 on the absorbance scale is equivalent to elution with 100% Buffer B (salt concentration 0.75 M KCl) as indicated on the profile. The wash stage occurs at 0-75 mL and the elution stage occurs at 75-150 mL. Flow rate is 5 mL/min.

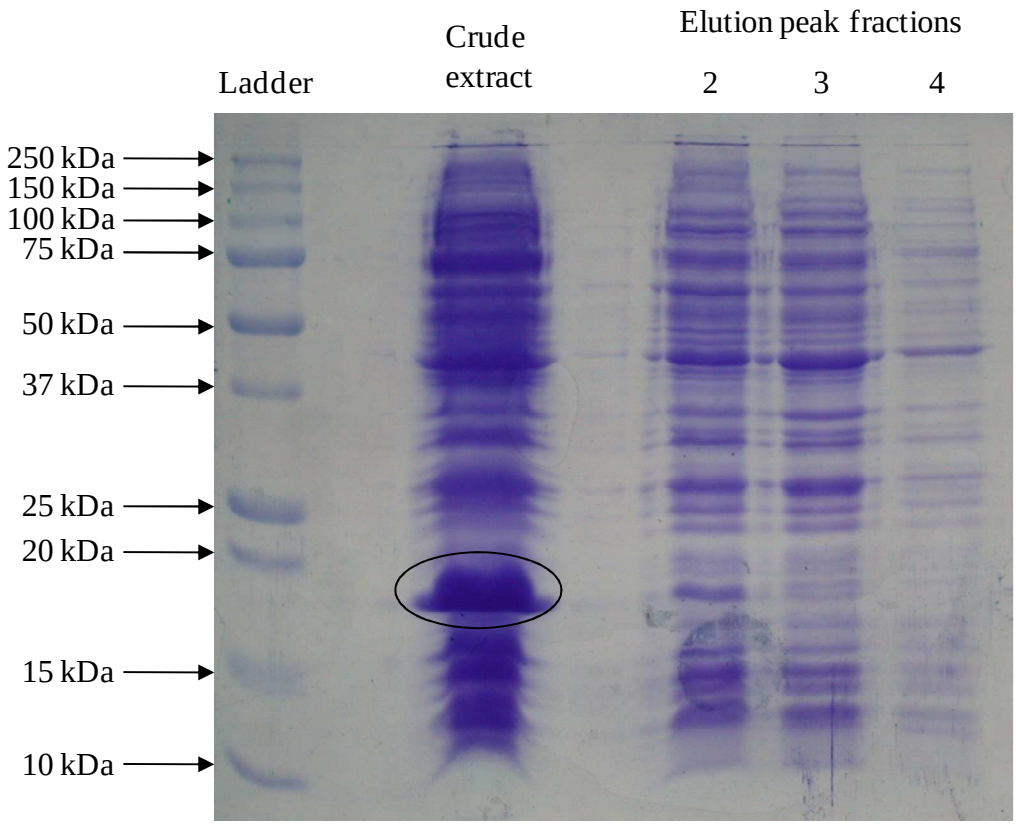

Figure 3.05: 12% SDS-PAGE gel showing the wash fractions (fractions 2-4) corresponding to the large peak at 5-20 mL in the elution profile for one Heparin column run (Figure 3.04). The wash fractions show no significant indication of overexpressed RirA, compared to a sample of crude extract (unpurified RirA) that clearly shows overexpressed RirA (circled).

Once the overexpression has been confirmed, the next stage is the Heparin purification to remove the majority of contaminants. During Heparin purification, an elution profile was plotted from the absorbances at 280 nm (Figure 3.04). The elution profile shows two significant peaks where the fractions contain protein. The first peak occurs in the wash stage at 0-30 mL. RirA is expected not to be here, since RirA binds to Heparin in Buffer A. 5 mL fractions of the wash stage were collected. Fractions of interest were analysed by SDS-PAGE. Analysis of SDS-PAGE gels of fractions collected at the 0-30 mL first peak show no significant bands that could be attributed to RirA (Figure 3.05). The second peak occurs at the elution stage at 95-

130 mL, corresponding to a gradient of 50% Buffer B. RirA is anticipated to elute at or near this salt concentration because it binds Heparin strongly and requires a high salt concentration for elution.

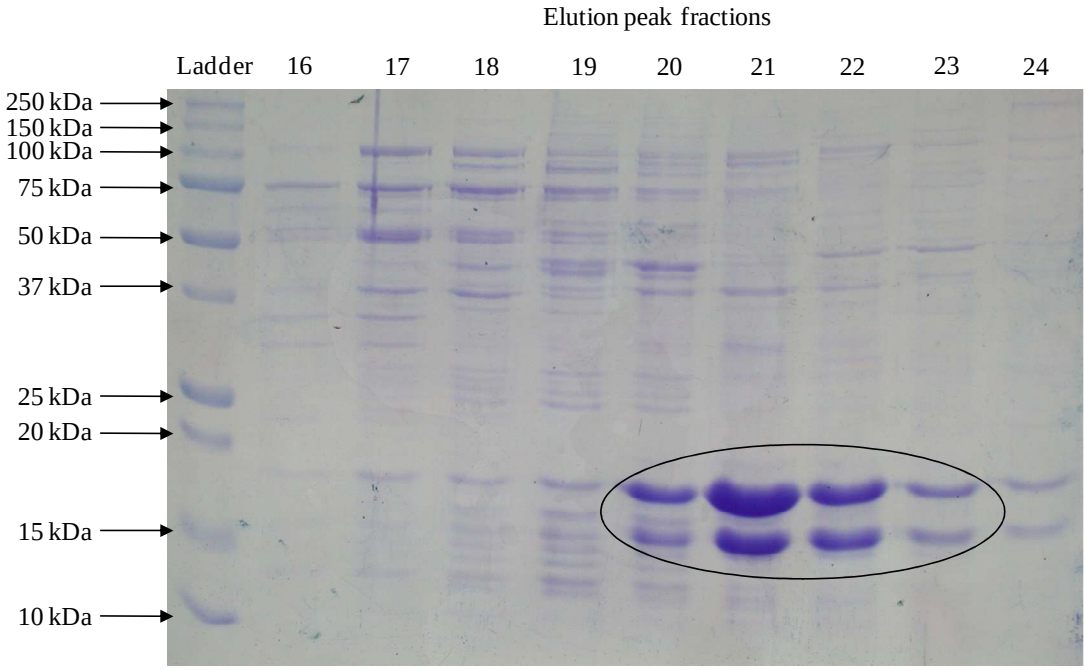

Figure 3.06: 12% SDS-PAGE gel showing the elution fractions 16-24 for one Heparin column run. These correspond to the total volume range 75-120 mL in the elution profile (Figure 3.04). The RirA (circled) is below the 20 kDa marker on the ladder and the breakdown product is above 15 kDa on the ladder. The majority of the RirA is eluted at fractions 21 and 22. This corresponds to 100 and 105 mL total collected volume in Figure 3.04. Protein loadings for lanes 20-23 are 20 µg, 71 µg, 41 µg and 12 µg respectively.

There is also a third peak at 70-80 mL. However, the A_{280nm} trace indicates only a small amount of protein and the peak corresponds to the transition between the wash and elution stages. Therefore it is unlikely that RirA is present in these fractions. Again 5 mL fractions were collected for the elution stage. The elution fractions of interest, corresponding to the peaks at 70-80 mL and 95-130 mL were analysed on SDS-PAGE to locate overexpressed RirA (Figure 3.06).

The elute fractions 20-23 on Figure 3.06 (corresponding to the elution peak at 95-130 mL in Figure 3.04) show a large band between the 15 kDa and 20 kDa mark corresponding to RirA. These fractions were pooled. Also there is a large band nearer the 15 kDa mark for the same fractions. This is thought to be a breakdown product of RirA where a small chain of amino acids is lost from one of the terminal ends. Evidence for the breakdown product is provided by SDS-PAGE in the next section. If RirA is stored at 4°C in a fridge and not flash frozen, and RirA samples are checked periodically on SDS-PAGE gels, over time the band that corresponds to RirA becomes less intense and narrower, whereas the band that corresponds to what is thought to be a breakdown product becomes more intense and broader.

Another problem encountered with the RirA purifications was that the Heparin purification stage was inconsistent. The amount of contaminants removed was variable, with some preparations pure and others with many contaminants remaining. To remedy this problem the pooled Heparin fractions containing RirA that had contaminants were further purified using a S200 gel filtration column connected to an ÄKTA Prime system. The results of the gel filtration profile are shown in Figure 3.07. The higher molecular weight contaminants are largely removed as shown in the sharp peak at ~ 100 mL in Figure 3.07. This results in highly pure protein but the protein is dilute and spread across many fractions. This can be clearly seen if the fractions are analysed by SDS-PAGE. Figure 3.08 shows an example of such a gel. The RirA is highly pure, with only very faint contaminating bands around the 50 kDa area. This degree of purity is necessary as the reconstitution technique used is not specific and can actually reconstitute an iron-sulphur cluster non-specifically into other proteins.

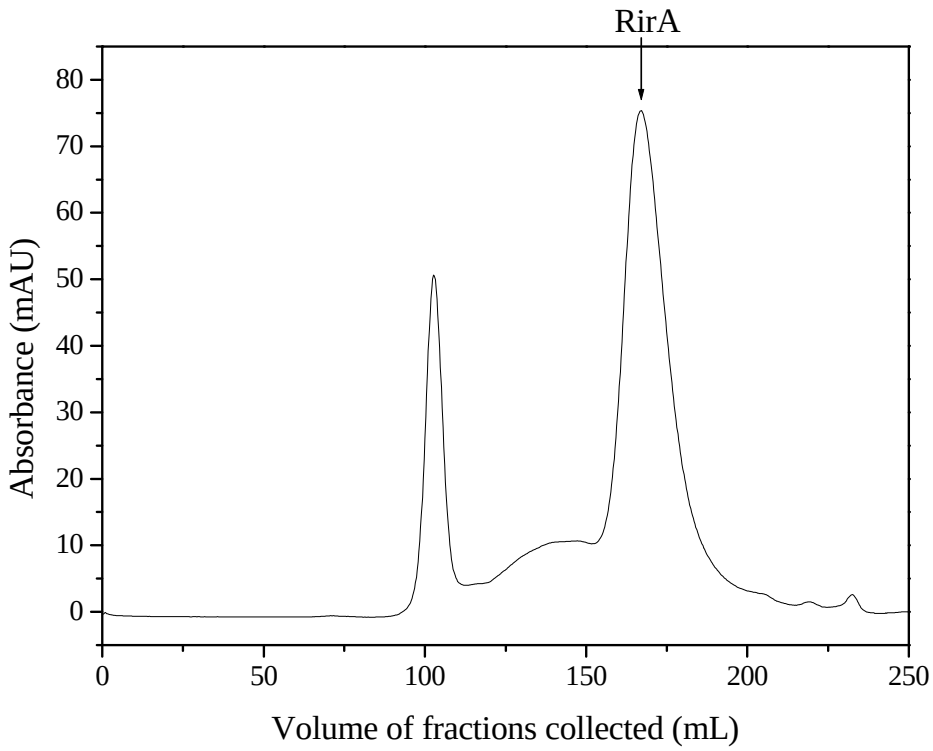

Figure 3.07: S200 gel filtration profile of pooled Heparin-purified RirA showing the presence of contaminants and RirA (indicated) through measurement at 280 nm. The column is run at 1 mL/min.

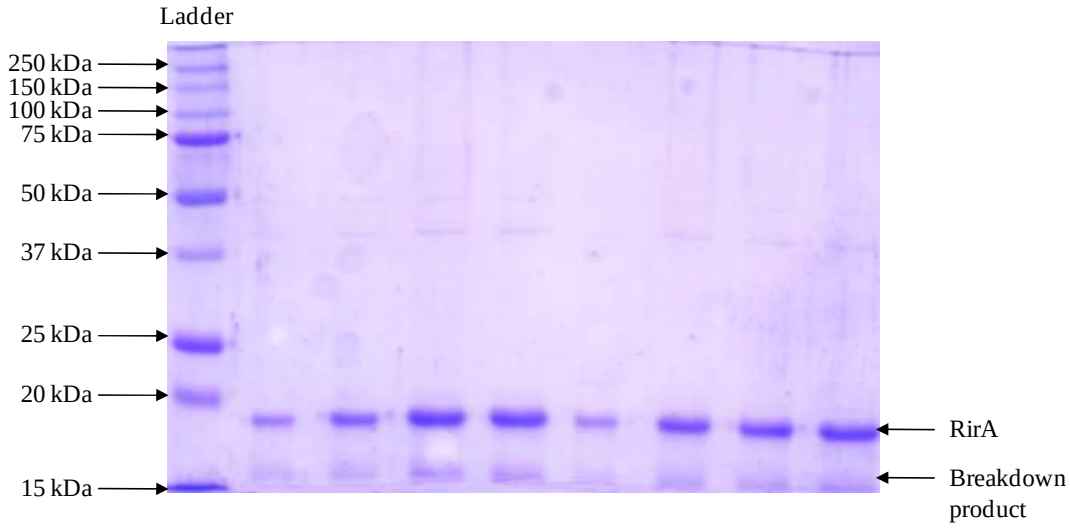

Figure 3.08: 12% SDS gel showing some of the fractions that correspond to the RirA peak shown in Figure 3.07. The protein loading for each lane is 14-16 µg

All protein fractions that contain significant amounts of RirA were pooled and filtered through a single-use syringe filter. Depending on how concentrated the final fractions containing RirA were, the fractions were concentrated using an Amicon ultrafiltration stirred cell model 8050 (using an YM5 membrane disc) or spin columns. This sometimes led to RirA precipitating during concentration and so was only performed if the RirA concentration was particularly low. Once the concentration of RirA is known then appropriate amounts of L-cysteine and ammonium iron (II) sulphate can be calculated and reconstitution can proceed. The concentration needs to be such in that a yellow colour can be easily detected as clusters are formed and the volume is small enough to fit into the special reconstitution chamber.

3.3.2: Investigation of RirA Overexpression and Breakdown Product.

Protein degradation can be a significant problem in purification. Often this is caused by proteases hydrolysing peptide bonds. Solutions to the problem of protein degradation by proteases include the use of inhibitors and changing to a bacterial host strain deficient in proteases (for example, BL21 lacks cytoplasmic *lon* and periplasmic *ompT* proteases [14]). In this study, RirA degradation occurs if IPTG incubation is left for too long. It also appears that formation of the breakdown product occurs over time once the protein is extracted from the cells, and is linked to free iron in solution.

As described in the previous section, the RirA apoprotein is prone to forming a breakdown product. Even before the RirA is purified using column chromatography, it can suffer degradation. As shown in Figure 3.09 the timing of the

IPTG incubation is important for the quantity of protein gained during overexpression.

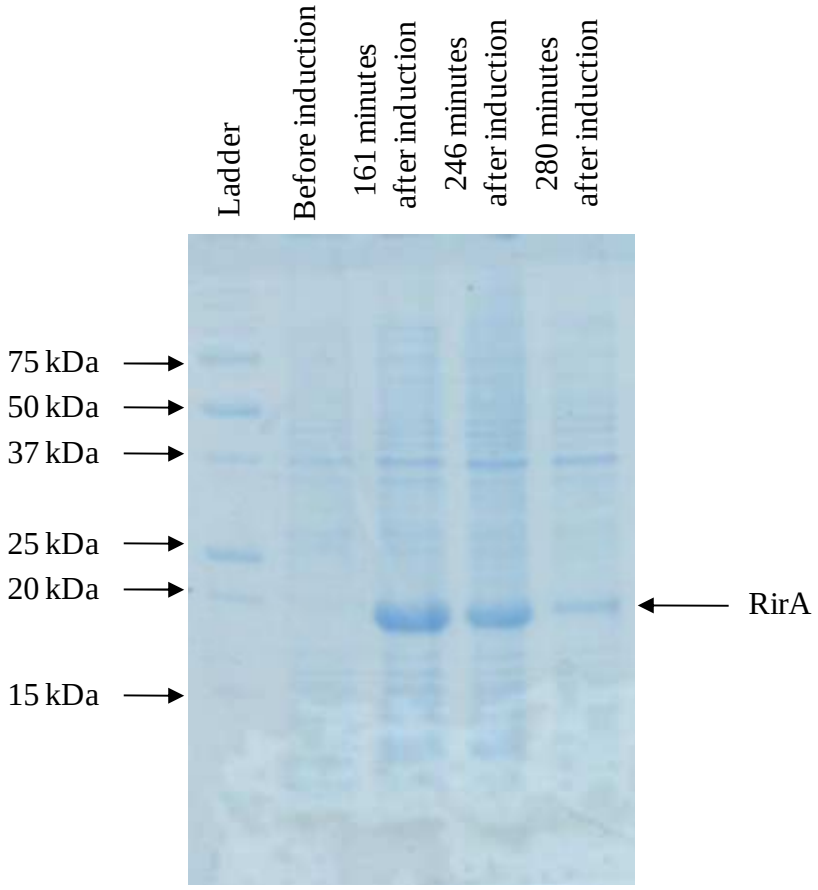

Figure 3.09: 12% SDS-PAGE gel showing the degradation of RirA if IPTG induction is left for too long a time period. Key markers from the ladder are indicated. RirA can be seen just above the 20 kDa marker as indicated by the arrowed RirA label, which correlates with the estimated 17441 Da size from sequencing. SDS-PAGE gel kindly performed and photographed by Nick Cull.

SDS-PAGE analysis (Nick Cull, personal communication) shows that RirA degrades when the cells are left to incubate for too long a time period. This is clearly different from the formation of breakdown product during the preparation and purification of RirA. As the RirA bands decrease in intensity over longer incubation times there is no trace of a growing breakdown product band at ~ 15 kDa. This correlates with the

observation that RirA can be stored without any breakdown product formation in BL21 *E. coli* cells if they are frozen as a pellet. Presumably the presence of RirA at high concentration has a disadvantageous effect on the BL21 *E. coli* cells, and therefore the cell takes measures to reduce the amount of intracellular RirA. The protein is not toxic to the BL21 cells since cell growth is not slowed down and overexpression is consistently high.

Once RirA is overexpressed and cell extract is acquired after sonication the breakdown product begins to form. The breakdown product forms at around 15 kDa, below the intact RirA band at ~ 20 kDa. Eventually all of the RirA breaks down into the breakdown product over a period of weeks as shown in Figure 3.10.

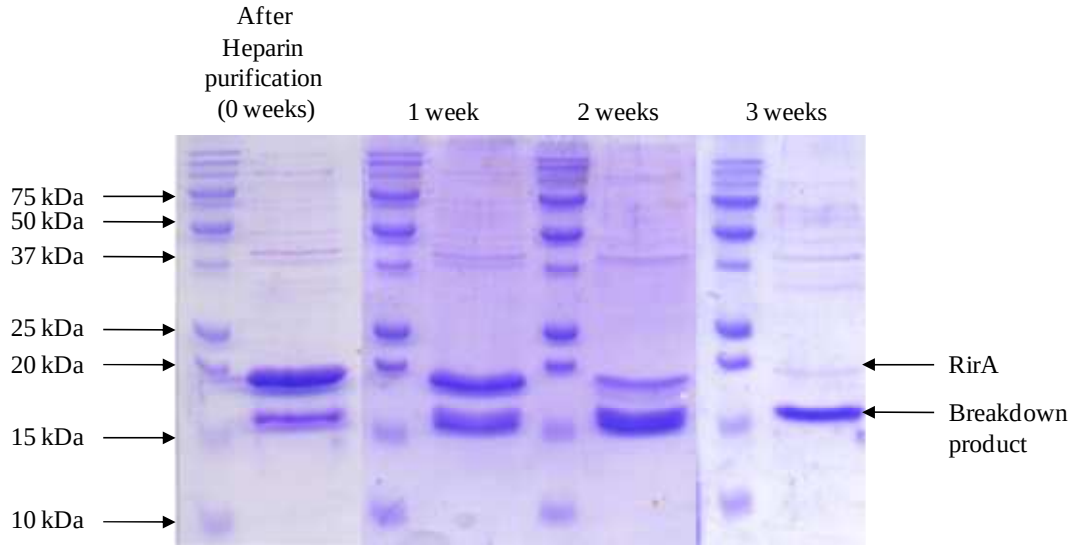

Figure 3.10: 15% SDS PAGE of Heparin purified RirA showing the timescale of formation of breakdown product over a period of weeks at room temperature. Protein loading for lanes 0, 1 and 2 weeks 54 µg. The week 3 lane contains 47 µg protein due to a small amount of precipitation occurring.

By adding 10 mM EDTA to all buffers and carrying out the preparation in an anaerobic cabinet, the formation of the breakdown product is slowed. From this

effect of EDTA it was postulated that free metals may have had an effect on the degradation of RirA. This was tested by adding ferrous iron (100 µM $Fe(NH_4)_2(SO_4)_2.6H_2O$) to RirA protein in both aerobic and anaerobic environments at 4°C. The resulting SDS-PAGE is shown in Figure 3.11.

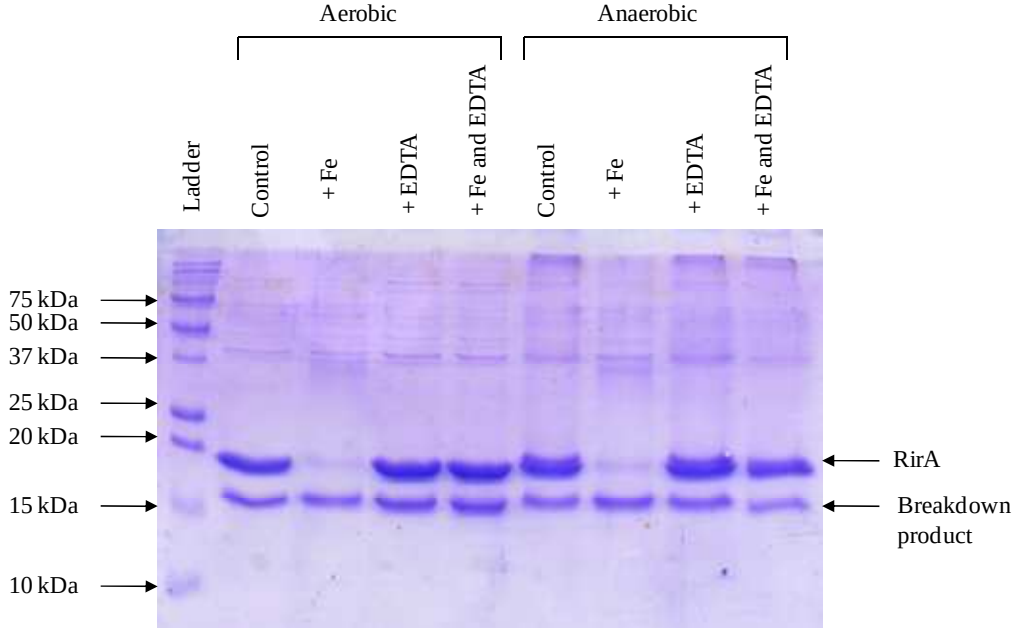

Figure 3.11: 15% SDS PAGE gel showing the effects of iron and oxygen on RirA degradation at 4°C. Protein loading for all lanes is 53 µg. Samples containing iron had 100 µM $Fe(NH_4)_2(SO_4)_2.6H_2O$ added and samples containing EDTA had 1 mM EDTA added.

From Figure 3.11 there appears to be evidence of iron having an effect on breakdown product formation. The band corresponding to intact RirA is almost removed in both the aerobic and anaerobic sample containing iron. There is however no evidence for oxygen causing rapid breakdown product formation on its own, as the corresponding aerobic and anaerobic samples look very similar to each other. The EDTA would chelate any free iron in solution and stop any acceleration in breakdown product formation, therefore the samples containing EDTA and Fe + EDTA should look

similar to the control sample which contains no iron or EDTA. Figure 3.12 shows a gel after Heparin purification with much less breakdown product then that shown in

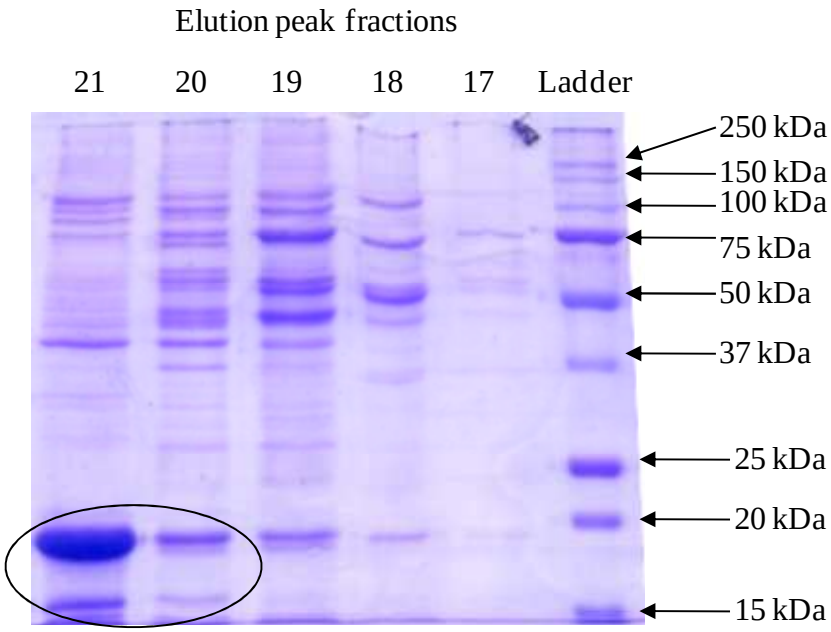

Figure 3.12: 12% SDS PAGE of Heparin purified RirA with a small amount of breakdown product (circled). Note the comparative size of the breakdown product to the corresponding earlier preparation SDS PAGE shown in Figure 3.06. Elution fractions are comparative to those of Figure 3.06, and therefore also correspond to the elution profile shown in Figure 3.04. Protein loadings for lanes 20 and 21 are 24 µg and 69 µg respectively.

Figure 3.07 due to the use of EDTA. However, the EDTA chelated with the ammonium iron (II) sulphate in the reconstitution stage. Reconstitutions involving EDTA would develop no colour in the time period, show no characteristic shoulder in the electronic absorbance spectrum and would result in black precipitation. The chelation of iron by EDTA resulted in more and more iron becoming unavailable and therefore clusters could not be produced. The black precipitate was the result of formation of iron (II) sulphide occurring through sulphide generation becoming

uncontrolled or accumulation of too much unreacted sulphide in the reaction mixture. Thus EDTA was only used in buffers up until the Heparin purification stage.

3.3.3: Sequencing of the RirA Apoprotein.

DNA sequencing is an important tool in the identification of genes. Sequencing of DNA can be performed through chain-termination methods such as the use of dideoxyribonucleotides [15] or through the use of next generation sequencing methods [16]. Once the sequence of a gene is known and is linked to a function then it can be used for many purposes, such as identifying genes with similar functions in other organisms, or confirming whether a correct gene is inserted into a plasmid and checking for mutations, as in this study.

To confirm that the overexpressed protein was indeed RirA, the pET21a plasmid containing the RirA insert was sequenced using Eurofin MWG sequencing. The sequence data shows that the insert is 100% identical to the amino acid sequence shown in Figure 3.01. The sequence data for the pET21a plasmid with the RirA insert is shown in Figure 3.13. The sequence has been translated using the ExPASy translate tool. Features of the plasmid such as the ribosome binding site, the two restriction sites *Nde*I and *Bam*HI, the His.Tag region and the T7 terminator were checked against a pET21a cloning/expression region map on the Novagen website and found to be exactly the same in sequence. However, examination of the sequence of the plasmid around and at the *Xba*I restriction site showed significant mutation. The *Xba*I site is close to the T7 promotor that controls expression. Any mutations at the T7 promotor could adversely affect expression. These mutations could be an explanation as to why overexpression of the protein using pET21a in the third year was largely unsuccessful. The sequence requested was not extensive enough to tell

whether the T7 promotor or other important sites such as the *lacI* operon were mutated.

The replacement pET11a plasmid artificially constructed by GenScript has also been sequenced. The sequence data is shown in Figure 3.14.

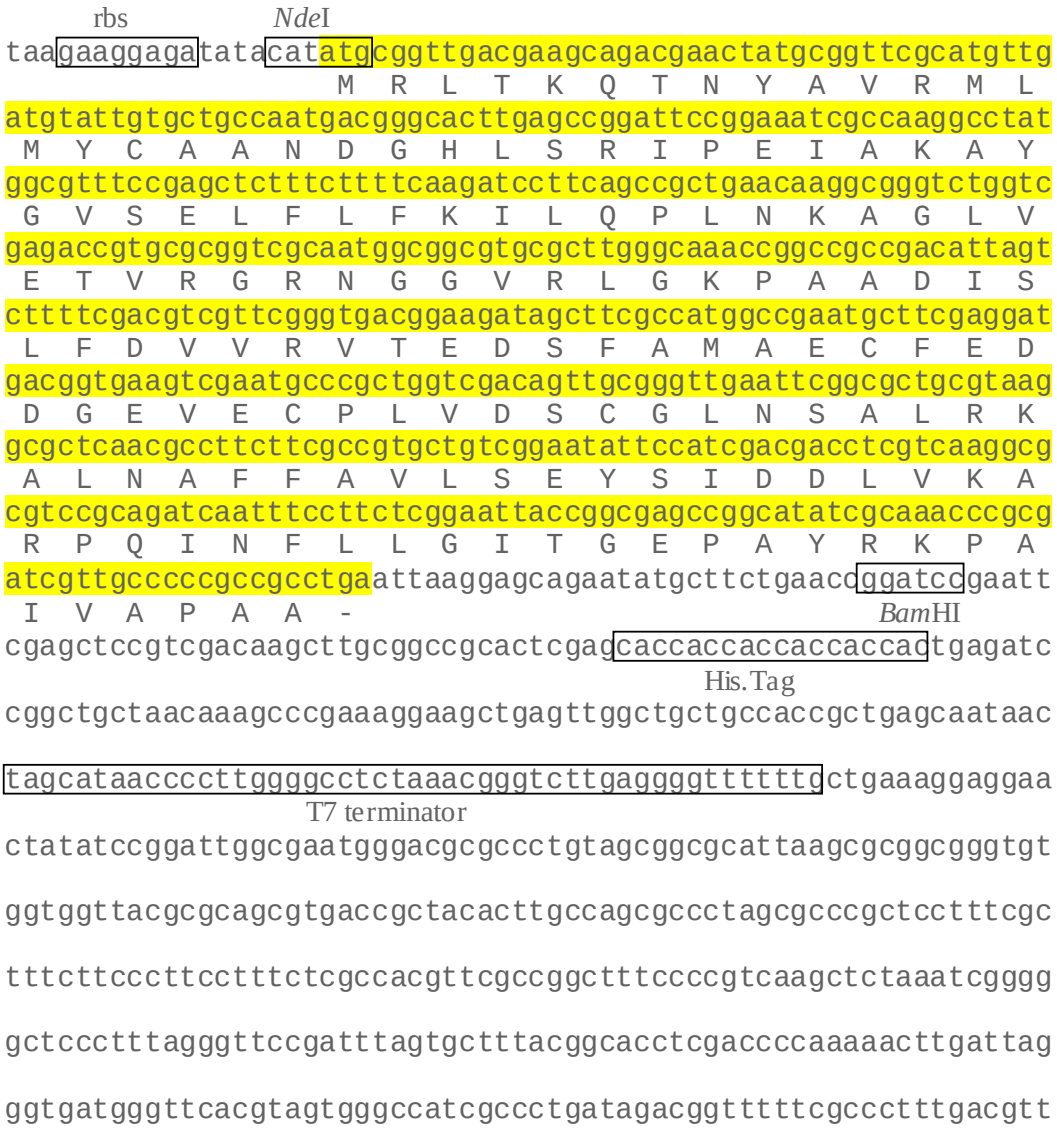

Figure 3.13: Sequence data of the pET21a plasmid with the RirA insert. The RirA sequence is highlighted in yellow with the amino acid corresponding to the codon below. Features of the pET21a plasmid that fall into the sequence given are boxed and labelled.

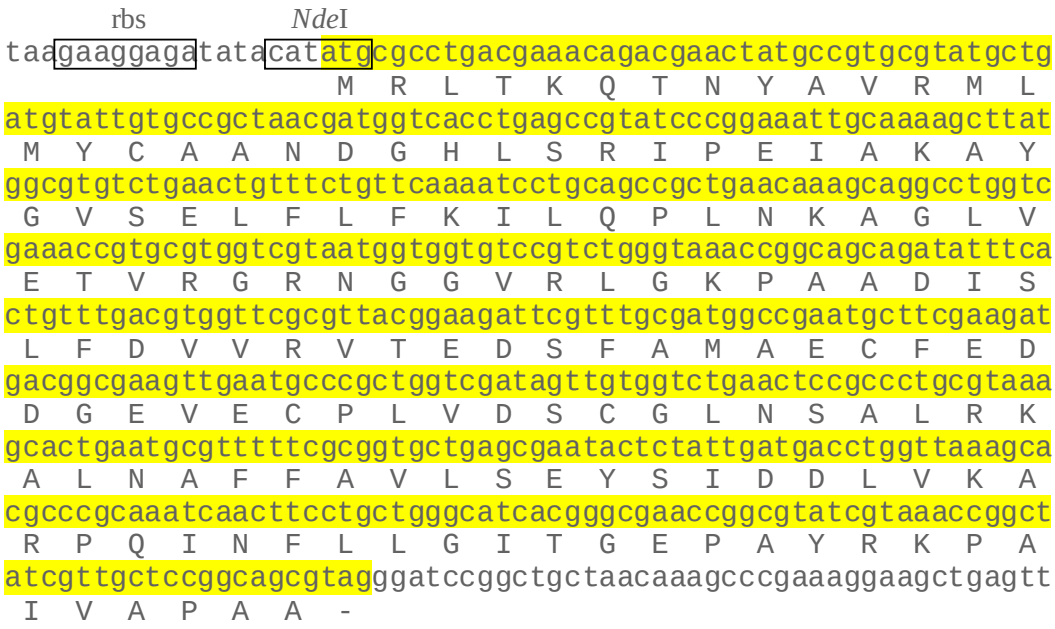

Figure 3.14: Sequence data of the pET11a plasmid with the RirA insert. The RirA sequence is highlighted in yellow with the amino acid corresponding to the codon below. Features of the pET11a plasmid that fall into the sequence given are boxed and labelled.

The insert for the pET21a plasmid and pET11a plasmid has 100% identity to the sequence identified as RirA by Todd and co-workers [6]. This alignment is shown in Figure 3.15. The multiple sequence alignment demonstrates that the protein overexpressed throughout the study has been RirA from which the sequence was determined by Todd *et al* [6]. It also demonstrates that the insert in the pET21a plasmid has no mutations which affect the amino acid sequence. Thus, the problems encountered with pET21a can easily be rectified through restriction digestion with *Nde*I and *Bam*HI to remove the insert from the mutated vector. The RirA insert can then be religated to fresh pET21a plasmid and prepared as before.

```
Todd 2002 MRLTKQTNYAVRMLMYCAANDGHLSRIPEIAKAYGVSELF 40
pET11a    MRLTKQTNYAVRMLMYCAANDGHLSRIPEIAKAYGVSELF 40
pET21a    MRLTKQTNYAVRMLMYCAANDGHLSRIPEIAKAYGVSELF 40

Todd 2002 LFKILQPLNKAGLVETVRGRNGGVRLGKPAADISLFDVVR 80
pET11a    LFKILQPLNKAGLVETVRGRNGGVRLGKPAADISLFDVVR 80
pET21a    LFKILQPLNKAGLVETVRGRNGGVRLGKPAADISLFDVVR 80

Todd 2002 VTEDSFAMAECFEDDGEVECPLVDSCGLNSALRKALNAFF 120
pET11a    VTEDSFAMAECFEDDGEVECPLVDSCGLNSALRKALNAFF 120
pET21a    VTEDSFAMAECFEDDGEVECPLVDSCGLNSALRKALNAFF 120

Todd 2002 AVLSEYSIDDLVKARPQINFLLGITGEPAYRKPAIVAPAA 160
pET11a    AVLSEYSIDDLVKARPQINFLLGITGEPAYRKPAIVAPAA 160
pET21a    AVLSEYSIDDLVKARPQINFLLGITGEPAYRKPAIVAPAA 160
```

Figure 3.15: Multiple sequence alignment showing the sequence of RirA as published in Todd *et al.* 2002 [6] compared to the RirA inserts of the pET21a and pET11a plasmids used in this work. All residues are conserved for all three sequences. Alignment constructed using ClustalW2 and Jalview [17, 18].

3.3.4: Characterisation of Protein by Size Exclusion Chromatography

Determining the oligomeric state of a protein can reveal information relevant to function and structure. Oligomerization gives proteins functional and structural advantages, including increased control over active site accessibility and specificity, higher complexity and improved stability. It can also be disadvantageous; leading to the formation of structures that are pathogenic [19]. There are several methods that can be used to determine the oligomeric state including analytical centrifugation, gluteraldehyde crosslinking [20] and size exclusion chromatography. For the

purposes of this study size exclusion chromatography was performed to determine whether the unreconstituted RirA apoprotein was monomeric or multimeric. This is a technique whereby proteins of known sizes are applied to a gel filtration column under the same conditions. The proteins elute at differing elution volumes (V_e). From this a size exclusion calibration curve can be plotted. The protein of unknown oligomeric state can then be applied to the column. The elution volume of this protein can then be compared with the known standards to determine the molecular weight and oligomeric state.

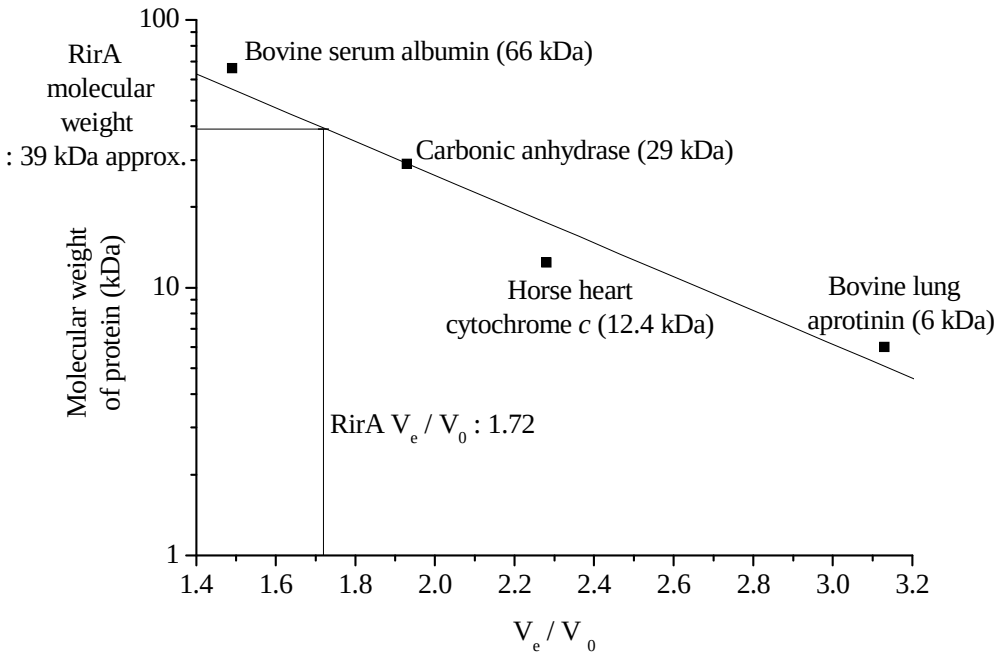

Figure 3.16: Size exclusion chromatography calibration curve showing the protein standards and the associated trendline. RirA has a V_e / V_0 of 1.72 which gives a molecular weight of 39 kDa as indicated on the logarithmic scale.

A HiPrep 26/60 S200 gel filtration column was used. The calibration was performed using blue dextran (~ 2,000,000 Da) for determining the void volume,

bovine serum albumin (66,000 Da), carbonic anhydrase (29,000 Da), horse heart cytochrome *c* (12,400 Da) and aprotinin from bovine lung (6,500 Da). The calculated molecular weight of RirA is shown in Figure 3.16.

The deduced molecular weight of 39 kDa is close to the molecular weight anticipated for dimeric RirA (each monomer is 17.4 kDa). The size exclusion chromatography was also tried with protein containing the cluster. However this was unsuccessful due to cluster degradation during chromatography. Analysis of the collected protein using electronic absorbance spectroscopy revealed no characteristic iron-sulphur cluster shoulder at 410 nm (Figure 3.18).

3.3.5: Characterisation of Protein by Determination of Extinction Coefficients and Recording of Electronic Absorbance Spectra.

Extinction coefficients can be used to accurately quantify the amount of protein in a given sample. Approximate extinction coefficients can be estimated through assigning a molar extinction coefficient value to each tryptophan, tyrosine and cystine (disulphide-bonded cysteine) in the protein sequence. From the figures of Pace *et al*. the extinction coefficients for tryptophan, tyrosine and cystine are 5,500, 1,490 and 125 M^{-1} cm^{-1} respectively [21]. Adding all the tryptophans, tyrosines and cystines in a sequence would give an estimate of the extinction coefficient of the protein. This calculation can be performed through a computer program such as the ExPASy extinction coefficient calculator.

The extinction coefficient can be more accurately determined through measuring absorbances at 280 nm of native protein and the same protein sample denatured by 6.6 M guanidine-HCl. The extinction coefficient of the denatured protein can then be calculated using the extinction coefficients of tryptophan,

tyrosine and cystine as reported by Pace *et al.* [21]. The native extinction coefficient can then be calculated through Equation 2.

$$\varepsilon_{\text{Native 280 nm}} = \varepsilon_{\text{Denatured 280 nm}} \times (A_{\text{Native 280 nm}}/A_{\text{Denatured 280 nm}}) \quad (2)$$

An extinction coefficient for the RirA apoprotein was calculated by using the ExPASy extinction coefficient calculator and by electronic absorption spectroscopy of native and unfolded forms (See section 2.2.2). Experimental calculations from the ExPASy extinction coefficient calculator predicted a value of 7450 $M^{-1} cm^{-1}$ for RirA that has not broken down. This doubled to take into account that RirA is a dimer is 14900 $M^{-1} cm^{-1}$. Determination of the extinction coefficient by measuring the absorbances of folded and unfolded protein at 280 nm gave a similar value of

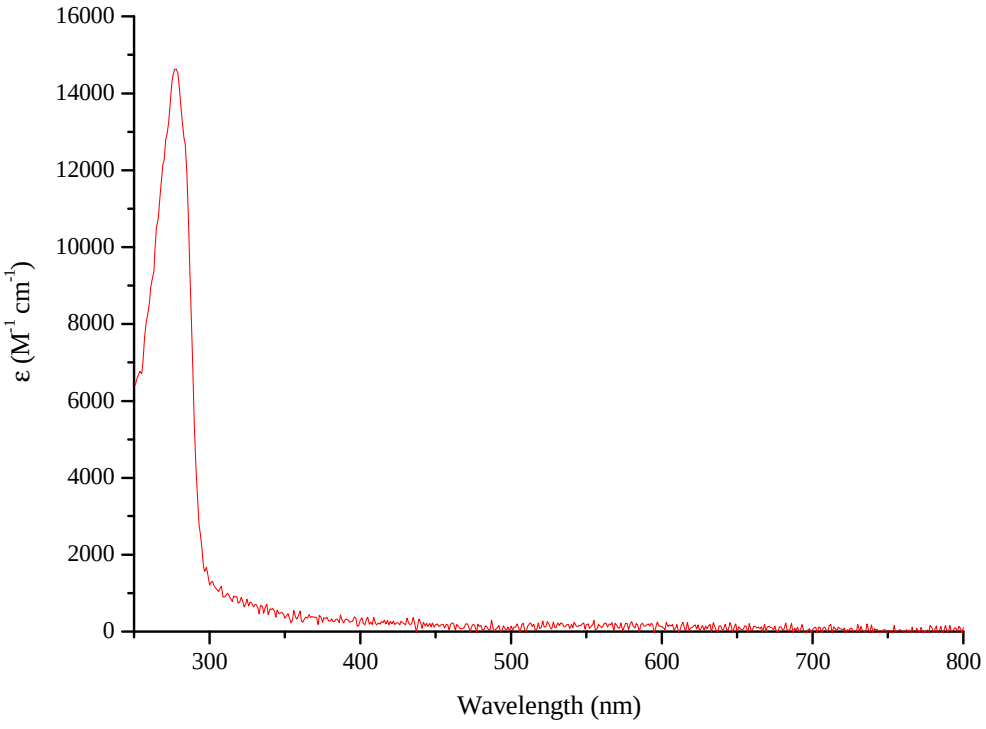

Figure 3.17: Electronic absorption spectrum of RirA apoprotein showing the extinction coefficient at 280 nm as 14800 $M^{-1} cm^{-1}$.

14800 $M^{-1}\,cm^{-1}$. This was calculated using the 14900 $M^{-1}\,cm^{-1}$ denatured extinction coefficient and dividing by ($A_{Native\ 280\ nm}/A_{Denatured\ 280\ nm}$). These extinction coefficients may have significant error however due to the lack of tryptophan in the RirA sequence [21]. An electronic absorption spectrum of RirA apoprotein can be seen in Figure 3.17.

An estimation of the extinction coefficient of the holoprotein was also calculated by taking an electronic absorption spectrum at the same concentration of protein as the apoprotein as shown in Figure 3.18.

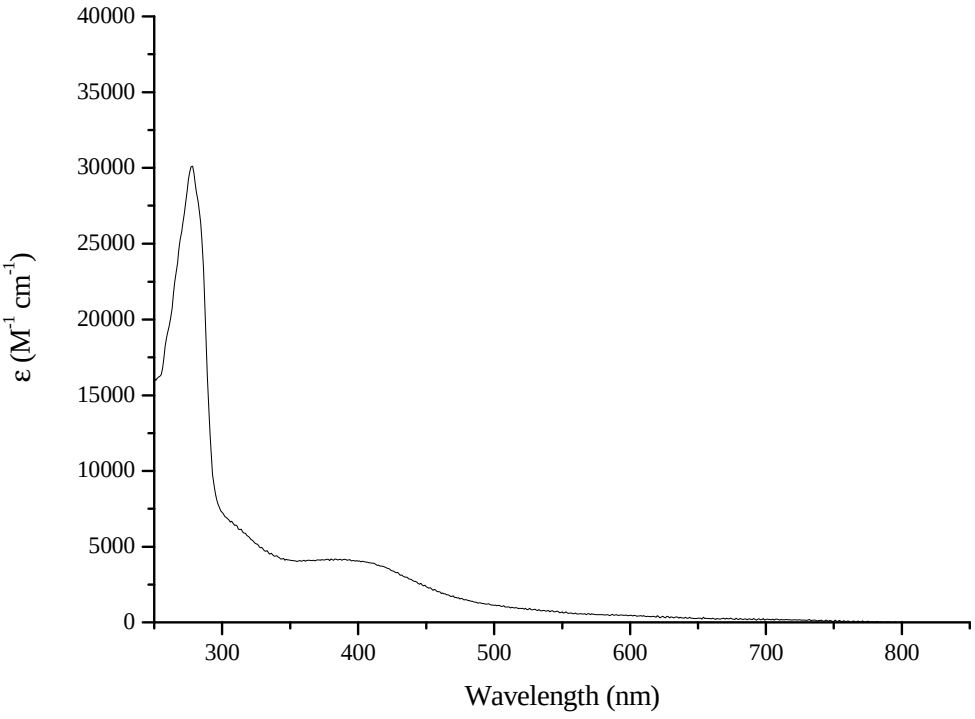

Figure 3.18: Electronic absorbance spectrum of RirA holoprotein that is 11.8% cluster loaded. An extinction coefficient of 32986 $M^{-1}\,cm^{-1}$ per RirA monomer at 410 nm is calculated for 100% loading.

By applying the same multiplication factor using to convert the apoprotein absorbance to ε the two spectra can be compared. However, the reconstituted protein does not have 100% loading of cluster. Iron and sulphur assays of the reconstituted protein shown in Figure 3.18 revealed a dimeric protein concentration of 313 μM, a sulphide concentration of 296 μM and an iron concentration of 315 μM. The electronic absorption spectra shown in Figure 3.18 is characteristic of a [3Fe-4S] or [4Fe-4S] spectrum, since the [2Fe-2S] clusters have more features present in their electronic absorbance spectra [22]. If the protein and sulphide concentrations are compared, since these would be the same for both [3Fe-4S] and [4Fe-4S], then the sulphide concentration suggests that 11.8% of the total sulphide required for complete loading has been reconstituted. The sulphide concentration should be eight times that of the protein concentration for 100% loading, as the RirA dimer has two sites for a [3Fe-4S] or [4Fe-4S] iron sulphur cluster (one per monomer). This gives an extinction coefficient of ~ 33000 $M^{-1} cm^{-1}$ at 410 nm, which correlates to two [4Fe-4S] clusters at around 4000 $M^{-1} cm^{-1}$ per iron [22]. The apoprotein in Figure 3.17 gives no significant absorbance in the 350-500 nm range. Therefore the total absorbance from 300-500 nm in Figure 3.18 must be due solely to the cluster. Therefore the extinction coefficient can be estimated at 410 nm as there are no underlying bands due to protein absorbance.

3.3.6: Dithionite Reduction and EPR of Reconstituted Protein.

Spectroscopic techniques such as UV-visible, EPR and MCD can be used as tools to identify the type and oxidation state of an iron-sulphur cluster present in a protein. The common iron-sulphur cluster types [2Fe-2S], [3Fe-4S] and [4Fe-4S] have characteristic EPR and MCD spectra [22]. Further analysis of cluster type can

also be performed through reduction or oxidation of the iron-sulphur cluster. Oxidised and reduced iron-sulphur clusters can be identified through MCD fingerprinting. EPR, used to detect species with unpaired electrons, is also particularly effective. Reduction or oxidation of an iron sulphur cluster can restore or silence EPR signals, providing additional information for assigning cluster types. In this study, electronic absorbance and EPR spectra were recorded for the reconstituted RirA in reduced and oxidised states. Dithionite and ferricyanide were used to reduce and oxidise the clusters respectively.

The RirA was first checked by recording an electronic absorbance spectrum of the reconstituted protein such as that shown in Figure 3.18. The reconstituted protein was also checked by SDS PAGE to ascertain that the protein that has been reconstituted is indeed RirA (Figure 3.19). A sample of the reconstituted protein was then reduced using sodium dithionite. A reconstituted sample was used containing an estimated 125 μM of dimeric protein, 126 μM of iron and 119 μM of sulphide. The concentration of iron-sulphur cluster can be estimated, for either a [3Fe-4S] or [4Fe-4S], by assuming an extinction coefficient of 4000 M^{-1} cm^{-1} *per iron* [22]. This allows comparison of cluster concentration with the EPR data. Originally 2 μL of 0.88 mM dithionite was to be delivered to the sample for each spectrum recorded. A spectrum was recorded of the original reconstituted protein and the protein containing eight 2 μL additions (final dithionite concentration 33.85 μM) of dithionite (Figure 3.20). The main difference is the disappearance of the shoulder at the 360 nm to 460 nm range when the sodium dithionite is added.

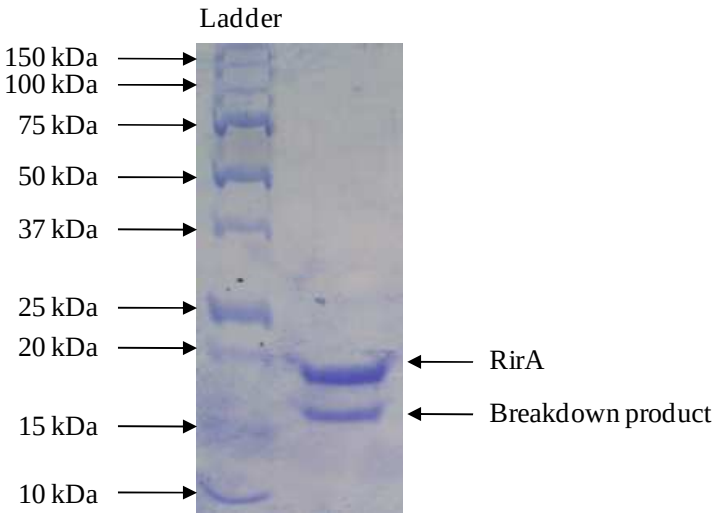

Figure 3.19: 12% SDS PAGE of a small sample of reconstituted protein showing RirA and its breakdown product below the 20 kDa marker and above the 15 kDa marker respectively. Protein loading was 23 µg.

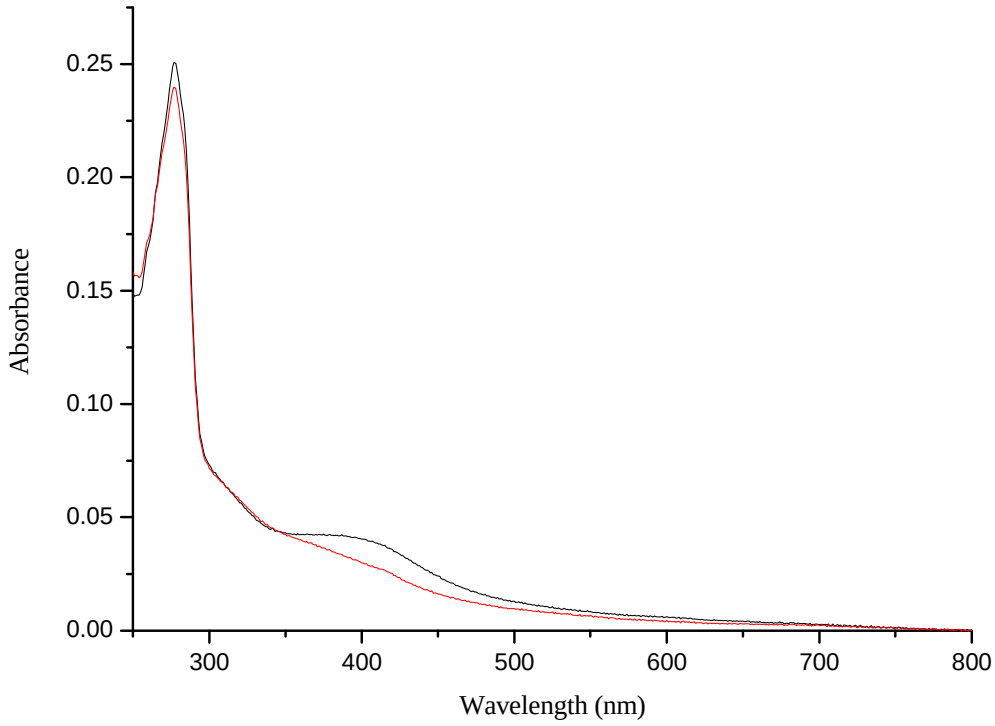

Figure 3.20: Electronic absorption spectra of reconstituted RirA holoprotein (black line) and after treatment with eight 2 µL additions of dithionite (total concentration 33.85 µM dithionite) (red line).

Subsequent additions resulted in no significant shape changes at the shoulder or 280 nm band. There was however an emergence of a peak at 315 nm associated with dithionite. The dithionite solution used in the reduction of the RirA holoprotein was used to reduce a solution of cytochrome *c* of known concentration. Dithionite is a reductant that donates two electrons. However, the purity of dithionite stocks can alter the quantity required to completely reduce a sample. Using oxidised cytochrome *c* a titration was performed to determine what concentration of dithionite was required for complete reduction. The resulting titration demonstrated that 21.5 μM of dithionite was required to completely reduce 26 μM of cytochrome *c*. Since each *c* heme in cytochrome *c* requires one electron for reduction, this equates to 1.21 electrons. From an iron concentration of 126 μM and a dithionite concentration of 33.85 μM (41 μM electrons) the total of 0.32 electrons per iron can be deduced. This is in close agreement with [3Fe-4S] clusters (0.33 electrons per iron) and near to [4Fe-4S] clusters (0.25 electrons per iron).

As well as addition of dithionite, ferricyanide (0.88 mM) was also added in 2 μL aliquots to reconstituted protein to see if any changes could be observed in the electronic absorbance spectrum. The observed spectra of reconstituted protein with ferricyanide additions showed no changes to the original reconstituted spectrum.

The reconstituted protein in oxidised and dithionite-reduced form, as shown in Figure 3.20, were transferred into quartz EPR tubes in an anaerobic cabinet and flash frozen in liquid nitrogen for EPR spectroscopy. A ferricyanide-oxidised sample of reconstituted protein was also analysed through EPR spectroscopy.

The EPR spectra of reconstituted RirA oxidised with ferricyanide (Figure 3.21) were recorded at three different temperatures. At 10 K the spectrum contains a sharp derivative-shaped feature at g = 2.02.

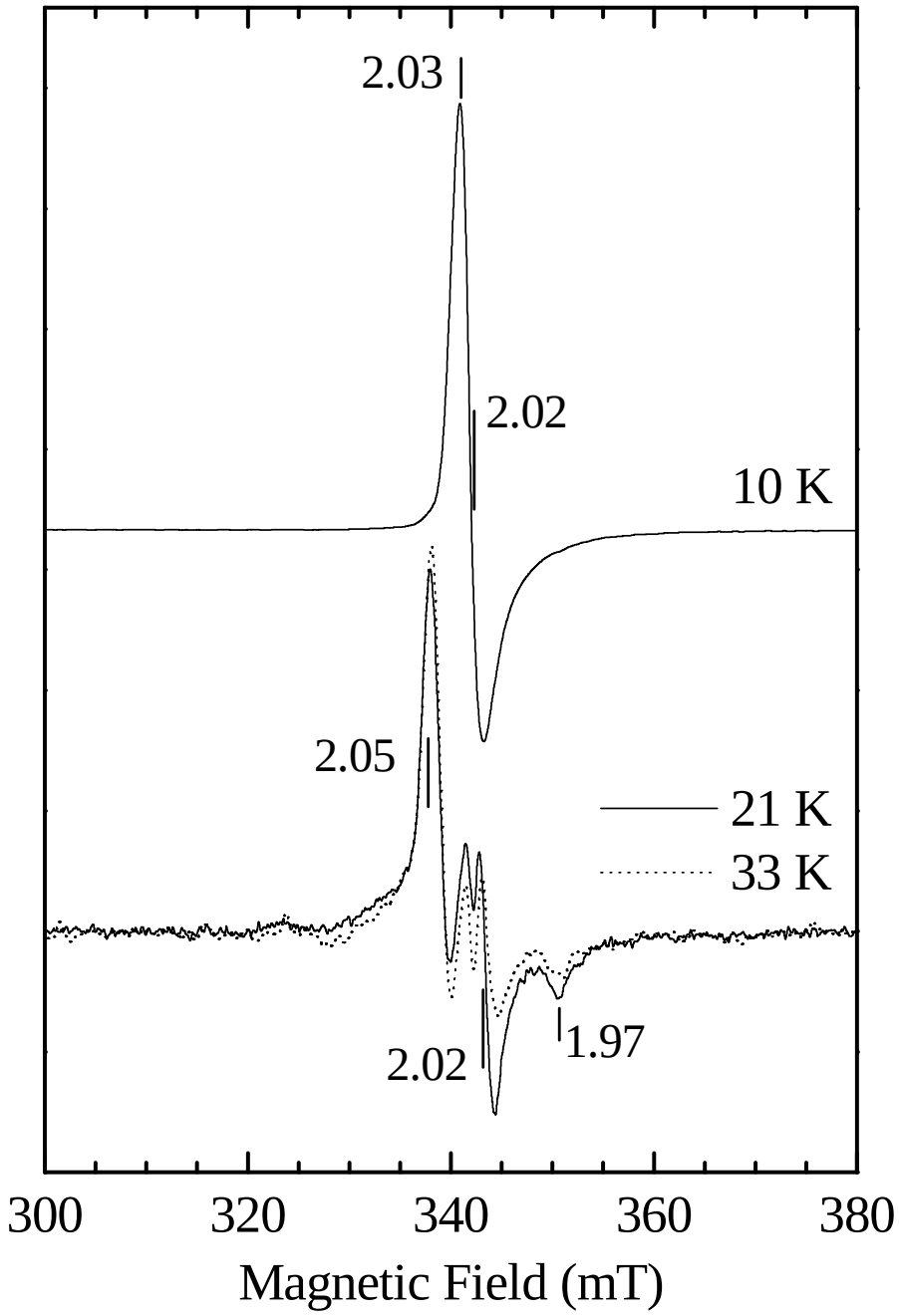

Figure 3.21: EPR spectra for ferricyanide-oxidised reconstituted RirA protein measured at different temperatures. The microwave power was kept at a constant 2 mW and the modulation amplitude was 1 mT. Protein was in 25 mM HEPES, 2.5 mM $CaCl_2$, and 50 mM NaCl at pH 7.5. Protein concentration was 125 µM, iron concentration 126 µM and sulphide concentration 119 µM. The total ferricyanide concentration was 28 µM.

The shape and g-value is absolutely typical for $[3Fe\text{-}4S]^{+}$ clusters, the spin S = 1/2 oxidised state of a three-iron cluster, as typified by the EPR spectra of oxidised ferredoxins from certain *Desulfovibrio* bacteria and aconitase from *E. coli* [22-26]. The g-value of 2.02 is also close to the reported typical value of 2.01 reported for these ferredoxins and aconitase. Another typical feature of $[3Fe\text{-}4S]^{+}$ clusters that is observed in Figure 3.21 is the temperature dependence. The pronounced decrease in intensity with increasing temperature is typical for this species. Due to rapid relaxation, such spectra cannot generally be observed at temperatures above 20 K.

The EPR spectra of reconstituted RirA reduced with dithionite (Figure 3.22) were recorded at two different powers. The small shoulder at low field from the sharp 2.05 feature and the trough at high field at 1.93 become more pronounced at higher power. The increase in size of these features is indicative of a fast relaxing species. They could be tentatively assigned to an interacting pair of paramagnetic species such as two $[4Fe\text{-}4S]^{+}$ clusters, which have been observed to undergo electron spin relaxation at a more rapid rate in 2[4Fe-4S] ferredoxins [27]. $[4Fe\text{-}4S]^{+}$ clusters have a spin S = 1/2 and can be either axial or rhombic with one of the g-values lower than 2 [28]. Reduced ferredoxins from several *Desulfovibrio* bacteria typify a classic $[4Fe\text{-}4S]^{+}$ rhombic signal with g-values of around 2.06, 1.94 and 1.90 [22, 24-26]. The g-values indicated on Figure 3.22 at 2.05, 1.97 and 1.93 are suggestive of those typical $[4Fe\text{-}4S]^{+}$ g-values.

The EPR spectra of the as reconstituted samples of RirA are complex and contain signals from several species (Figures 3.23 and 3.24). Since RirA holoprotein is also thought to be dimeric there could be many combinations of different iron-sulphur cluster types interacting with each other to produce complicated spectra.

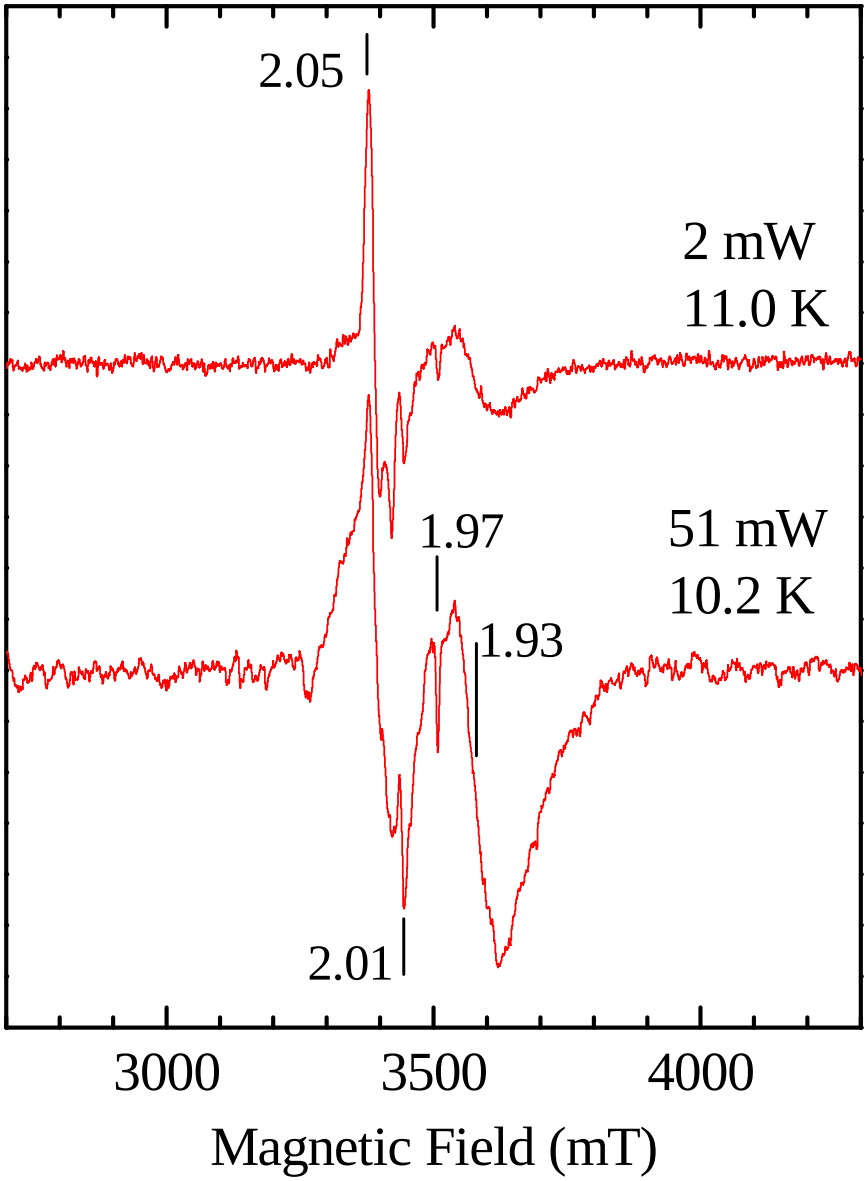

Figure 3.22: EPR spectra for dithionite-reduced reconstituted RirA protein measured at different microwave powers. The temperatures are indicated on the figure and the modulation amplitude was 1 mT. Protein was in 25 mM HEPES, 2.5 mM $CaCl_2$, and 50 mM NaCl at pH 7.5. Protein concentration was 125 µM, iron concentration 126 µM and sulphide concentration 119 µM. The same sample is used in Figure 3.20 so therefore the total dithionite concentration was 33.85 µM.

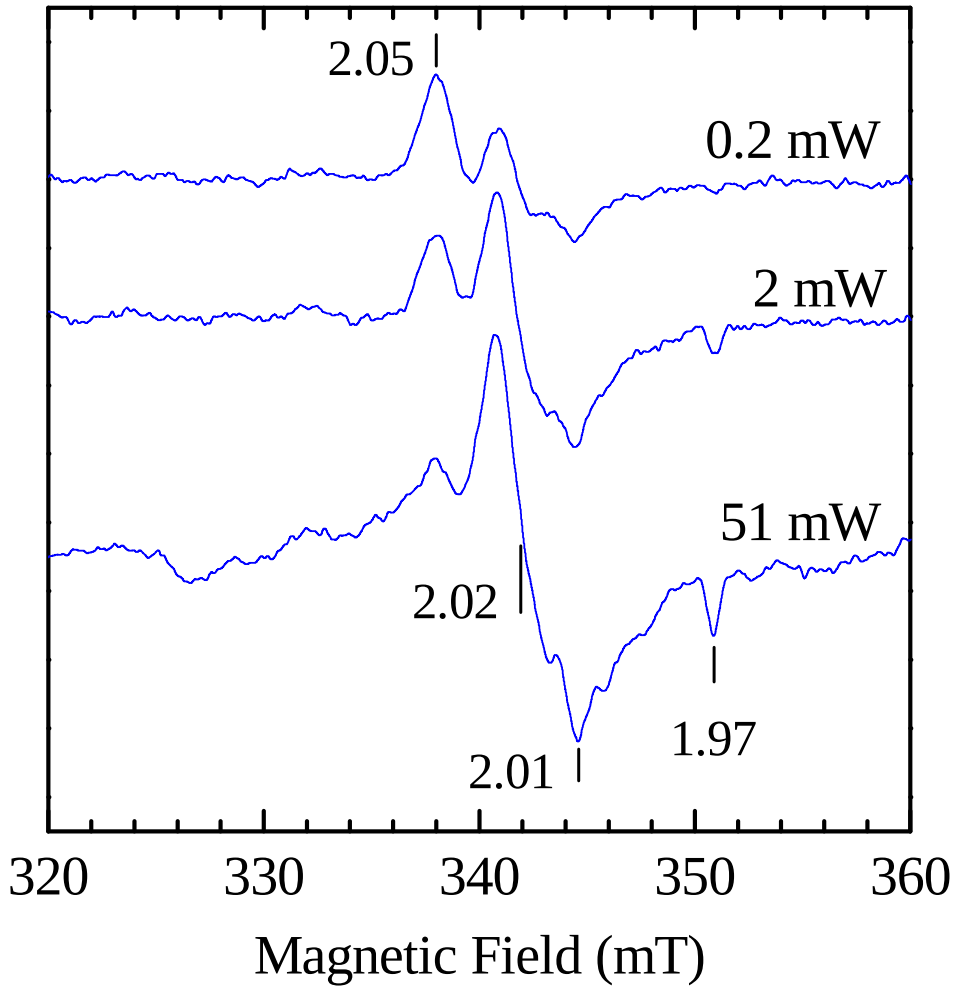

Figure 3.23: EPR spectra for as reconstituted RirA protein measured at different microwave powers. The temperature was kept at a constant 10 K and the modulation amplitude was 1 mT. Protein was in 25 mM HEPES, 2.5 mM $CaCl_2$, and 50 mM NaCl at pH 7.5. Protein concentration was 125 μM, iron concentration 126 μM and sulphide concentration 119 μM.

Because of this it is difficult to assign iron-sulphur cluster types to particular EPR spectral features. Figure 3.23 shows EPR spectra measured at a constant temperature of 10 K but at different powers. From these spectra an axial spectrum with features at 2.02 and 1.97 can be identified.

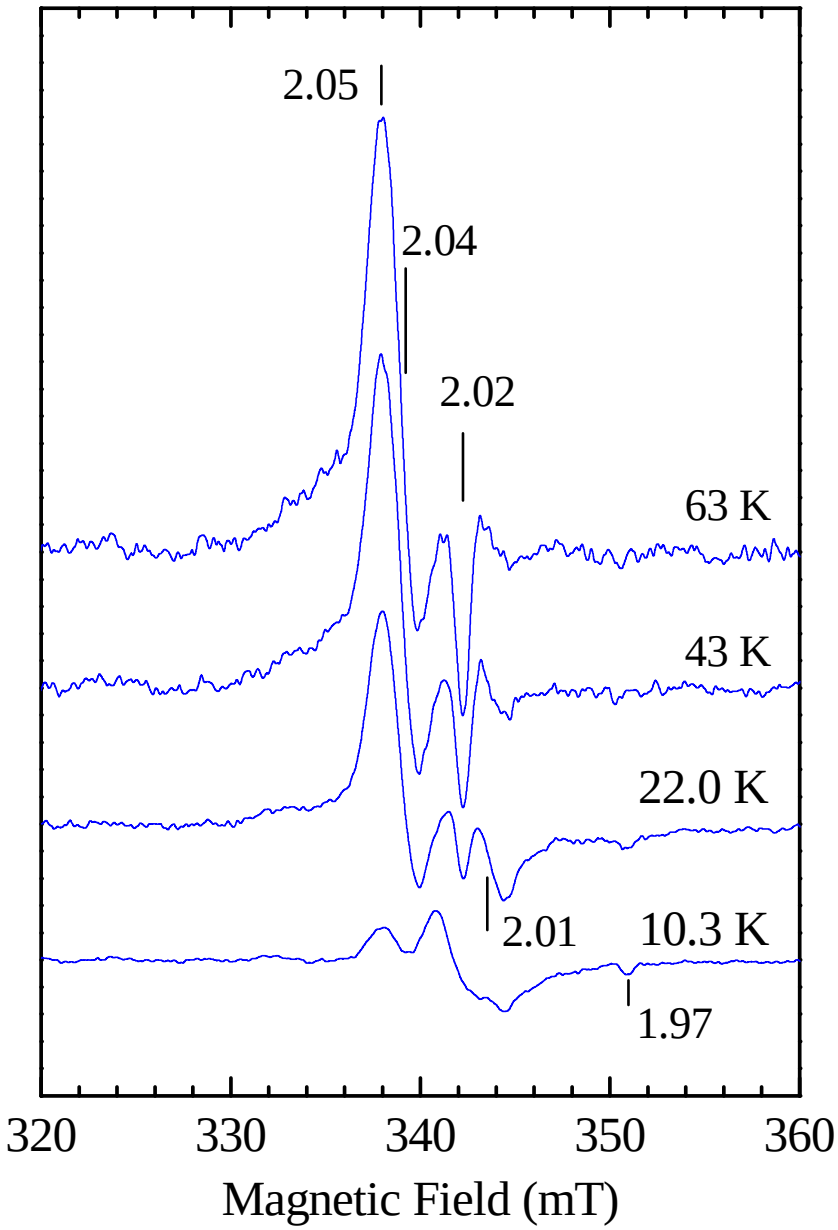

Figure 3.24: EPR spectra for as reconstituted RirA protein measured at different temperatures. The microwave power was kept at a constant 2 mW and the modulation amplitude was 1 mT. Protein was in 25 mM HEPES, 2.5 mM $CaCl_2$, and 50 mM NaCl at pH 7.5. Protein concentration was 125 μM, iron concentration 126 μM and sulphide concentration 119 μM.

The features at these g-values increase in size with increasing power. From this power dependency it can be deduced that this axial species is a fast relaxer. Figure 3.24 shows EPR spectra measured at a constant power of 2 mW but at different temperatures. An axial spectrum can again be identified with features at 2.04 and 2.02. In contrast to the axial spectrum that can be deduced from Figure 3.23, this spectrum indicates this species is a slow relaxer, due to the increase in the size of the features at higher temperature.

In principle, MCD spectroscopy could also be used. The paramagnetic forms of these clusters, $[3Fe\text{-}4S]^{+}$, $[3Fe\text{-}4S]^{0}$, $[4Fe\text{-}4S]^{+}$, all give, at low temperatures, characteristic MCD signals that could be used to identify and quantitate these clusters in oxidised and reduced samples. Unfortunately it proved possible to prepare samples of only 150 μM concentration, well short of the 400 μM needed to prepare MCD samples. Furthermore, samples require the addition of equal volumes of ethanediol or glycerol in order that they form optically transparent glasses when frozen. In the presence of either of these glassing agents, reconstituted RirA precipitated on freezing and we were unable to carry out an MCD characterisation.

3.4: RirA: Summary and Conclusions

The rhizobial iron regulator protein RirA has been expressed, purified and characterised by electronic absorbance and EPR data. Success with iron-sulphur cluster reconstitution has yielded EPR spectra that provide valuable insight into the type of cluster present, as well as allowing observation of properties such as the cluster degradation in the presence of oxygen. However, problems arose during protein overexpression with the pET21a plasmid.

Initially the overexpression of RirA using the pET21a plasmid worked well. However, instances of RirA failing to overexpress became more frequent. Many cell cultures revealed no overexpression of the RirA protein when analysed by SDS-PAGE. This occurred when cultures were grown from glycerol stocks of BL21 cells containing the plasmid and also from freshly transformed BL21 *E. coli* cells. It appeared from looking at the sequence data of the plasmid that there were mutations around and at the *Xba*I restriction site. The limitations of the sequence data meant that other coding sequences could not be investigated for mutations. However the sequence in and around the *Xba*I site was certainly mutated. The T7 promotor is in close proximity to the *Xba*I site and could also contain mutations. This would be likely to have a significant effect on overexpression. The pET21a plasmid has now been replaced with a pET11a plasmid containing the RirA insert synthesised by GenScript. This plasmid has many of the same features of pET21a. It has the T7 promoter, the pBR322 origin of replication, the ampicillin resistance gene as a selection marker and the *lac*I repressor as the target gene for overexpression through induction with IPTG.

Another problem encountered was that the purified RirA contains two forms of the protein due to the formation of a degradation product. Around 10-20 amino acids are lost from the C-terminal end of the RirA protein. Initially, just after producing the crude extract very little of the RirA breaks down. With time more of the RirA turns to breakdown product. The change can be observed via SDS-PAGE electrophoresis as shown in Figure 3.08. The RirA protein band is at ~20 kDa, whereas the breakdown product can be observed closer to the 15 kDa marker. There is no indication that NsrR or IscR behaves in this way [1, 29]. As described, RirA also degrades if the IPTG overexpression stage is allowed to go on for too long

(Figure 3.03). This suggests that the RirA protein at a certain level of expression is possibly cytotoxic. This may result in the *E. coli* cells degrading the protein in response to the cytotoxic effect. The possibility that the protein is being cleaved by a protease in the cell extract is unlikely. The addition of 1 mM AEBSF (and later PMSF) to the buffers was used to combat this, but it had only a minor effect. A protease inhibitor cocktail tablet by Roche was also used to completely eliminate any form of protease activity. This was not successful in stopping the breakdown. Therefore post cell break, protease activity can be ruled out up to a point, dependant on whether the inhibitors were effective at blocking activity of their target proteases. The breakdown product formation was slowed down significantly by the inclusion of EDTA in the purification buffers. This suggests that free metals such as iron may play a part in the degradation of RirA in the cell extract. Oxygen was also tested for a role in the breakdown of RirA once the cell extract was obtained. There is however no evidence of this from SDS-PAGE analysis (Figure 3.09). From Figure 3.03 it appears that RirA degradation to breakdown product does not happen in the cell, but only once the RirA is extracted out of the cells. It is also unlikely that RirA has an oxygen sensing role. Oxygen dependent cluster degradation is linked to function in other proteins. For instance FNR, an oxygen responsive transcriptional regulator of over 100 genes, has a cluster that converts from a $[4Fe\text{-}4S]^{2+}$ to a $[3Fe\text{-}4S]^{+}$ with a pseudo first order reaction of 0.0611 s^{-1} [30]. In contrast WhiD converts from a [4Fe-4S] to apoprotein approximately 300 times more slowly than this at 2.403×10^{-4} s^{-1} [31]. It has been suggested that WhiD does not have a role in sensing oxygen on the basis of comparison with proteins such as aconitase [32]. Reconstituted RirA when left exposed to oxygen does not see rapid cluster degradation of that described for FNR.

RirA solubility posed problems, with precipitation occurring during protein preparation and concentration. NsrR was also found to be unstable in the apo-form with precipitation occurring readily (Dr Jason Crack, personal communication). With both the apo-forms of RirA and NsrR prone to precipitation, it was considered whether the cysteines associated with the iron sulphur clusters were responsible for the instability. The stability of RirA when concentrated is greatly improved when the protein is reconstituted with an iron-sulphur cluster. Dithiothreitol is used in the preparation of NsrR to keep the protein stable [1]. Trials using dithiothreitol in the buffers to stop RirA precipitating only delayed precipitation but did not prevent it. Apoprotein stability did not seem to significantly increase with the inclusion of 5-10% glycerol or 50 mM arginine and glutamic acid in the buffer solution [33]. Guruprasad *et al.* devised an instability index of proteins from analysing their primary sequences. A score of 40 or less predicts that the protein is most likely stable, whereas a score of over 40 predicts the protein is most likely unstable. If the RirA sequence is inputted into the instability index through ExPASy and ProtParam, the prediction is slightly unstable at 41.63 [34].

Through size exclusion chromatography the RirA apoprotein was shown to be a dimer. This technique was also attempted with the iron-sulphur reconstituted protein but the cluster fell apart on application of the protein to the gel filtration column. Two of the Rrf2 family members that contain the conserved cysteines, NsrR and IscR, are also homodimers [1, 35], and therefore the proposal that RirA is a dimer would correlate with the structure of these two related proteins. The Rrf2 family members that do not have the capacity to accommodate iron-sulphur clusters can also provide insight into the structure of RirA. A recent study by Shepard *et al.* [36] described the crystal structure of CymR, a cysteine biosynthesis repressor. This

study described the possible structure of RirA and the positions of the clusters. This is described in more detail in Chapter 5. The likelihood is that the holoprotein is also dimeric and can accommodate two clusters. The presence of four cysteines at each site allows the possibility of the cluster types to be either [2Fe-2S], [3Fe-4S] and [4Fe-4S]. The clusters present were characterised through electronic absorbance and EPR spectroscopy. The significance of the spectroscopic data obtained is discussed next.

Despite the problems encountered, it was possible to obtain highly pure overexpressed RirA and reconstitute it. The reconstitution technique is not specific and can insert a cluster into proteins that normally would not possess one such as bovine serum albumin [37]. It was therefore important to have pure protein so that contaminants could be ruled out of any iron-sulphur cluster signals observed. Iron sulphur clusters observed in IscR and NsrR have been of the [2Fe-2S] type, although there is now a question mark to whether NsrR actually binds a [4Fe-4S] cluster [1, 3, 29, 38]. However, the presence of a [2Fe-2S] cluster in RirA is unlikely. The electronic absorbance spectrum of RirA in Figure 3.18 only shows a characteristic shoulder at ~ 400 nm. Most examples of [2Fe-2S] electronic absorbance spectra have more than one distinct feature. For example the benzene dioxygenase from *Pseudomonas putida* has features at ~ 350 nm, 450 nm and ~ 550 nm [22]. However, the electronic absorbance spectra of [3Fe-4S] and [4Fe-4S] clusters can be very similar in appearance, and therefore cannot be used solely to identify the cluster present. The $[4Fe\text{-}4S]^{2+}$ of aconitase and the $[3Fe\text{-}4S]^{+}$ of native *Thermus aquaticus* ferredoxin have similar features in their electronic absorbance spectra [22, 39].

The EPR of ferricyanide-oxidised reconstituted RirA (Figure 3.21) shows a characteristic S = 1/2 $[3Fe\text{-}4S]^{+}$ signal in terms of shape and g-values that correspond

with $[3Fe\text{-}4S]^{+}$ clusters in aconitase and ferredoxins [22-26]. Figure 3.21 also shows typical temperature dependence of $[3Fe\text{-}4S]^{+}$ clusters, with increasing temperature resulting in a decrease in signal. No $[3Fe\text{-}4S]^{+}$ has been reported for as isolated, oxidised or reduced forms of NsrR or IscR [1, 2, 29, 40]. A [3Fe-4S] cluster intermediate has been observed in NsrR as the result of exposing [4Fe-4S] clusters to oxygen in the presence of DTT [2]. As well as the EPR data, the presence of [3Fe-4S] clusters in the reconstituted protein is consistent with iron and sulphide assays which give the average ratio as 1 iron to 1.33 sulphides. This is close to the 1 iron to 1.25 sulphide ratio of a [3Fe-4S], as opposed to the 1 iron to 1 sulphide ratio of [2Fe-2S] and [4Fe-4S]. It is also consistent with the calculated value of 0.32 electrons per iron in titrations with dithionite. A [3Fe-4S] cluster would have a value of 0.33 electrons per iron to reduce. It is however also close to the value of 0.25 electrons per iron for [4Fe-4S]. It is not known whether the [3Fe-4S] is as a result of incomplete construction of a [4Fe-4S] or if it is physiologically relevant.

The EPR of dithionite-reduced reconstituted RirA shows features that undergo fast relaxation and g-values suggestive of interacting $[4Fe\text{-}4S]^{+}$ clusters. Reduced [4Fe-4S] NsrR has a fast relaxing, axial EPR signal at g = 2.04, 1.93 which is assigned to $[4Fe\text{-}4S]^{+}$ clusters [2]. In comparison the spectra of dithionite-reduced RirA (Figure 3.22) also has features that show fast relaxation at g ~ 2.06 and 1.93. The existence of a [4Fe-4S] cluster per monomer is supported by the calculated extinction coefficient of the holoprotein. At 16493 $M^{-1}\,cm^{-1}$ per monomer it supports a [4Fe-4S] cluster at approximately 4000 $M^{-1}\,cm^{-1}$ per iron [22]. A single non-interacting S = 1/2 $[4Fe\text{-}4S]^{+}$ cluster, such as those seen in reduced ferredoxins [24-26], show a typical rhombic signal with g-values 2.06, 1.94, 1.90. Figure 3.22 has g-values at 2.05, 1.97 and 1.93 that are suggestive of a single $[4Fe\text{-}4S]^{+}$. This suggests

that there is a proportion of reconstituted RirA with two interacting $[4Fe\text{-}4S]^{+}$ clusters and another proportion with a $[4Fe\text{-}4S]^{+}$ cluster in one monomer only. For a single $[4Fe\text{-}4S]^{+}$ cluster to show a rhombic g = 2.05, 1.97, 1.93 signal in reconstituted RirA the other monomer site would have to be occupied by an EPR silent species such as $[3Fe\text{-}4S]^{0}$ or it would have to be empty.

It is certain that [3Fe-4S] clusters are one of the many species that has been reconstituted into RirA in this study. There is evidence for [4Fe-4S] clusters present also. However, there is still much to be done on the characterisation of the iron-sulphur clusters in reconstituted RirA. The as reconstituted EPR spectra of RirA are very complex, with several species present that relax at different rates. Further work to elucidate the identity and proportions of the different species would involve simulation of the EPR spectra. Further spectroscopic work to characterise RirA would also include preparing a MCD sample. This would provide further information that would aid in identifying the clusters. Unfortunately attempts to prepare a MCD sample were unsuccessful, due to problems with concentration and precipitation from addition of the glassing agent. Methods in the future to combat this could include trying a less common glassing agent instead, simply adding the glycerol or ethanediol very slowly or employing different buffers and/or detergents to stabilise the protein.

3.5: References

1. Tucker, N. P., Hicks, M. G., Clarke, T. A., Crack, J. C., Chandra, G., Le Brun, N. E., Dixon, R., Hutchings, M. I. (2008) *PLoS One **3***, e3623.

2. Yukl, E. T., Elbaz, M. A., Nakano, M. M., Moenne-Loccuz, P. (2008) *Biochemistry **47***, 13084-13092.

3. Schwartz, C. J., Giel, J. L., Patschkowski, T., Luther, C., Ruzicka, F. J., Beinert, H., Kiley, P. J. (2001) *Proc. Natl. Acad. Sci. U. S. A.* ***98***, 14895-14900.

4. Yeoman, K. H., Curson, A. R. J., Todd, J. D., Sawers, G., Johnston, A. W. B. (2004) *Microbiology* ***150***, 4065-4074.

5. Todd, J. D., Sawers, G., Johnston, A. W. B. (2005) *Mol. Genet. Genomics* ***273***, 197-206.

6. Todd, J. D., Wexler, M., Sawers, G., Yeoman, K. H., Poole, P. S., Johnston, A. W. B. (2002) *Microbiology* ***148***, 4059-4071.

7. Ngok-Ngam, P., Ruangkiattikul, N., Mahavihakanont, A., Virgem, S. S., Sukchawalit, R., Mongkolsuk, S. (2009) *J. Bacteriol.* ***191***, 2083-2090.

8. Viguier, C. O., Cuiv, P., Clarke, P., O'Connell, M. (2005) *FEMS Microbiol. Lett.* ***246***, 235-242.

9. Chao, T. C., Buhrmester, J., Hansmeier, N., Pühler, A., Weidner, S. (2005) *Appl. Environ. Microbiol.* ***71***, 5969-5982.

10. Hibbing, M. E., Fuqua, C. (2011) *J. Bacteriol.*, [Epub ahead of print]

11. Hannig, G., Makrides, S. C. (1998) *Trends Biotechnol.* ***16***, 54-60.

12. Crack, J. C., Green, J., Thomson, A. J. (2004) *J. Biol. Chem.* ***279***, 9278-9286.

13. Crack, J. C., Gaskell, A. A., Green, J., Cheesman, M. R., Le Brun, N. E., Thomson, A. J. (2008) *J. Am. Chem. Soc.* ***130***, 1749-1758.

14. Terpe, K. (2006) *Appl. Microbiol. Biotechnol.* ***72***, 211-222.

15. Sanger, F., Nicklen, S., Coulsen, A. R. (1977) *Proc. Natl. Acad. Sci. U. S. A.* ***74***, 5463-5467.

16. Zhang, J., Chiodini, R., Badr, A., Zhang, G. (2011) *J. Genet. Genomics* ***38***, 95-109.

17. Chenna, R., Sugawara, H., Koike, T., Lopez, R., Gibson, T. J., Higgins, D. G., Thompson, J. D. (2003) *Nucleic Acids Res.* ***31***, 3497-3500.

18. Clamp, M., Cuff, J., Searle, S. M., Barton, G. J. (2004) *Bioinfomatics* ***20***, 426-427.

19. Marianayagam, N. J., Sunde, M., Matthews, J. M. (2004) *Trends Biochem. Sci.* ***29***, 618-625.

20. Fadouloglou, V. E., Kokkinidis, M., Glykos, N. M. (2008) *Anal. Biochem.* ***373***, 404-406.

21. Pace, C. N., Vajdos, F. Fee, L., Grimsley, G., Gray, T. (1995) *Protein Sci.* ***4***, 2411-2423.

22. George, S. J. (1986) PhD Thesis.

23. Bennett, B., Gruer, M. J., Guest, J. R., Thomson, A. J. (1995) *Eur. J. Biochem.* ***233***, 317-326.

24. Grazina, R., de Sousa, P. M., Brondino, C. D., Carepo, M. S., Moura, I., Moura, J. J. (2011) *Bioelectrochemistry* ***82***, 22-28.

25. Busch, J. L., Breton, J. L., Bartlett, B. M., James, R., Hatchikian, E. C., Thomson, A. J. (1996) *Biochem. J.* ***314***, 63-71.

26. Rodrigues, P., Graca, F., Macedo, A. L., Moura, I., Moura, J. J. (2001) *Biochem. Biophys. Res. Commun.* ***289***, 630-633.

27. Rupp, H., Rao, K. K., Hall, D. O., Cammack, R. (1978) *Biochim. Biophys. Acta* ***537***, 255-260.

28. Sweeney, W. V., Rabinowitz, J. C. (1980) *Ann. Rev. Biochem.* ***49***, 139-161.

29. Zeng, J., Zhang, K., Liu, J., Qiu, G. (2008) *J. Microbiol. Biotechnol.* ***18***, 1672-1677.

30. Crack, J. C., Green, J., Cheesman, M. R., Le Brun, N. E., Thomson, A. J. (2007) *Proc. Natl. Acad. Sci. U. S. A.* ***104***, 2092-2097.

31. Crack, J. C., den Hengst, C. D., Jakimowicz, P., Subramanian, S., Johnson, M. K., Buttner, M. J., Thomson, A. J., Le Brun, N. E. (2009) *Biochemistry* ***48***, 12252-12264.

32. Kennedy, M. C., Emptage, M. H., Dreyer, J. L., Beinert, H. (1983) *J. Biol. Chem.* ***258***, 11098–11105.

33. Golovanov, A. P., Hautbergue, G. M., Wilson, S. A., Lian, L. Y. (2004) *J. Am Chem. Soc.* ***126***, 8933-8939.

34. Guruprasad, K., Reddy, B. V., Pandit, M. W. (1990) *Protein Eng.* ***4***, 155-161.

35. Nesbit, A. D., Giel, J. L., Rose, J. C., Kiley, P. J. (2009) *J. Mol. Biol.* ***387***, 28-41.

36. Shepard, W., Soutourina, O., Courtois, E., England, P., Haouz, A., Martin-Verstraete, I. (2011) *FEBS J.*, [Epub ahead of print].

37. Arakawa, S., Kimura, T. (1979) *Biochim. Biophys. Acta.* ***580***, 382-391.

38. Tucker, N. P., Le Brun, N. E., Dixon, R., Hutchings, M. I. (2010) *Trends Microbiol.* ***18***, 149-156.

39. Emptage, M. H., Dreyer, J. L., Kennedy, M. C., Beinert, H. (1983) *J. Biol. Chem.* ***258***, 11106-11111.

40. Schwartz, C. J., Giel, J. L., Patschkowski, T., Luther, C., Ruzicka, F. J., Beinert, H., Kiley, P. J. (2001) *Proc. Natl. Acad. Sci. U. S. A.* ***98***, 14895-14900.

Chapter 4.

Novel heme derivatives formed in the reactions of oxidised (as-prepared) cd_1 with NO_2^- substrate and other nitrogenous ligands.

4.1: Introduction

A long established method of probing the transition metal sites of metalloproteins is to monitor their interactions with, and accessibility to, small exogenous ligands. This approach was used extensively in the analysis of the hemes in cd_1, particularly in the case of *Pseudomonas aeruginosa*. Some ligands bind to the d_1 heme of cd_1 in a straightforward coordinative manner. For example fluoride, cyanide and imidazole ligands show simple coordination to the heme d_1 ferric ion, modifying but still exhibiting the Fe^{III} EPR spectrum [1, 2]. In the case of fluoride coordination, the heme d_1 EPR spectrum changes from rhombic to axial. Cyanide complexation with cd_1 causes more extensive changes to both *c* and d_1 EPR features. A peak attributable to heme *c* moves from $g = 2.98$ to $g = 3.31$. The d_1 spectrum is rhombic with *g* values 2.47, 2.35 and 1.61. By comparison with cyanide-complexed sperm whale myoglobin the authors concluded that cyanide binds to the *c* heme of cd_1 [3]. Imidazole-complexed *P. aeruginosa* cd_1 also has a resonance attributable to the d_1 heme at $g_{xy} = 2.58$. The *c* heme is again affected, with the g_z resonance shifted to $g = 3.55$. Some unliganded *c* heme also remains at $g = 2.98$ [2]. It is unclear whether histidine or methionine is displaced by cyanide or imidazole. nIR MCD spectroscopy may elucidate which amino acid residue is displaced. The histidine-methionine charge transfer band has a peak at ~1775 nm. Both cyanide and imidazole give rise to IR charge transfer MCD wavelengths that are similar to

histidine. Therefore if these ligands displace the histidine, the wavelength at ~1775 nm will not change significantly. If the methionine is displaced however then the new ligand set will appear as bis-histidine. The wavelength at which a bis-histidine charge transfer band occurs is ~1550 nm. Therefore the displaced amino acid ligand can be identified. Thus with fluoride, cyanide and imidazole, although heme *c* may also be involved in binding, heme d_1 remains low-spin ferric with detectable EPR. In contrast it has been reported that additions of nitrite, NO or azide lead to the complete removal of all d_1 EPR features [1, 2, 4].

Although cd_1 was first identified as a cytochrome oxidase, it is now accepted that its physiological substrate is nitrite. Nitrite is ambidentate, being able to bind to heme in two different confirmations. Both are monodentate. The first is bound via the nitrogen atom and is termed nitro, while the second is bound by one of the oxygen atoms and is termed nitrito. In inorganic models nitrite is always bound to iron by the nitrogen atom whether the iron is in the ferrous or ferric state. Protein heme-nitrite structures are limited. Three protein structures have been reported in which NO_2^- binds via the nitrogen atom: cd_1 from *Paracoccus pantotrophus* [5]; sulphite reductase hemoprotein from *Escherichia coli* [6]; and cytochrome *c* nitrite reductase from *Wolinella succinogenes* [7]. However there is an example of a protein heme-nitrite structure that does not conform to the N-binding mode. Horse heart met-myoglobin binds nitrite in the oxygen atom binding nitrito conformation, although this is changed to the nitro conformation when the distal heme pocket residue histidine-64 is mutated to a valine [8, 9].

Both cd_1 and myoglobin have nitrite reductase properties with the resulting product being NO [10-12]. NO is a very strong binding ligand to heme, especially so when the heme iron is in the ferrous state. The formation constants (K_f) for NO

binding to ferrous and ferric heme are generally 10^{11}-10^{12} and 10^{3}-10^{7} M^{-1} respectively [13 and refs therein]. This is obviously a potential problem for a heme-containing enzyme that makes NO as a product. The NO ligands are bound to the heme iron by the nitrogen atom in an arrangement that has a relatively strong ligand field strength. In inorganic chemistry, NO as a ligand can vary in character between two common types. The first is the linear nitrosonium ligand with an M-N-O bond angle in the range 160-180°. This is the NO^+ species, a 2-electron σ-donor with an N-O bond order of 3. The true NO^+ species has a high stretching frequency ν_{NO} of 2200-2400 cm^{-1} as demonstrated by the nitrosonium salt $NO^+BF_4^-$. The second type is the bent nitrosyl arrangement with a bond angle of 120-140°. This is the NO species that has a bond order of 2.5. The NO species has a lower ν_{NO} than the NO^+ species. The figure for the gaseous form is 1876 cm^{-1}. Ferric heme bound NO adopts the linear mode of binding becoming Fe^{II}-NO^+ whereas ferrous heme bound NO adopts the bent conformation as shown in Figure 4.01. There is a third nitroxyl species, NO^-, but this is rare. The ν_{NO} for this form of NO is 1150-1170 cm^{-1}.

The azide ligand has weak to intermediate ligand field strength. Like the nitrite ligands it is monoanionic and monodentate. The azide ligand has two resonance forms as shown in Figure 4.02. In horse heart metmyoglobin the azide ligand favours an angled conformation when bound to the haem iron [14, 15]. The binding to heme only requires one of the lone pairs from the three on the N^{2-}. Horse heart myoglobin with an azide ligand bound displays a mixture of high and low spin species [16]. This is very similar to tyrosinate-bound *P. pantotrophus cd*$_1$ in that a high spin / low spin equilibrium also exists for the d_1 heme [17].

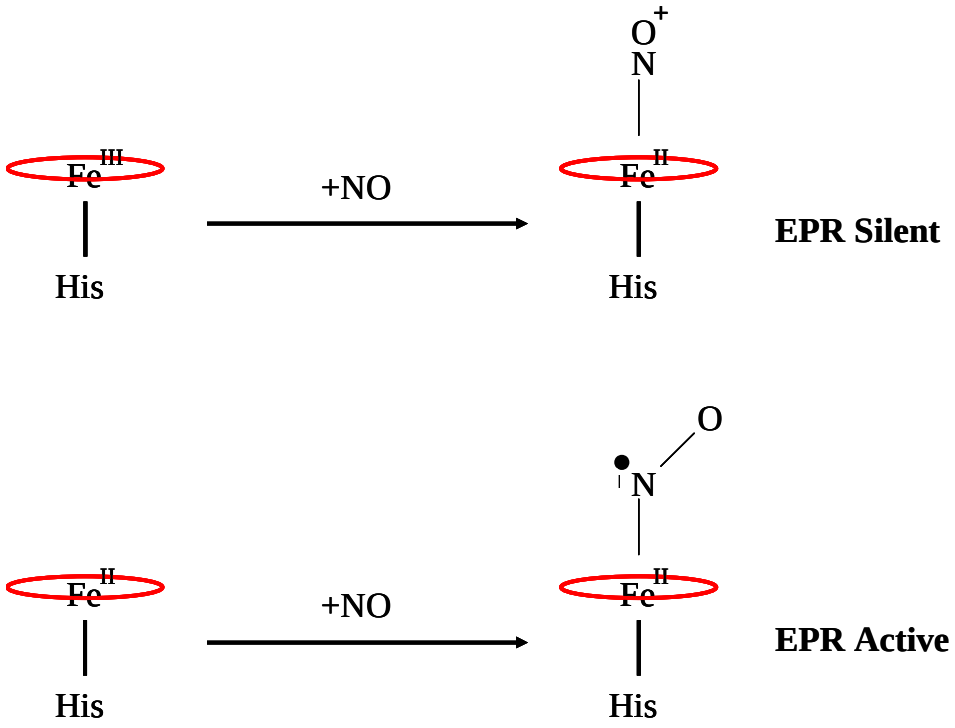

Figure 4.01: The two NO conformations formed from the binding of NO to ferric and ferrous heme. The ferric linear conformation is diamagnetic and therefore EPR silent, whereas the bent conformation is s = 1/2 at the NO· and therefore EPR active.

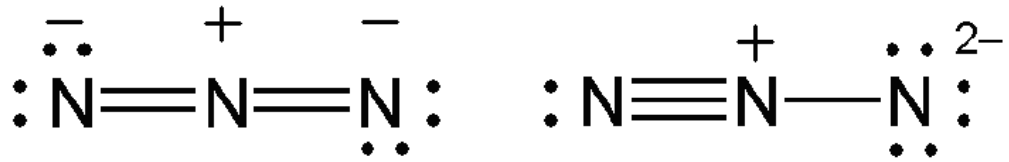

Figure 4.02: The two Lewis Structures for azide ion.

At room temperature the population of high spin (S = 5/2) and low spin (S = 1/2) is three quarters high spin to one quarter low spin. This is due to a degeneracy of two for the S = 1/2 and six for S = 5/2. The ligand field strength of azide is also close to the spin crossover when histidine is the fifth ligand. Therefore the difference of the

energy level between high and low spin states is small. It is also worth noting that histidine / hydroxide is similar in ligand field strength and can also give a high spin and low spin mixture. However it can exist also as purely low spin.

It was reported that nitrite would bind to ferric d_1 heme in a form of the active site made transiently accessible by redox cycling. Work using hydroxylamine to reoxidise the enzyme suggested that NO_2^- bound immediately after product (NH_3) formation [18]. The conclusion was that NO_2^- binds ferric d_1 heme at the distal site before the tyrosine 25 can rebind as illustrated in Figure 4.03. However, as the authors pointed out, this model did not fully explain all observations. The "nitrite-bound" form appeared to take longer to stabilise than the time required for reversion to the as-prepared form, approximately 20 minutes at room temperature. Also the EPR data showed no characteristic signals of low spin ferric d_1 heme, an observation reminiscent of those reported for azide and nitrite addition to the as prepared form. Only a single species was observed, with g-values similar to those of the histidine/methionine coordinated heme *c* in the putative ammonia-bound intermediate (Figure 4.03) [18].

Subsequently, Van Wonderen *et al* [4] showed that, following addition of NO_2^- to as-prepared cd_1 (*Paracoccus* and *Pseudomonas* species), the low-spin Fe^{III} heme d_1 is made EPR silent through spin-coupling to a radical formed in a reaction with the nitrite. They proposed a novel nitrosyl species involving NO bound to Fe^{III} heme d_1 but one in which the usual electron transfer to the iron had not taken place i.e. a true Fe^{III}-$NO^{\bullet}$ species and not the Fe^{II}-NO^+ form usually encountered in hemes. The absorbance spectra of these species showed some similarities to those of cd_1 treated with NO and ferrous d_1 heme reacted with NO_2^- [19-22]. However, Wang

and Averill reported a species with a 1913 cm^{-1} FTIR band consistent with a Fe^{II}-NO^{+} form [19].

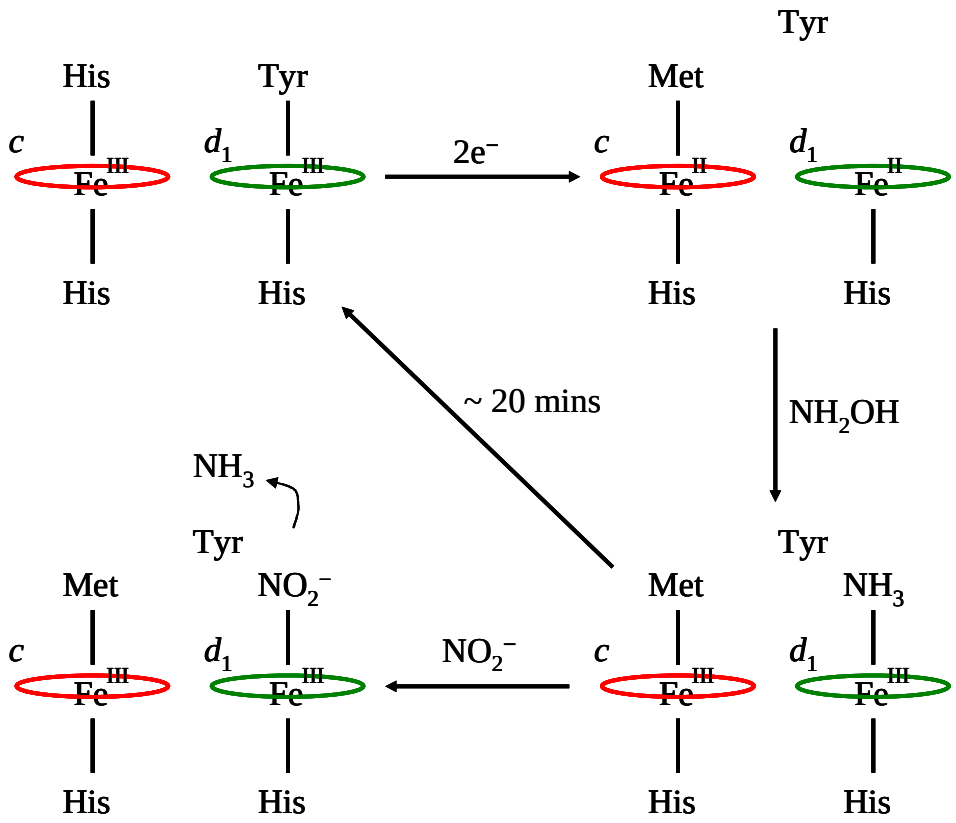

Figure 4.03: Scheme showing the reoxidation of reduced *P. pantotrophus* cd_1 with hydroxylamine followed by a gradual reversion to the oxidised form. The proposed reaction of NO_2^- with ferric d_1 heme at the distal site is also shown as suggested by Allen *et al* [18]. Adapted from Scheme 1 shown in van Wonderen *et al* [4].

Added to *P. aeruginosa* cd_1, azide ion was reported to remove the majority of the d_1 EPR signal in a similar way to nitrite [2]. Muhoberac and Wharton describe two features at g = 2.50 and g = 1.73 as being similarly reduced in intensity by both ligands [1]. This observation was never further investigated and it is not known whether or not the azide-treated cd_1 contains the same form of EPR silent heme d_1 as with nitrite. While it is obvious that *reduction* of nitrite can lead to the radical $NO^{\bullet}$, the only known radical form of azide is $N_3^{\bullet}$, formed by *oxidation* of N_3^-.

The work described in this chapter was undertaken with the aims of understanding the nature of the reaction of NO_2^- with oxidised cd_1 and of identifying the novel species formed at heme d_1. The product formed with azide was also prepared for spectroscopic comparison.

4.2: Oxidised (as Prepared) *Pseudomonas aeruginosa* and *Paracoccus pantotrophus* cd_1: Characterisation of Starting Material.

The electronic absorption spectra of two samples of as purified, oxidised cd_1 from *P. aeruginosa* and *P. pantotrophus* are shown in Figure 4.04. The *Pseudomonas* and *Paracoccus* oxidised enzymes both have absorption maxima at 526-527 nm and 406-411 nm. The Soret band at 406-411 nm and the αβ band at 526-527 nm are assigned to the *c* heme for both cd_1 enzymes. The Soret and αβ bands of the d_1 heme both appear to longer wavelength than the corresponding *c* heme features. The d_1 features take the form of a shoulder at 450-470 nm and a peak at 640-646 nm. Again, these are present in both oxidised enzymes. The shoulders at 450-470 nm appear very different however between the two enzymes. For *Pseudomonas* cd_1, the shoulder is located at ~ 470 nm and is much broader than the *Paracoccus* cd_1 equivalent, which is narrower and located at 450 nm. The bands at 640-646 nm are from ferric d_1 in the low spin state. In *P. aeruginosa* cd_1, all d_1 heme is in this spin state. But the *Paracoccus* enzyme has an additional peak at 702 nm. This is due to the presence of the high spin state of ferric d_1 heme. This was originally deduced from low temperature absorption and MCD spectra [17]. The spectrum of *Paracoccus* cd_1 at 1.5 K resembles the spectra of *P. aeruginosa* cd_1 at all temperatures with a single d_1 α-band at ~ 640 nm. Thus d_1 has an S = 1/2 ground state with a high spin S = 5/2 state at higher energy and thermally accessible at room

temperature. The two spectra shown in Figure 4.04 are representative of the preparations of cd_1 prepared as described in Materials and Methods and used for the experiments described here.

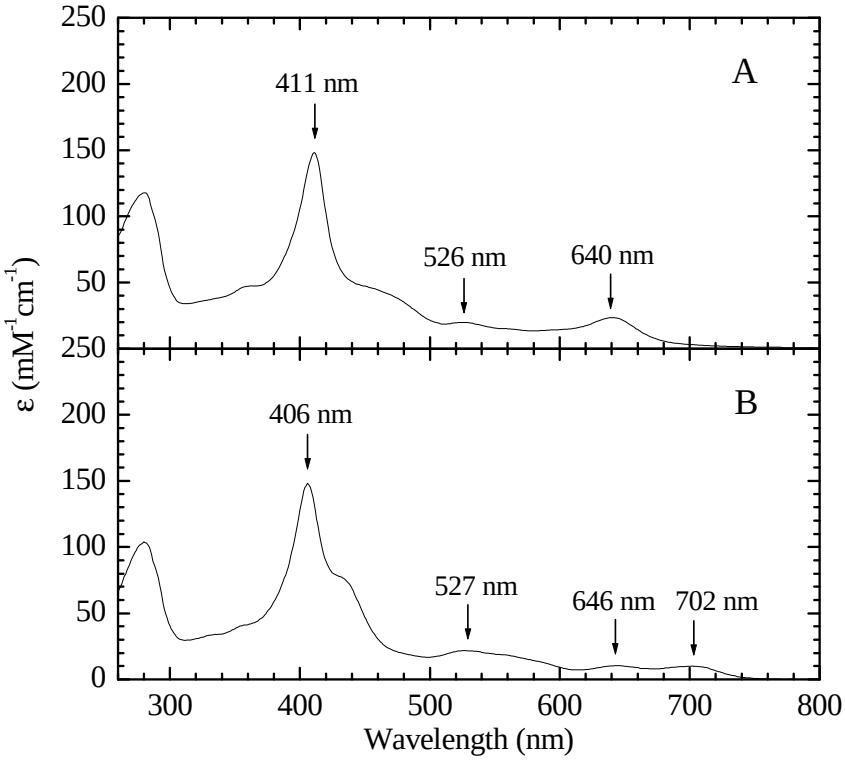

Figure 4.04: UV-Visible electronic absorption spectra of oxidised (as-prepared) cd_1 from *P. aeruginosa* (A) and *P. pantotrophus* (B). The *P. aeruginosa* cd_1 is at a concentration of 32 μM in 20 mM potassium phosphate buffer pH 6. The *P. pantotrophus* cd_1 is at a concentration of 185 μM in 100 mM Tris buffer pH 8.

4.3: Oxidised (as Prepared) *Pseudomonas aeruginosa* cd_1:

pH Dependence of Electronic Absorption and EPR.

The nitrite reductase activity of *P. pantotrophus* cd_1 is reported to be higher at acidic pH [23]. This could be due to consumption of protons during the reaction and there has been no report of pH dependent changes in the spectroscopic properties

of the oxidised enzyme. The electronic absorbance spectra of *P. pantotrophus* cd_1 show no significant changes in the pH range 5.5-9.0 [24]. However EPR spectra of samples at the two extremes of pH show significant differences [24]. At 10 K, a significant high-spin ferric d_1 signal is present in the pH 6.5 sample. It was suggested that lowering the pH protonates a histidine in the distal pocket; this hydrogen-bonds to the distal tyrosinate weakening its ligand field strength and so reducing the energy gap between the two spin-states (Figure 4.05).

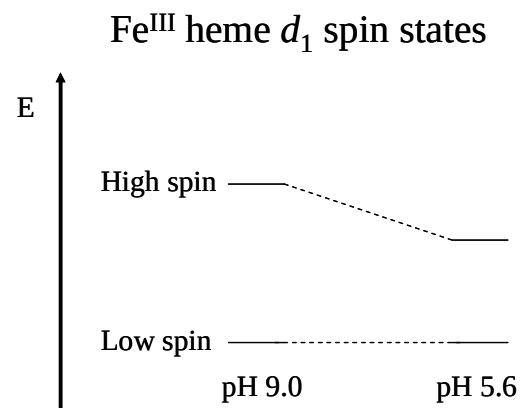

Figure 4.05: Energy diagram showing the energy differences at pH extremes for high and low spin ferric d_1 heme.

A protonated histidine residue interacting with the distal heme d_1 ligand can in principle also be present in the case of the *Pseudomonad* cd_1s because two histidine residues in the distal pocket are conserved. We therefore examined *P. aeruginosa* at different pHs using electronic absorbance spectroscopy and EPR to seek evidence for analogous behaviour. Four samples of 0.5 mL, 233 μM *P. aeruginosa* cd_1 were buffer exchanged into mixed buffer (12 mM acetate, 12 mM MES, 12 mM MOPS and 12 mM Tris) in D_2O. Mixed buffer is chosen to cope with the pH range required. Each cd_1 sample is buffer exchanged into a mixed buffer of a specific pH* in D_2O (see Chapter 2 for explanation of pH*). The set pH* values for the four samples were 5.5, 6.5, 7.5 and 8.5. The buffer exchange is continued until

the original buffer is less than a hundredth of the total volume. Electronic absorbance spectra were recorded for the four samples using a 1 mm pathlength cuvette. The electronic absorbance spectra of the two extreme pH* values, shown in Figure 4.06, reveal only very minor spectral changes but these do occur at bands from both hemes.

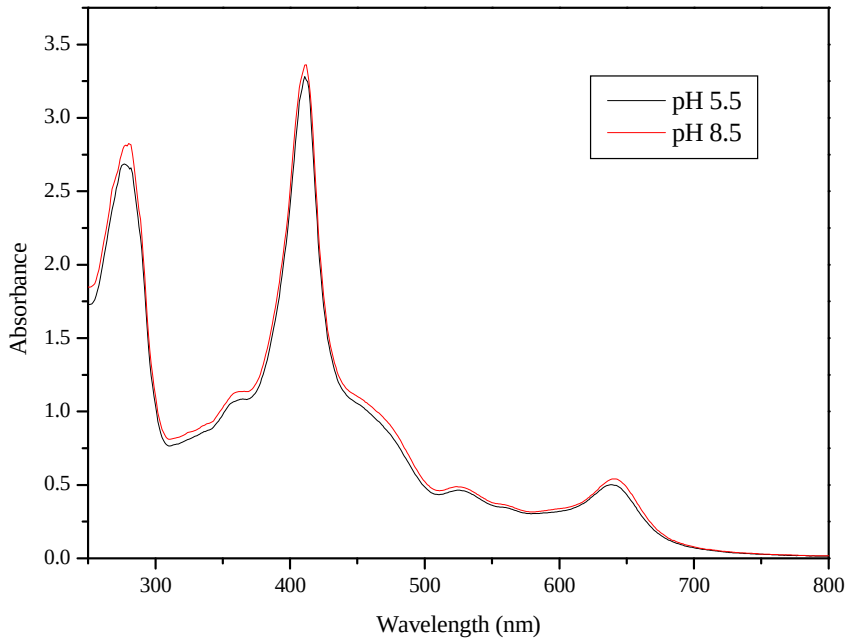

Figure 4.06: Electronic absorbance spectra of *P. aeruginosa* cd_1. The samples are in mixed buffer (12 mM acetate, 12 mM MES, 12 mM MOPS and 12 mM Tris) in D_2O at pH 5.5 and 8.5. Concentration of sample at pH* 5.5 is at 204 μM, the pH* 8.5 sample is at 211 μM.

The four samples were concentrated using microcons so that each was approximately 450 μM in a volume of 250 μL. This concentration left the absorption spectrum unchanged at visible wavelengths (not shown). The four samples were then frozen in quartz tubes for examination using X-band EPR spectroscopy. The results are shown in Figure 4.07: g-values of the features are indicated on the figure.

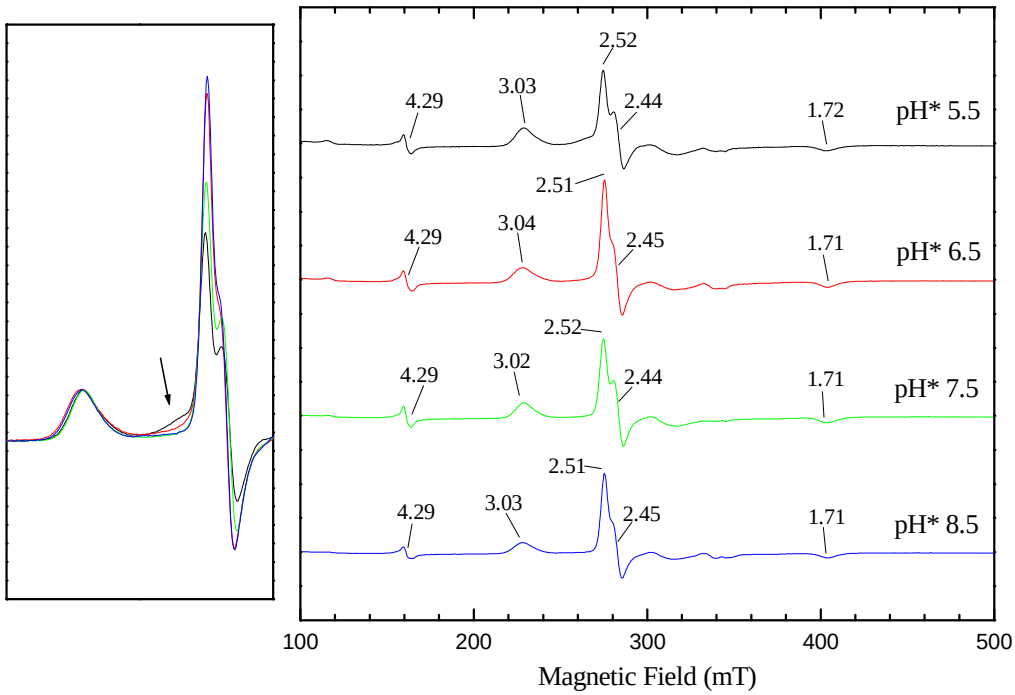

Figure 4.07: X-band EPR spectra of *P. aeruginosa cd*$_1$ at pH* values 5.5, 6.5, 7.5 and 8.5. Buffer used was a mixed buffer (12 mM acetate, 12 mM MES, 12 mM MOPS and 12 mM Tris) in D_2O set to the pH* required. Microwave power was 2 mW and temperature was 10 K for each spectrum.

Changes in heme spin-state, as were observed for the *Paracoccus* enzyme, are not evident here. Minor but unmistakable changes are seen in the envelope of the g_{xy} features of heme d_1. However, the shifts are not systematic across the four samples, possible indicating that more than one change is occurring over this pH* range (the distal pocket contains two conserved histidines). The magnetic field scales for the spectra were adjusted to account for small differences in the microwave frequencies; the intensities were normalised to the g_z feature of *heme c* ($g \sim 3$) and the resulting spectra are overlaid in the panel to the left of the figure. The broad feature at ~265 mT (arrowed) is assigned to heme d_1 (see simulations later in this chapter and

in the Appendix). Thus overall the spectral shifts indicate that the heme d_1 is responding to changes in external pH* but any changes in heme *c* are negligible. In this respect the results mirror those for the *Paracoccus* cd_1.

4.4: Oxidised (as Prepared) *Pseudomonas aeruginosa* and *Paracoccus pantotrophus* cd_1: Quantitation of EPR Species.

It is well established that EPR spectra of cd_1 contain signals of two distinct types. The first is a highly recognisable low-spin ferric heme spectrum as is frequently observed for the ubiquitous *b*- and *c*-type hemes. Such spectra fall into two classes, referred to as rhombic and large g_{max}. Both give a g_z usually in the 2.7-3.5 range. For large g_{max} spectra, the g_z-value is to the higher side of ~ 3; g_y and especially g_x may be broad and undetected. This signal in cd_1 arises from heme *c*. In both *P. aeruginosa* and *Pseudomonas stutzeri* the heme *c* EPR tends to the rhombic type and all three *g*-values can often be identified. In as-prepared *Paracoccus* cd_1, heme *c* gives rise to EPR more large g_{max} in nature and arises from heme *c* with *bis*-histidine ligation in a form with approximately perpendicular ligand planes [17, 25]. The large g_{max} EPR arises because of the ligand orientation, not the ligand identity. There are also examples of large g_{max} spectra from hemes with histidine-methionine coordination [26]. The second type of signal in the EPR of cd_1 is unusual. It has a narrow spread of *g*-values, generally with sharp features. The g-values are also reversed in order so that the g_x value is at low field [25]. This signal arises from the heme d_1. The three *g*-values of the d_1 heme can all be identified in the cd_1 species collected in Table 4.01. The EPR spectra for d_1 heme can be axial or rhombic. Here "rhombic" is in the general sense of three different g-values rather than the specific meaning for normal hemes. Each of these distinctive *c* and d_1 signal types described

are usually heterogeneous. Thus electronic absorbance spectra of as-isolated cd_1 contain signatures for heme *c* and for heme d_1 in only the Fe^{III} oxidation state and two distinct types of Fe^{III} heme are observed in the EPR. Previously, therefore, there was no reason to suppose that all the hemes observed in the absorbance were not represented in the EPR. It would not have been straightforward to quantitate the *c* and d_1 hemes from EPR spectra because of the heterogeneity and extensive signal overlap. However, work by van Wonderen *et al* [4] raised the possibility of a Fe^{III}-$NO^{\bullet}$ form of cd_1 which would contain EPR-silent heme d_1 but which would still appear as low-spin ferric in the absorbance spectrum. This has important implications because it would be a form with product still bound. When the physiological ligand NO_2^- is added, to solutions of cd_1 from *P. stutzeri* and *P. pantotrophus*, the typical low-spin, ferric d_1 EPR features are no longer observed. However, electronic absorbance spectra still show low-spin ferric features at ~640 nm [4]. *P. stutzeri* cd_1 shows no significant change at 640 nm when nitrite is added but the heme d_1 signals disappear from the EPR [4]. The oxidised *P. pantotrophus* cd_1 enzyme exists as a thermal equilibrium of low-spin ground state (S = 1/2) and high-spin excited state (S = 5/2). These give rise to bands at 640 nm and 702 nm respectively. Following treatment with nitrite, the 702 nm band corresponding to the high-spin disappears; the low-spin band shifts from 644 nm to 631 nm and intensifies consistent with a low-spin/high-spin mixture becoming entirely low-spin [4]. But retention of low-spin ferric characteristics in the electronic absorbance spectrum with an absence of heme d_1 features in the EPR requires a more complex explanation than a simple spin-state transition. The visible region heme d_1 band is relatively insensitive to oxidation state changes (compared to *b*- and *c*-type hemes) but high-spin Fe^{II} heme d_1 in reduced enzyme gives rise to intense Soret region MCD that is

not observed for this species. One explanation for the lack of EPR is that nitrite has created a radical species that has coupled to the low-spin, ferric d_1 heme. Two possible explanations for the nature of the radical were suggested [4]. One was a single nitrite turnover creating a radical on an amino-acid residue near the heme (possibly tyrosine or tryptophan) and dissociation of NO. This then spin couples to the low-spin Fe^{III} d_1 heme. Another nitrite ion may act as the distal ligand on the d_1 heme. A second explanation again involves a single turnover of nitrite but with retention of NO as the d_1 ligand. The NO radical then couples to the low-spin, ferric d_1 heme. This would require a very unusual form of heme-NO complex. The common form of an NO molecule bound to a ferric heme is best represented as nitrosyl heme in the Fe^{II}-NO^+ configuration. This species is diamagnetic and EPR silent but is assumed that Fe^{II}-NO^+ on d_1 heme would present a ferrous character that would be observed in an absorbance spectrum. The second candidate is a novel Fe^{III}-$NO^{\bullet}$ on the d_1 heme. The ferric iron component is S = 1/2 and the $NO^{\bullet}$ radical component is also S = 1/2, resulting in a silent EPR species.

Work was therefore undertaken with two aims related to questions concerning the nature of NO_2^--treated *cd*$_1$:

(i) In as-prepared samples of *cd*$_1$, are there sub-populations of "Fe^{III}-$NO^{\bullet}$" that have gone undetected because they appear as low-spin Fe^{III} heme d_1 in the EPR?

Samples of *cd*$_1$, in the as-prepared form, from *P. pantotrophus* and *P. aeruginosa* were carefully characterised by EPR spectroscopy under normal and under non-saturating conditions. The spectra were deconvoluted into the contributions from individual heme *c* and heme d_1 species by simulation. By double integrations of the simulations, the contributions of heme s d_1 and *c* to the EPR were quantified;

(ii) Can it be proved that the NO_2^--treated form of oxidised cd_1 does indeed contain a novel Fe^{III}-$NO^{\bullet}$ species?

This question was approached by attempting to make the NO-bound form of oxidised cd_1 and characterising it using ratio-data MCD methods (RD-MCD) so as to make a comparison with RD-MCD of the NO_2^--treated form.

4.4.1: Preparation of EPR Samples

A 200 μL portion of 500 μM *P. aeruginosa* cd_1 was buffer exchanged into 50 mM phosphate buffer in D_2O at pH 6.5* using microcon filtration devices. This D_2O based buffer system was chosen so that samples could be used, if necessary, for MCD studies. Once exchanged, an absorption spectrum was recorded to ensure that the sample remained in the oxidised state. The sample was then transferred to a quartz tube and frozen in liquid nitrogen for EPR studies. EPR spectra were then recorded for at two combinations of temperature and power: 10 K/2 mW and 20 K/0.64 mW. These are chosen because, although the "standard" 10 K/2 mW combination gives excellent signal-to-noise (and allows comparison to previously reported spectra), the d_1 heme saturates significantly under these conditions and is quantitatively underrepresented in the spectrum. Saturation at 20 K/0.64 mW is negligible and so spectra recorded under these conditions can be used to quantitate the relative spin concentrations of heme *c* and heme d_1.

The sample was then thawed and, in preparation for possible low-temperature MCD studies, the glassing agent deuterated glycerol was added ("deuterated" here means that the exchangeable protons have been replaced by deuterons by repeatedly mixing glycerol with D_2O and then removing the H_2O/D_2O under vacuum until exchange is >99.5%). This D_3-glycerol is added to the concentrated *P. aeruginosa*

cd_1 solution in a slight excess such that the glycerol constitutes ~55% of the total volume. The sample is then again frozen and characterised by EPR spectroscopy at 10 K/2 mW and 20 K/0.64 mW.

These procedures were repeated with the *P. pantotrophus* cd_1, which is also quantitated by EPR. A 200 μL portion of 500 μM *P. pantotrophus* cd_1 was buffer exchanged into mixed buffer (12 mM acetate, 12 mM MES, 12 mM MOPS, 12 mM Tris) in D_2O at pH 6.5* using microcons. Once buffer exchanged, EPR spectra were recorded for *P. pantotrophus* cd_1 at the same combinations of power and temperature used for the *Pseudomonas* enzyme. Then, as before, D_3-glycerol is added to the concentrated *P. pantotrophus* cd_1 solution so that the volume of glycerol is ~55% of the total volume and EPR again recorded at 10 K/2 mW and 20 K/0.64 mW.

4.4.2: Simulation of EPR

The subsequent pages show the EPR data recorded for the samples described above. They are presented along with simulated EPR data of the full spectrum and of the individual species of both heme *c* and heme d_1 in Table 4.02A and 4.02B (spectra are shown in Appendix). For each sample, the following simulation strategy was used. The EPR spectrum recorded under non-saturating conditions for heme d_1 (20 K/0.64 mW) is the one to be used for quantitation of the EPR signals. However, since heme *c* gives broad and often relatively weaker features under these conditions, each simulation was started by first using the 10 K/2 mW spectrum. This provided a set of simulation parameters that could then be used as a starting point for simulation of the 20 K/0.64 mW spectra in which the heme *c* features were less pronounced. Furthermore, where assignment of features between heme *c* and heme d_1 was ambiguous, comparison of the spectra under these two sets of conditions provided a

guide: parts of the spectrum saturating at 10 K/2 mW could be assumed to belong to heme d_1.

Spectra were initially simulated using the program "S_HALF" (Dr. J. Bradley, unpublished). This allows additive simulations of several S = ½ species. Input parameters, for each species, are g_{xyz}-values and linewidths for individual features. The program allows for a degree of automated fitting at each feature. Once a reasonable set of parameters was obtained, further refinement was achieved manually using the program SimFonia v1.1 (Bruker Biospin). Quantitation of the final simulations, in order to obtain heme *c* / heme d_1 spin concentration ratios, was achieved by performing double integrations in WinEPR (Bruker Biospin).

Where one, or both, of heme *c* and heme d_1 gave rise to heterogeneous features, then previously reported EPR spectra of *cd*$_1$s were used to guide the initial choice of g-value sets. Table 4.01 summarises the currently available EPR data used for this purpose.

Where g-values cannot be detected, for example the high-field g_x-value of heme *c*, parameters were chosen on the assumption that the sum of the squared g-values $\Sigma g_i^2 = 16$ and the linewidth set to an arbitrary large value. This is indicated in Table 4.02B by brackets around the g-value and * on the linewidth.

Species and state	Heme *c* g_x g_y g_z	Heme d_1 g_z g_y g_x	References
Pseudomonas aeruginosa			
Oxidised, as isolated cd_1	2.97, 2.25, 1.4	2.52, 2.43, 1.7	[1, 20]
cd_1 with NO_2^-	2.95, 2.30, 1.42	-	[1]
cd_1 with F^- ligand	2.94, 2.26, 1.48	2.53, 2.53, 1.62	[1]
cd_1 with CN^- ligand	3.31, -, -	2.47, 2.35, 1.61	[1]
cd_1 with imidazole ligand	3.55, -, -	2.58, -, -	[2]
cd_1 with N_3^- ligand	3.02, -, -	-	[2]
cd_1 with NO ligand	3.02, 2.24, 1.34	-	[2]
Pseudomonas stutzeri			
Oxidised, as isolated cd_1	2.96, 2.27, 1.62	2.54, 2.40, 1.85	[16]
cd_1 with NO_2^-	2.99, 2.29, -	-	[4]
Paracoccus pantotrophus			
Oxidised, as isolated cd_1	3.04, -, -	2.51, 2.20, 1.85	[16]
cd_1 transient intermediate (His/Met at *c* heme) designated cd_1*	2.94, 2.33, 1.40	2.67, 2.53, -	[27]
cd_1 with NO_2^-	2.93, 2.32, 1.40	-	[4, 17]
Thiobacillus denitrificans			
Oxidised, as isolated cd_1	3.60, -, -	2.52, 2.44, 1.70	[28]

Table 4.01: Experimental EPR g-values of low spin ferric *c* and d_1 hemes in different species and states of cytochrome cd_1. Note that the g-values are reversed in the d_1 heme to represent the $(d_{xz,yz})^4(d_{xy})^1$ ground state. " - " represent g-values not determined from the EPR spectra. The g-values can vary to those shown in this table by a small degree. This includes spread caused by a two-fold heterogeneity that is often seen in cd_1 EPR spectra.

Description of cd_1 EPR sample and state	**Species type and % contribution (for 20 K / 0.64 mW spectra)**	**g_{xyz}**	**W_{xyz}**
***Pseudomonas aeruginosa* cd_1**			
Oxidised, as isolated. 10 K / 2 mW	d_1 heme	2.518, 2.44, 1.723	44, 72, 125
	d_1 heme	2.638, 2.44, 1.70	160, 190, 250
	c heme	1.42, 2.28, 2.99	480, 160, 130
Oxidised, as isolated. 20 K / 0.64 mW	d_1 heme, 59.0	2.518, 2.44, 1.723	44, 72, 110
	d_1 heme, 41.4	2.633, 2.40, 1.72	170, 190, 190
	c heme, 100.0	1.410, 2.282, 2.98	480, 155, 140
Oxidised, as isolated with ~ 55% deuterated glycerol added 10K / 2 mW	d_1 heme	2.518, 2.445, 1.709	34, 46, 78
	d_1 heme	2.565, 2.267, 1.85	55, 32, 26
	c heme	1.38, 2.326, 3.011	450, 80, 93
	c heme	1.38, 2.245, 2.918	450, 100, 80
Oxidised, as isolated with ~ 55% deuterated glycerol added 20K / 0.64 mW	d_1 heme, 67.8	2.518, 2.445, 1.709	34, 46, 78
	d_1 heme, 23.9	2.53, 2.26, 1.85	55, 23, 26
	c heme, 59.7	1.38, 2.326, 3.011	450, 80, 93
	c heme, 40.3	1.38, 2.275, 2.918	450, 70, 80

Table 4.02A: Simulated EPR data for a series of *P. aeruginosa* cd_1 samples, showing contributions, g-values (g_{xyz}) and linewidths (W_{xyz}). Experimental and simulated EPR spectra of samples are shown in the Appendix. Samples are in 50 mM phosphate D_2O buffer, pH 6.5*. Spectrometric parameters for all samples are modulation frequency, 100 KHz; modulation amplitude, 10 G; time constant, 40.96 ms; and sweep time, 83.886 s.

Description of cd_1 EPR sample and state	**Species type and % contribution (for 20 K / 0.64 mW spectra)**	**g_{xyz}**	**W_{xyz}**
***Paracoccus pantotrophus* cd_1**			
Oxidised, as isolated. 10 K / 2 mW	d_1 heme	2.526, 2.223, 1.8417	46, 17, 65
	d_1 heme	2.6, 2.208, 1.8598	80, 22, 43
	c heme	(1.150), 2.24, 3.108	1000*, 80, 93
	c heme	(1.369), 2.29, 2.98	1000*, 100, 80
Oxidised, as isolated. 20 K / 0.64 mW	d_1 heme, 61.7	2.534, 2.223, 1.8417	43, 17, 65
	d_1 heme, 59.9	2.59, 2.208, 1.8598	80, 22, 43
	c heme, 91.4	(1.192), 2.24, 3.092	1000*, 110, 155
	c heme, 8.6	(1.350), 2.29, 2.989	1000*, 100, 80
Oxidised, as isolated with ~ 55% deuterated glycerol added 10K / 2 mW	d_1 heme	2.518, 2.226, 1.853	32, 18, 42
	d_1 heme	2.562, 2.214, 1.87	68, 20, 30
	c heme	(1.089), 2.19, 3.165	1000*, 170, 115
	c heme	(1.350), 2.29, 2.989	1000*, 100, 80
Oxidised, as isolated with ~ 55% deuterated glycerol added 20K / 0.64 mW	d_1 heme, 57.3	2.518, 2.221, 1.853	32, 22, 42
	d_1 heme, 80.1	2.557, 2.218, 1.871	80, 18, 30
	c heme, 89.8	(0.0992), 2.24, 3.162	1000*, 110, 120
	c heme, 10.2	(1.350), 2.29, 2.989	1000*, 100, 80

Table 4.02B: Simulated EPR data for a series of *P. pantotrophus* cd_1 samples, showing contributions, g-values (g_{xyz}) and linewidths (W_{xyz}). Experimental and simulated EPR spectra of samples are shown in the Appendix. Samples are in 12 mM acetate, 12 mM MES, 12 mM MOPS and 12 mM Tris D_2O buffer, pH 6.5*. Spectrometric parameters for all samples are modulation frequency, 100 KHz; modulation amplitude, 10 G; time constant, 40.96 ms; and sweep time, 83.886 s. As mentioned earlier, where g-values cannot be detected, for example the high-field g_x-value of heme *c*, parameters were chosen on the assumption that the sum of the squared g-values $\Sigma g_i^2 = 16$ and the linewidth set to an arbitrary large value. This is indicated by brackets around the g-value and * on the linewidth.

4.5: Activation / Deactivation of *Paracoccus pantotrophus* cd_1 - Activation of Oxidised cd_1 by NO_2^-.

The standard method of assaying cd_1 nitrite reductase activity uses excess reduced cytochrome *c* as an electron donor and excess NO_2^- ion as substrate. Following changes in the absorption spectrum of the cytochrome *c* as it is oxidised to the ferric state quantitates electron transfer during turnover.

It has been shown that reduction of the *P. pantotrophus* cd_1 enzyme results in a ligand switch at the heme *c* from bis-histidine to histidine-methionine coordination. Crystallography has shown that upon reduction histidine-17 is replaced with methionine-106 for both monomers, although the double histidine-methionine form has only been proven in crystal structures [5]. This ligation is reported to revert back to bis-histidine following reoxidation with hydroxylamine over a period of about 20 minutes [27]. Histidine-methionine coordinated ferric heme *c* can be detected using MCD to track reoxidation of *P. pantotrophus* cd_1 in solution [29]. Kinetic, structural and spectroscopic analysis led to the conclusion that the histidine-methionine form of *P. pantotrophus* cd_1 is the catalytically competent form and thus requires reduction for activation [5, 23, 29]. An argument for this conclusion is that bis-histidine coordinated heme *c* has a lower reduction potential than histidine-methionine coordination. Therefore the bis-histidine coordinated heme would require a lower driving force for electron transfer from pseudoazurin [30].

It was also reported by Richter *et al* [23] that oxidised, as isolated cd_1 exhibits a low 'background' catalytic activity using NO_2^- as substrate but amounting to no more than 6% of the full activity observed if the protein is first activated by reduction. Oxidised, as isolated *P. pantotrophus* cd_1 has a small population of the histidine-methionine coordinated form. This small population of 'catalytically

competent' enzyme could be responsible for the background activity, consistent with the model of reduction being required to convert all the cd_1 population to the fully active histidine-methionine coordinated form. But van Wonderen *et al* [4] reported that exposure of oxidised *P. pantotrophus* cd_1 to NO_2^- leads to the switching of ligands to histidine / methionine at heme *c* i.e. the conformational change that is proposed to be required for activity can be effected without the need for prereduction [4]. These observations, in combination, suggest the possibility that cd_1 can be activated by exposure to its own physiological substrate NO_2^-. Both the NO_2^- induced ligand switching [4] and NO_2^- turnover are more rapid at acidic pH. The effect on cd_1 activity of exposure to NO_2^- at several pHs prior to the assay was therefore investigated.

The method of assaying the activity of *P. pantotrophus* cd_1 was based on that of Richter *et al* [23]. The assay works by using an excess of reduced cytochrome *c* as an electron donor and an excess of NO_2^- as the substrate. The cd_1 enzyme can then catalyse the one electron reduction of NO_2^-. Cytochrome *c*, when reduced, exhibits a sharp band at 550 nm, whereas the oxidised form shows a much broader spectral feature with a weaker intensity at similar wavelengths. Therefore the changes of intensity at 550 nm are a direct measure of the donation of electrons by the reduced cytochrome *c* to cd_1, and therefore the rate of turnover. Richter *et al* [23] used the physiological electron donors pseudoazurin and cytochrome c_{550} as well as horse heart cytochrome *c*. Only the last of these three electron donors is used in this work due to its ready availability. The k_{cat}s of oxidised cd_1 that Richter reported using the electron donors pseudoazurin, cytochrome c_{550} and horse heart cytochrome *c* were 5.3, 2.1 and 2.4 s^{-1} respectively. i.e. activity using these two cytochromes was comparable but, with pseudoazurin, approximately twice as large. D-(+)-glucose,

glucose oxidase and catalase are also used in the assay mixture to remove traces of oxygen and peroxide respectively. This is important since cd_1 also has significant cytochrome oxidase activity: the cd_1 protein can also catalyse the four electron reduction of oxygen to water.

4.5.1: Preparation of Experiment

Solutions of reduced horse heart cytochrome *c* and glucose were prepared in batches for several assays. Solutions of reduced cytochrome *c* were prepared from lyophilised protein and degassed buffers inside an anaerobic glove-box. A sufficient quantity of horse heart cytochrome *c* was measured to produce a stock solution of 400 μM. The volume needed was dependent on the number of assays undertaken. Lyophilised cytochrome *c* was taken into an anaerobic glove box and dissolved in a minimum amount of deoxygenated buffer (see Figure 4.09 for different buffer conditions). A small quantity (~ 10 mg) of sodium dithionite was added to the cytochrome *c*. The solution changes from a dark crimson colour to a light cherry colour upon dithionite addition. This reduced protein was then passed through a 5 mL HiTrap desalting column. 1 ml of the reduced protein was passed through the desalting column in turn to remove the excess dithionite. The reduced cytochrome *c* solution can be kept in the glove box for up to 3 days, or it can be flash frozen and kept in the freezer for 6 months. The glucose solution was prepared using powdered D-(+)-glucose and degassed buffers inside a glove-box. A suitable amount was weighed to give a 4% w/v stock solution. The glucose was taken into the Belle glove box, where the appropriate deoxygenated buffer was added. The glucose was left overnight. This is because D-(+)-glucose in solution gradually mutarotates through equilibrium to one third α-D-glucose and two thirds β-D-glucose. The β-D-glucose is

the anomer on which glucose oxidase acts. Once these two solutions were ready, 4 mM sodium nitrite, glucose oxidase, catalase and ~200 μM oxidised *Paracoccus pantotrophus* cd_1 (as isolated) were prepared, also in the anaerobic glove box.

4.5.2: Assay Experimental Technique

To an anaerobic 1 cm pathlength cuvette in the anaerobic glove box was added 0.5 mL chosen buffer, 0.5 mL 4 mM sodium nitrite, 0.5 mL 400 μM reduced cytochrome *c*, 0.5 mL 4% glucose solution, 1 unit mL^{-1} glucose oxidase and 400 units mL^{-1} catalase. The anaerobic cuvette was then sealed with a rubber seal (Suba-Seal). The cd_1 protein was prepared by transferring 3 μL to a 0.5 mL deoxygenated Eppendorf tube. To that was added 1 μL of chosen buffer if the assay was a control or 1 μL of 4 mM sodium nitrite if nitrite incubation was taking place. Once the appropriate time for each incubation has elapsed the protein was taken up into a 10 μL Hamilton syringe. The cuvette of reaction mixture and the syringe was removed from the glove box. The cuvette was placed in a Jasco V550 spectrometer and the 550 nm absorbance recorded before cd_1 addition. The syringe needle was then used to pierce the rubber seal and the cd_1 is injected into the reaction mixture. The cuvette was quickly inverted to mix and then placed in the spectrophotometer. A time course measurement was then immediately recorded at 550 nm (Figure 4.08).

4.5.3: Analysis and Results

The 550 nm time traces have an initial linear form followed by a curve as the reduced cytochrome *c* is consumed. From the time of injection and closure of the spectrophotometer there is a period of 5 seconds during which the trace is

uninformative. The shape of the curve is therefore fitted from t ~ 5 seconds onwards and back extrapolated to t = 0.

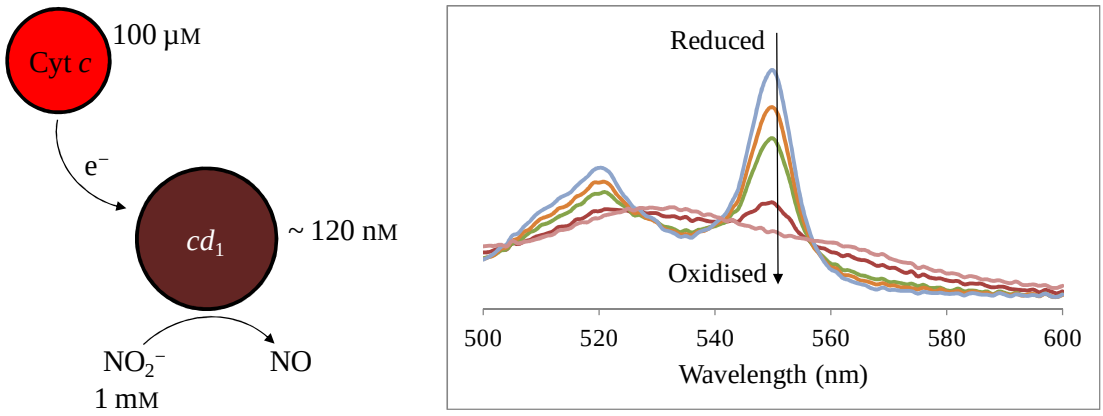

Figure 4.08: UV-Visible electronic absorbance spectra showing the 550 nm band disappearing as electrons are consumed by nitrite reduction, as indicated by the arrow. Included is a simple diagram of the reaction taking place. Reduced cytochrome *c* donates electrons to *cd*$_1$ resulting in the flattening of the 550 nm feature. Concentrations of nitrite, reduced cytochrome *c* and *cd*$_1$ in the reaction cuvette are also included.

Approximately 30 seconds of the time trace are fitted to a single exponential decay using Microcal Origin. Once the curve is fitted then Origin returns values for the y offset (y_0), the amplitude (A_1) and the decay constant (t_1) in the equation describing the exponential decay: $y = y_0 + A_1 \exp^{(-x/t_1)}$ (Equation 1)

$$\frac{df(x)}{dx} = A_1 \frac{de^{-x/t_1}}{dx} = -\frac{A_1}{t_1} e^{-x/t_1} \qquad (1)$$

The initial gradient is then calculated by setting x equal to 0. It is calculated in units of mAu/s. Multiple runs were performed. The values for one particular point are totalled and averaged. This is done for all points. The averages for all buffers and incubation times are shown in Figure 4.09.

The general buffer is a mixed buffer consisting of 12 mM acetate, 12 mM 2-(N-morpholino)-ethanesulphonic acid (MES), 12 mM 3-(N-morpholino)-propanesulphonic acid (MOPS) and 12 mM tris(hydroxymethyl)aminomethane (Tris). This mixed buffer has a wide ranging effective pH range of 3.6 to 9 (acetate 3.6-5.6, MES 5.5-6.7, MOPS 6.5-7.9, Tris 7.5-9). The conditions that have been altered are the pH and whether the buffer is in H_2O or D_2O. Initially the buffer system bis-tris propane (BTP) was used in the assays. However this showed some inhibitory effects by delaying or stopping the initial reaction rate.

Figure 4.09 is in general agreement with the findings of Richter *et al* in that the lower pH values give faster turnover rates with nitrite [23]. They use the physiological donor cytochrome c_{550} instead of horse heart cytochrome *c* however. Non-deuterated and deuterated data sets were performed for pH 5.5 and 6.5. The deuterated and non-deuterated results for both pHs are comparable to each other, which suggests that the aqueous environment has no effect on the initial rate. At pH 7.5 only a non-deuterated data set was generated to conserve D_2O. The pH 7.5 data set only showed a slight enhancement of initial activity, therefore the focus was on the other two pHs. In terms of nitrite incubation the longer the cd_1 is incubated with nitrite the faster the rate of turnover.

4.6: Activation / Deactivation of *Pseudomonas aeruginosa* cd_1 - Activation of Oxidised cd_1 by NO_2^-.

The preparation, experimental techniques and analysis of the *P. aeruginosa* cd_1 assays are conducted and recorded using the same methods as the *P. pantotrophus* cd_1 assays. The concentration of oxidised, as isolated *P. aeruginosa* cd_1 used in the assays was also ~ 200 μM.

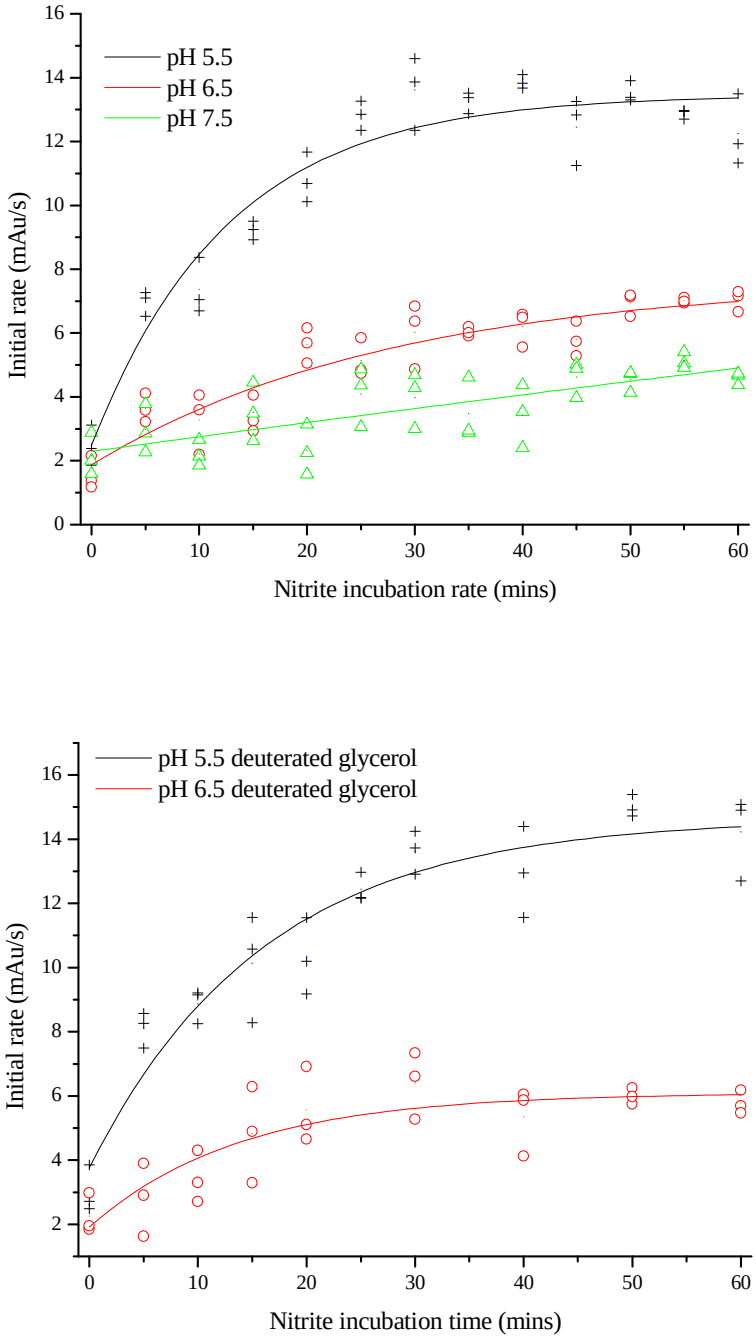

Figure 4.09: Plots of initial rates for different pH and buffer conditions for *P. pantotrophus* *cd*$_1$ (Top graph, buffers made using water. Bottom graph, buffers made using deuterium). Curves are fitted from sets of three rates measured using the same conditions. The curve used is a single exponential decay described using the equation $y = y_0 + A_1\exp^{(-x/t_1)}$. Individual rates measured shown as + (pH 5.5), ○ (pH 6.5) and Δ (pH 7.5).

Figure 4.09 shows a trend of increasing turnover rates with nitrite for the *Paracoccus* enzyme at lower pH. Similarly the *Pseudomonas* enzyme also shows increasing rates of turnover with acidic pH in Figure 4.10.

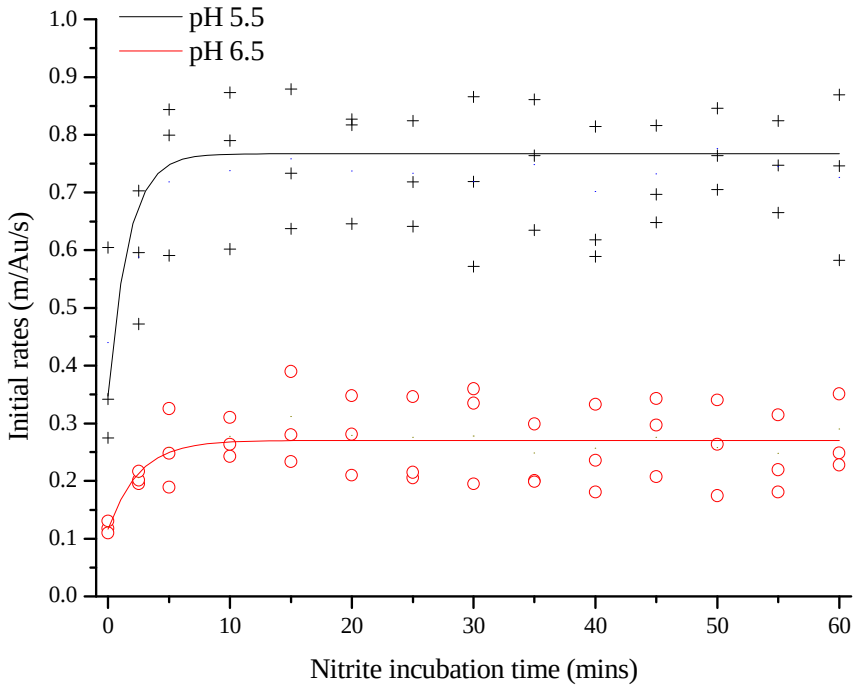

Figure 4.10: Plots of initial rates for different pH and buffer conditions for *P. aeruginosa* cd_1. Curves are fitted from sets of three rates measured using the same conditions. The curve used is a single exponential decay described using the equation $y = y_0 + A_1\exp^{(-x/t_1)}$. Individual rates measured shown as + (pH 5.5) and ○ (pH 6.5).

The activities of the nitrite incubation assays for *P. aeruginosa* cd_1 were only detectable at pH 5.5 and 6.5. A comparison of Figure 4.09 and Figure 4.10 indicates that the rates are markedly slower for the *Pseudomonas* enzyme. This is in agreement with published turnover numbers of 72 s^{-1} and 6 s^{-1} at pH 7 for *P. pantotrophus* and *P. aeruginosa* cd_1 respectively [23, 31]. The difference between the sets of data for

the two enzymes lies in the turnover increase due to nitrite incubation over a period of time. In the *P. pantotrophus* cd_1 enzyme the turnover rates increased with longer periods of nitrite incubation, whereas the *P. aeruginosa* cd_1 turnover rate increases instantly if nitrite incubation is performed but after ~ 5 minutes of incubation remains steady. This is due to the *P. pantotrophus* cd_1 having an activation phase, where the binding of nitrite to the d_1 heme of the oxidised heme drives a ligand change at heme *c* [4]. *P. aeruginosa* cd_1 requires no such activation, with the *c* heme ligands retained throughout a catalytic cycle. Therefore the initial rates remain the same after a small incubation period.

The variation in initial rates for the *P. aeruginosa* cd_1 assays measured using the same conditions was also smaller then the equivalent *P. pantotrophus* cd_1 assays. Differences of up to ~ 4 mAu/s were recorded for the *Paracoccus* assays, whereas the *Pseudomonas* data showed variation in the range of ~ ±0.15 mAu/s and ~ ±0.075 mAu/s for pH 5.5 and 6.5 respectively.

4.7: Reversion to the Oxidised State by Reaction of Reduced *Paracoccus pantotrophus* cd_1 with Hydroxylamine.

From the above section, it is clear that exposure of oxidised cd_1 to NO_2^- activates the protein to the standard nitrite-reductase assay without the need for reduction. The work of Van Wonderen *et al.* [4] demonstrated that NO_2^- treatment triggers a ligand switch to His/Met at heme *c* but also produces, at the active site, a novel form of heme d_1, the nature of which is addressed later in this chapter. It is not obvious whether one or both of these two factors, the ligand switch at heme *c* and the novel form of heme d_1, is required for activation. If heme *c* His/Met ligation is a critical factor, then activity should diminish over the same timescale that heme *c*

reverts to His/His coordination following reoxidation of the protein. It was therefore decided to measure activity as a function of time following reoxidation of reduced cd_1 by hydroxylamine. Bradley and Haynes (UEA, unpublished) have monitored the His/Met to His/His heme *c* ligand reversion, following reoxidation of reduced cd_1 by hydroxylamine, using near-infrared MCD spectroscopy (see Figure 4.03 for reaction scheme). Reversion was accelerated at acidic pH but was such that, at a pH of 6.5, it would be feasible to assay the protein at a series of times during reversion. This was therefore attempted.

Again, the method of assaying the activity of *P. pantotrophus* cd_1 was based on that of Richter *et al* [23]. Reduced cytochrome *c* and glucose solutions were prepared beforehand in the same way as for the nitrite incubation assays. The same assay mixture was also used. To an anaerobic 1 cm pathlength cuvette in the anaerobic glove box was added 0.5 mL buffer, 0.5 mL 4 mM sodium nitrite, 0.5 mL 400 μM reduced cytochrome *c*, 0.5 mL 4% glucose solution, 1 unit mL^{-1} glucose oxidase and 400 units mL^{-1} catalase. These were all prepared in anaerobic mixed buffer (12 mM acetate, 12 mM 2-(N-morpholino)-ethanesulphonic acid (MES), 12 mM 3-(N-morpholino)-propanesulphonic acid (MOPS) and 12 mM tris(hydroxymethyl)aminomethane (Tris)) pH 6.5 made in H_2O.

The cd_1 protein is reduced with sodium dithionite in a two-electron reduction: a 250 μL, 150 μM sample of *P. pantotrophus* cd_1 was reduced by adding a few grains of sodium dithionite and agitating to mix. The protein changes from a brown to a green colour. The protein is then passed through a 5 mL HiTrap desalting column in the same manner as the reduced cytochrome *c* to remove any excess sodium dithionite. An electronic absorbance spectrum is then recorded of the desalted protein to check for full reduction and also to calculate the new concentration of reduced

protein after dilution through the desalting column. If the band at 702 nm has completed disappeared then the protein is deemed to be reduced. The reduced cd_1 protein is prepared for hydroxylamine incubation by transferring 3 μL to a 0.5 mL deoxygenated Eppendorf tube. To that is added 1 μL of buffer if the assay is a control or 1 μL of 16 mM hydroxylamine hydrochloride if hydroxylamine incubation is taking place. As hydroxylamine is added to the reduced cd_1 a stop clock is started. At a set time after reoxidation, a sample of the cd_1 is removed with a 10 μL Hamilton syringe, injected into the reaction mixture in the cuvette and assayed by monitoring the change at 550 nm as was done following NO_2^- incubations. Again, initial rates were calculated using the first 30 seconds of each trace and using Origin to fit a first order, exponential decay curve. The results of the assays are shown in Figure 4.11.

4.8: MCD and EPR of *Pseudomonas aeruginosa* and *Paracoccus pantotrophus* cd_1 Treated with NO and NO_2^-. Reaction of Oxidised cd_1 with NO.

This section describes experiments to test the suggestion that the species formed at the active site following treatment of oxidised cd_1 with NO_2^- is a novel Fe^{III}-$NO^{\bullet}$ nitrosyl heme d_1. Using cd_1 from both *P. aeruginosa* and *P. pantotrophus*, attempts were made to bind NO directly to the Fe^{III} heme d_1 of the oxidised enzyme in order to prepare samples for examination by RD-MCD methods.

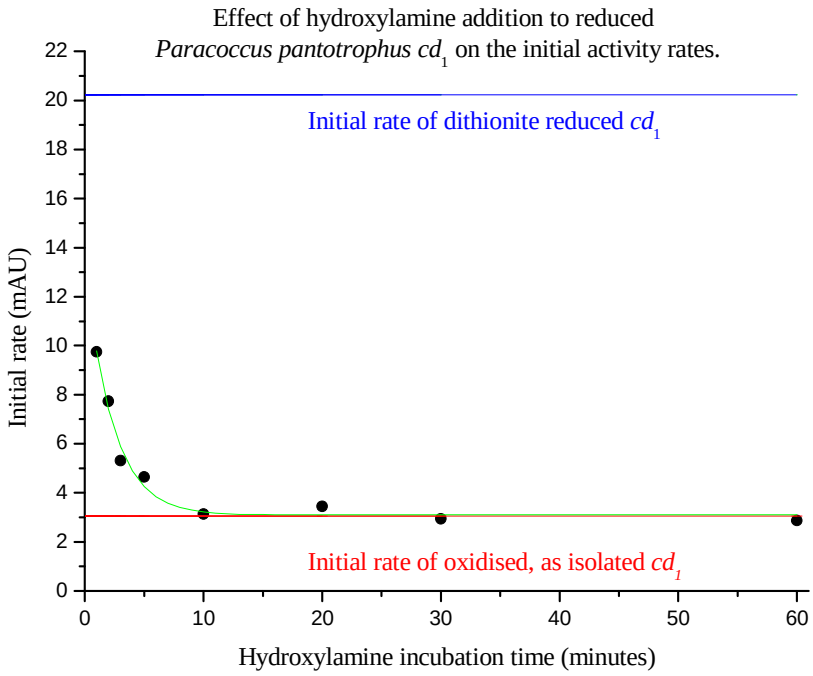

Figure 4.11: Plot of initial rates of *cd*$_1$ activity after incubation with hydroxylamine. The blue line is the initial rate of reduced *cd*$_1$ with no hydroxylamine added (equivalent volume of buffer added as a control). The red line is the initial rate of oxidised, as isolated *cd*$_1$ (protein not reduced by dithionite and no hydroxylamine added). Unlike the nitrite incubation assays this is just one set of data and not an average. The green line is a first order, exponential decay curve fitted using Origin with equation $y = y_0 + A_1\exp^{(-x/t_1)}$. Parameters:
y offset (y_0) = 3.1, amplitude (A_1) = 10.4, decay constant (t_1) = 2.3.

4.8.1: *Pseudomonas aeruginosa* with Bound NO.

The work of Yamanaka et al in 1961 first showed that *cd*$_1$ was capable of reducing nitrite to NO [10]. Since then much work to elucidate the catalytic mechanism of *cd*$_1$ has taken place [19, 32-35]. Given the nature of the product of this reaction and the extremely strong affinity of NO for hemes in both Fe^{II} and Fe^{III} oxidation states, a core question concerns the nature of the heme *d*$_1$-NO product complex or other nitrosyl-heme intermediates.

Using infrared spectroscopy, several studies have identified vibrational frequencies characteristic both of Fe^{II}-NO and of Fe^{II}-NO^+, the latter being the accepted best representation of the species usually formed when NO binds to a Fe^{III} heme (*b, c*-type etc.) [19, 21]. However, van Wonderen *et al* [4] found that, when oxidised cd_1 from *P. pantotrophus* and from *P. stutzeri* were exposed to NO_2^- the resulting form of heme d_1 appeared to be low-spin Fe^{III}, as judged by electronic absorption spectra, but was now EPR silent. On the basis of MCD spectroscopy, which showed heme d_1 to be paramagnetic, they proposed that a novel Fe^{III}-$NO^{\bullet}$ species had resulted from the scavenging of an electron to allow a single turnover of NO_2^-. Both the ferric heme iron and the NO radical are S = ½ species, resulting in an EPR-silent state but the coupling between the two spins is relatively weak and does not fully abolish the paramagnetism [4, 36]. The existence and nature of this putative novel species can be investigated by preparing it from NO and oxidised cd_1 and again characterising it using magneto-optical methods. The following section describes work attempted to achieve this.

4.8.2: *Pseudomonas aeruginosa* cd_1 + NO: UV-Visible Electronic Absorbance.

A sample of *P. aeruginosa* cd_1 of volume 200 μL and concentration 16 μM was exchanged into 50 mM bis-tris propane (BTP) buffer solution at pH 6.5 using Microcons with a 10000 molecular weight cut off. Concentration followed by dilution with new buffer was repeated until the original buffer made up less than 0.01 of the total volume. The cd_1 sample was then placed in a 1 mm pathlength cuvette and the electronic absorbance spectrum was recorded in the range 260-900 nm using a Jasco V550 UV-visible spectrophotometer.

The 1 mm cuvette was then taken into an anaerobic glove box and 4 µL of saturated NO solution added using a Hamilton gas tight syringe (see Preparation of NO solution in Materials, Methods and Techniques). This represents approximately one equivalent of NO per monomer. The 1 mm cuvette was sealed with a rubber stopper and taken out of the box. The spectrum was again recorded in the range 260-900 nm. NO additions and absorption spectroscopy were repeated until a total of six equivalents of NO had been added. The spectra are shown in Figure 4.12. The heme d_1 visible region band at 640 nm only shows minor changes. However, the heme *c* bands in the region 500-560 nm are significantly changed by the NO additions. These changes are typical for reduction of the Fe^{III} heme *c* to the Fe^{II} state. Only when cd_1 was exposed to gaseous NO could this autoreduction be avoided.

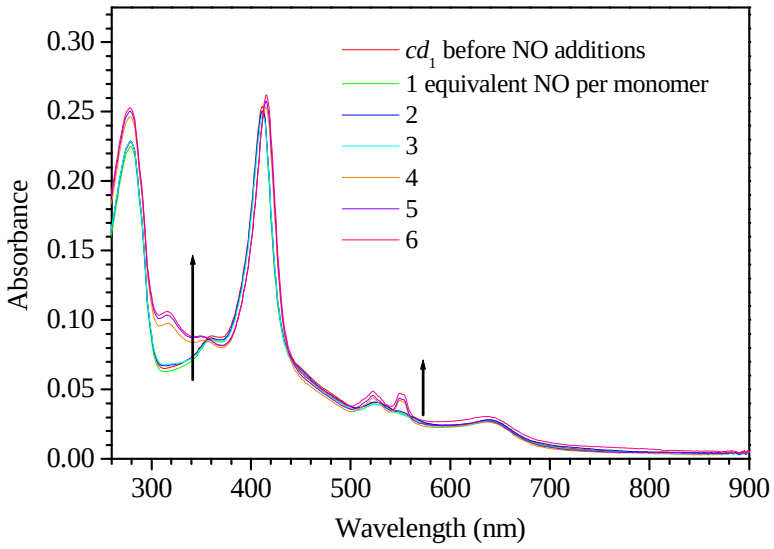

Figure 4.12: UV-Visible electronic absorbance spectra of 16 µM *P. aeruginosa* cd_1 protein and the effects of NO equivalents. The arrows denote the changes in the spectra with higher amounts of NO.

Again cd_1 protein was exchanged anaerobically until the original buffer made up less than 0.01 of the total volume. The sample was returned to the glove box and transferred into a pear shaped flask ready for NO treatment. The cd_1 was exposed to gaseous NO for 15 minutes. The absorption spectra before and after NO treatment are shown in Figure 4.13. There is a shift in the visible heme d_1 band from 642 nm to 636 nm. The heme *c* features remain largely unchanged.

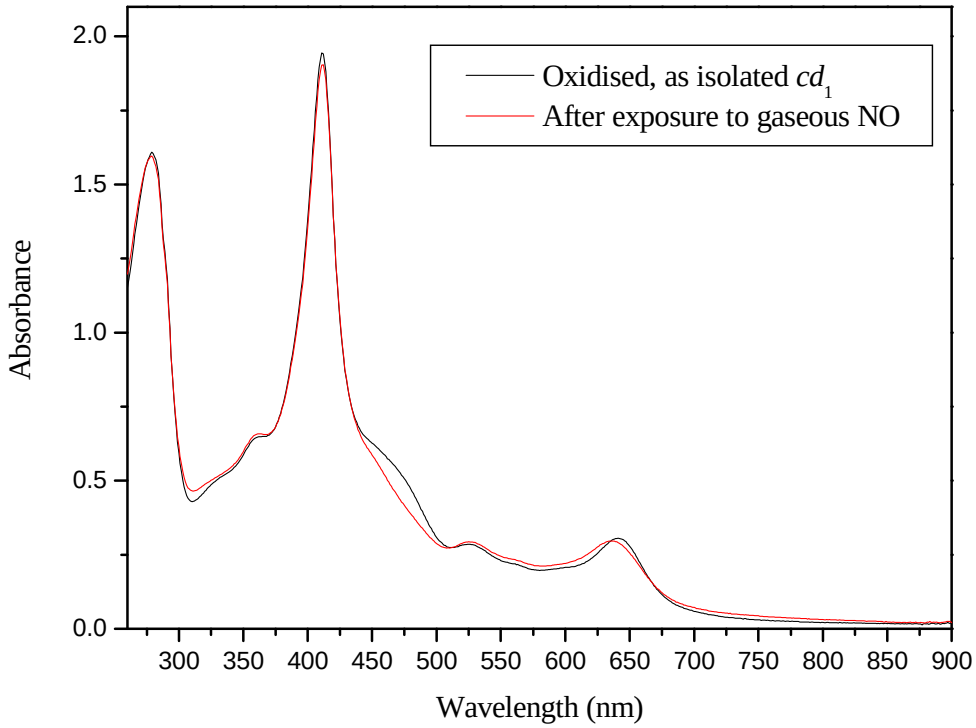

Figure 4.13: UV-Visible electronic absorbance spectra of 132 μM *P. aeruginosa* cd_1 protein before and after exposure to gaseous NO.

4.8.3: *Pseudomonas aeruginosa* cd_1 + NO: EPR.

In preparation for LT-MCD studies, glycerol glassing agent was added anaerobically (to ~55% glycerol by volume) to an NO-bound sample exhibiting no apparent autoreduction of heme *c*. The sample was frozen in a quartz tube for EPR (Figure 4.14). A derivative feature at g = 2.02 is due to a minority population (<5%) of Fe^{II}-NO heme. Therefore, although the heme *c* in this sample remains Fe^{III}, there has been some autoreduction of the nitrosyl heme d_1. The rest of heme d_1 is now EPR silent and the EPR is dominated by the rhombic spectrum of Fe^{III} heme *c* (g_{zyx} = 2.94,2.25,-).

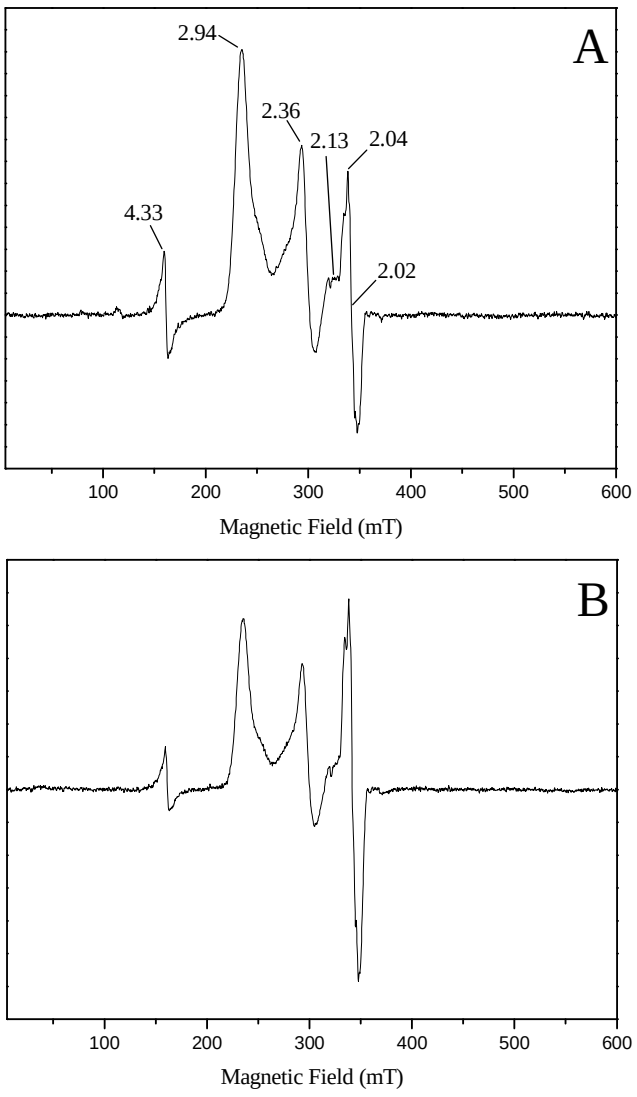

Figure 4.14: Experimental EPR spectra of NO bound *P. aeruginosa* cd_1 with the introduction of deuterated glycerol at ~55% of the total volume. Conditions used are 10 K / 2 mW (A) and 20 K / 0.64 mW (B). Spectrometric parameters are modulation frequency, 100 KHz; modulation amplitude, 10 G; time constant, 40.96 ms; and sweep time, 83.886 s.

4.8.4: *Pseudomonas aeruginosa* cd_1 + NO: RD-MCD.

The NO-treated cd_1 sample in buffer/glycerol was then frozen for MCD characterisation (Figure 4.15). These MCD spectra were recorded under "ratioed" conditions i.e. the four spectra were recorded at four different temperatures but the magnetic field was adjusted so as to keep the ratio of Magnetic Field / Temperature constant. Under these conditions, signals arising from species for which S = ½ will show fixed MCD intensity. At 450-550 nm the spectra are virtually the same since

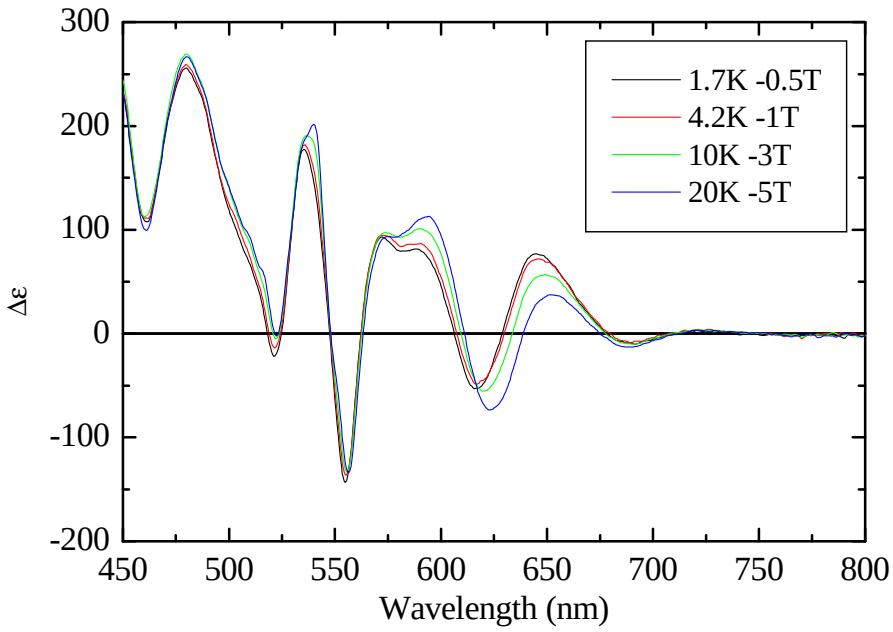

Figure 4.15: Ratio-data MCD spectra from NO bound *P. aeruginosa* cd_1. Sample is in 50 mM phosphate buffer in D_2O, pH 6.5* containing ~55% total volume deuterated glycerol. Key at the top right corner of the figure shows the temperature / magnetic field combinations.

these bands arise predominantly from the S = ½ low-spin Fe^{III} heme *c*. In the region 550-700 nm, although the bands are, in form, characteristic of a low-spin Fe^{II} heme d_1, the fact that they do not overlie indicates that the heme d_1 is not a simple S = ½ species. The spectra are, in fact, the same as were reported for the NO_2^-

treated forms of the oxidised cytochromes cd_1 from *P. pantotrophus* and *P. stutzeri* [4]. The link is thus made between the NO and NO_2^- treated forms in support of the suggestion of a novel Fe^{III}-$NO^{\bullet}$ form of heme d_1.

4.8.5: *Paracoccus pantotrophus* cd_1 + NO: EPR.

Previous attempts to bind NO to *P. pantotrophus* cd_1 at pH 7 resulted in only a trace of NO bound cd_1. But *P. pantotrophus* cd_1 is now known to react with nitrite more rapidly at lower pH [4]. Therefore concentrated *P. pantotrophus* cd_1 protein was buffer-exchanged into a mixed (12 mM acetate, 12 mM MES, 12 mM MOPS, 12 mM Tris) D_2O buffer at pH 5.5. A UV-visible electronic absorption spectrum was acquired of 200 μL, 224 μM oxidised, as isolated *P. pantotrophus* cd_1 (see Figure 5.04B). The 200 μL, 224 μM cd_1 solution was then taken into a glove box and transferred to a pear shaped flask ready for exposure to NO (see Preparation of NO solution in Materials, Methods and Techniques). After 1 hour of treatment the cd_1 was examined by electronic absorbance to see if any changes had occurred. The cd_1 solution was then replaced in the pear shaped flask in the glove box and left exposed to NO overnight. An electronic absorbance spectrum was again recorded. The electronic absorbance spectra are shown in Figure 4.16. There is a slight trace of autoreduction of heme *c* as shown by the increase at 561 nm. The low spin d_1 feature at 635 nm has increased in intensity whereas the high spin d_1 feature at 705 nm has decreased.

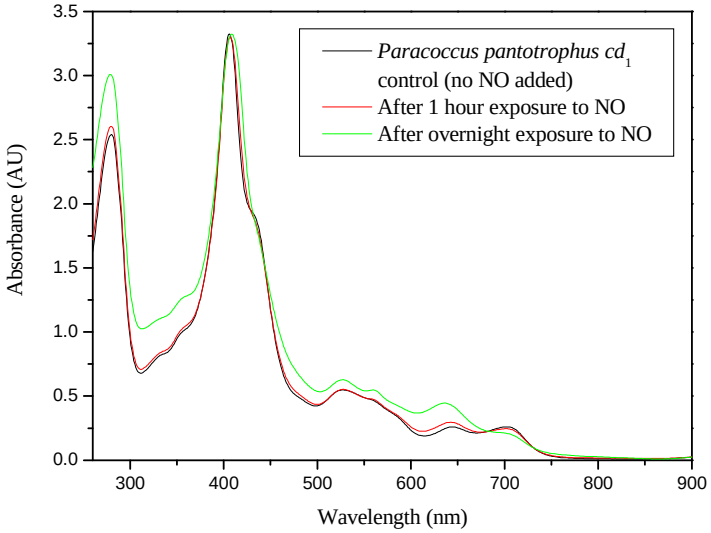

Figure 4.16: Electronic absorption spectra of *P. pantotrophus* cd_1. Legend in figure indicates what cd_1 state corresponds to which spectrum. The sample is in mixed buffer (12 mM acetate, 12 mM MES, 12 mM MOPS and 12 mM Tris) in D_2O at pH 5.5. Concentration of cd_1 protein is 224 μM.

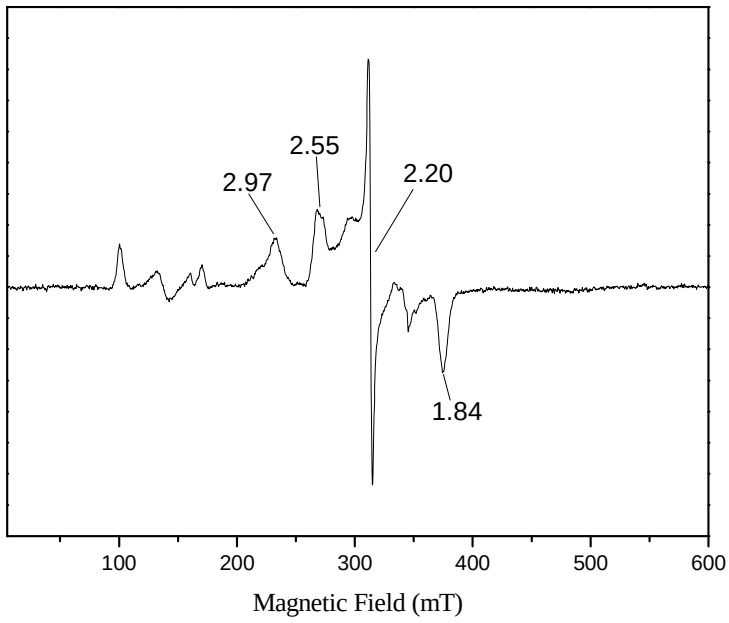

Figure 4.17: Experimental EPR spectrum of *P. pantotrophus* cd_1 after overnight exposure to NO. The sample is in mixed buffer (12 mM acetate, 12 mM MES, 12 mM MOPS and 12 mM Tris) in D_2O at pH 5.5. Conditions are 10 K / 2 mW. Spectrometric parameters are modulation frequency, 100 KHz; modulation amplitude, 10 G.

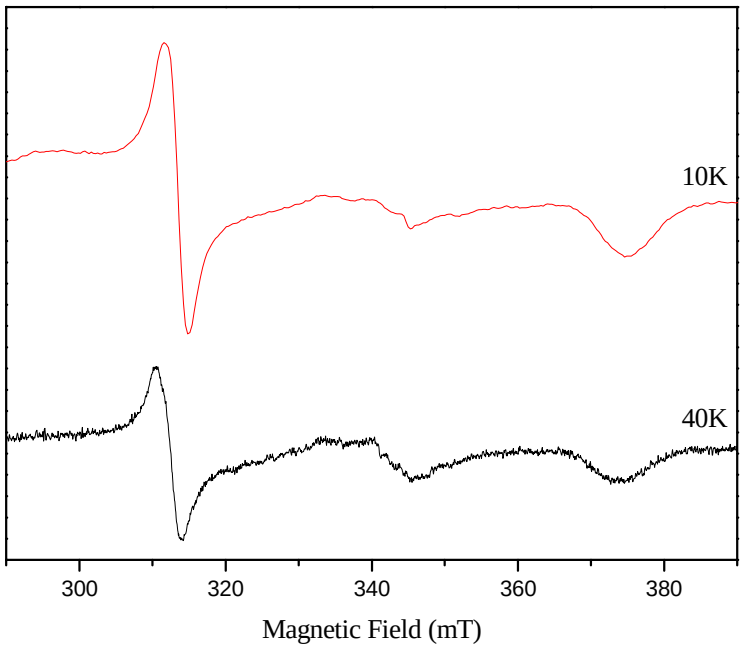

Figure 4.18: Experimental EPR spectra at 10 K / 2 mW and 40 K / 2 mW of *P. pantotrophus* cd_1 after overnight exposure to NO, focusing on the 290-390 mT regions. The sample is in mixed buffer (12 mM acetate, 12 mM MES, 12 mM MOPS and 12 mM Tris) in D_2O at pH 5.5. Spectrometric parameters are modulation frequency, 100 KHz; modulation amplitude, 10 G for 10 K, 4 G for 40 K; time constant, 20.48 ms; and sweep time, 41.943 s.

Also the shoulder at 430 nm, another d_1 heme feature, flattens with increasing exposure to NO. The cd_1 exposed to NO overnight was then transferred to a quartz tube to record EPR spectra. Spectra recorded at 10 K and 40 K are shown in Figures 4.17 and 4.18. Figure 4.17 still shows signals from both hemes but the heme d_1 features appear to have diminished in intensity relative to those of heme *c*. Furthermore there has been a change in the lineshape of both signals. The g_z feature of heme *c* is still two-fold heterogeneous but there is now more of the rhombic form with $g_z = 2.97$. Similarly, the ratio of the two heme d_1 species that contributed to the feature at 2.5-2.6 has switched in slight favour of the lower field component.

4.8.6: Reaction of Oxidised *cd*$_1$ with NO_2^-.

There have been reports of infrared spectroscopic studies of *cd*$_1$ that detect a 1913 cm^{-1} band that is characteristic of a "normal" Fe^{II}-NO^+ heme (19,21). However, RD-MCD studies [4] gave rise to the suggestion that a novel Fe^{III}-$NO^{\bullet}$ species can exist at heme *d*$_1$. But there have also been significant differences in the wavelength reported for the heme *d*$_1$ in this species, varying between 631 and 640 nm [4, 18]. We therefore considered the possibility that there is a pH dependence in the form of this nitrosyl complex as shown below (Equation 2).

low-pH Fe^{III}-$NO^{\bullet}$ $\rightleftharpoons$ Fe^{II}-NO^+ high-pH (2)

Unlike the Fe^{III}-$NO^{\bullet}$ species, which is paramagnetic, Fe^{II}-NO^+ is a diamagnetic form and its presence would lead to a reduction in MCD intensity at low-temperature. We have therefore investigated the MCD properties of the NO_2^--treated *cd*$_1$ at several different pHs in order to probe for the presence of a variable Fe^{III}-$NO^{\bullet}$/Fe^{II}-NO^+ mixture. However, since reaction with NO_2^- is extremely slow at higher pH values, the approach adopted was to perform the reaction with concentrated *cd*$_1$ at low pH and to dilute small aliquots into volumes of buffer at the required higher pH values.

4.8.7: pH on the Nature of NO_2^- Treated *Paracoccus pantotrophus cd*$_1$.

The binding of NO_2^- to *P. pantotrophus cd*$_1$ was investigated at three pHs. Concentrated *P. pantotrophus* (~150-200 μM) *cd*$_1$ was buffer-exchanged into a dilute mixed buffer (1.2 mM acetate, 1.2 mM MES, 1.2 mM MOPS, 1.2 mM Tris) at pH 6.5. The buffer-exchanged *cd*$_1$ was then aliquoted into three 25 μL volumes. To each 25 μL aliquot was added 130 μL of 100% glycerol and 95 μL of concentrated mixed buffer (120 mM acetate, 120 mM MES, 120 mM MOPS, 120 mM Tris) set at either pH 6.5, 7.5 or 8.5. Measurement of the pH of the samples after dilution into the three

buffers gave pH values of 7.2 (pH 6.5 concentrated buffer), 8.0 (pH 7.5 concentrated buffer) and 8.7 (pH 8.5 concentrated buffer). Prior to refreezing for MCD, the electronic absorbance spectrum of each sample was recorded (Figure 4.19).

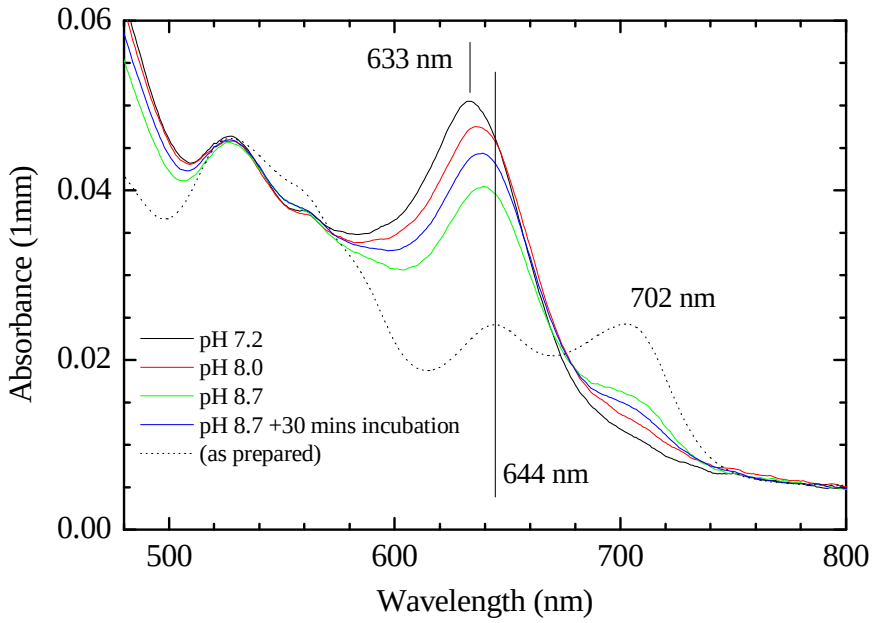

Figure 4.19: Electronic absorbance spectra of NO_2^--treated *P. pantotrophus* cd_1 at three different pHs. The concentration of cd_1 for each sample was ~ 150-200 μM. Buffer used was a mixed buffer of final concentration 12 mM acetate, 12 mM MES, 12 mM MOPS and 12 mM Tris. The dotted line denotes oxidised, as isolated, cd_1 with the d_1 bands at 644 nm and 702 nm indicated. The blue shifted peak at 633 nm of NO_2^--treated *P. pantotrophus* cd_1 at pH 7.2 is also indicated. The blue trace at pH 8.7 has had 30 minutes incubation to minimise the 702 nm band.

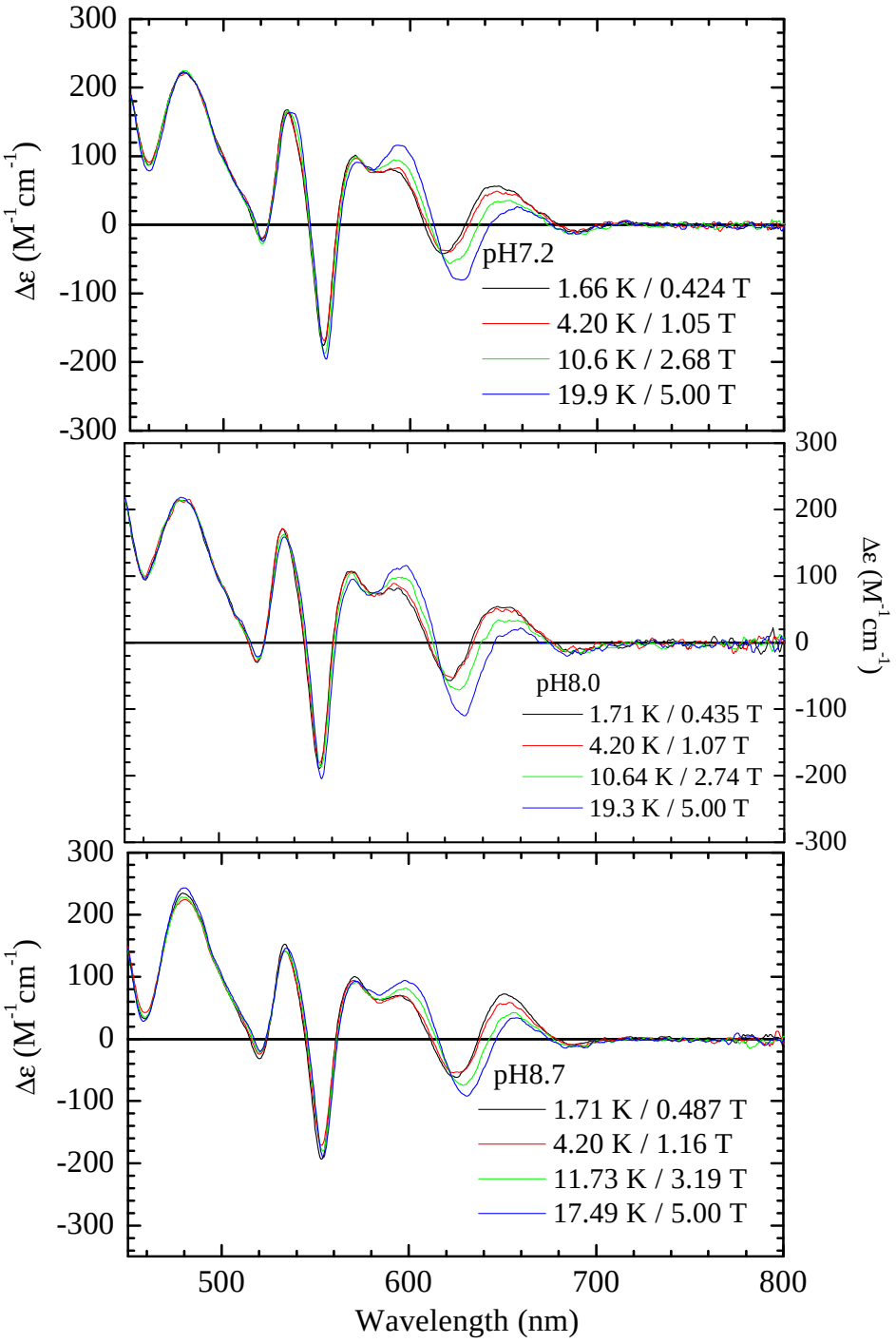

Figure 4.20: RD-MCD of NO_2^--treated *P. pantotrophus cd*$_1$. Samples are in mixed buffer (12 mM acetate, 12 mM MES, 12 mM MOPS and 12 mM Tris) at pH denoted in legend. Temperatures and magnetic field combinations shown in legends.

In the spectra of the NO_2^--treated samples, the low-spin Fe^{III} heme d_1 band (at 644 nm in the as-prepared protein) shifts to the blue with decreasing pH (633 nm at pH 7.2, 639 nm at pH 8.7). Judged by absence of the 702 nm band, the reaction is complete in the pH 7.2 and 8.0 samples. At pH 8.7, a further 30 minutes incubation was required to minimise the 702 nm band.

The RD-MCD data for these three samples are shown in Figure 4.20. For all three samples, bands in the 450-580 nm region arise from heme *c* and overlie, consistent with the S = ½ spin of this centre. However for ALL three samples, at 580-700 nm where the bands come mainly from heme d_1, the spectra do not overlie but spread in the same manner as was reported for NO_2^--treated *Paracoccus* cd_1 at pH6.5 [4] and has been observed earlier here for the NO-treated *P. aeruginosa* cd_1. Although there is a shift in the wavelength of these bands that reflects that seen in the absorbance spectra, all show the same Ratioed-Data MCD effect that results from the coupling of two S = ½ species in the Fe^{III}-$NO^{\bullet}$ heme d_1. Changes in pH that cause significant shifts in the wavelength of the heme d_1 bands do not result in major changes to the intensity of the corresponding RD-MCD bands. There is therefore no evidence for the presence of a diamagnetic Fe^{II}-NO^+ species.

4.9: Reaction of Oxidised cd_1 with N_3^-

The reaction of oxidised cd_1 with NO_2^- discussed in this chapter displays similarities to the behaviour reported when azide was added to cd_1 from *P. aeruginosa*. Exposure to sodium azide led to a significant reduction in the intensity of the low-spin ferric heme d_1 EPR features but MCD showed that the heme d_1 species produced was still paramagnetic [2]. The product of the reaction

with azide has therefore been characterised by absorption, EPR and MCD spectroscopies.

4.9.1: UV-Visible Absorption Spectra of *Pseudomonas aeruginosa* and *Paracoccus pantotrophus* cd_1 Treated with N_3^-.

As with the samples used for binding NO, the nitrite reductases were buffer-exchanged into a 50 mM BTP buffer at pH 6.5. For each experiment 200 µL of cd_1 protein at a concentration of 150-200 µM was used to obtain a "pre-azide" spectrum with good signal/noise in a 1 mm pathlength cuvette. 5 µL of 820 mM sodium azide was added and mixed to give a total concentration of 20 mM azide. The protein-azide mixture is allowed to incubate in the cuvette for 30 minutes before recording absorption spectra until no further change was observed.

The *P. aeruginosa* cd_1 (Figure 4.21) shows small but clear changes at bands

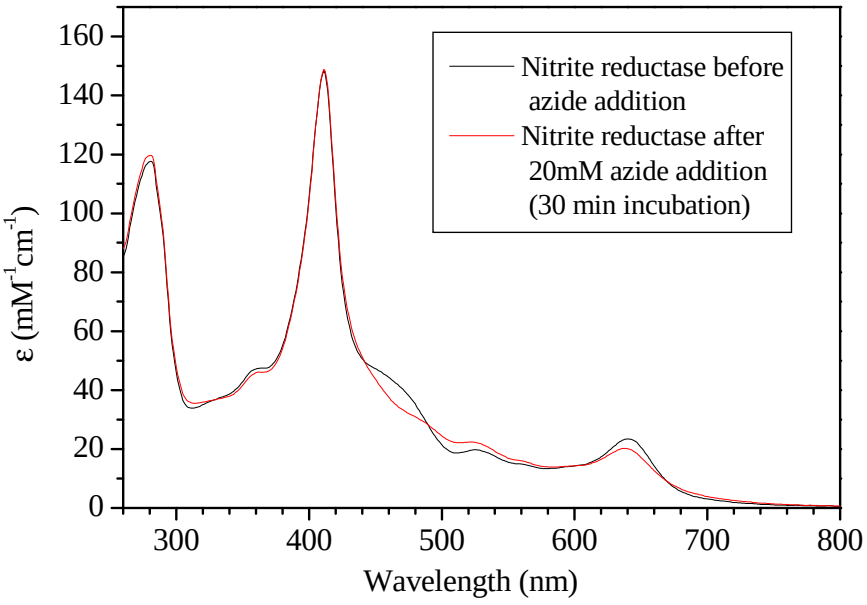

Figure 4.21: UV-Vis electronic absorbance spectra showing the changes in d_1 features of *P. aeruginosa* cd_1 in the presence of 20 mM azide. The concentration of protein used in this experiment was 186 µM.

associated with heme d_1. The 460 nm shoulder flattens significantly and the peak at 640 nm becomes less pronounced and shifts to 638 nm.

The *P. pantotrophus* cd_1 was exposed to azide with the same procedure as the *Pseudomonas* cd_1. The spectrum of *Paracoccus* cd_1 before the azide addition and the spectrum 30 minutes after the addition of azide were almost identical, showing only very minor changes in intensities but no detectable shifts (not shown). The sample was then left at 4°C overnight. The spectral changes were enhanced by this incubation but still minor (Figure 4.22).

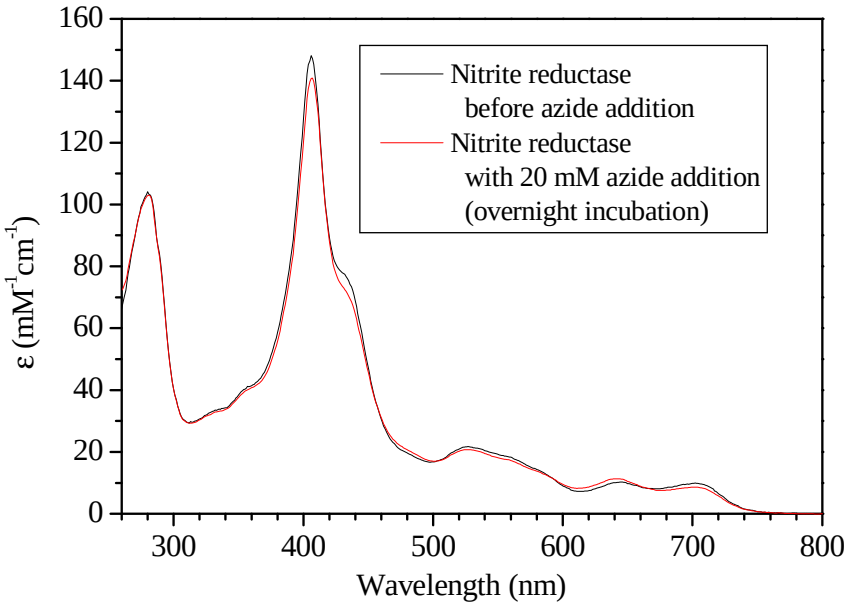

Figure 4.22: UV-Visible electronic absorbance spectra showing the slight difference in the 440 nm feature of *P. pantotrophus* cd_1 without azide and in the presence of 20 mM azide (incubation time overnight). The concentration of protein used in this experiment was 148 μM.

4.9.2: EPR and MCD of *Pseudomonas aeruginosa* cd_1 Azide Derivative.

In preparation for MCD, glycerol was added to the azide-treated *Pseudomonas* cd_1 sample (to a level of ~55% v/v). This was then frozen in a quartz tube for EPR (Figure 4.23). As previously suggested [2], with the exception of a

trace at g = 2.46, the spectrum now lacks the EPR features associated with Fe^{III} heme d_1. Apart from the g = 2.98 and 2.32 features of low-spin Fe^{III} heme *c*, the only other feature is a derivative at g = 4.3. This is often indicative of adventitious Fe^{III} ion but here is unusually pronounced. A similar signal was reported by Walsh *et al* [2].

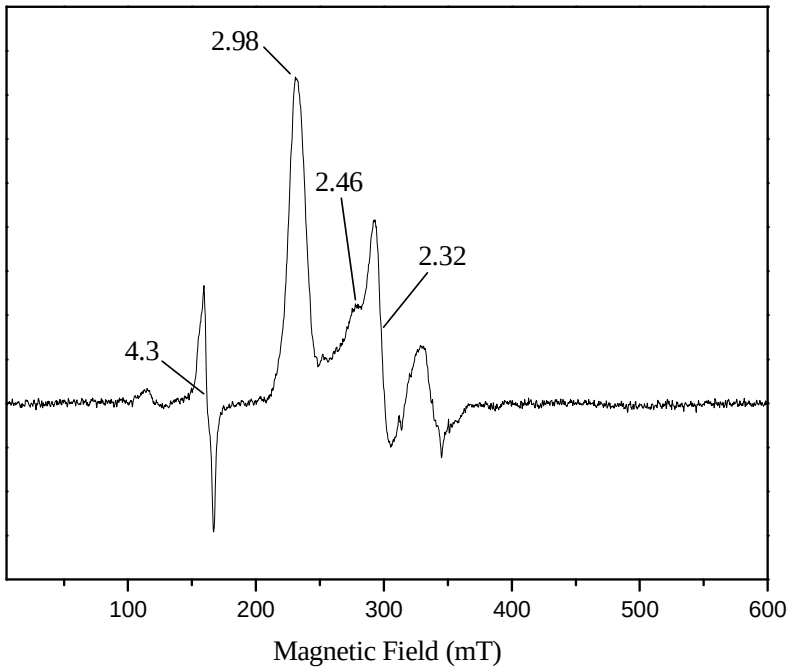

Figure 4.23: Experimental EPR spectrum of azide-treated *P. aeruginosa* cd_1 in buffer/glycerol mix. Conditions used were 10 K / 2 mW.

This sample was transferred into a 250 μL quartz cell and frozen in the MCD cryostat. RD-MCD spectra then recorded are shown in Figure 4.24. As was observed for the NO-derivatives of *Pseudomonas* cd_1, these spectra show clear regions where the spectra do not "ratio" i.e. they do not overlie. This is observed in regions associated with heme d_1, especially the 600-700 nm region, but the spectra are in detail different to those of the NO-derivative. The broad band at 460-540 nm, which

contains bands from both hemes, does not ratio and is almost double the intensity observed for the *Pseudomonas* cd_1 NO-derivative. Therefore, heme d_1 again appears to be low-spin Fe^{III} in nature but rendered EPR silent presumably by coupling to a radical species. But the nature of this species is clearly different to that found in the NO derivative.

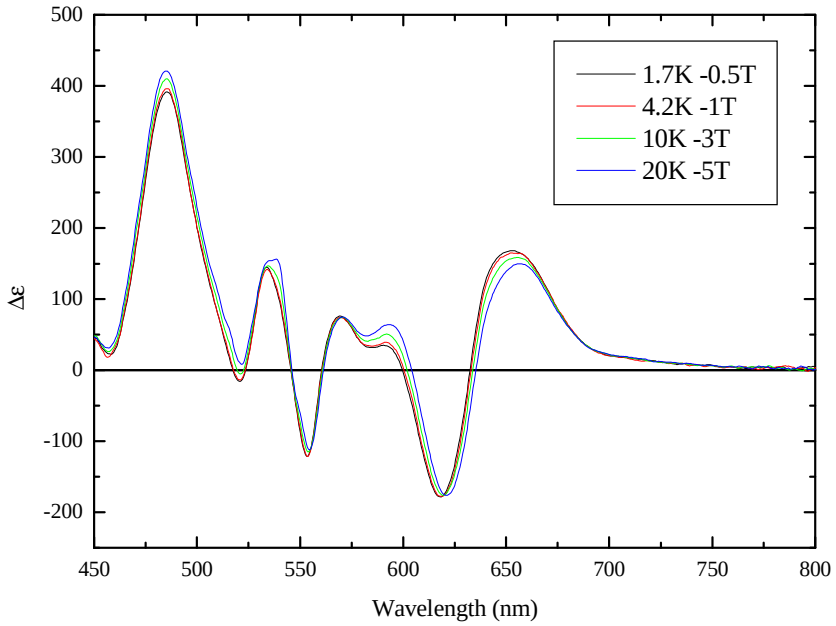

Figure 4.24: Ratio-data MCD spectra from azide bound *P. aeruginosa* cd_1. Sample is in 50 mM phosphate buffer in D_2O, pH 6.5* containing ~55% total volume deuterated glycerol. Key at the top right corner of the figure shows the temperature / magnetic field combinations.

4.9.3: EPR of the Azide-treated *Paracoccus pantotrophus* cd_1

The *Paracoccus* cd_1 sample treated with azide (absorption in Figure 4.22) was transferred to a quartz tube for EPR measurements (Figure 4.25). Signals from heme *c* are observed at g_{zyx} = 2.92, ~2.2, 1.55. The contribution from heme d_1, now an axial signal with g_{xy} = 2.51 has diminished in relative intensity but not disappeared entirely as was observed with the *Pseudomonas* cd_1.

This sample was not examined by MCD. On addition of glycerol, the EPR spectrum reverted to that of the oxidised as-prepared *Paracoccus* cd_1.

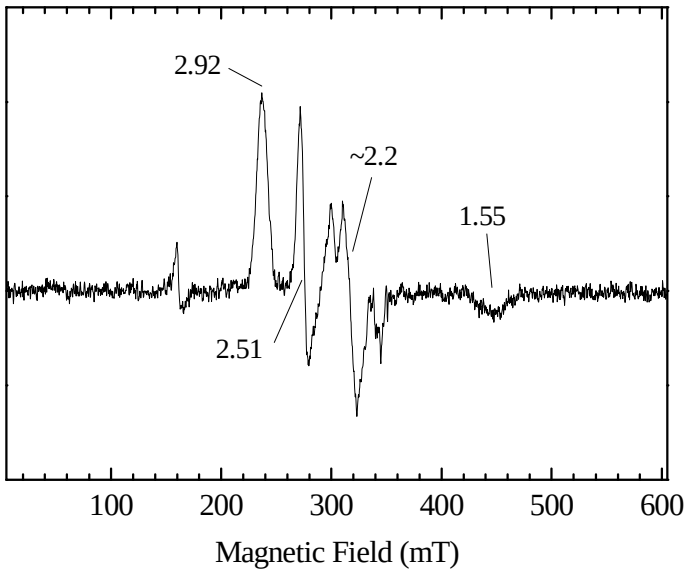

Figure 4.25: EPR spectrum of *P. pantotrophus* cd_1 treated with azide at a concentration of 20 mM. Sample is in 12 mM acetate, 12 mM MES, 12 mM MOPS and 12 mM Tris D_2O buffer, pH 6.5*. Conditions are 10 K / 2 mW. Spectrometric parameters are modulation frequency, 100 KHz; modulation amplitude, 10 G; time constant, 82 ms; and sweep time, 168 s.

4.10: cd_1: Summary and Conclusions

At acidic pH cd_1 has a higher nitrite reductase activity and the reaction of the oxidised form with NO_2^- is more rapid [4, 20, 23, 34]. There are however no published spectra showing actual pH dependence for any type of cd_1 spectrum. The work of Bennett in these laboratories showed that despite the absorbance spectra of *P. pantotrophus* cd_1 having no sensitivity to pH change, the EPR does [24]. Changes in the EPR at acidic pH were assigned to protonation of histidine(s) in the distal heme d_1 pocket, which then hydrogen-bond to tyrosine, resulting in a weakening of

its ligand strength at heme d_1 [5]. The *P. aeruginosa* cd_1 was investigated for similar behaviour. This work has shown that absorbance spectra give rise to only minor changes with changes in pH. Between pH 5.5 and 8.5 there is only a 2 nm shift. However EPR again responds to changes in pH. There is no spin-state change as observed with the *Paracoccus* enzyme. Instead there is more complicated behaviour observed in *P. aeruginosa* cd_1 at the pH range 5.5-8.5. This could indicate more than one process, such as the protonation of both distal histidines [37].

The suggestion of a novel Fe^{III}-NO$^{\cdot}$ form of heme d_1 raised the possibility that product bound enzyme could exist in cd_1 preparations without being detected [4]. The Fe^{III}-NO$^{\cdot}$ species appears as normal low-spin ferric in absorbance spectra. In EPR, unless there were extremely high proportions of Fe^{III}-NO$^{\cdot}$ this would not be immediately apparent. Therefore an EPR study of as isolated cd_1 from both *P. pantotrophus* and *P. aeruginosa* was undertaken. The aim of this study was to simulate spectra recorded under non-saturating conditions and therefore be able to quantify the relative levels of EPR active heme *c* and d_1. Although EPR features of both heme *c* and d_1 are heterogeneous, the integrations of the simulated spectra showed that in *Pseudomonas* cd_1 the EPR contained 1.00 heme d_1 per heme *c* as isolated. This indicates that no Fe^{III}-NO$^{\cdot}$ species is present in preparations of *P. aeruginosa* cd_1. The best simulation that could be achieved for the *P. pantotrophus* cd_1 EPR gave figures for the heme d_1 that were in excess of 1 compared to the heme *c*. There is no evidence for EPR silent heme d_1. Work on simulating EPR for as isolated *P. stutzeri* cd_1 indicated a proportion of d_1 heme that was EPR silent [4]. It is noted that, although the residues are not equivalent in the sequence, both the *P. aeruginosa* and *P. pantotrophus* cd_1 have a tyrosine residue

that interacts with heme d_1 or its distal ligand [38, 39]. The sequence of *P. stutzeri* has no equivalent tyrosine [40].

When oxidised cd_1 was reported to undergo an unexpected reaction with nitrite, it was also demonstrated that in *P. pantotrophus* cd_1 this reaction triggers the bis-histidine to histidine/methionine ligand switch that was believed essential for activity [4]. It was previously believed that reduction was required to initiate this switching of ligands. In this work, assay methods have clearly shown that (i) nitrite exposure activates cd_1 without the need for reduction and (ii) activation is more rapid at acidic pH. While these rates are orders of magnitude too slow to be part of the catalytic cycle, they do provide the method of activation of resting cd_1. The deactivation process was also studied. Using nIR-MCD, Bradley and Haynes have followed the ligand changes at heme *c* following reoxidation of reduced *P. pantotrophus* cd_1 with hydroxylamine (UEA, unpublished). They identified a new intermediate, with heme *c* switching to a bis-histidine form with parallel ligand planes, before slowly reverting to the perpendicular ligand conformation of the as-isolated form (which was observed in the first crystal structure [38]). By sampling and assaying activity following reoxidation it has now been shown that the loss of activity parallels the histidine/methionine to the parallel bis-histidine switch, and not the reversion to the true as-isolated form.

The work described here has provided the first clear evidence that the species formed by reaction of nitrite with oxidised cd_1 is indeed a novel Fe^{III}-$NO^{\cdot}$ form of heme d_1. Detailed VFVT MCD studies of the NO derivative of oxidised *P. aeruginosa* cd_1 showed that the NO-bound heme d_1 has identical magneto-optical properties to those of *P. aeruginosa* or *P. pantotrophus* cd_1 treated with NO_2^-. However, it was not possible to stoichiometrically displace the tyrosinate bound to

Fe^{III} heme d_1 of the *P. pantotrophus* cd_1 to produce the analogous fully NO-bound form.

Other work here at UEA has shown that when the fully (two-electron) reduced *P. pantotrophus* cd_1 is one-electron oxidised by nitrite, a mixture of two forms that differ in the location of the remaining electron results:

$$Fe^{II}\text{-heme } c \text{ / heme } d_1\text{-}Fe^{II}\text{-}NO^{+} \rightleftharpoons Fe^{III}\text{-heme } c \text{ / heme } d_1\text{-}Fe^{II}\text{-NO}$$

The position of the equilibrium is dependent on the protonation of one or both of the distal heme d_1 pocket histidine residues. This raised the possibility that the result of nitrite reaction with the oxidised enzyme was a mixture of two forms of heme d_1: Fe^{III}-$NO^{\cdot}$ and Fe^{II}-NO^{+}. The former is the novel species identified in this work. The latter is the "normal" form of ferric heme nitrosyl that is diamagnetic in nature and so would not appear in the low-temperature MCD spectra. RC-MCD spectra were therefore recorded, at three different pH values, for the product of nitrite treatment of the *P. pantotrophus* cd_1. Although there are detectable shifts in the band positions, at all pHs studied, the heme d_1 was in the Fe^{III}-$NO^{\cdot}$ form. It therefore appears that the Fe^{II}-NO^{+} form of heme d_1 only occurs when heme *c* is reduced.

Oxidised cd_1 from *P. pantotrophus* and *P. aeruginosa* both reacted with azide. However, for *P. pantotrophus* cd_1, it was not possible to prepare a sample in glycerol/buffer for VTVF MCD studies. This was achieved for the *P. aeruginosa* cd_1. Exposure to azide led to a complete removal of the heme d_1 EPR and the RD-MCD suggested a low-spin Fe^{III} heme d_1 interacting with a radical. However the data indicate this is not a form equivalent to the Fe^{III}-$NO^{\cdot}$ heme d_1 that results from addition of NO_2^{-} or NO. It is not clear what is happening in this reaction. Azide is known to form a $N_3^{\cdot}$ radical but this is an oxidative process and not reductive as $NO_2^{-} \rightarrow NO$.

4.11: References

1. Muhoberac, B. B., Wharton, D. C. (1983) *J. Biol. Chem.* ***258***, 3019-3027.
2. Walsh, T. A., Johnson, M. K., Thomson, A. J., Barber, D., Greenwood, C. (1981) *J. Inorg. Biochem.* ***14***, 1-14.
3. Hori, H. (1971) *Biochim. Biophys. Acta* ***251***, 227-235.
4. Van Wonderen, J. H., Knight, C., Oganesyan, V. S., George, S. J., Zumft, W. G., Cheesman, M. R. (2007) *J. Biol. Chem.* ***282***, 28207-28215.
5. Williams, P. A., Fulop, V., Garman, E. F., Saunders, N. F. W., Ferguson, S. J., Hadju, J. (1997) *Nature* ***389***, 406-412.
6. Crane, B. R., Siegel, L. M., Getzoff, E. D. (1997) *Biochemistry* ***36***, 12120–12137.
7. Einsle, O., Messerschmidt, A., Huber, R., Kroneck, P. M. H., Neese, F. (2002) *J. Am. Chem. Soc.* ***124***, 11737–11745.
8. Yi, J., Heinecke, J., Tan, H., Ford, P. C., Richter-Addo, G. B. (2009) *J. Am. Chem. Soc.* ***131***, 18119-18128.
9. Copeland, D. M., Soares, A. S., West, A. H., Richter-Addo, G. B. (2006) *J. Inorg. Biochem.* ***100***, 1413-1425.
10. Yamanaka, T., Ota, A., Okunuki, K. (1961) *Biochim. Biophys. Acta* ***53***, 294-308.
11. Moir, J. W. B., Baratta, D., Richardson, D. J., Ferguson, S. J. (1993) *Eur. J. Biochem.* ***212***, 377-385.
12. Gladwin, M. T., Kim-Shapiro, D. B. (2008) *Blood* ***112***, 2636-2647.
13. Mayburd, A. L., Kassner, R. J. (2002) *Biochemistry* ***41***, 11582-11591.
14. Maurus, R., Bogumil, R., Nguyen, N. T., Mauk, A. G., Brayer, G. (1998) *Biochem. J.* ***332***, 67-74.

15. Stryer, L., Kendrew, J. C., Watson, H. C. (1964) *J. Mol. Biol.* ***8***, 96-104.

16. Bogumil, R., Hunter, C. L., Maurus, R., Tang, H. L., Lee, H., Lloyd, E., Brayer, G. D., Smith, M., Mauk, A. G. (1994) *Biochemistry* ***33***, 7600-7608.

17. Cheesman, M. R., Ferguson, S. J., Moir, J. W. B., Richardson, D. J., Zumft, W. G., Thomson, A. J. (1997) *Biochemistry* ***36***, 16267-16276.

18. Allen, J. W. A., Higham, C. W., Zajicek, R. S., Watmough, N. J., Ferguson, S. J. (2002) *Biochem. J.* ***366***, 883-888.

19. Wang, Y. N., Averill, B. A. (1996) *J. Am. Chem. Soc.* ***118***, 3972-3973.

20. Silvestrini, M. C., Colosimo, A., Brunori, M., Walsh, T. A., Barber, D., Greenwood, C. (1979) *Biochem. J.* ***183***, 701-709.

21. George, S. J., Allen, J. W. A., Ferguson, S. J., Thornley, R. N. F. (2000) *J. Biol. Chem.* ***275***, 33231-33237.

22. Zajicek, R. S., Cartron, M. L., Ferguson, S. J. (2006) *Biochemistry* ***45***, 11208-11216.

23. Richter, C. D., Allen, J. W., Higham, C.W., Koppenhöfer, A., Zajicek, R. S., Watmough, N. J., Ferguson, S. J. (2002) *J. Biol. Chem.* ***277***, 3093-3100.

24. Bennett, M. S., Cheesman, M. R. *unpublished.*

25. Walker, F. A., Huynh, B. H., Scheidt, W. R., Osvath, S. (1986) *J. Am. Chem. Soc.* ***108***, 5288-5297.

26. Spinner, F., Cheesman, M. R., Thomson, A. J., Kaysser, T., Gennis, R. B., Peng, Q., Peterson, J. (1995) *Biochem. J.* ***308***, 641-644.

27. Allen, J. W. A., Watmough, N. J., Ferguson, S. J. (2000) *Nat. Struct. Biol.* ***7***, 885-888.

28. Legall, J., Payne, W. J., Morgan, T. V., Dervartanian, D. (1979) *Biochem. Biophys. Res. Commun.* ***87***, 355-362.

29. Allen, J. W. A., Cheesman, M. R., Higham, C. W., Ferguson, S. J., Watmough, N. J. (2000) *Biochem. Biophys. Res. Commun.* ***279***, 674-677.

30. Pettigrew, G. W., Moore, G. R. (1987) *Cytochromes c: Biological Aspects*, Springer, Berlin.

31. Rinaldo, S., Arcovito, A., Brunori, M., Cutruzzolà, F. (2007) *J. Biol. Chem.* ***282***, 14761-14767.

32. Das, T. K., Wilson, E. K., Cutruzzolà, F., Brunori, M., Rousseau, D. L. (2001) *Biochemistry* ***40***, 10774-10781.

33. Kim, C. H., Hollocher, T. C. (1983) *J. Biol. Chem.* ***258***, 4861-4863.

34. Silvestrini, M. C., Tordi, M. G., Musci, G., Brunori, M. (1990) *J. Biol. Chem.* ***265***, 11783-11787.

35. Cutruzzolà, F., Rinaldo, S., Centola, F., Brunori, M. (2003) *IUBMB Life* ***55***, 617-621.

36. Cheesman, M. R., Oganesyan, V. S., Watmough, N. J., Butler, C. S., Thomson, A. J. (2004) *J. Am. Chem. Soc.* ***126***, 4157-4166.

37. Cutruzzolà, F., Brown, K., Wilson, E. K., Bellelli, A., Arese, M., Tegoni, M., Cambillau, C., Brunori, M. (2001) *Proc. Natl. Acad. Sci. USA* ***98***, 2232-2237.

38. Fulop, V., Moir, J. W. B., Ferguson, S. J., Hadju, J. (1995) *Cell* ***81***, 369-377.

39. Nurizzo, D., Silvestrini, M. C., Mathieu, M., Cutruzzolà, F., Bourgeois, D., Fülöp, V., Hajdu, J., Brunori, M., Tegoni, M., Cambillau, C. (1997) *Structure* ***15***, 1157-1171.

40. Smith, G. B., Tiedje, J. M. (1992) *Appl. Environ. Microbiol.* ***58***, 376-384.

Chapter 5.

General discussion.

5.1: Introduction

This thesis presents the studies of two proteins that have important functions in microorganisms that are involved in the nitrogen cycle. The first is RirA, a transcriptional suppressor in conditions of iron sufficiency. This regulator is found in the symbiotic, nitrogen-fixing bacterium *Rhizobium leguminosarum*, as well as many of the other *Rhizobia*, *Bartonella* and *Brucella*. The aims of this section of the project were to purify and characterise the RirA protein from *R. leguminosarum*, investigating the proposal that RirA is an iron-sulphur protein by attempting to reconstitute and identify the nature of the cluster through spectroscopic methods.

The second protein is cd_1 nitrite reductase, a denitrification enzyme that catalyses the one electron reduction of nitrite to nitric oxide. The focus here was on the cd_1 nitrite reductases from *Paracoccus pantotrophus* and *Pseudomonas aeruginosa*.

The possibility that the reaction of NO_2^- with oxidised cd_1 produces an unusual Fe^{III}-NO heme d_1 nitrosyl species was tested in a variable-temperature MCD study of cd_1 exposed to nitric oxide. This heme d_1 species would appear as low-spin Fe^{III} in the electronic absorption spectrum but would not appear in the EPR spectrum. The possible presence of this product-bound form in as-prepared samples of cd_1 from both species was investigated by simulation, and quantitation, of the X-band EPR spectra of these proteins.

The reaction of oxidised cd_1 with NO_2^-, which originally led to the suggestion of a novel Fe^{III}-NO form, also led to the switching of the ligands at heme *c* from His/His to the His/Met coordination associated with activity. The dependence of this activation on pH and time was investigated using nitrite reductase assays of cd_1 pre-incubated with NO_2^- for variable periods at several pH values.

5.2: RirA from *Rhizobium leguminosarum*

These studies of RirA involved the first purification and cluster reconstitution of the protein, [1-7]. Comparisons can now be made with data reported for other members of the Rrf2 family and there are strong similarities to the well studied family members, NsrR and IscR. All three proteins have three conserved cysteine residues in which iron sulphur clusters could be accommodated (see Figure 1.30). Size exclusion chromatography in this work has shown that RirA apoprotein is dimeric. This correlates with published work on NsrR and IscR, which has determined that these proteins are also dimeric [8, 9] Specifically, NsrR and IscR are dimeric in both apo- and holo- forms. Apart from the genetic analysis (Figure 1.30) [10, 11], no characterisation of the Rrf2 protein has been reported and there are no crystal structures published for RirA, NsrR, IscR or Rrf2. The PDB [12] has five crystal structures available for the Rrf2 family members. None of these contain the three cysteines that are found in the sequence of RirA, IscR, Rrf2 or NsrR [2, 11, 13, 14]. These are YwnA (pdb 1XD7) from *Bacillus subtilis*, BC1842 (pdb 1YLF) from *Bacillus cereus*, LP_0360 (pdb 3K69) from *Lactobacillus plantarum*, Lin1550 (pdb 3LWF) from *Listeria innocua* and CymR (pdb 2Y75) in *B. subtilus* [15]. CymR is a repressor of cysteine biosynthesis and cystine uptake genes. The Lin1550 gene is also a CymR repressor.

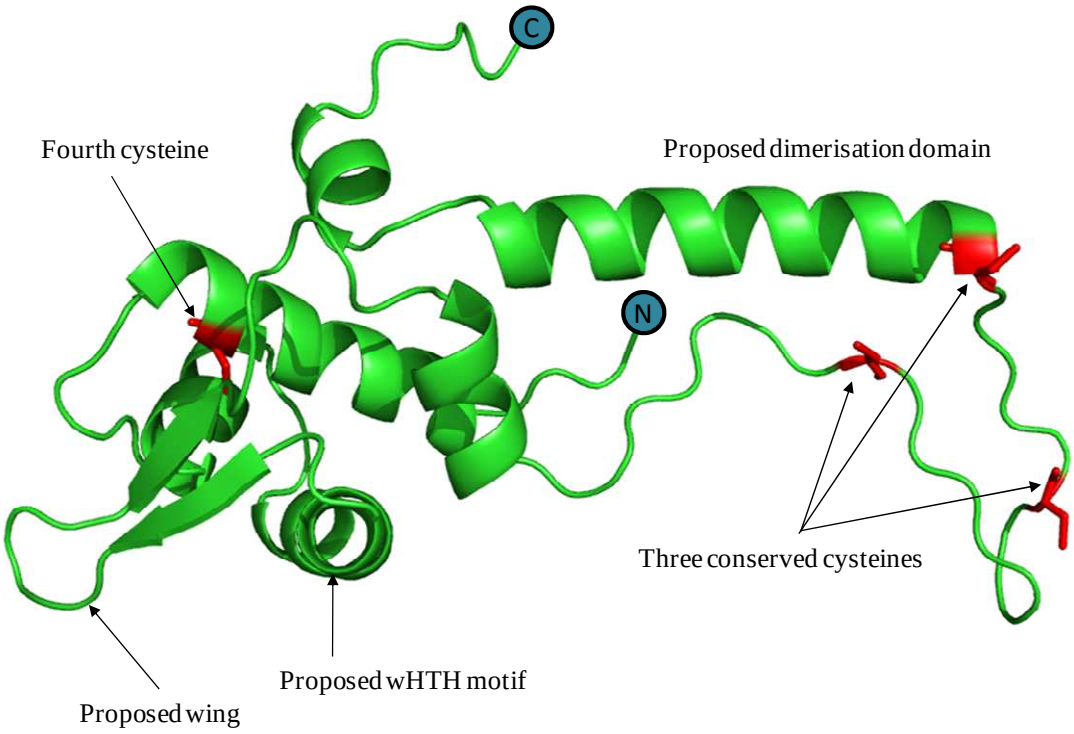

Figure 5.01: SWISS-MODEL generated Pymol cartoon representation of RirA using Lin1550 (pdb 3LWF) as a template. Cysteines are shown in red as stick representations.

If the RirA sequence is put into SWISS-MODEL [16-18] then the resulting predicted model is constructed as a result of comparison with the Lin1550 structure (The CymR (pdb 2Y75) shares 70% identity with Lin1550). The model only has ~23% sequence identity but it can be used to predict the location of iron-sulphur clusters in the Rrf2 family members such as RirA. The predicted model for RirA from SWISS-MODEL is shown in Figure 5.01. The three conserved cysteines in this model are located at an open loop, equivalent to the α6 and β3 regions of the dimerisation domain in the CymR structure [15]. These three cysteines are openly exposed and may be the cause of the precipitation of the apoprotein during concentration and preparation. The fourth cysteine (Cys 17) is located at the equivalent of the α1 helix

in CymR, close to the wing and helix-turn-helix DNA binding domain [15]. If RirA does form a physiologically relevant dimer, like CymR and many other prokaryotic transcription factors, then it appears that an iron-sulphur cluster requiring four cysteine ligands such as [2Fe-2S] or [4Fe-4S] could be formed from the three conserved cysteines of one monomer combined with the fourth cysteine of the opposing monomer. However, the fourth cysteine may not be a ligand. IscR only has three cysteines in its sequence. The fourth ligand is therefore a non-cysteine residue. A glutamate residue has been reported as the fourth ligand [19]. NsrR is also thought to have a non-cysteine fourth ligand. A conserved histidine in the helix-turn helix DNA binding domain is predicted to be the fourth ligand [20]. This suggests that RirA could also have a fourth non-cysteine ligand also.

RirA would form a dimer with two iron-sulphur clusters in close contact with the wing and helix-turn-helix motifs that bind DNA at the minor and major grooves respectively [15]. Evidence for the existence of a dimeric complex when RirA is reconstituted with the clusters was sought through analytical gel filtration. Unfortunately, several attempts resulted in the iron-sulphur clusters dissociating from the reconstituted protein rapidly when applied to the column. Clusters would be incorporated when iron levels are high, activating the RirA dimer and allowing it to bind to IRO sequences, repressing the target genes. The method of regulation could indeed be more complicated. For example, a non-DNA binding form could already contain two [3Fe-4S] clusters bound at the sites of the conserved cysteines. As a repressor of iron uptake genes in conditions of iron sufficiency it may utilise two additional iron atoms to form two [4Fe-4S] clusters. This may induce conformational changes that allow binding of RirA to the DNA to repress its target genes. A comparable example of a protein activated by incorporation of a further iron ion into

a [3Fe-4S] cluster to form a [4Fe-4S] is aconitase [21], an enzyme that converts citrate to isocitrate.

The identification of reconstituted iron sulphur clusters in the RirA is the other key part of this work. On the basis of the electronic absorbance spectrum of reconstituted RirA, it can be postulated that the clusters are unlikely to be [2Fe-2S] in nature. The spectra of [2Fe-2S] clusters from various ferredoxins, xanthine oxidase and benzene dioxygenase have several features additional to the ~ 400 nm shoulder observed in Figure 3.18 [22 and refs. therein]. This single feature is more indicative of [3Fe-4S] and [4Fe-4S] clusters [22 and refs. therein]. Interestingly, studies on both NsrR and IscR have identified [2Fe-2S] clusters, but there is some dispute whether or not the physiologically relevant clusters are [4Fe-4S] [9, 14, 20, 23-25]. The electronic absorbance spectrum shown in Yukl *et al.* for the [4Fe-4S] containing NsrR is strikingly similar to that of RirA in this work [9]. So far, only IscR containing [2Fe-2S] clusters have been reported [14, 24].

These studies have provided evidence of [3Fe-4S] and [4Fe-4S] clusters in many different combinations in reconstituted RirA. The EPR of the reduced reconstituted RirA (Figure 4.22) shows a shoulder at low field from the sharp feature at g = 2.05 and a trough at high field at g ~ 1.93. These spectral features increase in size with increasing temperature, indicative of a fast relaxer. These fast relaxing features can be tentatively assigned to spin-coupled $[4Fe\text{-}4S]^{+}$ clusters. Interacting paramagnetic species such as $[4Fe\text{-}4S]^{+}$ undergo much more rapid relaxation [26]. Reduced NsrR has a fast relaxing EPR signal at g = 2.04 and 1.93 assigned to a $[4Fe\text{-}4S]^{+}$ also [9].

The g-values 2.05, 1.97 and 1.93 indicated on Figure 4.22 are also suggestive of $[4Fe\text{-}4S]^{+}$ cluster g-values observed in reduced 7Fe ferredoxins [22, 27-29]. These

ferridoxins have a [3Fe-4S] and [4Fe-4S] cluster. Reduction renders the [3Fe-4S] EPR silent, leaving $[4Fe\text{-}4S]^{+}$ as the sole detectable species. The reduced EPR spectra of reconstituted RirA show g-values of 2.05, 1.97 and 1.93 which is suggestive of a single $[4Fe\text{-}4S]^{+}$ cluster. This may occur if one monomer of the reconstituted RirA dimer has a $[4Fe\text{-}4S]^{+}$ and the other monomer has no cluster or an EPR silent species such as $[3Fe\text{-}4S]^{0}$.

The spectroscopic data proves the presence of $[3Fe\text{-}4S]^{+}$ clusters. The EPR of oxidised reconstituted RirA at 10 K (Figure 4.21) clearly shows a typical shape for a $[3Fe\text{-}4S]^{+}$ cluster. The typical g-value of 2.01 reported for many [3Fe-4S] clusters in 7Fe ferredoxins and aconitase corresponds closely to the g = 2.02 indicated on the 10 K, oxidised spectrum [22, 27-30]. There is also a classic temperature dependence observed for [3Fe-4S]. As the temperature increases, the [3Fe-4S] signal decreases. The EPR of the oxidised [3Fe-4S] can also be quantitated. The concentration of 127 μM iron from assays correspond directly to the as reconstituted absorbance spectrum in Figure 3.20 (the ferricyanide-oxidised absorbance spectrum at the same concentration showed no change at the 410 nm shoulder from the as reconstituted). The shoulder at 410 nm gives a crude estimated iron concentration of ~ 100 μM using the extinction coefficient for iron of 4000 M^{-1} cm^{-1}. If the absorbance is all due to [3Fe-4S] clusters then the concentration of cluster is ~ 33 μM. Integration of the oxidised [3Fe-4S] cluster gave a concentration of ~ 25 μM. The presence of [3Fe-4S] in reconstituted RirA is unusual as [2Fe-2S] and [4Fe-4S] clusters are far more common in transcription factors such as FNR, SoxR, NsrR and IscR than [3Fe-4S] [31, 32]. The [3Fe-4S] clusters appear to act more as an intermediate stage such as in FNR or as the result of [4Fe-4S] cluster degradation [33, 34].

The as reconstituted RirA EPR spectra are complicated and therefore assigning cluster types is difficult. Two axial species, a slow relaxer at g = 2.04, 2.02 and a fast relaxer at g = 2.02, 1.97, can be identified from spectra recorded at different temperatures and microwave powers. There appears to be a similar behaviour for the two [4Fe-4S] clusters in the NQO9 subunit of *Paracoccus denitrificans* NADH-quinone oxidoreductase, with an axial slow relaxing species at g = 2.05, 1.93 and an axial fast relaxing species at g = 2.08, 1.90 [35]. The axial spectra themselves are not similar, however. The g-values for the NQO9 subunit are spread further apart than the equivalent RirA values, and the axial spectra identified in the NQO9 subunit are of the type $g_x = g_y < g_z$, whereas the axial spectra derived from the reconstituted RirA is of the type $g_x = g_y > g_z$.

Future work would involve simulating the EPR data to identify the different signals contributing to the spectra. To definitively identify the clusters and establish that RirA is indeed a dimer, MCD fingerprinting and X-ray crystallography would be useful tools. Low temperature MCD would allow identification not only of the cluster but of its oxidation state as well, using the standards of *Desulphovibrio gigas* ferredoxin II for [3Fe-4S] and *Desulphovibrio africanus* ferredoxin II for [4Fe-4S] [22, 36]. The crystal structure of RirA would confirm the dimeric structure, positions of the cysteine residues and the type of clusters present. This would also allow more accurate predictions to be made for NsrR, IscR and Rrf2, as current crystal structures of Rrf2 family members are those without iron-sulphur clusters. Once the cluster type and protein characterisation are confirmed, studies could then be focused on the DNA binding mechanisms of RirA and the role of the clusters.

5.3: The cd_1 Nitrite Reductases of *Paracoccus pantotrophus* and *Pseudomonas aeruginosa*.

One of the key focuses of this work was to provide further evidence for the EPR silent d_1 species Fe^{III}-$NO^{\bullet}$. The work of van Wonderen *et al*. suggested the presence of EPR silent d_1 Fe^{III}-$NO^{\bullet}$ in both oxidised *P. pantotrophus* and *Pseudomonas stutzeri* cd_1 preparations following treatment with nitrite [37]. For the 'as isolated' preparations of *P. pantotrophus* cd_1, this work confirms that there are no significant levels of the EPR silent d_1 species, as determined by spectral simulation and integration. In contrast the *P. stutzeri* cd_1 EPR simulation showed a population of EPR silent d_1 heme. The same methods were here applied to the cd_1 from *P. aeruginosa*. As with the *P. pantotrophus* enzyme, the as prepared *P. aeruginosa* cd_1 appears to contain no product-bound EPR silent d_1 heme. The presence of a tyrosine residue near the N-terminal of the *P. pantotrophus* (Tyrosine 25) and *P. aeruginosa* (Tyrosine 10) enzymes may play a role in displacing the product NO. However, in the protein sequences, these two tyrosines are inequivalent residues and, in the structures of the oxidised enzymes, they behave very differently: in *Paracoccus* cd_1, the tyrosine is a ligand to the heme d_1 but, in the structure of the *P. aeruginosa* enzyme it serves to hydrogen-bond a water/hydroxide ligand. Both tyrosines have been shown not to be essential to catalysis but may play a role in stabilising the heme [38, 39]. The *P. stutzeri* enzyme has no tyrosine residue, and indeed no potential heme ligand at all, near the N-terminal and may therefore lack a method of assisting NO dissociation.

For nitrite to be reduced by as prepared cd_1, an electron is required. The origin of the electron is unknown. It is however not unknown for metalloproteins with high reduction potentials to undergo autoreduction [40, 41]. One explanation is

that certain buffers can donate electrons. Piperazine ring-based buffers such as HEPES have been shown to form radical species, whereas morpholine based buffers such as MES do not [42]. However, it has been suggested that the morpholine based buffer MOPS can form a reducing radical [43]. If this is the case then this could be the electron source, since MOPS is part of the mixed buffer used in this study. It has also been shown that the reaction of nitrite with as prepared cd_1 is several times slower in phosphate buffer than in Good's buffers [44] (Dr Myles Cheesman and Josh Dunne, personal communication).

This work provides the first evidence that the reaction of nitrite with oxidised cd_1 enzyme produces a novel Fe^{III}-$NO^{\bullet}$ species of heme d_1. Previous suggestions for the product of this reaction included Fe^{III}-NO_2^-, Fe^{IV}=O and Fe^{II}-NO^+ but these have been discounted [37, 45-48]. Fe^{III}-NO_2^- was dismissed on the grounds that the EPR spectrum shows no low-spin Fe^{III} d_1 heme, which would be present. Fe^{IV}=O was ruled out due to the lack of saturation at high field of the MCD signals at ultralow temperatures. This is more characteristic of a weakly coupled spin system (S_1 = 1/2 plus S_2 = 1/2) rather than a ferryl form of heme d_1. Fe^{II}-NO^+ has been suggested in previous studies [47]. Fe^{II}-NO^+ would not however give rise to a Fe^{III} spectrum and is diamagnetic, so would not give rise to intense MCD at low temperatures. From studies of the pH dependence of the VFVT MCD of *P. aeruginosa* cd_1 in this work there is no evidence for the presence of populations of Fe^{II}-NO^+. The Fe^{II}-NO^+ form of heme d_1 is reported only when heme *c* is reduced [49, 50].

The VFVT MCD spectra for nitrite treated oxidised cd_1 from both *P. pantotrophus* and *P. stutzeri* from van Wonderen *et al*. [37] are identical to the VFVT MCD spectrum of the NO treated oxidised *P. aeruginosa* cd_1 in this work. This suggests that the Fe^{III}-$NO^{\bullet}$ species formed from nitrite reacting with the d_1 heme

of cd_1s is a general process throughout this class of enzymes. Unfortunately it was not possible to produce a fully bound NO form of *P. pantotrophus* cd_1, apparently due to the presence of the tyrosinate residue. Through VFVT MCD this would have provided a direct comparison with the nitrite treated *P. pantotrophus* cd_1 VFVT MCD spectrum published in van Wonderen *et al.* [37].

As well as NO, *P. aeruginosa* cd_1 was treated with azide and analysed by EPR and VFVT MCD. The EPR spectrum was identical to that reported in Muhoberac and Wharton [51] and Walsh *et al*. [52]. The VFVT MCD of azide treated oxidised *P. aeruginosa* cd_1 shows again that low spin Fe^{III} d_1 heme is interacting with a radical, as observed for NO treated oxidised *P. aeruginosa* cd_1. Unreacted N_3^- is not a radical and so not the ligand. It has not been possible to assign the radical species in the azide treated *P. aeruginosa* cd_1. $N_3^{\bullet}$ is a known radical derived from azide but would be produced by an oxidative process and not a reductive process such as that which occurs with nitrite. The low temperature MCD of the azide derivative of the *Paracoccus* enzyme could not be obtained. An EPR spectrum was acquired but the addition of glycerol for MCD caused the return of the EPR signals of the 'as isolated' enzyme.

At increasingly acidic pH the reaction of oxidised cd_1 with nitrite was significantly more rapid and the enzymatic activity higher [37, 53-55]. Bennett showed that despite no change in the electronic absorbance spectrum of *P. pantotrophus* cd_1 with varying pH, the EPR shows significant change [56]. A suggestion for this behaviour is protonation of histidines in the d_1 distal pocket. The protonation of the histidines results in hydrogen-bonding to the distal tyrosinate residue. Through this hydrogen-bonding interaction the energy gap between spin-states is narrowed, due to the weakening of the ligand field strength of the tyrosinate.

The two histidines located in the d_1 distal pocket of *P. pantotrophus* cd_1, histidines 327 and 369, are also conserved in *P. aeruginosa* cd_1 (see Figure 1.12) and have been shown to be essential to activity [57]. As with the electronic absorbance spectra of *P. pantotrophus* cd_1 the *P. aeruginosa* cd_1 spectra over the pH range 5.5-8.5 exhibit no significant changes. The EPR spectra of *P. aeruginosa* cd_1 do not show changes with pH. There are subtle changes in features attributed to the d_1 heme. At ~ 265 mT there is a feature which becomes more prominent at more acidic pH. There are also changes at the g_{xy} of the d_1 heme but these are not systematic, possibly due to the protonation of more than one histidine. The *c* heme features of the EPR spectra remain unchanged at different pHs for both the *P. aeruginosa* and *P. pantotrophus* cd_1.

Richter *et al*. first described an activation of cd_1 when pre-exposed to nitrite [55]. In *P. pantotrophus* oxidised cd_1 the reaction with nitrite triggers the bis-histidine to histidine / methionine switch thought to be essential for enzyme activity [37]. Assays of enzyme activity were conducted with *Paracoccus* cd_1 samples incubated with nitrite for different lengths of time. They demonstrated that cd_1 is activated by nitrite without the need for reduction, and that this is more rapid at more acidic pH. This work also includes nitrite incubation studies of *P. aeruginosa* cd_1. The *P. aeruginosa* cd_1 shows no activation step when exposed to nitrite as observed for the cd_1 of *P. pantotrophus*, and this is reflected in the shape of the curves in Figure 4.09 and 4.10. For the *P. pantotrophus* enzyme, longer incubation times with nitrite results in a faster initial rate. For *P. aeruginosa*, the initial rate is only faster with longer incubation times within the first 5 minutes. After 5 minutes, longer nitrite incubation times do not change the initial rate. Like the *P. pantotrophus* enzyme, *P. aeruginosa* cd_1 has faster initial rates at more acidic pH. Comparison of the two

cd$_1$s shows that the *P. pantotrophus* enzyme has initial rates many orders of magnitude faster than *P. aeruginosa cd*$_1$. This is in agreement with published turnover numbers of 72 s^{-1} and 6 s^{-1} for *P. pantotrophus* and *P. aeruginosa cd*$_1$ at pH 7 respectively [55, 58]. The rates in this work are magnitudes of order too slow to be involved in the catalytic cycle.

As well as following activation of *P. pantotrophus cd*$_1$ using assays studies on the deactivation were also performed. Bradley and Haynes (UEA, unpublished) observed changes in ligands at heme *c* following hydroxylamine reoxidation of reduced *Paracoccus* enzyme. Through nIR-MCD they discovered a new heme *c* intermediate, a bis-histidine coordinated form with parallel ligand planes. This form slowly reverts to the perpendicular ligand conformation seen in the first crystal structure of the oxidised *Paracoccus* enzyme [59]. Through assaying activities of the hydroxylamine-treated, reduced *Paracoccus cd*$_1$ at different time stages it has been observed that loss of enzyme activity occurs from reversion of the reduced form to the bis-histidine, parallel plane form, and not the 'as isolated' perpendicular plane form.

This work has provided insight into the mechanism of nitrite reduction by *cd*$_1$. There have already been many revisions of the mechanism, particularly for *P. aeruginosa cd*$_1$ [50, 58, 60, 61]. This work provides further evidence that the species resulting from the reaction of oxidised *cd*$_1$ with nitrite is a novel Fe^{III}-$NO^{\bullet}$ form of heme *d*$_1$. Further evidence has also been provided of activation of *P. pantotrophus cd*$_1$ through exposure to nitrite without the need for reduction, and that this activation is more rapid at acidic pH. In conjunction with the work of Bradley and Haynes these studies have also provided new insight into the deactivation mechanism of *P. pantotrophus cd*$_1$. Through continued research such as

this the mechanism of the cd_1 enzymes can be clearly defined. This knowledge could provide key information on denitrification, useful for world issues such as the greenhouse effect, global warming and effective use of nitrogenous fertilisers [62].

5.4: References

1. Todd, J. D., Sawers, G., Johnston, A. W. B. (2005) *Mol. Genet. Genomics* ***273***, 197-206.
2. Todd, J. D., Wexler, M., Sawers, G., Yeoman, K. H., Poole, P. S., Johnston, A. W. B. (2002) *Microbiol-SGM* ***148***, 4059-4071.
3. Yeoman, K. H., Curson, A. R. J., Todd, J. D., Sawers, G., Johnston, A. W. B. (2004) *Microbiol-SGM* ***150***, 4065-4074.
4. Ngok-Ngam, P., Ruangkiattikul, N., Mahavihakanont, A., Virgem, S. S., Sukchawalit, R., Mongkolsuk, S. (2009) *J. Bacteriol.* ***191***, 2083-2090.
5. Viguier, C. O., Cuív, P., Clarke, P., O'Connell, M. (2005) *FEMS Microbiol. Lett.* ***246***, 235-242.
6. Hibbing, M. E., Fuqua, C. (2011) *J. Bacteriol.*, [Epub ahead of print]
7. Chao, T. C., Buhrmester, J., Hansmeier, N., Pühler, A., Weidner, S. (2005) *Appl. Environ. Microbiol.* ***71***, 5969-5982.
8. Nesbit, A. D., Giel, J. L., Rose, J. C., Kiley, P. J. (2009) *J. Mol. Biol.* ***387***, 28-41.
9. Yukl, E. T., Elbaz, M. A., Nakano, M. M., Moenne-Loccoz, P. (2008) *Biochemistry* ***47***, 13084-13092.
10. Rossi, M., Pollock, W. B., Reij, M. W., Keon, R. G., Fu, R., Voordouw, G. (1993) *J. Bacteriol.* ***175***, 4699-4711.
11. Keon, R. G., Fu, R. D., Voordouw, G. (1997) *Arch. Microbiol.* ***167***, 376-383.
12. Berman, H. M., Westbrook, J., Feng, Z., Gilliland, G., Bhat, T. N., Weissig, H., Shindyalov, I. N., Bourne, P. E. (2000) *Nucleic Acids Res.* ***28***, 235-242.

13. Beaumont, H. J. E., Lens, S. I., Reijnders, W. N. M., Westerhoff, H.V., van Spanning, R. J. M. (2004) *Mol. Microbiol.* ***54***, 148-158.

14. Schwartz, C. J., Giel, J. L., Patschkowski, T., Luther, C., Ruzicka, F. J., Beinert, H., Kiley, P. J. (2001) *Proc. Natl. Acad. Sci. U. S. A.* ***98***, 14895-14900.

15. Shepard, W., Soutourina, O., Courtois, E., England, P., Haouz, A., Martin-Verstraete, I. (2011) *FEBS J.*, [Epub ahead of print].

16. Arnold, K., Bordoll, L., Kopp, J. Schwede, T. (2006) *Bioinfomatics* ***22***, 195-201.

17. Schwede, T., Kopp, J., Guex, N., Peltsch, M. C. (2003) *Nucleic Acids Res.* ***31***, 3381-3385.

18. Guex, N., Peltsch, M. C. (1997) *Electrophoresis* ***18***, 2714-2723.

19. Zeng, J., Zhang, X., Wang, Y., Ai, C., Liu, Q., Qiu, G. (2008) *FEBS Lett.* ***582***, 3889-3892.

20. Tucker, N. P., Le Brun, N. E., Dixon, R., Hutchings, M. I. (2010) *Trends Microbiol.* ***18***, 149-156.

21. Kent, T. A., Dreyer, J. L., Kennedy, M. C., Huynh, B. H., Emptage, M. H., Beinert, H., Munck, E. (1982) *Proc. Nat. Acad. Sci. U.S.A.* ***79***, 1096-1100.

22. George, S. J. (1986) PhD Thesis.

23. Tucker, N. P., Hicks, M. G., Clarke, T. A., Crack, J. C., Chandra, G., Le Brun, N. E., Dixon, R., Hutchings, M. I. (2008) *PLoS One* ***3***, e3623.

24. Zeng, J., Zhang, K., Liu, J., Qiu, G. (2008) *J. Microbiol. Biotechnol.* ***18***, 1672-1677.

25. Chandramouli, K. (2006) *Dissertation (University of Georgia Theses and Dissertations).*

26. Sweeney, W. V., Rabinowitz, J. C. . (1980) *Ann. Rev. Biochem.* ***49***, 139-161.

27. Rodrigues, P., Graca, F., Macedo, A. L., Moura, I., Moura, J. J. (2001) *Biochem. Biophys. Res. Commun.* ***289***, 630-633.

28. Grazina, R., de Sousa, P. M., Brondino, C. D., Carepo, M. S., Moura, I., Moura, J. J. . (2011) *Bioelectrochemistry* ***82***, 22-28.

29. Busch, J. L., Breton, J. L., Bartlett, B. M., James, R., Hatchikian, E. C., Thomson, A. J. . (1996) *Biochem. J.* ***314***, 63-71.

30. Bennett, B., Gruer, M. J., Guest, J. R., Thomson, A. J. . (1995) *Eur. J. Biochem.* ***233***, 317-326.

31. Johnson D. C., D., D. R., Smith, A. D., Johnson, M. K. (2005) *Annu. Rev. Biochem.* ***74***, 247-281.

32. Fleischhacker, A. S., Kiley, P. J. (2011) *Curr. Opin. Chem. Biol.* ***15***, 335-341.

33. Crack, J. C., Jervis, A. J., Gaskell, A. A., White, G. F., Green, J., Thomson, A. J., Le Brun, N. E. . (2008) *Biochem. Soc. Trans.* ***36***, 1144-1148.

34. Crack, J. C., Gaskell, A. A., Green, J., Cheesman, M. R., Le Brun, N. E., Thomson, A. J. (2008) *J. Am Chem. Soc.* ***130***, 1749-1758.

35. Yano, T., Magnitsky, S., Sled, V. D., Ohnishi, T., Yagi, T. (1999) *J. Biol. Chem.* ***274***, 28598-28605.

36. Thomson, A. J., Robinson, A. E., Johnson, M. K., Moura, J. J., Moura, I., Xavier, A. V., Legall, J. (1981) *Biochim. Biophys. Acta.* ***670***, 93-100.

37. van Wonderen, J. H., Knight, C., Oganesyan, V. S., George, S. J., Zumft, W. G., Cheesman, M. R. (2007) *J. Biol. Chem.* ***282***, 28207-28215.

38. Cutruzzola, F., Arese, M., Grasso, S., Bellelli, A., Brunori, M. (1997) *FEBS Lett.* ***412***, 365- 369.

39. Radoul, M., Bykov, D., Rinaldo, S., Cutruzzolà, F., Neese, F., Goldfarb, D. (2011) *J. Am Chem. Soc.* ***133***, 3043-3055.

40. Tanaka, K., Takahashi, K., Asada, K. (1978) *J. Biol. Chem.* ***253***, 7397-7403.

41. Takabe, T., Niwa, S., Ishikawa, H. (1980) *J. Biochem.*, 1335-1339.

42. Grady, J. K., Chasteen, N. D., Harris, D. C. (1988) *Anal. Biochem.* ***173***, 111-115.

43. Burkitt, M. J., Gilbert, B. C. (1991) *Free Radic. Res. Commun.* ***14***, 107-123.

44. Good, N. E., Winget, G. D., Winter, W., Connolly, T. N., Izawa, S., Singh, R. M. M. (1966) *Biochemistry* ***5***, 467-477.

45. Allen, J. W. A., Higham, C. W., Zajicek, R. S., Watmough, N. J., and Ferguson, S. J. (2002) *Biochem. J.* ***366***, 883-888.

46. Oganesyan, V. S., Cheesman, M. R., Thomson, A. J. (2007) *Inorg. Chem.* ***46***, 10950-10952.

47. Wang, Y. N., Averill, B. A. (1996) *J. Am Chem. Soc.* ***118***, 3972-3973.

48. George, S. J., Allen, J. W. A., Ferguson, S. J., Thornley, R. N. F. (2000) *J. Biol. Chem.* ***275***, 33231-33237.

49. Sam, K. A., Strampraad, M. J. F., de Vries, S., Ferguson, S. J. (2008) *J. Biol. Chem.* ***283***, 27403-27409.

50. Rinaldo, S., Sam, K. A., Castiglione, N., Stelitano, V., Arcovito, A., Brunori, M., Allen, J. W., Ferguson, S. J., Cutruzzolà, F. (2011) *Biochem. J.* ***435***, 217-225.

51. Muhoberac, B. B., Wharton, D. C. (1983) *J. Biol. Chem.* ***258***, 3019-3027.

52. Walsh, T. A., Johnson, M. K., Thomson, A. J., Barber, D., Greenwood, C. (1981) *Inorg. Biochem.* ***14***, 1-14.

53. Silvestrini, M. C., Tordi, M. G., Musci, G., Brunori, M. (1990) *J. Biol. Chem.* ***265***, 11783-11787.

54. Silvestrini, M. C., Colosimo, A., Brunori, M., Walsh, T. A., Barber, D., Greenwood, C. (1979) *Biochem. J.* ***183***, 701-709.

55. Richter, C. D., Allen, J. W., Higham, C. W., Koppenhöfer, A., Zajicek, R. S., Watmough, N. J., Ferguson, S. J.,. (2002) *J. Biol. Chem.* ***277***, 3093-3100.

56. Bennett, M. S., Cheesman, M. R. *unpublished*.

57. Cutruzzola, F., Brown, K., Wilson, E., Bellelli, A., Arese, M., Tegoni, M., Cambillau, C., Brunori, M. (2001) *Proc. Nat. Acad. Sci. U.S.A.* ***98***, 2232-2237.

58. Rinaldo, S., Arcovito, A., Brunori, M., Cutruzzola, F. (2007) *J. Biol. Chem.* ***282***, 14761-14767.

59. Fulop, V., Moir, J. W. B., Ferguson, S. J., Hadju, J. (1995) *Cell* ***81***, 369-377.

60. Cutruzzola, F., Rinaldo, S., Centola, F., Brunori, M. (2003) *IUBMB Life **55***, 617-621.

61. Rinaldo, S., Giardina, G., Castiglione, N., Stelitano, V., Cutruzzola, F. (2011) *Biochem. Soc. Trans. **39***, 195-200.

62. Socolow, R. H. (1999) *Proc. Nat. Acad. Sci. U.S.A. **96***, 6001-6008.

Appendix.

Experimental and Simulated EPR Spectra of *Paracoccus pantotrophus* and *Pseudomonas aeruginosa* cd_1

This appendix shows the recorded experimental and simulated EPR spectra for *P. aeruginosa* and *P. pantotrophus* cd_1 from Tables 4.02A and 4.02B. Each figure contains the experimental spectrum, the sum of the simulated spectra and the simulated spectra for each *c* and d_1 heme species. Each figure has a table detailing the % contributions of each species at 20 K / 0.64 mW, the g-values of each signal (g_{xyz}) and the linewidths (W_{xyz}). As with Tables 4.02A and 4.02B, where g-values cannot be detected, such as the high-field g_x of heme *c*, parameters were chosen on the assumption that the total of the squared g-values is 16 ($\Sigma g_i^2 = 16$) and the linewidth set to an arbitrary large value. This is indicated by brackets around the g-value and * on the linewidth.

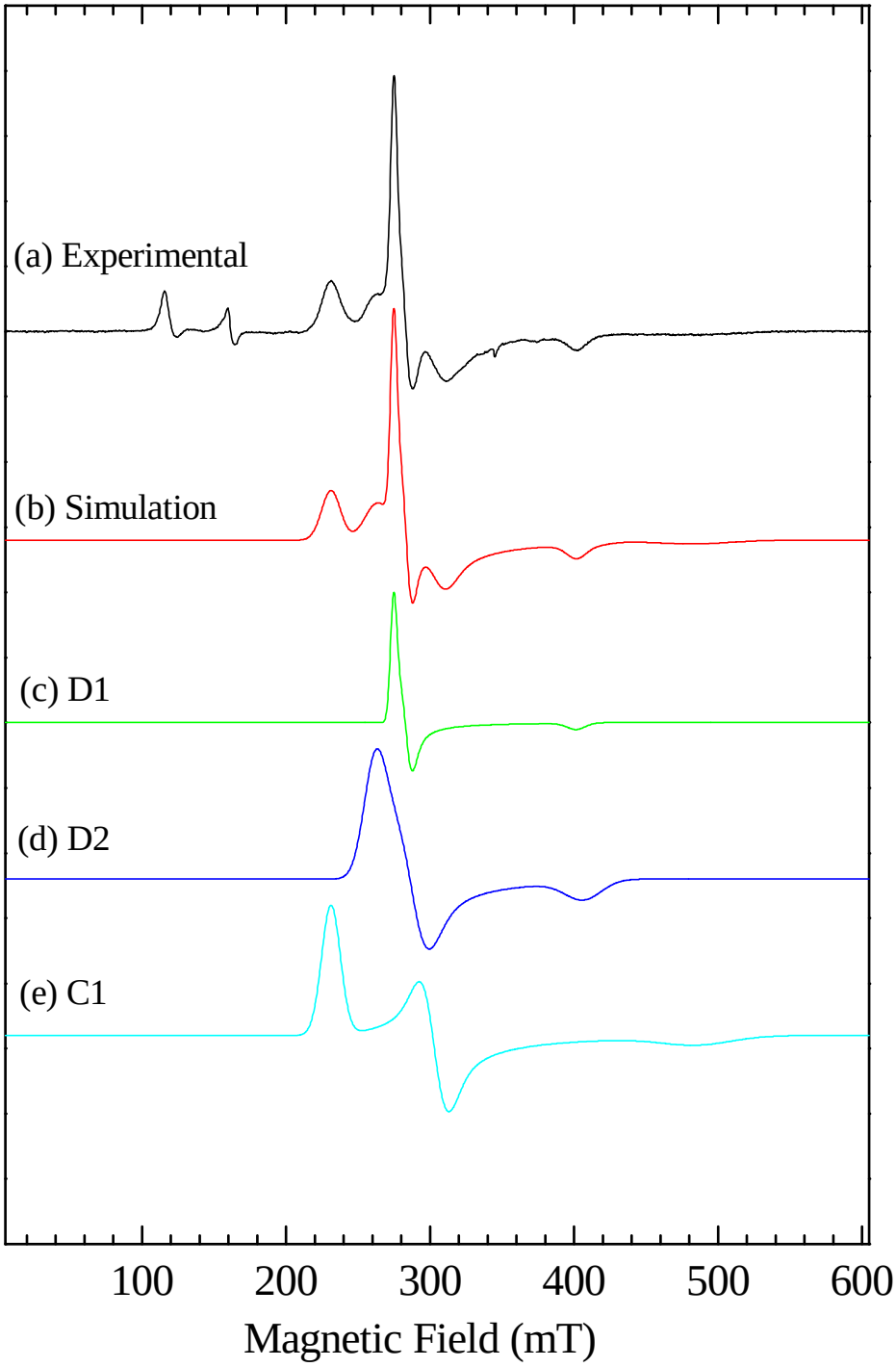
(a) Experimental
(b) Simulation
(c) D1
(d) D2
(e) C1
100
200
300
400
500
600
Magnetic Field (mT)

Figure A.01: (Previous page) Experimental and simulated EPR of oxidised, as isolated *P. aeruginosa* cd_1. Conditions are 10 K / 2 mW. Samples are in 50 mM phosphate D_2O buffer, pH 6.5*. Spectrometric parameters are modulation frequency, 100 KHz; modulation amplitude, 10 G; time constant, 40.96 ms; and sweep time, 83.886 s.

Constituent number	g_{xyz}	W_{xyz}	Species type
D1	2.518, 2.44, 1.723	44, 72, 125	d_1 heme
D2	2.638, 2.44, 1.70	160, 190, 250	d_1 heme
C1	1.42, 2.28, 2.99	480, 160, 130	*c* heme

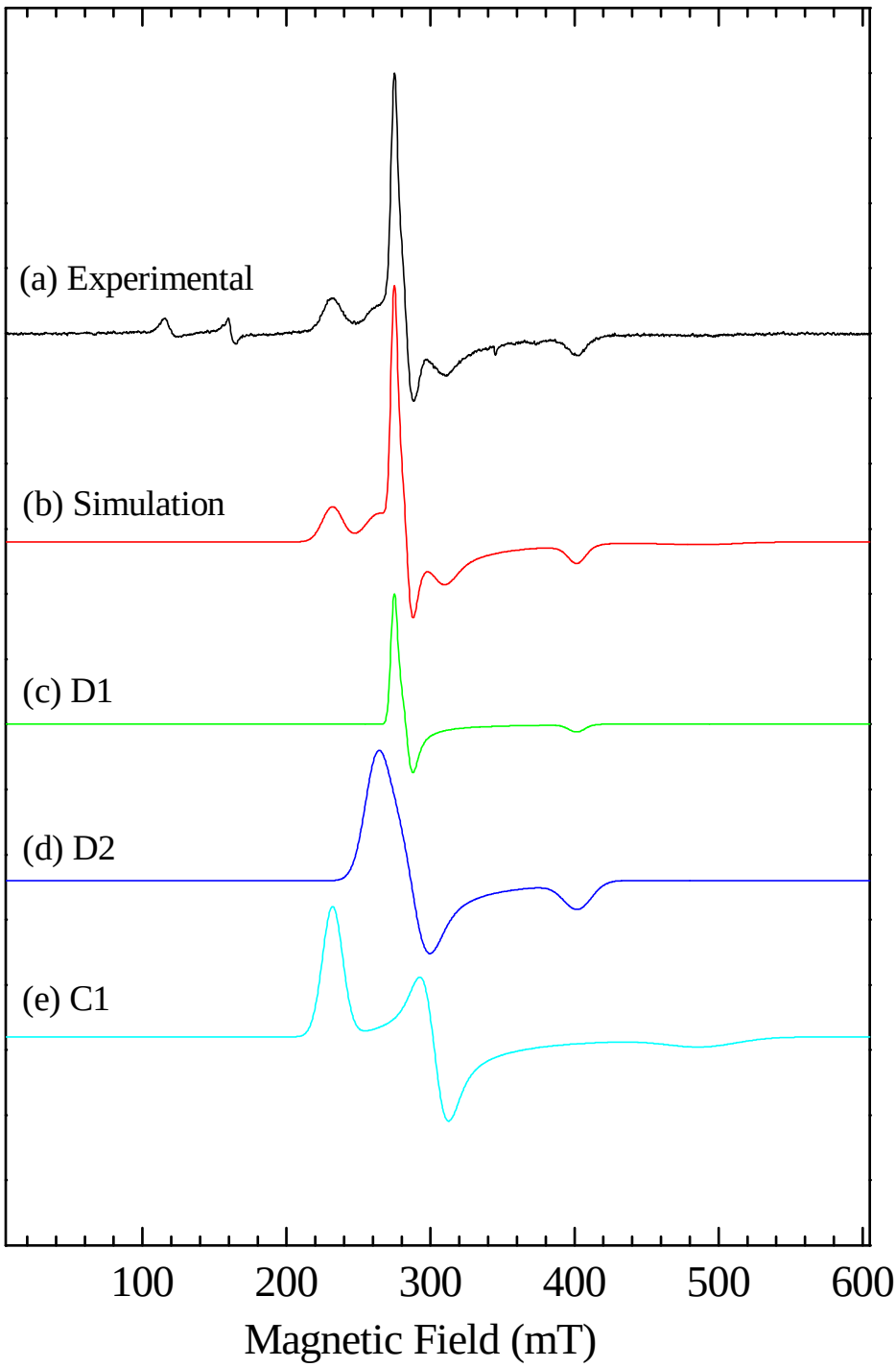
(a) Experimental
(b) Simulation
(c) D1
(d) D2
(e) C1
100
200
300
400
500
600
Magnetic Field (mT)

Figure A.02: (Previous page) Experimental and simulated EPR of oxidised, as isolated *P. aeruginosa* cd_1. Conditions are 20 K / 0.64 mW. Samples are in 50 mM phosphate D_2O buffer, pH 6.5*. Spectrometric parameters are modulation frequency, 100 KHz; modulation amplitude, 10 G; time constant, 40.96 ms; and sweep time, 83.886 s.

Constituent number	g_{xyz}	W_{xyz}	Species type and % contribution
D1	2.518, 2.44, 1.723	44, 72, 110	d_1 heme, 0.590
D2	2.633, 2.40, 1.72	170, 190, 190	d_1 heme, 0.414
C1	1.410, 2.282, 2.98	480, 155, 140	*c* heme, 1.000

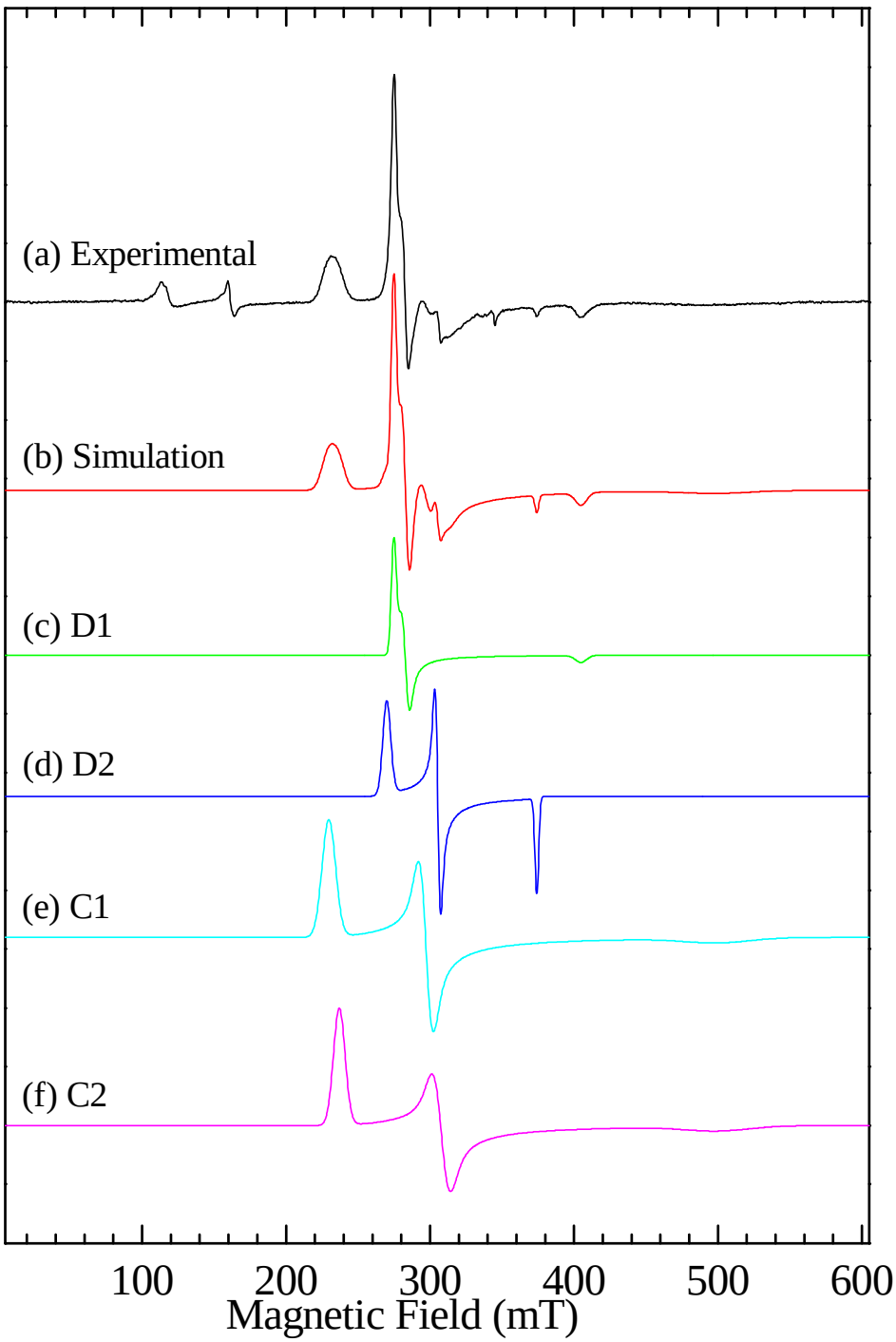
(a) Experimental
(b) Simulation
(c) D1
(d) D2
(e) C1
(f) C2
100
200
300
400
500
600
Magnetic Field (mT)

Figure A.03: (Previous page) Experimental and simulated EPR spectra of oxidised *P. aeruginosa* cd_1 as in Figure A.01 but with deuterated glycerol at ~55% total volume. Conditions used are 10 K / 2 mW. Spectrometric parameters are modulation frequency, 100 KHz; modulation amplitude, 10 G; time constant, 40.96 ms; and sweep time, 83.886 s.

Constituent number	g_{xyz}	W_{xyz}	Species type
D1	2.518, 2.445, 1.709	34, 46, 78	d_1 heme
D2	2.565, 2.267, 1.85	55, 32, 26	d_1 heme
C1	1.38, 2.326, 3.011	450, 80, 93	*c* heme
C2	1.38, 2.245, 2.918	450, 100, 80	*c* heme

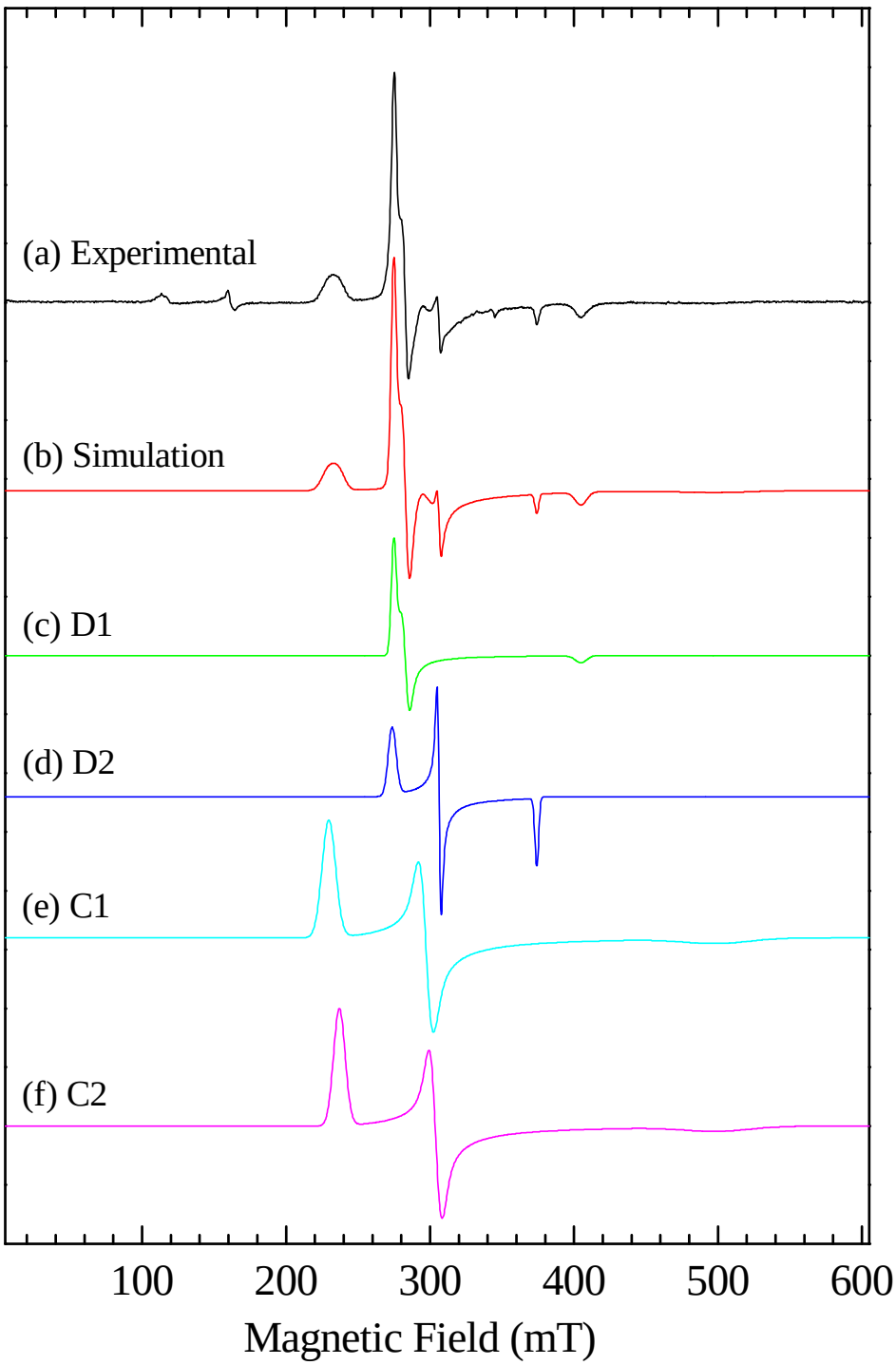
(a) Experimental
(b) Simulation
(c) D1
(d) D2
(e) C1
(f) C2
100
200
300
400
500
600
Magnetic Field (mT)

Figure A.04: (Previous page) Experimental and simulated EPR spectra of oxidised *P. aeruginosa* cd_1 as in Figure A.02 but with deuterated glycerol at ~55% total volume. Conditions used are 20 K / 0.64 mW. Spectrometric parameters are modulation frequency, 100 KHz; modulation amplitude, 10 G; time constant, 40.96 ms; and sweep time, 83.886 s.

Constituent number	g_{xyz}	W_{xyz}	Species type and % contribution
D1	2.518, 2.445, 1.709	34, 46, 78	d_1 heme, 0.678
D2	2.53, 2.26, 1.85	55, 23, 26	d_1 heme, 0.239
C1	1.38, 2.326, 3.011	450, 80, 93	*c* heme, 0.597
C2	1.38, 2.275, 2.918	450, 70, 80	*c* heme, 0.403

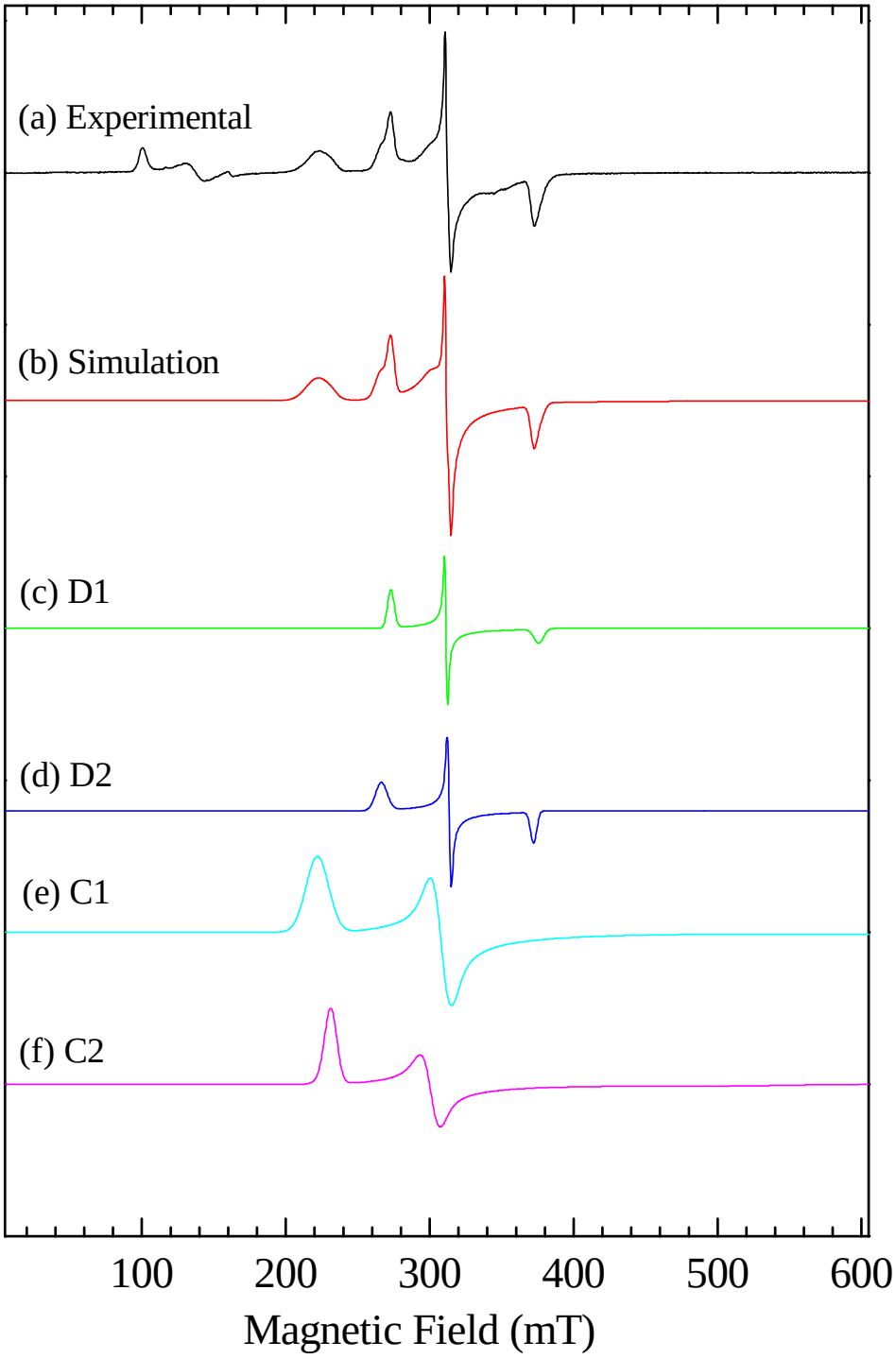
(a) Experimental
(b) Simulation
(c) D1
(d) D2
(e) C1
(f) C2
100
200
300
400
500
600
Magnetic Field (mT)

Figure A.05: (Previous page) Experimental and simulated EPR of oxidised, as isolated *P. pantotrophus* cd_1. Sample is in 12 mM acetate, 12 mM MES, 12 mM MOPS and 12 mM Tris D_2O buffer, pH 6.5*. Conditions are 10 K / 2 mW. Spectrometric parameters are modulation frequency, 100 KHz; modulation amplitude, 10 G; time constant, 40.96 ms; and sweep time, 83.886 s.

Constituent number	g_{xyz}	W_{xyz}	Species type
D1	2.526, 2.223, 1.8417	46, 17, 65	d_1 heme
D2	2.6, 2.208, 1.8598	80, 22, 43	d_1 heme
C1	(1.150), 2.24, 3.108	1000*, 80, 93	*c* heme
C2	(1.369), 2.29, 2.98	1000*, 100, 80	*c* heme

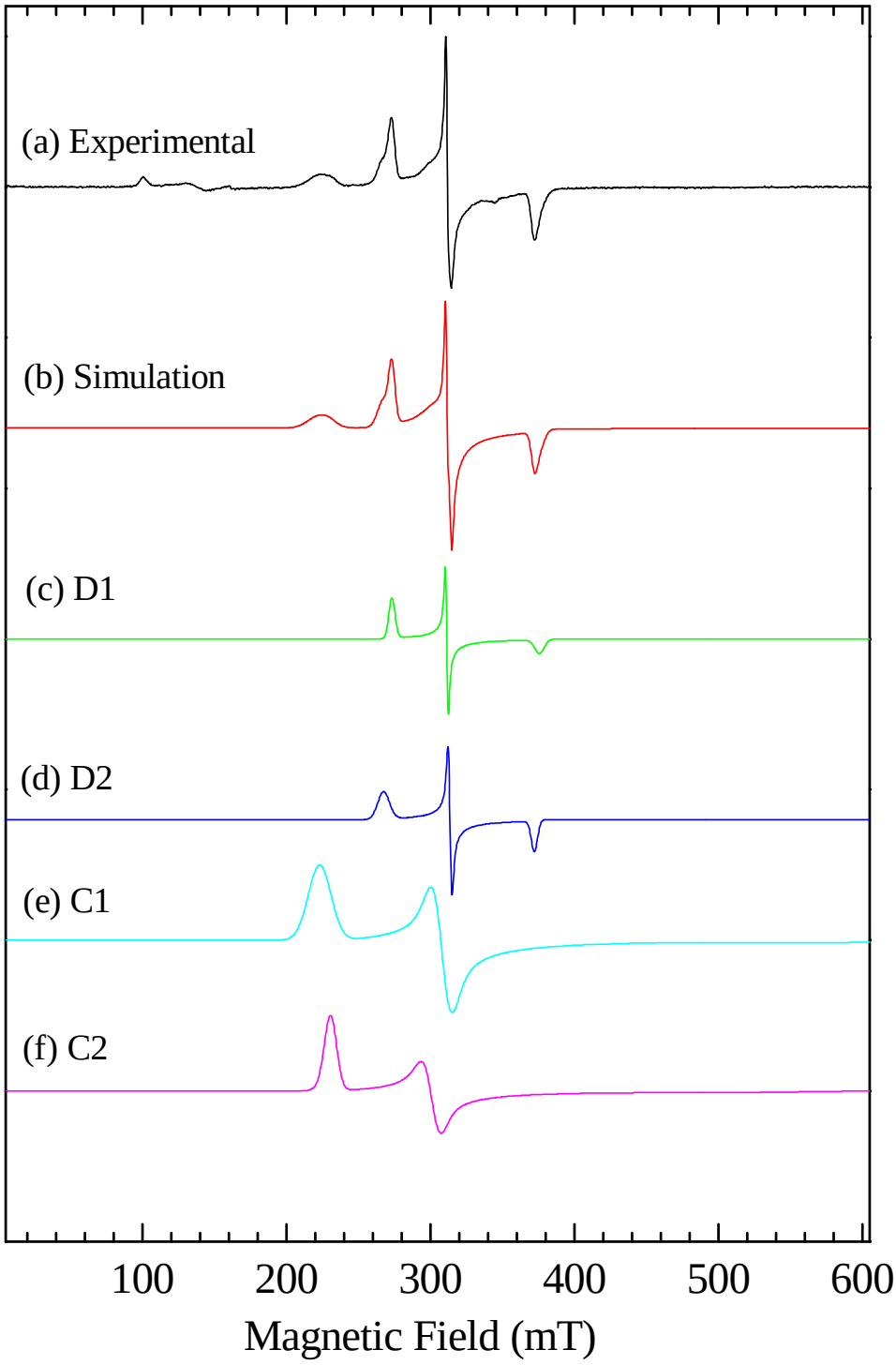
(a) Experimental
(b) Simulation
(c) D1
(d) D2
(e) C1
(f) C2
100
200
300
400
500
600
Magnetic Field (mT)

Figure A.06: (Previous page) Experimental and simulated EPR of oxidised, as isolated *P. pantotrophus* cd_1. Sample is in 12 mM acetate, 12 mM MES, 12 mM MOPS and 12 mM Tris D_2O buffer, pH 6.5*. Conditions are 20 K / 0.64 mW. Spectrometric parameters are modulation frequency, 100 KHz; modulation amplitude, 10 G; time constant, 40.96 ms; and sweep time, 83.886 s.

Constituent number	g_{xyz}	W_{xyz}	Species type and % contribution
D1	2.534, 2.223, 1.8417	43, 17, 65	d_1 heme, 0.617
D2	2.59, 2.208, 1.8598	80, 22, 43	d_1 heme, 0.599
C1	(1.192), 2.24, 3.092	1000*, 110, 155	*c* heme, 0.914
C2	(1.350), 2.29, 2.989	1000*, 100, 80	*c* heme, 0.086

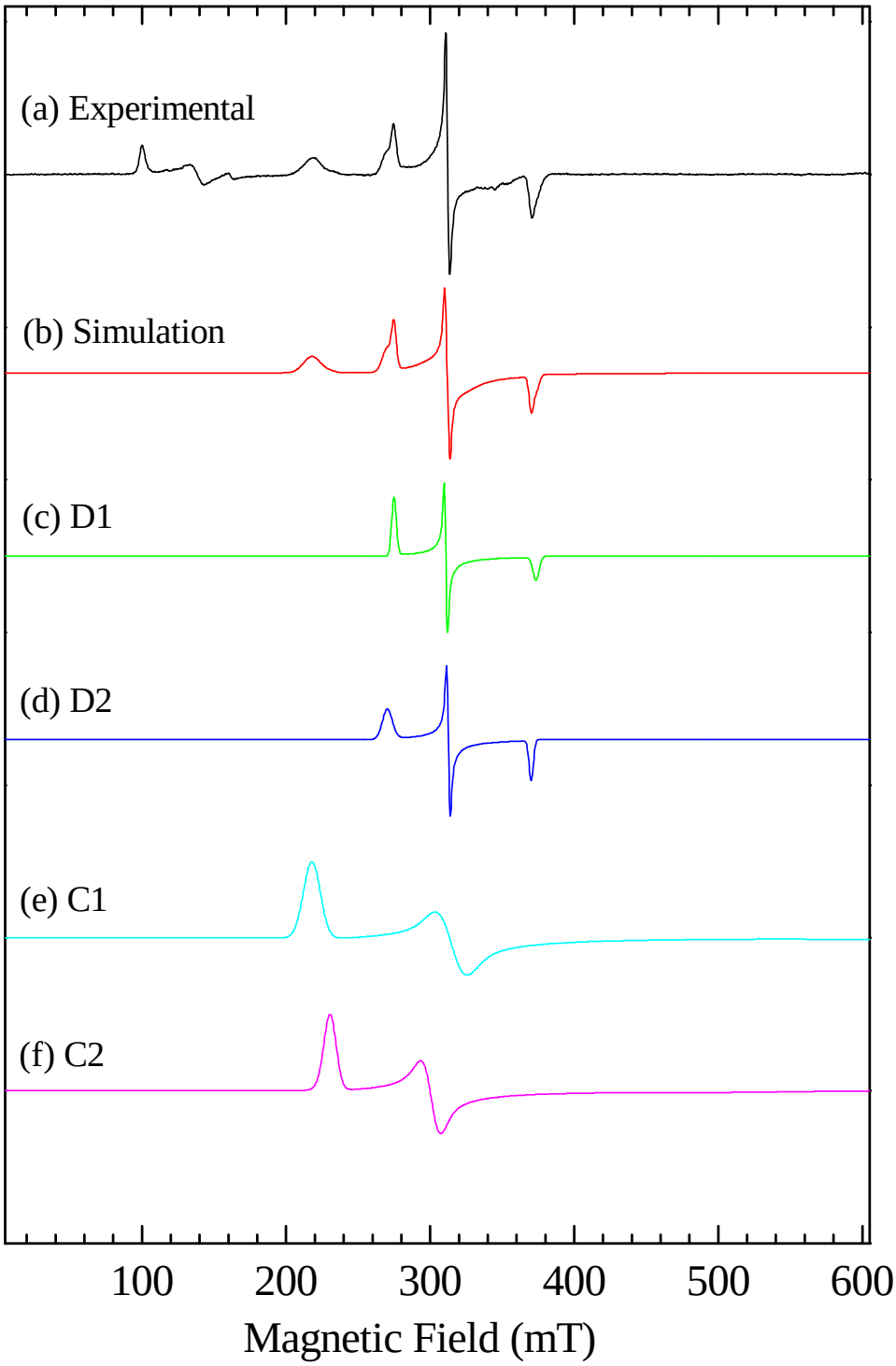
(a) Experimental
(b) Simulation
(c) D1
(d) D2
(e) C1
(f) C2
100
200
300
400
500
600
Magnetic Field (mT)

Figure A.07: (Previous page) Experimental and simulated EPR spectra of oxidised, as isolated *P. pantotrophus* cd_1 as in Figure A.05 but with the introduction of deuterated glycerol at ~55% of the total volume. Conditions used are 10 K / 2 mW. Spectrometric parameters are modulation frequency, 100 KHz; modulation amplitude, 10 G; time constant, 40.96 ms; and sweep time, 83.886 s.

Constituent number	g_{xyz}	W_{xyz}	Species type
D1	2.518, 2.226, 1.853	32, 18, 42	d_1 heme
D2	2.562, 2.214, 1.87	68, 20, 30	d_1 heme
C1	(1.089), 2.19, 3.165	1000*, 170, 115	*c* heme
C2	(1.350), 2.29, 2.989	1000*, 100, 80	*c* heme

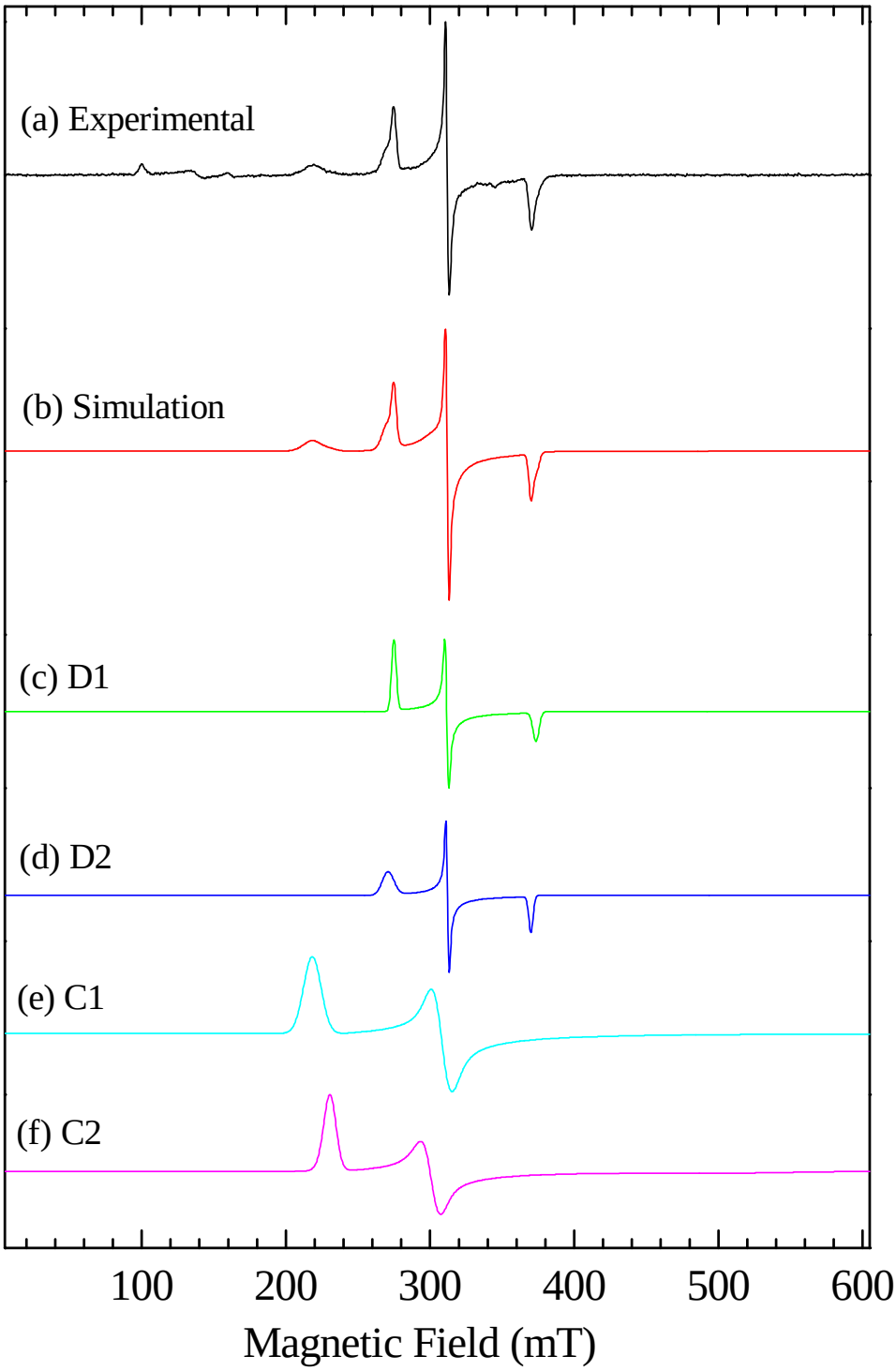
(a) Experimental
(b) Simulation
(c) D1
(d) D2
(e) C1
(f) C2
100
200
300
400
500
600
Magnetic Field (mT)

Figure A.08: (Previous page) Experimental and simulated EPR spectra of oxidised, as isolated *P. pantotrophus* cd_1 as in Figure A.06 but with the introduction of deuterated glycerol at ~55% of the total volume. Conditions used are 20 K / 0.64 mW. Spectrometric parameters are modulation frequency, 100 KHz; modulation amplitude, 10 G; time constant, 40.96 ms; and sweep time, 83.886 s.

Constituent number	g_{xyz}	W_{xyz}	Species type and % contribution
D1	2.518, 2.221, 1.853	32, 22, 42	d_1 heme, 0.573
D2	2.557, 2.218, 1.871	80, 18, 30	d_1 heme, 0.801
C1	(0.0992), 2.24, 3.162	1000*, 110, 120	*c* heme, 0.898
C2	(1.350), 2.29, 2.989	1000*, 100, 80	*c* heme, 0.102